DISSERTATION

BIOPOLYMER NANOMATERIALS FOR GROWTH FACTOR STABILIZATION AND DELIVERY

Submitted by

Laura Walker Place

Graduate Degree Program in Bioengineering

In partial fulfillment of the requirements

For the Degree of Doctor of Philosophy

Colorado State University

Fort Collins, Colorado

Summer 2014

Doctoral Committee:

Advisor: Matt J. Kipper

Susan James
Ketul C. Popat
Benjamin Miller

ABSTRACT

BIOPOLYMER NANOMATERIALS FOR GROWTH FACTOR STABILIZATION AND DELIVERY

Biopolymers are useful in tissue engineering due to their inherent biochemical signals, including interactions with growth factors. There are six biopolymers used in this work, the glycosaminoglycans (GAGs), heparin (Hep), chondroitin sulfate (CS), and hyaluronan (HA), chitosan (Chi), a GAG-like molecule derived from arthropod exoskeletons, a Chi derivative *N,N,N*-trimethyl chitosan (TMC), and an extracellular matrix (ECM)-derived material, demineralized bone matrix (DBM). The direct delivery of growth factors is complicated by their instability. GAG side chains of proteoglycans stabilize growth factors. GAGs also regulate growth factor-receptor interactions at the cell surface. The majority of proteoglycan function is derived from its GAG side chain composition. Here we report the development of nanoparticles, proteoglycan-mimetic graft copolymers, incorporation of nanoparticles into electrospun nanofibers, and processing methods for electrospinning demineralized bone matrix to fabricate bioactive scaffolds for tissue engineering. The nanoparticles were found to show similar size, composition, and growth factor binding and stabilization as the proteoglycan aggrecan. We use basic fibroblast growth factor (FGF-2) as a model heparin-binding growth factor, demonstrating that nanoparticles can preserve its activity for more than three weeks.

Graft copolymers were synthesized with either CS or Hep as the side chains at four different grafting densities. Their chemistry was confirmed via ATR-FTIR and proton NMR. They were shown to increase in effective hydrodynamic diameter with grafting density, resulting

in a size range from 90-500 nm. Graft copolymers were tested for their ability to deliver FGF-2 to cells. The CS conditions and the Hep 1:30 performed equally as well as when FGF-2 was delivered in solution. Preliminary dynamic mechanical testing demonstrated that hydrogels containing the copolymers exhibit changes in compressive modulus with cycle frequency.

Two electrospinning techniques were developed, using an emulsion and a coaxial needle, for incorporating growth factor into electrospun nanofibers. We bound FGF-2 to aggrecan-mimetic nanoparticles for stabilization throughout electrospinning. The two techniques were characterized for morphology, nanoparticle and FGF-2 incorporation, cytocompatibility, and FGF-2 delivery. We demonstrated that both techniques result in nanofibers within the size range of collagen fiber bundles and dispersion of PCNs throughout the fiber mat, and exhibit cytocompatibility. We determined via ELISA that the coaxial technique is superior to the emulsion for growth factor incorporation. Finally, FGF-2 delivery to MSCs from coaxially electrospun nanofibers was assessed using a cell activity assay.

We developed a novel method for tuning the nanostructure of DBM through electrospinning without the use of a carrier polymer. This work surveys solvents and solvent blends for electrospinning DBM. The effects of DBM concentration and dissolution time on solution viscosity are reported and correlated to observed differences in fiber morphology. We also present a survey of techniques to stabilize the resultant fibers with respect to aqueous environments. Glutaraldehyde vapor treatment is successful at maintaining both macroscopic and microscopic structure of the electrospun DBM fibers. Finally, we report results from tensile testing of stabilized DBM nanofiber mats, and preliminary evaluation of their cytocompatibility. The DBM nanofiber mats exhibit good cytocompatibility toward human dermal fibroblasts (HDF) in a 4-day culture.

ACKNOWLEDGEMENTS

I would like to acknowledge my advisor, Dr. Matt Kipper, my committee members Dr. Ketul Popat, Dr. Sue James, and Dr. Benjamin Miller. Thank you for your knowledge and thoughtful questions.

I would like to thank faculty and staff at Colorado State University and University of Wyoming for collaborations, training, and equipment use, Dr. Melissa Reynolds, Dr. Vinod Damodaran, Dr. Travis Bailey, Dr. Tammy Donahue, Dr. Salman Khetani, Dr. John Kisiday, Dr. Pat Mccurdy, and Dr. Patrick Johnson. I would also like thank the undergraduate students that did large amounts of experimental work reported here, Sean Kelly, Maria Seyki, Julia Taussig, and Natalee Franz.

I would like to thank current and past members of the group, particularly my good friend, Dr. Jorge Almodóvar for teaching me all he knows, Dr. Fabio Zomer Valpato, Rai Romero, and Selin Akgul. I would like to thank my colleagues for their help and support in and out of the lab, Dr. Victoria Leszczak, Dr. Nathan Trujillo, Dr. Anthony Schwartz, Nabila Huq, Hannah Pauly, and Justin Weaver, and my editor, Taylor Hinton. I would like acknowledge my funding sources, without which none of this would be possible, the National Science Foundation and Allosource.

Finally I would like to thank my friends and family for all of their support throughout this endeavor, particularly my parents, Kirk and Michelle Place, and my grandparents for teaching me the value of hard work.

TABLE OF CONTENTS

CHAPTER 1

Introduction

1.1 MOTIVATION.

Tissue engineering and regenerative medicine seek to repair tissues damaged by injury or disease. In 2010 there were over one million total joint replacements, 438,000 internal fixation devices for bone fractures, and 849,000 coronary artery stents and vascular grafts implanted.[1] Current procedures and devices have many drawbacks, including immune response, hemocompatibility, secondary surgeries, and implant lifetime. These techniques could be improved or replaced by applying tissue engineering principles. The tissue engineering paradigm combines a scaffold with biochemical cues and cells to create a material that takes advantage of the body's natural pathways to integrate and heal more effectively.

1.2 BIOMIMETIC CONSTRUCTS FOR TISSUE ENGINEERING.

The principle of biomimetics is one strategy for developing biologically functional materials for tissue engineering and regenerative medicine. This approach imitates structural and chemical attributes seen *in vivo*. These include feature size, shape, organization, and presentation of ligands and signaling molecules.[2-4] Tissues are made up of cells surrounded by the extracellular matrix (ECM). The ECM has a complex three-dimensional architecture that gives rise to the function of the tissue.[5] Cells receive cues from the ECM to adhere, migrate, proliferate, and differentiate.[6] By mimicking key features of the ECM, we may achieve improved cell recognition, adhesion, and improved control over cell function, which could be translated into reduced immune response and better tissue integration of an implant. Two important features of the ECM that could be mimicked are biomechanics, and biochemistry. These are described below. The research described in this dissertation is guided by a biomimetic approach.

1.2.1 Biomechanical Cues. Tissues are comprised of a hierarchical structure from the nano to the macro scale.[7] It has been shown that feature size, surface area, porosity, and organization affect cell adhesion and differentiation.[6, 8-10] A number of studies have investigated the effects of nanofeatures on cell behavior. Balasandaram et al. showed increased chondrocyte activity on nanostructured polymeric surfaces versus flat surfaces.[11] Coburn et al. observed higher chondrogenesis from mesenchymal stem cells (MSCs) when cultured in a nanofiber construct over a pellet culture that had no nanofeatures.[12] A review by Karageorgiou et al. determined that larger pore sizes lead to increased vascularization and osteogenesis whereas smaller pores result in cartilaginous tissue.[13] These studies demonstrate that the nanostructure of a material affects cell behavior.

The nanostructure dictates the macrostructure, and thus the mechanical function of the tissue. For example, articular cartilage is a load-bearing material that provides support and lubrication in joints.[14] It is primarily made up of collagen II, proteoglycans, and water.[15] The structure of these components gives rise to its function.[16] Collagen II is arranged into long fibrils that provide tensile strength; the proteoglycans are brush-like structures made up of a protein backbone with glycosaminoglycan (GAG) side chains. GAGs are highly sulfated polysaccharides that carry a strong negative charge. This results in electrostatic repulsions and makes them very hydrophilic, leading to compressive strength and lubricity. The nanostructure of these elements is imperative to achieve these mechanical properties. Incorporating biomimetic nanofeatures into constructs is an important theme throughout the following chapters.

1.2.2 Biochemical Cues. Cells respond to biochemical cues from their surrounding environment, including the chemistry of the environment itself and the presentation of growth factors and other proteins.[6, 17-19] The use of natural polymers that closely imitate the chemistry of

the ECM is one way to present these cues. There are many research groups incorporating natural polymers for various tissue engineering applications, such as collagen and GAGs into coatings, hydrogels, porous composites, and nanofibers.[20] Badrossamay et al. seeded several different cell types onto polycaprolactone and polycaprolactone-collagen blend fibers and saw higher cell adhesion and spreading on the collagen blend fibers.[21] Mathews et al. showed increased osteoblast differentiation on tissue culture polystyrene coated with different glycosaminoglycans.[22] Mimicking the ECM composition provides cues for cell adhesion and differentiation.[23]

The ECM contains adhesion proteins and growth factors that provide cells with signals.[24] Several commonly used adhesion proteins are fibronectin, vitronectin, laminin, and collagen. These support cell attachment and spreading. Specific motifs in these proteins, such as RGD, YIGSR, and GFOGER, have been identified and are often used in place of the full molecule. Many studies show improved cell interactions with a scaffold after the addition of these molecules.[6, 25-29]

Growth factors are signaling molecules that stimulate cells to proliferate, migrate, and differentiate.[30] There are a variety of growth factors in the ECM, including members of the fibroblast growth factor (FGF) family, the transforming growth factor beta (TGF-β) superfamily, insulin-like growth factors (IGF), platelet-derived growth factor (PDGF), and vascular endothelial growth factor (VEGF).[31-34] These growth factors stimulate cells and have been shown to improve wound healing.[33, 35] However, they are unstable in solution.[36, 37] Many growth factors, including members of the TGF- β superfamily and FGF family, can bind to GAGs in the ECM where they are protected and localized.[10, 19, 38, 39] For example, when FGF-2 is bound to heparin it is more likely that the cell receptor for FGF-2 will bind.[38] These characteristics can be exploited

to engineer a bioactive scaffold. This will be a common thread throughout the chapters of this dissertation.

1.2.3 Engineering Biomimetics. The previous sections have described the importance of the structural and biochemical properties of the ECM. Thus, when engineering a material, the structure and chemistry may be designed to control cell behavior.[40] There are a variety of options for the material and structure, which are ultimately dictated by the final application. For example, if the application is cartilage, a soft porous gel containing chondroitin sulfate would be preferable. For bone, a hard porous material containing minerals such as calcium phosphate and hydroxyapatite may provide superior results. For a vascular graft, an elastic construct rich in heparan sulfate would be desireable.[8, 17, 41-43] Design boundaries and limitations such as cost, time, and dose required arise throughout material development. These issues can limit a material or open doors to new applications. Materials science approaches can be used to tailor the material properties to present different biological signals and drugs in a controlled way, and at different concentrations, for new applications. This work engineers materials intelligently to incorporate all of these features to create biomimetic constructs for a variety of applications.

1.4 PROJECT DESCRIPTION.

Current methods for repairing damaged or diseased tissue have limitations, including immune response and tissue integration. As stated previously, one strategy to overcome these limitations is biomimetics. This principle seeks to create a therapeutic material by imitating chemical makeup, hierarchical structure, and delivery of biochemical cues expressed *in vivo*. The work herein strives to accomplish this through the use of biopolymers constructed in a variety of geometries and incorporation of the growth factor FGF-2.

Six biopolymers are used to create three different geometries of nanoassemblies. These include, chitosan (CHI), *N*,*N*,*N*-trimethylchitosan (TMC), heparin (HEP), chondroitin sulfate (CS), hyaluronan (HA), and demineralized bone matrix (DBM). HEP, CS, and HA are GAGs; HEP and CS are strong polyanions, while HA is a weak polyanion. CHI and one of its derivatives, TMC, are structurally similar to GAGs; CHI is a weak polycation and TMC is a strong polycation. DBM is derived from human bone and contains a mixture of ECM proteins and polysaccharides.

These biopolymers are used in combination with FGF-2 to create and evaluate biomimetic nanoassemblies for use in tissue engineering.

1.4.1 Hypothesis and Research Aims. This dissertation investigates the hypothesis that the inherent properties of biopolymers can be exploited to create biomimetic nanoassemblies capable of stabilizing and delivering growth factors. This will be tested through a literature review, the investigation of the following four specific aims, and finally summarized with conclusions and future work:

Hypothesis 1: GAG-rich polyelectrolyte complex nanoparticles will protect growth factor from heat and proteolytic degradation.

Specific Aim 1: Investigate stabilization of growth factors by polyelectrolyte complex nanoparticles made from four different combinations of polysaccharides, and compare them to each other and to aggrecan.

Hypothesis 2: A graft-on approach will produce GAG-based synthetic graft copolymers with a bottlebrush conformation of different sizes and different functionalities with respect to growth factor delivery and mechanical properties.

Specific Aim 2: Synthesize and characterize proteoglycan-mimetic graft copolymers with controllable grafting density.

Hypothesis 3: GAG-rich polyelectrolyte complex nanoparticles will protect growth factor through processing conditions for electrospinning.

Specific Aim 3: Incorporate growth factor into electrospun nanofibers through two methods, an emulsion and coaxial electrospinning.

Hypothesis 4: An ECM derived scaffold made from demineralized bone matrix without a carrier polymer can be formed through electrospinning.

Specific Aim 4: Determine processing conditions to form a nanostructured tissue engineering scaffold made from demineralized bone matrix without a carrier polymer.

Specific Aim 1 focuses on polyelectrolyte complex nanoparticles (PCNs). PCNs made from HEP and CHI have been thoroughly characterized by our lab.[44] The purpose of Specific Aim 1 is to increase the repertoire of polysaccharides to include CHI, TMC, HEP, and CS. In addition to expanding the polysaccharides used, the different PCN formulations are compared to see if any combination protects or stimulates growth factor activity more effectively than the other combinations. Aggrecan is a molecule found in cartilage that provides crucial structural support and has the ability to bind and stabilize growth factors.[39, 45] The different PCNs are also contrasted with aggrecan to evaluate how they compare to a natural nanoassembly. This study provides insights regarding how nanostructure and GAG composition of nanoparticles influence their ability to stabilize and deliver growth heparin-binding growth factors.

Specific Aim 2 uses synthetic chemistry to create a proteoglycan mimetic copolymer using natural polysaccharides. These nanoassemblies imitate both the structure and the biochemical function of proteoglycans. These graft copolymers have controllable graft density

designed to tune their structure and function to desired applications. They have been thoroughly characterized to confirm their chemical composition, physical properties, and biochemical activity.

Specific Aim 3 introduces a geometry that mimics the ECM. Electrospinning is used to create biomimetic nanofibers. Two different electrospinning methods, an emulsion and coaxial electrospinning, are explored to incorporate growth factor into nanofibers to create a bioactive scaffold. In the emulsion, an aqueous phase containing growth factor, PCNs, or growth factor bound to PCNs is mixed with a CHI-containing organic phase using Tween20 to create an emulsion. In coaxial electrospinning, two solutions are spun out of a compound needle to produce a blended fiber mat containing two phases. Phase One contains CHI and Phase Two contains growth factor, PCNs, or growth factor bound to PCNs in polyvinyl alcohol (PVA) as a carrier polymer. Two arrangements, Phase One in excess and Phase Two in excess, are created and tested for growth factor delivery to MSCs.

Specific Aim 4 surveys a variety of processing conditions to electrospin demineralized bone matrix (DBM) without the use of a carrier polymer. An appropriate solvent system is determined and effects of DBM concentration and dissolution time on fiber morphology are studied. A number of crosslinking strategies are explored in detail to stabilize DBM nanofibers. DBM nanofibers are then tested for mechanical properties and cytocompatibility to ensure suitability for tissue engineering applications.

The final chapter of this dissertation summarizes the findings from the previous chapters. This includes a brief synopsis of the specific aims, conclusions, a description of limitations, and recommendations for future work from each chapter.

REFERENCES

1. Number of all-listed procedures for discharges from short-stay hospitals, by procedure category and age: United States, 2010.

2. Daley, W. P.; Peters, S. B.; Larsen, M., Extracellular matrix dynamics in development and regenerative medicine. *Journal of Cell Science* **2008,** 121, (3), 255-264.

3. Shin, H.; Jo, S.; Mikos, A. G., Biomimetic materials for tissue engineering. *Biomaterials* **2003,** 24, (24), 4353-4364.

4. Chen, R.; Hunt, J. A., Biomimetic materials processing for tissue-engineering processes. *Journal of Materials Chemistry* **2007,** 17, (38), 3974-3979.

5. Ratner, B. D.; Bryant, S. J., Biomaterials: Where we have been and where we are going. *Annual Review of Biomedical Engineering* **2004,** 6, 41-75.

6. von der Mark, K.; Park, J.; Bauer, S.; Schmuki, P., Nanoscale engineering of biomimetic surfaces: cues from the extracellular matrix. *Cell and Tissue Research* **2010,** 339, (1), 131-153.

7. Deng, M.; Kumbar, S. G.; Nair, L. S.; Weikel, A. L.; Allcock, H. R.; Laurencin, C. T., Biomimetic Structures: Biological Implications of Dipeptide-Substituted Polyphosphazene-Polyester Blend Nanofiber Matrices for Load-Bearing Bone Regeneration. *Advanced Functional Materials* **2011,** 21, (14), 2641-2651.

8. Fernandez-Muinos, T.; Suarez-Munoz, M.; Sanmarti-Espinal, M.; Semino, C. E., Matrix Dimensions, Stiffness, and Structural Properties Modulate Spontaneous Chondrogenic Commitment of Mouse Embryonic Fibroblasts. *Tissue Engineering Part A* **2014,** 20, (7-8), 1145-1155.

9. Ross, A. M.; Lahann, J., Surface engineering the cellular microenvironment via patterning and gradients. *Journal of Polymer Science Part B-Polymer Physics* **2013,** 51, (10), 775-794.

10. Kim, S. H. K. S. H.; Turnbull, J.; Guimond, S., Extracellular matrix and cell signalling: the dynamic cooperation of integrin, proteoglycan and growth factor receptor. *Journal of Endocrinology* **2011,** 209, (2), 139-151.

11. Balasundaram, G.; Storey, D. M.; Webster, T. J., Novel nano-rough polymers for cartilage tissue engineering. *International Journal of Nanomedicine* **2014,** 9, 1845-1853.

12. Coburn, J. M.; Gibson, M.; Monagle, S.; Patterson, Z.; Elisseeff, J. H., Bioinspired nanofibers support chondrogenesis for articular cartilage repair. *Proceedings of the National Academy of Sciences of the United States of America* **2012,** 109, (25), 10012-10017.

13. Karageorgiou, V.; Kaplan, D., Porosity of 3D biomaterial scaffolds and osteogenesis. *Biomaterials* **2005,** 26, (27), 5474-5491.

14. Hunter, D. J.; Felson, D. T., Osteoarthritis. *British Medical Journal* **2006,** 332, (7542), 639-642B.

15. van den Berg, W. B., The role of cytokines and growth factors in cartilage destruction in osteoarthritis and rheumatoid arthritis. *Zeitschrift Fur Rheumatologie* **1999,** 58, (3), 136-141.

16. Gentili, C.; Cancedda, R., Cartilage and Bone Extracellular Matrix. *Current Pharmaceutical Design* **2009,** 15, (12), 1334-1348.

17. Bryant, S. J.; Arthur, J. A.; Anseth, K. S., Incorporation of tissue-specific molecules alters chondrocyte metabolism and gene expression in photocrosslinked hydrogels. *Acta Biomaterialia* **2005,** 1, (2), 243-252.

18. Bosnakovski, D.; Mizuno, M.; Kim, G.; Takagi, S.; Okumura, M.; Fujinaga, T., Chondrogenic differentiation of bovine bone marrow mesenchymal stem cells (MSCs) in different hydrogels: Influence of collagen type II extracellular matrix on MSC chondrogenesis. *Biotechnology and Bioengineering* **2006,** 93, (6), 1152-1163.

19. Uebersax, L.; Merkle, H. P.; Meinel, L., Biopolymer-Based Growth Factor Delivery for Tissue Repair: From Natural Concepts to Engineered Systems. *Tissue Engineering Part B-Reviews* **2009,** 15, (3), 263-289.

20. Renth, A. N.; Detamore, M. S., Leveraging "Raw Materials" as Building Blocks and Bioactive Signals in Regenerative Medicine. *Tissue Engineering Part B-Reviews* **2012,** 18, (5), 341-362.

21. Badrossamay, M. R.; Balachandran, K.; Capulli, A. K.; Golecki, H. M.; Agarwal, A.; Goss, J. A.; Kim, H.; Shin, K.; Parker, K. K., Engineering hybrid polymer-protein super-aligned nanofibers via rotary jet spinning. *Biomaterials* **2014,** 35, (10), 3188-3197.

22. Mathews, S.; Mathew, S. A.; Gupta, P. K.; Bhonde, R.; Totey, S., Glycosaminoglycans enhance osteoblast differentiation of bone marrow derived human mesenchymal stem cells. *Journal of Tissue Engineering and Regenerative Medicine* **2014,** 8, (2), 143-152.

23. Chen, A. K.; Delrio, F. W.; Peterson, A. W.; Chung, K.-H.; Bhadiraju, K.; Plant, A. L., Cell Spreading and Proliferation in Response to the Composition and Mechanics of Engineered Fibrillar Extracellular Matrices. *Biotechnology and Bioengineering* **2013,** 110, (10), 2731-2741.

24. Badylak, S. E., The extracellular matrix as a scaffold for tissue reconstruction. *Seminars in Cell & Developmental Biology* **2002,** 13, (5), 377-383.

25. Brun, P.; Scorzeto, M.; Vassanelli, S.; Castagliuolo, I.; Palu, G.; Ghezzo, F.; Messina, G. M. L.; Iucci, G.; Battaglia, V.; Sivolella, S.; Bagno, A.; Polzonetti, G.; Marietta, G.; Dettin, M.,

Mechanisms underlying the attachment and spreading of human osteoblasts: From transient interactions to focal adhesions on vitronectin-grafted bioactive surfaces. *Acta Biomaterialia* **2013,** 9, (4), 6105-6115.

26. Mhanna, R.; Oeztuerk, E.; Vallmajo-Martin, Q.; Millan, C.; Mueller, M.; Zenobi-Wong, M., GFOGER-Modified MMP-Sensitive Polyethylene Glycol Hydrogels Induce Chondrogenic Differentiation of Human Mesenchymal Stem Cells. *Tissue Engineering Part A* **2014,** 20, (7-8), 1165-1174.

27. Alvarez-Barreto, J. F.; Landy, B.; VanGordon, S.; Place, L.; DeAngelis, P. L.; Sikavitsas, V. I., Enhanced osteoblastic differentiation of mesenchymal stem cells seeded in RGD-functionalized PLLA scaffolds and cultured in a flow perfusion bioreactor. *Journal of Tissue Engineering and Regenerative Medicine* **2011,** 5, (6), 464-475.

28. Missirlis, D.; Spatz, J. P., Combined Effects of PEG Hydrogel Elasticity and Cell-Adhesive Coating on Fibroblast Adhesion and Persistent Migration. *Biomacromolecules* **2014,** 15, (1), 195-205.

29. Tseng, L.-L.; Ho, C.-M.; Liang, W.-Z.; Hsieh, Y.-D.; Jan, C.-R., Comparison of efficacies of different bone substitutes adhered to osteoblasts with and without extracellular matrix proteins. *Journal of Dental Sciences* **2013,** 8, (4), 399-404.

30. Babensee, J. E.; McIntire, L. V.; Mikos, A. G., Growth factor delivery for tissue engineering. *Pharmaceutical Research* **2000,** 17, (5), 497-504.

31. Worster, A. A.; Nixon, A. J.; Brower-Toland, B. D.; Williams, J., Effect of transforming growth factor beta 1 on chondrogenic differentiation of cultured equine mesenchymal stem cells. *American Journal of Veterinary Research* **2000,** 61, (9), 1003-1010.

32. Lieberman, J. R.; Daluiski, A.; Einhorn, T. A., The role of growth factors in the repair of bone - Biology and clinical applications. *Journal of Bone and Joint Surgery-American Volume* **2002,** 84A, (6), 1032-1044.

33. Lee, S.-H.; Shin, H., Matrices and scaffolds for delivery of bioactive molecules in bone and cartilage tissue engineering. *Advanced Drug Delivery Reviews* **2007,** 59, (4-5), 339-359.

34. Santo, V. E.; Gomes, M. E.; Mano, J. F.; Reis, R. L., Controlled Release Strategies for Bone, Cartilage, and Osteochondral Engineering-Part I: Recapitulation of Native Tissue Healing and Variables for the Design of Delivery Systems. *Tissue Engineering Part B-Reviews* **2013,** 19, (4), 308-326.

35. Boateng, J. S.; Matthews, K. H.; Stevens, H. N. E.; Eccleston, G. M., Wound healing dressings and drug delivery systems: A review. *Journal of Pharmaceutical Sciences* **2008,** 97, (8), 2892-2923.

36. Place, L. W.; Sekyi, M.; Kipper, M. J., Aggrecan-Mimetic, Glycosaminoglycan-Containing Nanoparticles for Growth Factor Stabilization and Delivery. *Biomacromolecules* **2014,** 15, (2), 680-689.

37. Almodovar, J.; Bacon, S.; Gogolski, J.; Kisiday, J. D.; Kipper, M. J., Polysaccharide-Based Polyelectrolyte Multi layer Surface Coatings can Enhance Mesenchymal Stem Cell Response to Adsorbed Growth Factors. *Biomacromolecules* **2010,** 11, (10), 2629-2639.

38. Macri, L.; Silverstein, D.; Clark, R. A. F., Growth factor binding to the pericellular matrix and its importance in tissue engineering. *Advanced Drug Delivery Reviews* **2007,** 59, (13), 1366-1381.

39. Boddohi, S.; Kipper, M. J., Engineering Nanoassemblies of Polysaccharides. *Advanced Materials* **2010,** 22, (28), 2998-3016.

40. Desai, T. A., Micro- and nanoscale structures for tissue engineering constructs. *Medical Engineering & Physics* **2000,** 22, (9), 595-606.

41. Suh, J. K. F.; Matthew, H. W. T., Application of chitosan-based polysaccharide biomaterials in cartilage tissue engineering: a review. *Biomaterials* **2000,** 21, (24), 2589-2598.

42. Chowdhury, S.; Thomas, V.; Dean, D.; Catledge, S. A.; Vohra, Y. K., Nanoindentation on porous bioceramic scaffolds for bone tissue engineering. *Journal of Nanoscience and Nanotechnology* **2005,** 5, (11), 1816-1820.

43. Divya, P.; Krishnan, L. K., Glycosaminoglycans restrained in a fibrin matrix improve ECM remodelling by endothelial cells grown for vascular tissue engineering. *Journal of Tissue Engineering and Regenerative Medicine* **2009,** 3, (5), 377-388.

44. Boddohi, S.; Moore, N.; Johnson, P. A.; Kipper, M. J., Polysaccharide-Based Polyelectrolyte Complex Nanoparticles from Chitosan, Heparin, and Hyaluronan. *Biomacromolecules* **2009,** 10, (6), 1402-1409.

45. Horkay, F.; Basser, P. J.; Hecht, A. M.; Geissler, E., Gel-like behavior in aggrecan assemblies. *Journal of Chemical Physics* **2008,** 128, (13).

CHAPTER 2

Engineering Biopolymers into Structures for Tissue Engineering: Harnessing Inherent Biophysical and Biochemical Properties

2.1 SUMMARY

Tissue engineering combines a scaffold with signaling molecules and cells to form a bioactive material for tissue healing. Two principle approaches are to modify a material with exogenous biochemical signals, or to use a material that inherently contains biochemical signals. This review focuses on the latter. The extracellular matrix (ECM) is comprised of a complex network of polysaccharides and proteins. These perform both biophysical and biochemical functions. This review summarizes the different components of the ECM, including glycosaminoglycans (GAGs), elastin, laminin, collagen, and growth factors. Their structure-function relationships and roles in cell signaling are described. The functions of these components are intimately linked through complex pathways, but understanding them would provide tools for designing bioactive constructs. Finally, the state of the art for engineering biopolymers to harness these innate properties is summarized.

2.2 INTRODUCTION.

The classical tissue engineering scheme combines a scaffold with signaling molecules and cells to create a bioactive construct that replaces or repairs tissue damaged by injury or disease.[1-5] Two primary strategies for accomplishing this are 1.) Modification with exogenous signaling molecules, and 2.) The use of a biopolymer that inherently contains signaling molecules. A wide range of materials including metals, synthetic and natural polymers, and ECM-derived materials have been researched to achieve this end.[5]

Cells constantly interact with their surroundings. They receive a wealth of information from the structure and chemistry of their microenvironnment.[4, 6-8] Thus it is important to design a tissue engineering scaffold that imparts information rather than merely being inert. In tissues, cells are surrounded by the extracellular matrix (ECM). The ECM is composed of polysaccharides and cytokines surrounded by a framework of structural proteins.[6, 9] Differences in ratios and geometrical arrangements of these components at the nanometer and micrometer levels are responsible for the wide variety seen in structure, topography, and physical properties of tissues.[6, 10, 11] These components act in concert to regulate cell adhesion, migration, proliferation, and differentiation.[6] Researchers can learn from the mechanisms nature uses to control cell function to engineer bioactive materials.

Both synthetic and natural polymers have been studied for tissue engineering applications. Synthetic polymers can be chemically modified to tailor many important features such as degradation kinetics and mechanical properties.[12] However, they are not recognized by cells, which may inhibit cell attachment, proliferation, and differentiation unless proteins or peptides are incorporated.[13, 14] Although synthetic polymers are described as biocompatible and biodegradable, foreign body reactions inhibit tissue integration, which is imperative for implant success.[15-18] Natural polymers are similar to the ECM, providing cell recognition. This innate cell signaling allows for cell adhesion, metabolism of the scaffold, and mitigating toxicity and chronic inflammatory response.[3, 5, 9, 19] Additionally, they inherently interact with cytokines and cell surface receptors imparting biochemical function.[9, 20] These characteristics lead to increased cell infiltration and tissue integration. A selection of natural polymers and methods for imparting signals through proteins and nanostructure using a biomimetic approach are reviewed here.

2.3 NATURAL POLYMERS

The ECM is comprised of a complex mixture of polysaccharides and proteins.[6, 9, 21-23] These molecules impart structure and function to tissues. A class of molecules called proteoglycans is a prime example. These are made up of a core protein with glycosaminoglycan (GAG) side chains.[24, 25] The composition and number of GAG side chains gives rise to functionality. GAGs are hydrophilic, providing lubricity and compressive strength to tissues. In addition to structure, these also serve a biochemical purpose. They bind to cell surface integrins and act as a reservoir for signaling molecules, controlling cell adhesion and presentation of cytokines.[6, 9, 26] The ECM contains a variety of proteins that perform structural and signaling purposes. Collagen, elastin, and laminin provide a structural framework whose geometry and composition lead to the shape and function of a tissue.[10, 27] Additionally these proteins provide ligands to cell receptors and interact with cytokines.[9, 28, 29] Cytokines such as growth factors stimulate cells to migrate, proliferate, and differentiate.[30-32] These molecules work in conjunction to dictate the properties and performance of tissues.

2.3.1 Polysaccharides. Polysaccharides are a class of biological macromolecules derived from plants, animals, and microbes.[33, 34] They can exhibit a variety of structures with several common pendant groups giving them multivalency and allowing them to participate in a vast range of biochemical and biomechanical functions.[35] Many polysaccharides behave as polyelectrolytes at physiological pH. This feature can be used to tailor nanostructures such as multilayers and nanoparticles. This review focuses on several polysaccharides derived from animal sources including the GAGs heparin (Hep), chondroitin sulfate (CS), and hyaluronan (HA), and the GAG-like polymer chitosan (Chi).

2.3.1.1 Glycosaminoglycans. GAGs are prevalent in the ECM and on the cell surface.[36, 37] These are linear polysaccharides comprised of repeating disaccharide units containing one hexuronic acid (D-glucoronic acid or L-iduronic acid) or hexose (D-galactose) and one hexosamine (D-galactosamine or D-glucosamine).[20, 35, 36, 38-40] GAGs vary in subunit composition and modification, and in geometry of the glycosidic linkage (α or β) resulting in highly complex, heterogeneous structures.[20, 38, 39] Representative chemical structures of the GAGs presented in this review are shown in Figure 2.1

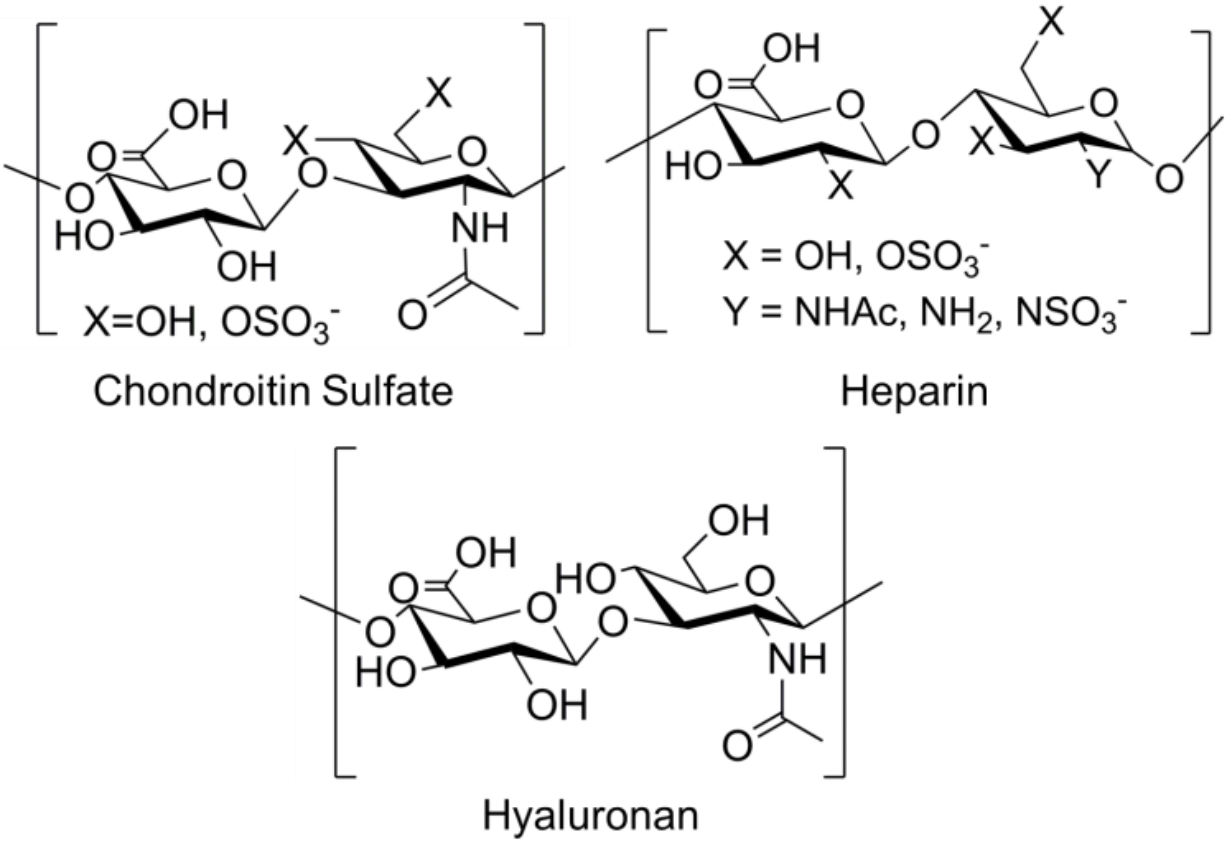

Figure 2.1. Representative chemical structures of GAGs described in this review.

CS and Hep are both sulfated, whereas HA is not; all three are negatively charged, and can have molecular weights ranging from thousands of Daltons to millions of Daltons. Biological function of GAGs is dictated by their sulfation pattern and polymer length.[38] The sulfated GAGs

are often covalently bound to a protein to form proteoglycans, which consequently derive much of their function from their GAG side chains.[3, 35, 38, 39, 41, 42] It is worth noting that the sulfated GAGs are generally much smaller than HA, and while HA does not form proteoglycans it does interact with them organizing them into complex assemblies. At physiological pH, carboxylic acid and sulfate groups are deprotonated, leading to high negative charge densities on the GAGs. When GAGs are densely packed, as is often the case in proteoglycans, regions of high anionic charge are created resulting in high osmotic pressure.[35, 39, 41] This high osmotic pressure leads to high water content, which in turn provides lubricity and compressive strength to tissues. Additionally, GAGs control the nanoscale structure and organization of the ECM by regulating collagen fibril and proteoglycan assembly.[35, 39, 43]

Due to the heterogeneity in structure, GAGs are able to interact with a wide range of proteins with varying levels of discrimination.[35, 37] They are known to bind and regulate a number of signaling molecules, including cytokines, enzymes, and adhesion proteins.[38, 42] They act as receptors, often forming growth factor-receptor complexes on the cell surface. Additionally, GAGs localize cytokines in the ECM, acting as a depot and protecting them from proteolytic degradation.[20, 44] The positioning of protein-binding motifs on a GAG determines if a protein is activated, inhibited, or sequestered in the ECM. [35, 38] Thus, GAGs regulate cellular processes such as adhesion, migration, proliferation, and differentiation. [3, 39]

2.3.1.1.1 CS. CS is an important GAG in tissues such as cartilage, the intervertebral disc, and the vitreous humor of the eye.[35, 45] CS can be sulfated at a number of different positions, giving it a high negative charge. CS is the primary GAG in the proteoglycan aggrecan shown in Figure 2.2.

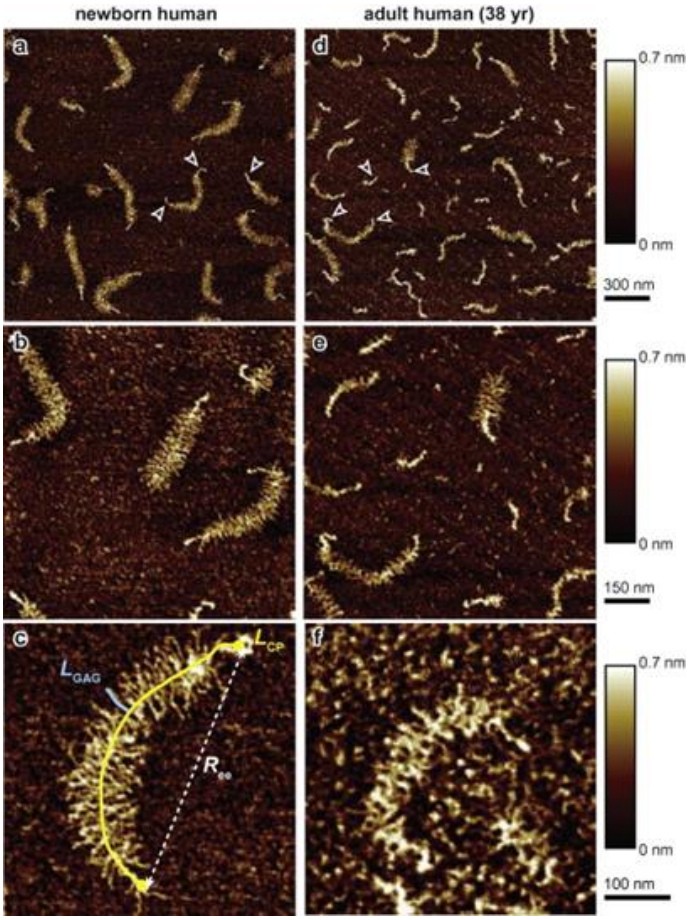

Figure 2.2. AFM images of (a, b, and c) human aggrecan from a newborn and (d, e, f) human aggrecan from a 38-year old adult. Bottlebrush structure is clearly visible. A core protein trace length, L_{cp}, end-to-end distance, R_{ee}, GAG length, L_{GAG} are shown in c. (Reprinted from Journal of Structural Biology, 181/3, H. Lee, L. Han, P.J. Roughley, A.J. Grodzinsky, C. Ortiz, Age-related nanostructural and nanomechanical changes of individual human cartilage aggrecan monomers and their glycosaminoglycan side chains, 264-273, Copyright 2013, with permission from Elsevier.)

Aggrecan is the largest proteoglycan, made up of a core protein with GAG side chains, including up to 100 densely packed (4-5 nm apart) CS chains.[35, 46-49] Strong electrostatic repulsion between the GAG chains results in a bottle brush structure. Several studies have found that aggrecan exhibits a contour length of 300–500 nm, and the individual GAG side chains range from 30–40 nm.[35, 49, 50] These aggrecan monomers bind to hyaluronan via a link protein to form a secondary bottle brush structure known as the aggrecan aggregate. Each hyaluronan molecule can have over 100 aggrecan monomers bound to it, forming an assembly with a length

ranging from 500-4000 nm.[35, 46, 51, 52] This assembly of tightly packed CS chains results in a high charge density generating substantial osmotic pressure. Thus, aggrecan is hydrophilic and retains large amounts of water, forming gel-like structures that are highly swollen in three dimensions.[48, 52, 53] This provides compressive strength with minimal deformation during dynamic loading and lubricity for near frictionless movement.[11, 37, 41, 46, 52, 54, 55]

In addition to biomechanical properties, CS also plays a role in biochemical signaling. CS has been used in biomaterials due to its ability to bind growth factors and support cell function.[39, 56-58] CS has been seen to improve wound healing and has been used for the treatment of osteoarthritis and atherosclerosis[56, 59-63] These inherent properties of CS make it an exceptional material for tissue engineering applications. CS has been used in coatings, nanofibers, nanoparticles, and hydrogels among others.

2.3.1.1.2 Hep and HS. Hep is a highly sulfated negatively charged GAG, normally found in intracellular granules of mast cells.[35, 38] It has the highest negative charge density of any known biomolecule and has primarily been used in clinical applications as an anticoagulant.[37, 38, 59] Hep was first isolated from the liver around 1920 and has been in clinical use for decades.[64] Hep is structurally similar to the GAG heparan sulfate (HS), but Hep is more highly sulfated than HS and has fewer acetylated glucosamine groups.[38] Because of its similarity and commercial availability, Hep is often used as a model for or in place of HS in experimental work.[20] HS performs many biological functions and is found on the cell surface and in the ECM.[35, 65]

The glycocalyx is a prime example of the dynamic biological roles played by HS. The glycocalyx is present on the surface of most eukaryotic cells, and is particularly important in the endothelium.[35] It is made up of a matrix of membrane-bound proteoglycans and glycoproteins, hyaluronan, and plasma proteins coating the luminal surface of blood vessels.[66-69] HS is the most

common GAG found in the glycocalyx, attributing 50-90 % of the total GAG content. The remainder is made up of CS and HA.[35, 68] Generally, HS and CS exist in a 4:1 ratio in vascular tissue, but these numbers can vary depending on stimuli and microenvironment conditions.[69] These GAGs exist primarily on three different types of proteoglycans. These include syndecans, glypicans, and perlecans, shown in Figure 2.3.

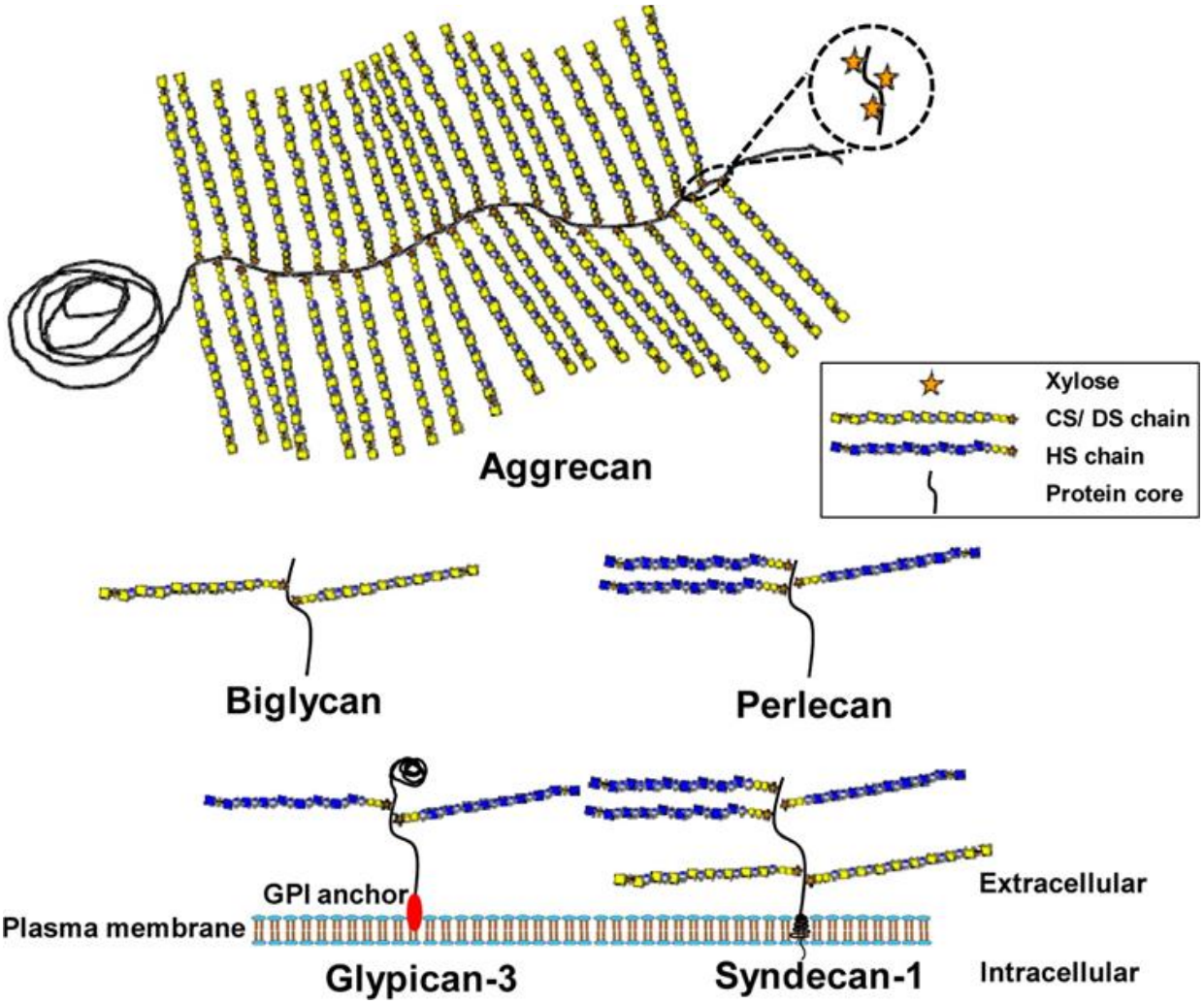

Figure 2.3. Schematic of common proteoglycans. (Reprinted from ACS Chemical Biology, 8/5, V.M. Tran, T.K.N. Nguyen, V. Sorna, D. Loganathan, B. Kuberan, Synthesis and Assessment of Glycosaminoglycan Priming Activity of Cluster-xylosides for Potential Use as Proteoglycan Mimetics, 949-957, Copyright 2013, with permission from American Chemical Society.)

Syndecans are the most common. These penetrate the cell membrane interacting with both the extracellular space and the cytoskeleton. Glypicans are similar to syndecans, but are bound only to the surface of the cell membrane. The least common of these three classes is perlecan. Perlecan carries only five GAG chains and is secreted rather than bound. Perlecan is either incorporated into the ECM where it assembles with collagen and other proteins to form basement membranes or diffuses into the blood stream. As mentioned earlier, the GAGs bound to these proteoglycans are sulfated and negatively charged under physiological conditions creating osmotic pressure and drawing in water. This leads to an extended brush-like nanostructure up to 750 nm thick, shown in Figure 2.4.[35, 67, 70, 71]

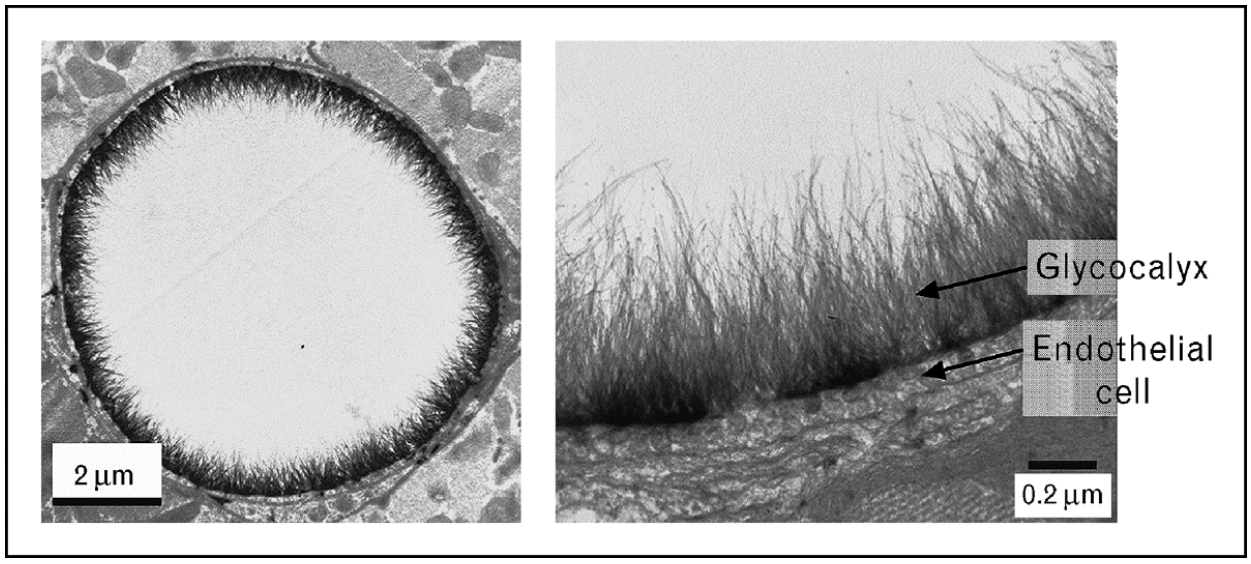

Figure 2.4. Electron microscopy of the glycocalyx in a blood vessel. (Reprinted from Current Opinion in Lipidology, 16/5, M. Nieuwdorp, M. Meuwese, H. Vink, J. Hoekstra, J. Kastelein, E. Stroes, The endothelial glycocalyx: a potential barrier between health and vascular disease, 507-511. Copyright 2005, with permission from Wolters Kluer Health.)

This structure forms a hydrophilic network that shapes the function of the endothelial glycocalyx.[66, 69, 70] This layer plays an integral role in regulating inflammation, leukocyte and platelet adhesion, mechanotransduction, and vascular permeability.[35, 66-72] The endothelial glycocalyx is lubricious, aiding in the motion of red blood cells and inhibiting platelet and

leukocyte adhesion unless perturbed by disease or injury.[35, 68, 70-72] Additionally, this surface is constantly exposed to shear stress from blood flow. Endothelial cells react to changes in shear stress, inducing alterations in cytoskeletal structure, gene expression, and production of signaling molecules. The transmembrane proteoglycan syndecan had been proposed to play an important role in shear stress transmittance.[69] This proteoglycan has a domain in the extracellular space for sensing shear and an intracellular component which interacts with actin and signaling molecules.[69] Endothelial cells are dynamic, always adapting the glycocalyx according to cues from the microenvironment through matrix turnover. The composition and geometry of the proteoglycans are highly dependent on the conditions of their local microenvironment, such as shear stress, nutrient content and concentration, and pH.[68] These features also affect vascular permeability. The glycocalyx controls exchange of nutrients, water, and signaling molecules between the endothelium and the lumen.[67, 71] In fact, this layer governs the interactions of all blood components with the blood vessel surface including plasma proteins, enzymes, growth factors, and cytokines, which are essential for homeostasis and preventing thrombosis.[35, 66, 68]

As described earlier, GAGs exhibit a wide variety of epitopes due to alterations in composition and geometry, particularly their sulfation pattern, yielding heterogeneous surfaces with various levels of protein binding promiscuity.[35, 66] The negative charge provided by the sulfate groups is of particular importance, as many proteins are cationic and bind electrostatically.[11, 54, 68, 71] Additionally, there is a class of growth factors that are stabilized through Hep/HS binding. Hep/HS also exhibit ligands to cell surface receptors that aid in signaling.[36, 54] These features make conjugation of Hep to tissue engineering scaffolds an attractive way to impart bioactivity for a variety of applications.

2.3.1.1.3 HA. HA is the only non-sulfated GAG and the only GAG that is secreted into the ECM without being bound to a protein core. It can have a molecular weight up to several million Daltons, making it much larger than the sulfated GAGs.[39] HA is widely distributed throughout many tissues, including skin, eye, connective, epithelial, endothelial, and neural tissues.[39, 56, 68, 73]

Although it is unbranched and does not form proteoglycans in the same manner as the sulfated GAGs, it does form complex networks with other macromolecules in the ECM.[54, 74-77] HA helps to shape the ECM by binding structural proteins such as collagen and fibrin as well as adhesion proteins.[54] Additionally, HA can further assemble proteoglycans into more complex structures via link proteins as in the aggrecan aggregate described earlier, or it can interact with other proteins via hydrodynamic properties.[78] HA behaves as a stiffened random coil in solution, and is able to trap 1000 times it weight in water, giving it an immense hydrated volume. This causes HA to interact with neighboring molecules, giving rise to its viscoelastic properties.[73, 77, 79] Due to its hydrophilicity, HA is imperative for the physical properties of many tissues such as lubrication in blood vessels via the glycocalyx, synovial joints, and articular cartilage.[38, 66, 73, 77, 80] It is used clinically to treat osteoarthritis. An injection directly into the joint is reported to restore lubricity and improve joint function.[56, 81, 82]

HA can be found either in the ECM or on the cell surface where it modulates signaling.[74] HA-binding proteins bind to cell surface integrins,which impact cell-cell and cell-substrate adhesion, migration, proliferation, and differentiation.[54, 56, 82] HA plays a major role in morphogenesis, development, remodeling, and wound healing.[11, 36, 38, 73, 78, 79, 82] It surrounds proliferating cells during wound healing, creates space, promotes angiogenesis, and prevents fibrosis.[11, 36, 54, 56, 78] The unique physical properties and active role in wound healing make HA

an excellent material to use in tissue engineering applications such as hydrogels, coatings, and drug delivery.

2.3.1.2 Chitosan. Chi is a naturally occurring polysaccharide derived from chitin, the primary structural component in the exoskeleton of arthropods. It is a linear polysaccharide composed of D-glucosamine and *N*-acetyl-D-glucosamine units in variable distributions and chain lengths. The N-acetyl-glucosamine groups in Chi are also found in the GAGs discussed in this review.[11, 60, 83] Chi has pendant amines along the polymer chain, giving rise to weak cationic properties and providing residues which can be modified to tailor biophysical and biochemical properties.[25, 60, 83] A variety of functional groups have been added to Chi, including acyl, alkyl, sulfate, thiol, and trimethyl groups.[60, 84-88] Our group has synthesized *N*,*N*,*N*-trimethyl chitosan (TMC) to form a strong polycation and to make a Chi derivative that is soluble at neutral pH. This modification made it possible to study the interactions of strong and weak polyelectrolytes in multilayers and to then use those multilayers to coat electrospun nanofibers for growth factor release.[89, 90] The chemical structures of Chi and TMC are displayed in Figure 2.5.

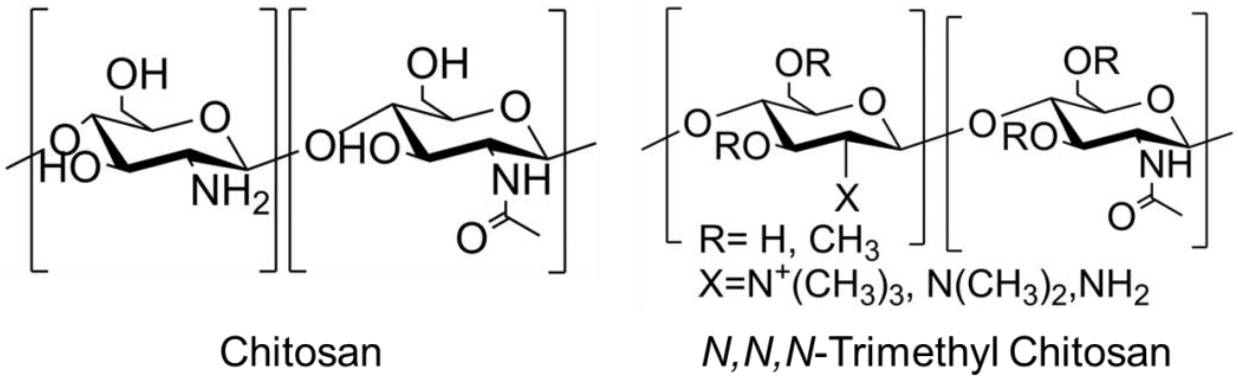

Figure 2.5. Chemical structures of Chi and TMC

Chi is known to be nontoxic, nonimmunogenic, mucoadhesive, hemostatic, biodegradable, antibacterial and antifungal.[11, 81, 83, 91, 92] Thus it has received much attention for use as a biomaterial. It has been investigated for wound healing, tissue engineering of bone,

cartilage, nerve, and intervertebral disc, as well as protein immobilization, and gene and drug delivery systems.[56, 81, 83, 91]

The cationic nature of Chi has often been used in research literature and by our group to form polyelectrolyte complexes with anionic polymers to form coatings, nanoparticles, and hydrogels with controlled biophysical and biochemical properties.[35, 81, 83, 89-91, 93-100] Many anionic polymers have been studied for this purpose, including poly(acrylic acid), alginate, pectin, DNA, collagen, and GAGs.[25, 83, 101] Due to their interaction with cell surface receptors and cytokines, complexation with GAGs is of particular interest. There have been a number of studies using nanoparticles made from Chi complexed with various GAGs for growth factor and drug delivery by intravenous, oral, and mucosal administration. Researchers have seen increased cell proliferation, vascularization, differentiation, and sustained release using these systems. [92, 99, 102-105] Due to its unique properties and ability to interact with GAGs, Chi is a promising biomaterial for tissue engineering.

2.3.2 Structural Proteins. The ECM contains a wide array of proteins that provide structure and signaling. These assemble into a hierarchical network shaping tissue function such as tensile strength in tendon and blood vessels, compressive strength in cartilage and meniscus, and the unique organizations seen in cornea and basement membranes.[10] Common proteins found in the ECM include elastin, laminin, and collagen. The most abundant is collagen, but all of these and the GAGs discussed in the previous section assemble to form tissues. [106]

2.3.2.1 Laminin and Elastin. Laminins are the most prevelant noncollagenous proteins in basement membranes. They are crucial in their architecture, and self-assemble into sheet-like structures over the cell surface. [107] Once assembled, laminins integrate with collagen and other ECM molecules into the complex two-dimensional polymer network that comprises basement

membranes.[106, 108, 109] The basement membranes are the principle scaffold underlying endothelium, and vasculature.[110]

Elastin is a largely amorphous structure that produces elastic properties in many tissues such as blood vessels. It is surrounded by a framework of a secondary component made of microfibrillar proteins.[111, 112] Additionally, this elastic structure forms a network with several different types of collagen to form blood vessel walls. Collagen in blood vessels is generally smaller and less tightly packed than in other tissues, and thus forms a meshwork with elastin resulting in more compliant properties. This allows the blood vessel to experience stresses without permanent deformation. This complex assembly is imperative for the preservation of vessel wall tensile strength and resilience. [108]

2.3.2.2 Collagen. Collagen has a unique hierarchical structure that leads to its impressive physical properties. It is composed of three alpha chains (two alpha-1 chains and one alpha-2 chain) that contain repeating motifs of several amino acids, glycine, proline, hydroxyproline, and sometimes hydroxylysine depending on collagen type, with glycine generally being repeated every third amino acid. Glycine is the smallest amino acid. Its position and small size allow the rotational freedom that leads to a helical structure. Inter-chain covalent and hydrogen bonding between these residues generates stability and rigidity in the molecule. These alpha chains form left-handed helices that further assemble into a triple helix exhibiting a diameter from 1.5-3.5 nm; these molecules then align into fibrils with diameters from 50-70 nm.[113-116] More than 20 types of collagen have been identified. They assembe into highly organized structures with different ratios of each type and interact with other macromolecules to give rise to the variety of structures and functions seen in tissues[106, 113, 115, 117] Collagen types I, II, III, V, and XI

are known for assembling into fibers roughly 150-250 nm wide in a quarter-staggered array that exhibits a banding pattern, shown in Figure 2.5. [106, 113, 115, 117]

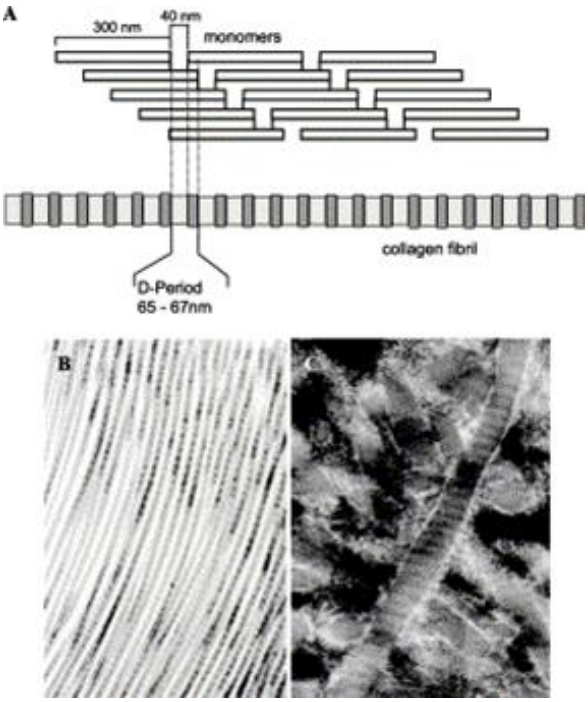

Figure 2.6. A.) Schematic of the hierarchical structure of collagen fibers. Electron microscopy of B.) Collagen type I in a tendon, C.) Collagen type II in articular cartilage (Reprinted from Advanced Drug Delivery Reviews, 55/12, K. Gelse , E. Pöschl , T. Aigner, Collagens—structure, function, and biosynthesis, 1531 – 1546, copyright 2003, with permission from Elsevier.)

Connective tissue such as bone and cartilage are primarily made up of collagen. The principle types of collagen found in these tissues are types I, II, III, V, and XI. [115, 117] Variations in ratios and geometry result in the very different mechanical properties seen in these tissues. Bone contains mostly type I and type V and the fibers are aligned in a transverse configuration. Bone is comprised of an ordered composite of collagen and minerals. The collagen fibers are arranged into concentric layers that provide a framework for the mineral phase.[106, 115, 117] Bone derives its great compressive strength from this complex architecture.

Cartilage is primarily made up of collagens type II and type XI and fibers are arranged differently depending on their location. Cartilage contains three different zones, the deep zone,

the middle zone, and the superficial zone. In the deep zone, near the bone, the collagen fibers are oriented perpendicular to the surface, much the same as collagen within the bone, to provide compressive strength. The fiber orientation gradually changes to a longitudinal alignment with higher concentrations of thinner fibers in the superficial zone.[118] Cartilage is hydrophilic and is generally in a swollen state, which puts the collagen fibers under constant tension, particularly in the superficial zone. The longitudinal orientation exhibited in this zone provides the necessary tensile strength.[106, 117 115, 118]

The cornea contains primarily type I and type V collagen. These collagens are arranged into parallel fibers with a uniform spacing of 30 nm. [106, 115] These further assemble into intricate lamellae. Crosslinking occurs within and between the collagen fibers to increase stability against proteolytic degradation and to provide desired mechanical properties. Within this framework GAGs are dispersed at intervals to reduce diffraction of light. The uniform spacing, shown in Figure 2.6., and GAGs dispersion are responsible for the transparency of the cornea.[115, 116, 119]

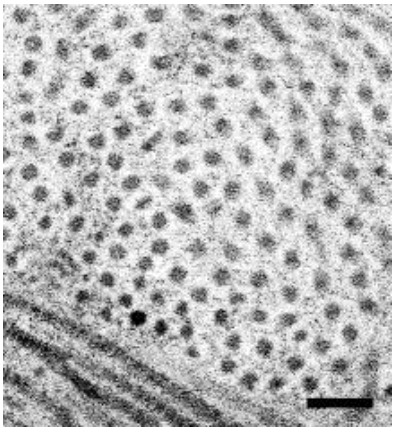

Figure 2.7. Electron microscopy of collagen fibrils in a chick cornea, scale bar 100 nm. (Reprinted from Developmental Dynamics, 237/10, A. J. Quantock, R. D. Young, Development of the corneal stroma, and the collagen–proteoglycan associations that help define its structure and function, 2607-2621, Copyright 2008, with permission from Wiley.)

Collagen is also implicated in cell signaling. Collagen provides ligands for cell receptors and organizes with other ECM macromolecules including other collagens and GAGs. Collagen

participates in the entrapment of cytokines for storage and delivery to cells. It has been demonstrated that collagen interacts with proteoglycans, mediating growth factor activity. Additionally, some types of collagen can bind to growth factors such as insulin growth factors (IGFs), transforming growth factor β (TGF-β), and bone morphogenetic protein 2 (BMP-2), which regulate cell activity.[106] Through these pathways, collagen is intimately involved in wound healing and tissue repair [106, 108, 115] Collagen has the ability to self-assemble into a wide array of structures and contains inherent cell signaling. These features make it an attractive material for tissue engineering scaffolds.

2.3.3 Growth Factors.

Growth factors are a class of cytokines that regulate cell processes. They are involved in a variety of pathways including wound healing, vascularization, and development.[32, 61, 120-124] There is a wide array of growth factors with different signaling pathways and different functions, including IGF, nerve growth factor (NGF), vascular endothelial growth factor (VEGF), platelet-derived growth factor (PDGF), members of the TGF- β superfamily, and the fibroblast growth factor (FGF) family.[125-129] Growth factors work in concert to regulate cell adhesion, migration, proliferation, and differentiation to maintain homeostasis.[32, 61, 93, 120-124, 128, 130-132] Growth factors hold much therapeutic promise. Some have been approved by the FDA and are used clinically in wound healing, and bone disease.[31] They have also been proposed for tissue engineering of nerves, bladders, blood vessels, and osteochondral defects.[133-139]

IGF and NGF have both been used in nerve tissue engineering. These growth factors promote axonal regeneration.[140, 141] IGF supports the survival and proliferation of Schwann cells. Schwann cells are essential for guiding and imparting nutrients to the regenerating axon. [140]

Additionally, both of these growth factors have been used for other tissue applications such as blood vessels, meniscus, and cartilage.[142-146]

Two primary growth factors that regulate angiogenesis are VEGF and PDGF. VEGF is significantly involved in neovascularization under both physiological and pathological conditions. VEGF is particularly mitogenic towards endothelial cells, and it stimulates endothelial progenitor cells to differentiate.[120, 121, 147] PDGF enhances the proliferation and migration of fibroblasts and smooth muscle cells.[121, 122] Through these functions, VEGF is significant in the initiation of angiogenesis, whereas PDGF is involved in the maturation of the blood vessel. Both are needed to form a fully developed blood vessel.[120]

TGF-β1 and bone morphogenetic protein 2 (BMP-2) are members of the TGF-β superfamily. TGF-β1 is implicated in cell proliferation, chondrogenesis, osteogenesis, and proteoglycan synthesis.[126, 131, 148, 149] BMP-2 is important for osteogenesis.[149, 150] Both of these proteins have been used in tissue engineering of bone and cartilage, individually and in conjunction with each other and other growth factors.[150-152]

FGF-2 is mitogenic and angiogenic.[122, 132, 150, 153] FGF-2 interacts with in complex ways with its environment; upon mechanical injury, FGF-2 is released and triggers a cascade of intracellular signaling pathways that control cell proliferation, migration, differentiation, and morphology. [61, 123, 124] Additionally, several groups have shown that FGF-2 has a biphasic effect on cell proliferation, with stimulation at low doses and inhibition at high doses.[93, 123] In angiogenesis, FGF-2 primarily stimulates endothelial cells, while eliciting little response from smooth muscle cells. Similar to VEGF, it is principally involved in the initiation of angiogenesis and is most effective when combined with other growth factors such as PDGF.[122] FGF-2 is expressed by many cell types and is involved in a number of signaling pathways. [61]

Growth factors have significant therapeutic applications, however, their potential is mitigated by their instability in solution.[93, 99] FGF-2 and TGF-β1 have a half-lives on the order of minutes when delivered by bolus injection.[154] To be clinically effective, high doses and multiple injections are required.[120, 155]

2.3.3.1 Growth Factor-GAG Interactions. In the ECM, growth factors are bound to GAGs where they are sequestered and protected from proteolytic degradation.[30, 35, 156, 157] A group of growth factors including members of the FGF family and TGF-β superfamily bind to Hep and HS, and to a lesser extent to CS in a conformation that stabilizes their three dimensional structure and preserves them from degradation.[20, 35, 61, 125, 153] This phenomenon primarily occurs through ionic interactions between the cationic amino acids such as arginine and lysine on the growth factor and the anionic sulfates and carboxylate groups on the GAG. The sulfation pattern on the GAGs and confirmation of the growth factor defines the binding affinity.[38] The heterogeneity in GAGs allows them to bind an array of growth factors and form gradients that are tissue specific.[26, 27, 38, 61, 158]

FGF activity is primarily derived from specific binding to FGF receptor tyrosine kinases (FGFRs) on the cell surface.[61] Hep/HS act as cofactors in this signaling complex. The composition of the GAG governs the FGF-FGFR specificity, modulating the cell response.[61, 124, 157] A scaffold designed with these GAG-growth factor interactions for controlled growth factor presentation would be advantageous in a variety of tissue engineering applications.

2.3.4 Tissue Engineering Scaffolds Made from Biopolymers. Materials using these natural polymers to impart cell signaling are prevalent in literature. Polysaccharides and proteins have been used to incorporate growth factors and to create a multitude of structures for tissue

engineering including multilayers, nanoparticles, and three dimensional constructs.[3, 5, 21, 27, 30, 60, 114]

Coatings are a simple method to impart biological function to a surface. Layer-by-layer assembly of polyelectrolyte multilayers (PEMs) is a method that has been used in our group. In this technique, two solutions containing oppositely charge polyelectrolytes are applied in an alternating pattern until desired thickness is reached. We have used this method to incorporate FGF-2 into a surface for delivery to mesenchymal stem cells (MSCs). We demonstrated enhanced cell proliferation with FGF-2 adsorbed to the surface over FGF-2 delivered in solution over a four day culture period.[93] Almodovar et al. created PEMs from poly(l-lysine) and hyaluronan using microfluidics to impregnated the surface with BMP-2 and BMP-7 in a spatially controlled pattern. They were able to induce osteogensis and myogenesis on the same scaffold.[159] Multilayers have been applied to flat, textured, and three dimensional surfaces to provide information to cells.[90, 160-162]

Nanoparticles are a common way to deliver growth factors to cells, either in soluble form or by incorporating them into a scaffold. Our group has created polyelectrolyte complex nanoparticles (PCNs) from various combinations of the GAGs Hep and CS, with Chi and TMC for FGF-2 stabilization and delivery. We showed sustained FGF-2 activity for 21 days, and superiority of our Hep-containg PCNs over aggrecan with respect to FGF-2 stability.[99] Parajo et al. formed PCNs using HA and chitosan to deliver a combination of VEGF and PDGF. They were able to maintain sustained release of PDGF over one week, while VEGF was completely released in the first 24 hours. This kind of design is useful for temporal control of growth factor release.[121] Nanoparticles have a vast range of applications from oral and intravenous delivery to modification of a scaffold.[102, 104, 163, 164]

Three dimensional scaffolds can be assembled through a variety of techniques including electrospinning, lyophilizing, salt and porogen leaching, and gelation. Our group has adsorbed FGF-2/PCN complexes to electrospun chitosan nanofibers and demonstrated sustained release over a period of 30 days.[100] Du et al. developed three dimensional chitosan porous hydrogel networks coated with CS using a layer-by-layer technique. FGF-2 was incorporated into the hydrogel and delivery to cells was confirmed.[165] Halili et al. fabricated a collagen type I scaffold with three different layers comprised of two foams with differing porosities and mechanical properties sandwiching an electrospun nanofiber mat. They cultured human fibrochondrocytes on these scaffolds and found that this layered scaffold had higher cell proliferation, collagen production, and GAG production than non-layered control foams after 45 days of culture.[166] Many other types of three dimensional constructs have been developed in wide range of sizes for various tissues.[34, 56, 131, 136, 158, 167-169]

As has been described, ECM is made up of a combination of polysaccharides and proteins that present innate biochemical cues, and the use of these polymers has been detailed. Another method for developing scaffolds with bioactive signals is to use unfractionated tissue ECM. This ECM would contain a mixture of polysaccharides and proteins. Some examples of these are demineralized bone matrix, decellularized adipose tissue, and small intestine submucosa.[5] Choi et al. tested porcine decellularized adipose tissue for post-processing properties and cytocompatibility with human cells. ECM components remained intact and cell exhibit adhesion and proliferation on the scaffold.[170] Small intestine submucosa and demineralized bone matrix are approved by the FDA and there are many commercial products currently in clinical use.[5] These materials are being studied for use in the trachea, bladder, soft tissue, skin, cartilage, and bone.[5, 21, 171, 172]

The materials described above primarily use physical techniques for fabrication. Proteoglycans impart crucial functionality to tissues, but isolating them from tissues is not always practical. Attempts have been made to mimic the structure and function of various proteoglycans. The Panitch group has published multiple papers on the synthesis and properties of proteoglycan-mimics using dermatan sulfate, CS, and a peptide chain, referred to as peptidoglycans.[173-180] They demonstrated that their dermatan sulfate-based peptidoglycans bind to collagen, delay fibrillogenesis, and increase mechanical properties of a collagen gel and of aligned collagen threads.[173-175] In proteoglycans, GAGs are bound only at their terminal end, thus functionalizing GAGs with a unique end-group is one approach for synthesizing a proteoglycan-mimetic. Sarkar et al. has successfully modified a terminal group on CS with vinyl monomers to these ends.[181] Tran et al. produced a library of xylosides that are able to activate multiple GAG chains to bind to a scaffold to form proteoglycan-mimcs.[182] These methods are promising for producing a synthetic proteoglycan that retains the inherent cell signaling properties of the natural material.

2.4 SUMMARY.

Natural polymers for tissue engineering have been reviewed here. The ECM is made up of an intricate network of polysaccharides and proteins. Proteoglycans found in the ECM and on the cell surface are crucial to tissue function. They are made up of a core protein and GAG side chains. The composition and geometry of the GAGs dictate the function of the proteoglycan. Aggrecan is an important proteoglycan in cartilage, the intervertebral disc, and vitreous humor of the eye. It is the largest of the proteoglycans with over 100 GAG side chains. The high density of anionic charges on aggrecan make it very hydrophilic, giving rise to the lubricity and compressive strength tissues such as cartilage. The glycocalyx coats eukaryotic cells and is

imperative to the function of the endothelium. It is made up of hyaluronan and membrane bound proteoglycans. The GAGs on the surface of the glycocalyx lead to lubricity, modulate filtration and interaction with blood components, and transduce signals across the cell membrane. Elastin, laminin, and collagen form structural components of the ECM. They align into hierarchical structures that give rise to mechanical properties of tissue. Additionally, they interact with other macromolecules in the ECM participating in cell signaling. Growth factors are signaling molecules on the cell surface and in the ECM of tissues. They are implicated in pathways that regulate homeostasis and wound healing. Growth factors have great therapeutic potential, but are unstable in solution. In the ECM, GAGs bind to growth factors protecting them from proteolytic degradation and participating in cell surface receptor-growth factor interactions. Different tissue engineering scaffolds fabricated from biopolymers are reviewed. Biomaterials using polysaccharides and proteins for growth factor delivery are the focus. Formats such as coatings, nanoparticles, three dimensional constructs, ECM-derived materials, and synthetic approaches are covered. There has been much research on these natural polymers and their functional roles in structure and cell signaling, but there are still gaps in our understanding. Harnessing the intricate relationship between growth factors and the ECM is a powerful tool for the design of bioactive tissue engineering scaffolds.

REFERENCES

1. Langer, R.; Vacanti, J. P., Tissue Engineering. *Science* **1993,** 260, (5110), 920-926.

2. Lavik, E.; Langer, R., Tissue engineering: current state and perspectives. *Applied Microbiology and Biotechnology* **2004,** 65, (1), 1-8.

3. Mano, J. F.; Silva, G. A.; Azevedo, H. S.; Malafaya, P. B.; Sousa, R. A.; Silva, S. S.; Boesel, L. F.; Oliveira, J. M.; Santos, T. C.; Marques, A. P.; Neves, N. M.; Reis, R. L., Natural origin biodegradable systems in tissue engineering and regenerative medicine: present status and some moving trends. *Journal of the Royal Society Interface* **2007,** 4, (17), 999-1030.

4. Hubbell, J. A., Biomaterials in Tissue Engineering. *Bio-Technology* **1995,** 13, (6), 565-576.

5. Renth, A. N.; Detamore, M. S., Leveraging "Raw Materials" as Building Blocks and Bioactive Signals in Regenerative Medicine. *Tissue Engineering Part B-Reviews* **2012,** 18, (5), 341-362.

6. Stevens, M. M.; George, J. H., Exploring and engineering the cell surface interface. *Science* **2005,** 310, (5751), 1135-1138.

7. Yang, S. F.; Leong, K. F.; Du, Z. H.; Chua, C. K., The design of scaffolds for use in tissue engineering. Part 1. Traditional factors. *Tissue Engineering* **2001,** 7, (6), 679-689.

8. Anderson, J. M.; Rodriguez, A.; Chang, D. T., Foreign body reaction to biomaterials. *Seminars in Immunology* **2008,** 20, (2), 86-100.

9. Chen, R.; Hunt, J. A., Biomimetic materials processing for tissue-engineering processes. *Journal of Materials Chemistry* **2007,** 17, (38), 3974-3979.

10. Gasiorowski, J. Z.; Murphy, C. J.; Nealey, P. F., Biophysical Cues and Cell Behavior: The Big Impact of Little Things. *Annual Review of Biomedical Engineering, Vol 15* **2013,** 15, 155-176.

11. Thiele, J.; Ma, Y.; Bruekers, S. M. C.; Ma, S.; Huck, W. T. S., 25th Anniversary Article: Designer Hydrogels for Cell Cultures: A Materials Selection Guide. *Advanced Materials* **2014,** 26, (1), 125-148.

12. Gunatillake, P. A.; Adhikari, R., Biodegradable synthetic polymers for tissue engineering. *Eur. Cells Mater.* **2003,** 5, 1-16.

13. Henderson, L. A.; Kipper, M. J.; Chiang, M. Y. M., Beyond Trial & Error: Tools to Advance the Engineering of Biomaterials. In *Polymers for Biomedical Applications*, Mahapatro, A.; Kulshrestha, A. S., Eds. ACS: Washington, D.C., 2008; Vol. 977, pp 118-152.

14. Yim, E. K. F.; Pang, S. W.; Leong, K. W., Synthetic nanostructures inducing differentiation of human mesenchymal stem cells into neuronal lineage. *Exp. Cell Res.* **2007,** 313, (9), 1820-1829.

15. Marotta, J. S.; Widenhouse, C. W.; Habal, M. B.; Goldberg, E. P., Silicone gel breast implant failure and frequency of additional surgeries: Analysis of 35 studies reporting examination of more than 8000 explants. *J. Biomed. Mater. Res.* **1999,** 48, (3), 354-364.

16. Tullberg, T., Failure of a Carbon Fiber Implant: A Case Report. *Spine* **1998,** 23, (16), 1804-1806.

17. van der Giessen, W. J.; Lincoff, A. M.; Schwartz, R. S.; van Beusekom, H. M. M.; Serruys, P. W.; Holmes, D. R.; Ellis, S. G.; Topol, E. J., Marked Inflammatory Sequelae to Implantation of Biodegradable and Nonbiodegradable Polymers in Porcine Coronary Arteries. *Circulation* **1996,** 94, (7), 1690-1697.

18. Leszczak, V.; Smith, B. S.; Popat, K. C., Hemocompatibility of polymeric nanostructured surfaces. *J. Biomater. Sci.-Polym. Ed.* **2013,** 24, (13), 1529-1548.

19. Nair, L. S.; Laurencin, C. T., Biodegradable polymers as biomaterials. *Progress in Polymer Science* **2007,** 32, (8-9), 762-798.

20. Mulloy, B.; Rider, C. C., Cytokines and proteoglycans: an introductory overview. *Biochemical Society Transactions* **2006,** 34, 409-413.

21. Badylak, S. E., The extracellular matrix as a scaffold for tissue reconstruction. *Seminars in Cell & Developmental Biology* **2002,** 13, (5), 377-383.

22. Daley, W. P.; Peters, S. B.; Larsen, M., Extracellular matrix dynamics in development and regenerative medicine. *Journal of Cell Science* **2008,** 121, (3), 255-264.

23. Gentili, C.; Cancedda, R., Cartilage and Bone Extracellular Matrix. *Current Pharmaceutical Design* **2009,** 15, (12), 1334-1348.

24. Schaefer, L.; Schaefer, R. M., Proteoglycans: from structural compounds to signaling molecules. *Cell and Tissue Research* **2010,** 339, (1), 237-246.

25. Suh, J. K. F.; Matthew, H. W. T., Application of chitosan-based polysaccharide biomaterials in cartilage tissue engineering: a review. *Biomaterials* **2000,** 21, (24), 2589-2598.

26. Cattaruzza, S.; Perris, R., Approaching the Proteoglycome: Molecular interactions of proteoglycans and their functional output. *Macromolecular Bioscience* **2006,** 6, (8), 667-680.

27. von der Mark, K.; Park, J.; Bauer, S.; Schmuki, P., Nanoscale engineering of biomimetic surfaces: cues from the extracellular matrix. *Cell and Tissue Research* **2010,** 339, (1), 131-153.

28. Garcia, A. J., Interfaces to control cell-biomaterial adhesive interactions. *Polymers for Regenerative Medicine* **2006**, 171-190.

29. Shin, H.; Jo, S.; Mikos, A. G., Biomimetic materials for tissue engineering. *Biomaterials* **2003,** 24, (24), 4353-4364.

30. Uebersax, L.; Merkle, H. P.; Meinel, L., Biopolymer-Based Growth Factor Delivery for Tissue Repair: From Natural Concepts to Engineered Systems. *Tissue Engineering Part B-Reviews* **2009,** 15, (3), 263-289.

31. Chen, R. R.; Mooney, D. J., Polymeric growth factor delivery strategies for tissue engineering. *Pharm. Res.* **2003,** 20, (8), 1103-1112.

32. Babensee, J. E.; McIntire, L. V.; Mikos, A. G., Growth factor delivery for tissue engineering. *Pharmaceutical Research* **2000,** 17, (5), 497-504.

33. Malafaya, P. B.; Silva, G. A.; Reis, R. L., Natural-origin polymers as carriers and scaffolds for biomolecules and cell delivery in tissue engineering applications. *Advanced Drug Delivery Reviews* **2007,** 59, (4-5), 207-233.

34. Lee, K. Y.; Jeong, L.; Kang, Y. O.; Lee, S. J.; Park, W. H., Electrospinning of polysaccharides for regenerative medicine. *Advanced Drug Delivery Reviews* **2009,** 61, (12), 1020-1032.

35. Boddohi, S.; Kipper, M. J., Engineering Nanoassemblies of Polysaccharides. *Advanced Materials* **2010,** 22, (28), 2998-3016.

36. Senni, K.; Pereira, J.; Gueniche, F.; Delbarre-Ladrat, C.; Sinquin, C.; Ratiskol, J.; Godeau, G.; Fischer, A.-M.; Helley, D.; Colliec-Jouault, S., Marine Polysaccharides: A Source of Bioactive Molecules for Cell Therapy and Tissue Engineering. *Marine Drugs* **2011,** 9, (9), 1664-1681.

37. Sasisekharan, R.; Raman, R.; Prabhakar, V., Glycomics approach to structure-function relationships of glycosaminoglycans. In *Annual Review of Biomedical Engineering*, 2006; Vol. 8, pp 181-231.

38. Gandhi, N. S.; Mancera, R. L., The Structure of Glycosaminoglycans and their Interactions with Proteins. *Chemical Biology & Drug Design* **2008,** 72, (6), 455-482.

39. Salbach, J.; Rachner, T. D.; Rauner, M.; Hempel, U.; Anderegg, U.; Franz, S.; Simon, J.-C.; Hofbauer, L. C., Regenerative potential of glycosaminoglycans for skin and bone. *Journal of Molecular Medicine-Jmm* **2012,** 90, (6), 625-635.

40. Bacakova, L.; Novotna, K.; Parizek, M., Polysaccharides as Cell Carriers for Tissue Engineering: the Use of Cellulose in Vascular Wall Reconstruction. *Physiological Research* **2014,** 63, S29-S47.

41. Yanagishita, M., Function of Proteoglycans in the Extracellular Matrix. *Acta Pathologica Japonica* **1993,** 43, (6), 283-293.

42. Weyers, A.; Linhardt, R. J., Neoproteoglycans in tissue engineering. *Febs Journal* **2013,** 280, (10), 2511-2522.

43. Scott, R. A.; Panitch, A., Glycosaminoglycans in biomedicine. *Wiley Interdisciplinary Reviews-Nanomedicine and Nanobiotechnology* **2013,** 5, (4), 388-398.

44. Zeyland, J.; Lipinski, D.; Juzwa, W.; Plawski, A.; Slomski, R., Structure and application of select glycosaminoglycans. *Medycyna Weterynaryjna* **2006,** 62, (2), 139-144.

45. Roughley, P. J.; Lee, E. R., Cartilage Proteoglycans - Structure and Potential Functions. *Microscopy Research and Technique* **1994,** 28, (5), 385-397.

46. Chandran, P. L.; Horkay, F., Aggrecan, an unusual polyelectrolyte: Review of solution behavior and physiological implications. *Acta Biomaterialia* **2012,** 8, (1), 3-12.

47. Dean, D.; Han, L.; Grodzinsky, A. J.; Ortiz, C., Compressive nanomechanics of opposing aggrecan macromolecules. *Journal of Biomechanics* **2006,** 39, (14), 2555-2565.

48. Kiani, C.; Chen, L.; Wu, Y. J.; Yee, A. J.; Yang, B. B., Structure and function of aggrecan. *Cell Research* **2002,** 12, (1), 19-32.

49. Ng, L.; Grodzinsky, A. J.; Patwari, P.; Sandy, J.; Plaas, A.; Ortiz, C., Individual cartilage aggrecan macromolecules and their constituent glycosaminoglycans visualized via atomic force microscopy. *Journal of Structural Biology* **2003,** 143, (3), 242-257.

50. Papagiannopoulos, A.; Waigh, T. A.; Hardingham, T.; Heinrich, M., Solution structure and dynamics of cartilage aggrecan. *Biomacromolecules* **2006,** 7, (7), 2162-2172.

51. Dudhia, J., Aggrecan, aging and assembly in articular cartilage. *Cellular and Molecular Life Sciences* **2005,** 62, (19-20), 2241-2256.

52. Horkay, F.; Basser, P. J.; Hecht, A. M.; Geissler, E., Gel-like behavior in aggrecan assemblies. *Journal of Chemical Physics* **2008,** 128, (13).

53. Heinegard, D., Proteoglycans and more - from molecules to biology. *International Journal of Experimental Pathology* **2009,** 90, (6), 575-586.

54. Baldwin, A. D.; Kiick, K. L., Polysaccharide-Modified Synthetic Polymeric Biomaterials. *Biopolymers* **2010,** 94, (1), 128-140.

55. Han, L.; Grodzinsky, A. J.; Ortiz, C., Nanomechanics of the Cartilage Extracellular Matrix. In *Annual Review of Materials Research, Vol 41*, Clarke, D. R.; Fratzl, P., Eds. Annual Reviews: Palo Alto, 2011; Vol. 41, pp 133-168.

56. Li, Y.; Rodrigues, J.; Tomas, H., Injectable and biodegradable hydrogels: gelation, biodegradation and biomedical applications. *Chemical Society Reviews* **2012,** 41, (6), 2193-2221.

57. Miller, R. E.; Grodzinsky, A. J.; Cummings, K.; Plaas, A. H. K.; Cole, A. A.; Lee, R. T.; Patwari, P., Intraarticular Injection of Heparin-Binding Insulin-like Growth Factor 1 Sustains Delivery of Insulin-like Growth Factor 1 to Cartilage Through Binding to Chondroitin Sulfate. *Arthritis and Rheumatism* **2010,** 62, (12), 3686-3694.

58. Thelin, M. A.; Bartolini, B.; Axelsson, J.; Gustafsson, R.; Tykesson, E.; Pera, E.; Oldberg, A.; Maccarana, M.; Malmstrom, A., Biological functions of iduronic acid in chondroitin/dermatan sulfate. *Febs Journal* **2013,** 280, (10), 2431-2446.

59. Volpi, N., Therapeutic applications of glycosaminoglycans. *Current Medicinal Chemistry* **2006,** 13, (15), 1799-1810.

60. Balakrishnan, B.; Banerjee, R., Biopolymer-Based Hydrogels for Cartilage Tissue Engineering. *Chemical Reviews* **2011,** 111, (8), 4453-4474.

61. Asada, M.; Shinomiya, M.; Suzuki, M.; Honda, E.; Sugimoto, R.; Ikekita, M.; Imamura, T., Glycosaminoglycan affinity of the complete fibroblast growth factor family. *Biochimica Et Biophysica Acta-General Subjects* **2009,** 1790, (1), 40-48.

62. Zou, X. H.; Foong, W. C.; Cao, T.; Bay, B. H.; Ouyang, H. W.; Yip, G. W., Chondroitin sulfate in palatal wound healing. *Journal of Dental Research* **2004,** 83, (11), 880-885.

63. Kosir, M. A.; Quinn, C. C. V.; Wang, W. L.; Tromp, G., Matrix glycosaminoglycans in the growth phase of fibroblasts: More of the story in wound healing. *Journal of Surgical Research* **2000,** 92, (1), 45-52.

64. Wardrop, D.; Keeling, D., The story of the discovery of heparin and warfarin. *British Journal of Haematology* **2008,** 141, (6), 757-763.

65. Sasisekharan, R.; Venkataraman, G., Heparin and heparan sulfate: biosynthesis, structure and function. *Current Opinion in Chemical Biology* **2000,** 4, (6), 626-631.

66. Reitsma, S.; Slaaf, D. W.; Vink, H.; van Zandvoort, M. A. M. J.; Egbrink, M. G. A. o., The endothelial glycocalyx: composition, functions, and visualization. *Pflugers Archiv-European Journal of Physiology* **2007,** 454, (3), 345-359.

67. Vink, H.; Duling, B. R., Identification of distinct luminal domains for macromolecules, erythrocytes, and leukocytes within mammalian capillaries. *Circulation Research* **1996,** 79, (3), 581-589.

68. Weinbaum, S.; Tarbell, J. M.; Damiano, E. R., The structure and function of the endothelial glycocalyx layer. *Annual Review of Biomedical Engineering* **2007,** 9, 121-167.

69. Florian, J. A.; Kosky, J. R.; Ainslie, K.; Pang, Z. Y.; Dull, R. O.; Tarbell, J. M., Heparan sulfate proteoglycan is a mechanosensor on endothelial cells. *Circulation Research* **2003,** 93, (10), E136-E142.

70. Becker, B. F.; Chappell, D.; Bruegger, D.; Annecke, T.; Jacob, M., Therapeutic strategies targeting the endothelial glycocalyx: acute deficits, but great potential. *Cardiovascular Research* **2010,** 87, (2), 300-310.

71. Tarbell, J. M.; Pahakis, M. Y., Mechanotransduction and the glycocalyx. *Journal of Internal Medicine* **2006,** 259, (4), 339-350.

72. Constantinescu, A. A.; Vink, H.; Spaan, J. A. E., Endothelial cell glycocalyx modulates immobilization of leukocytes at the endothelial surface. *Arteriosclerosis Thrombosis and Vascular Biology* **2003,** 23, (9), 1541-1547.

73. Bastow, E. R.; Byers, S.; Golub, S. B.; Clarkin, C. E.; Pitsillides, A. A.; Fosang, A. J., Hyaluronan synthesis and degradation in cartilage and bone. *Cellular and Molecular Life Sciences* **2008,** 65, (3), 395-413.

74. Murano, E.; Perin, D.; Khan, R.; Bergamin, M., Hyaluronan: From Biomimetic to Industrial Business Strategy. *Natural Product Communications* **2011,** 6, (4), 555-572.

75. Hargittai, I.; Hargittai, M., Molecular structure of hyaluronan: an introduction. *Structural Chemistry* **2008,** 19, (5), 697-717.

76. Chen, W. Y. J.; Abatangelo, G., Functions of hyaluronan in wound repair. *Wound Repair and Regeneration* **1999,** 7, (2), 79-89.

77. Anderegg, U.; Simon, J. C.; Averbeck, M., More than just a filler - the role of hyaluronan for skin homeostasis. *Experimental Dermatology* **2014,** 23, (5), 295-303.

78. Rooney, P.; Kumar, S., Inverse Relationship Between Hyaluronan and Collagens in Development and Angiogenesis. *Differentiation* **1993,** 54, (1), 1-9.

79. Olczyk, P.; Komosinska-Vassev, K.; Winsz-Szczotka, K.; Kuznik-Trocha, K.; Olczyk, K., Hyaluronan: Structure, metabolism, functions, and role in wound healing. *Postepy Higieny I Medycyny Doswiadczalnej* **2008,** 62, 651-659.

80. Reitinger, S.; Lepperdinger, G., Hyaluronan, a Ready Choice to Fuel Regeneration: A Mini-Review. *Gerontology* **2013,** 59, (1), 71-76.

81. Muzzarelli, R. A. A.; Greco, F.; Busilacchi, A.; Sollazzo, V.; Gigante, A., Chitosan, hyaluronan and chondroitin sulfate in tissue engineering for cartilage regeneration: A review. *Carbohydrate Polymers* **2012,** 89, (3), 723-739.

82. Itano, N.; Kimata, K., Hyaluronan synthase: New directions for hyaluronan research. *Trends in Glycoscience and Glycotechnology* **1998,** 10, (51), 23-38.

83. Hein, S.; Wang, K.; Stevens, W. F.; Kjems, J., Chitosan composites for biomedical applications: status, challenges and perspectives. *Materials Science and Technology* **2008,** 24, (9), 1053-1061.

84. Ho, Y. C.; Wu, S. J.; Mi, F. L.; Chiu, Y. L.; Yu, S. H.; Panda, N.; Sung, H. W., Thiol-Modified Chitosan Sulfate Nanoparticles for Protection and Release of Basic Fibroblast Growth Factor. *Bioconjugate Chemistry* **2010,** 21, (1), 28-38.

85. Schmitz, T.; Grabovac, E.; Palmberger, T. E.; Hoffer, M. H.; Bemkop-Schnurch, A., Synthesis and characterization of a chitosan-N-acetyl cysteine conjugate. *International Journal of Pharmaceutics* **2008,** 347, (1-2), 79-85.

86. Weltrowski, A.; Almeida, M. L. D.; Peschel, D.; Zhang, K.; Fischer, S.; Groth, T., Mitogenic Activity of Sulfated Chitosan and Cellulose Derivatives is Related to Protection of FGF-2 from Proteolytic Cleavage. *Macromolecular Bioscience* **2012,** 12, (6), 740-750.

87. Martins, A. F.; Pereira, A. G. B.; Fajardo, A. R.; Rubira, A. F.; Muniz, E. C., Characterization of polyelectrolytes complexes based on *N*,*N*,*N*-trimethyl chitosan/heparin prepared at different pH conditions. *Carbohydrate Polymers* **2011,** 86, (3), 1266-1272.

88. de Britto, D.; Assis, O. B. G., A novel method for obtaining a quaternary salt of chitosan. *Carbohydrate Polymers* **2007,** 69, (2), 305-310.

89. Almodovar, J.; Place, L. W.; Gogolski, J.; Erickson, K.; Kipper, M. J., Layer-by-Layer Assembly of Polysaccharide-Based Polyelectrolyte Multilayers: A Spectroscopic Study of Hydrophilicity, Composition, and Ion Pairing. *Biomacromolecules* **2011,** 12, (7), 2755-2765.

90. Almodovar, J.; Kipper, M. J., Coating Electrospun Chitosan Nanofibers with Polyelectrolyte Multilayers Using the Polysaccharides Heparin and N,N,N-Trimethyl Chitosan. *Macromolecular Bioscience* **2011,** 11, (1), 72-76.

91. Fajardo, A. R.; Lopes, L. C.; Valente, A. J. M.; Rubira, A. F.; Muniz, E. C., Effect of stoichiometry and pH on the structure and properties of Chitosan/Chondroitin sulfate complexes. *Colloid and Polymer Science* **2011,** 289, (15-16), 1739-1748.

92. Liu, Z. G.; Jiao, Y. P.; Liu, F. N.; Zhang, Z. Y., Heparin/chitosan nanoparticle carriers prepared by polyelectrolyte complexation. *Journal of Biomedical Materials Research Part A* **2007,** 83A, (3), 806-812.

93. Almodovar, J.; Bacon, S.; Gogolski, J.; Kisiday, J. D.; Kipper, M. J., Polysaccharide-Based Polyelectrolyte Multi layer Surface Coatings can Enhance Mesenchymal Stem Cell Response to Adsorbed Growth Factors. *Biomacromolecules* **2010,** 11, (10), 2629-2639.

94. Almodovar, J.; Mower, J.; Banerjee, A.; Sarkar, A. K.; Ehrhart, N. P.; Kipper, M. J., Chitosan-heparin polyelectrolyte multilayers on cortical bone: Periosteum-mimetic, cytophilic, antibacterial coatings. *Biotechnology and Bioengineering* **2013,** 110, (2), 609-618.

95. Boddohi, S.; Killingsworth, C. E.; Kipper, M. J., Polyelectrolyte multilayer assembly as a function of pH and ionic strength using the polysaccharides chitosan and heparin. *Biomacromolecules* **2008,** 9, (7), 2021-2028.

96. Boddohi, S.; Moore, N.; Johnson, P. A.; Kipper, M. J., Polysaccharide-Based Polyelectrolyte Complex Nanoparticles from Chitosan, Heparin, and Hyaluronan. *Biomacromolecules* **2009,** 10, (6), 1402-1409.

97. Boddohi, S.; Almodovar, J.; Zhang, H.; Johnson, P. A.; Kipper, M. J., Layer-by-layer assembly of polysaccharide-based nanostructured surfaces containing polyelectrolyte complex nanoparticles. *Colloids and Surfaces B-Biointerfaces* **2010,** 77, (1), 60-68.

98. Kipper, M. J.; Boddohi, S.; Yonemura, S. S., Polysaccharides with tailored nanostructures for biomedical applications. *Abstracts of Papers of the American Chemical Society* **2009,** 237.

99. Place, L. W.; Sekyi, M.; Kipper, M. J., Aggrecan-Mimetic, Glycosaminoglycan-Containing Nanoparticles for Growth Factor Stabilization and Delivery. *Biomacromolecules* **2014,** 15, (2), 680-689.

100. Volpato, F. Z.; Almodovar, J.; Erickson, K.; Popat, K. C.; Migliaresi, C.; Kipper, M. J., Preservation of FGF-2 bioactivity using heparin-based nanoparticles, and their delivery from electrospun chitosan fibers. *Acta Biomaterialia* **2012,** 8, (4), 1551-1559.

101. Grenha, A., Chitosan nanoparticles: a survey of preparation methods. *Journal of Drug Targeting* **2012,** 20, (4), 291-300.

102. Tan, Q.; Tang, H.; Hu, J. G.; Hu, Y. R.; Zhou, X. M.; Tao, Y. M.; Wu, Z. S., Controlled release of chitosan/heparin nanoparticle-delivered VEGF enhances regeneration of decellularized tissue-engineered scaffolds. *International Journal of Nanomedicine* **2011,** 6, 929-942.

103. Santo, V. E.; Gomes, M. E.; Mano, J. F.; Reis, R. L., Chitosan-chondroitin sulphate nanoparticles for controlled delivery of platelet lysates in bone regenerative medicine. *Journal of Tissue Engineering and Regenerative Medicine* **2012,** 6, s47-s59.

104. Chen, M. C.; Wong, H. S.; Lin, K. J.; Chen, H. L.; Wey, S. P.; Sonaje, K.; Lin, Y. H.; Chu, C. Y.; Sung, H. W., The characteristics, biodistribution and bioavailability of a chitosan-based nanoparticulate system for the oral delivery of heparin. *Biomaterials* **2009,** 30, (34), 6629-6637.

105. Paliwal, R.; Paliwal, S. R.; Agrawal, G. P.; Vyas, S. P., Chitosan nanoconstructs for improved oral delivery of low molecular weight heparin: In vitro and in vivo evaluation. *International Journal of Pharmaceutics* **2012,** 422, (1-2), 179-184.

106. Gelse, K.; Poschl, E.; Aigner, T., Collagens - structure, function, and biosynthesis. *Advanced Drug Delivery Reviews* **2003,** 55, (12), 1531-1546.

107. Torricelli, A. A. M.; Singh, V.; Santhiago, M. R.; Wilson, S. E., The Corneal Epithelial Basement Membrane: Structure, Function, and Disease. *Investigative Ophthalmology & Visual Science* **2013,** 54, (9), 6390-6400.

108. Plenz, G. A. M.; Deng, M. C.; Robenek, H.; Volker, W., Vascular collagens: spotlight on the role of type VIII collagen in atherogenesis. *Atherosclerosis* **2003,** 166, (1), 1-11.

109. Aumailley, M.; Gayraud, B., Structure and biological activity of the extracellular matrix. *Journal of Molecular Medicine-Jmm* **1998,** 76, (3-4), 253-265.

110. Yousif, L. F.; Di Russo, J.; Sorokin, L., Laminin isoforms in endothelial and perivascular basement membranes. *Cell Adhesion & Migration* **2013,** 7, (1), 101-110.

111. Green, E. M.; Mansfield, J. C.; Bell, J. S.; Winlove, C. P., The structure and micromechanics of elastic tissue. *Interface Focus* **2014,** 4, (2).

112. Rosenbloom, J.; Abrams, W. R.; Mecham, R., Extracellular-Matrix .4. The Elastic Fiber. *Faseb Journal* **1993,** 7, (13), 1208-1218.

113. Brodsky, B.; Ramshaw, J. A. M., The collagen triple-helix structure. *Matrix Biology* **1997,** 15, (8-9), 545-554.

114. Walters, B. D.; Stegemann, J. P., Strategies for directing the structure and function of three-dimensional collagen biomaterials across length scales. *Acta Biomaterialia* **2014,** 10, (4), 1488-1501.

115. Cen, L.; Liu, W.; Cui, L.; Zhang, W.; Cao, Y., Collagen tissue engineering: Development of novel biomaterials and applications. *Pediatric Research* **2008,** 63, (5), 492-496.

116. Ihanamaki, T.; Pelliniemi, L. J.; Vuorio, E., Collagens and collagen-related matrix components in the human and mouse eye. *Progress in Retinal and Eye Research* **2004,** 23, (4), 403-434.

117. Balasubramanian, P.; Prabhakaran, M. P.; Sireesha, M.; Ramakrishna, S., Collagen in Human Tissues: Structure, Function, and Biomedical Implications from a Tissue Engineering Perspective. *Polymer Composites - Polyolefin Fractionation - Polymeric Peptidomimetics - Collagens* **2013,** 251, 173-206.

118. Muir, H., The Chondrocyte, Architect of Cartilage - Biomechanics, Structure, Function and Molecular-Biology of Cartilage Matrix Macromolecules. *Bioessays* **1995,** 17, (12), 1039-1048.

119. Quantock, A. J.; Young, R. D., Development of the Corneal Stroma, and the Collagen-Proteoglycan Associations That Help Define Its Structure and Function. *Developmental Dynamics* **2008,** 237, (10), 2607-2621.

120. Richardson, T. P.; Peters, M. C.; Ennett, A. B.; Mooney, D. J., Polymeric system for dual growth factor delivery. *Nature Biotechnology* **2001,** 19, (11), 1029-1034.

121. Parajo, Y.; d'Angelo, I.; Welle, A.; Garcia-Fuentes, M.; Alonso, M. J., Hyaluronic acid/Chitosan nanoparticles as delivery vehicles for VEGF and PDGF-BB. *Drug Delivery* **2010,** 17, (8), 596-604.

122. d'Angelo, I.; Garcia-Fuentes, M.; Parajo, Y.; Welle, A.; Vantus, T.; Horvath, A.; Bokonyi, G.; Keri, G.; Alonso, M. J., Nanoparticles Based on PLGA:Poloxamer Blends for the Delivery of Proangiogenic Growth Factors. *Molecular Pharmaceutics* **2010,** 7, (5), 1724-1733.

123. De Luca, F.; Baron, J., Control of bone growth by fibroblast growth factors. *Trends in Endocrinology and Metabolism* **1999,** 10, (2), 61-65.

124. Eswarakumar, V. P.; Lax, I.; Schlessinger, J., Cellular signaling by fibroblast growth factor receptors. *Cytokine & Growth Factor Reviews* **2005,** 16, (2), 139-149.

125. Princz, M. A.; Sheardown, H., Heparin-modified dendrimer cross-linked collagen matrices for the delivery of basic fibroblast growth factor (FGF-2). *J. Biomater. Sci., Polym. Ed.* **2008,** 19, (9), 1201-1218.

126. Worster, A. A.; Nixon, A. J.; Brower-Toland, B. D.; Williams, J., Effect of transforming growth factor beta 1 on chondrogenic differentiation of cultured equine mesenchymal stem cells. *American Journal of Veterinary Research* **2000,** 61, (9), 1003-1010.

127. Lieberman, J. R.; Daluiski, A.; Einhorn, T. A., The role of growth factors in the repair of bone - Biology and clinical applications. *Journal of Bone and Joint Surgery-American Volume* **2002,** 84A, (6), 1032-1044.

128. Lee, S.-H.; Shin, H., Matrices and scaffolds for delivery of bioactive molecules in bone and cartilage tissue engineering. *Advanced Drug Delivery Reviews* **2007,** 59, (4-5), 339-359.

129. Santo, V. E.; Gomes, M. E.; Mano, J. F.; Reis, R. L., Controlled Release Strategies for Bone, Cartilage, and Osteochondral Engineering-Part I: Recapitulation of Native Tissue Healing and Variables for the Design of Delivery Systems. *Tissue Engineering Part B-Reviews* **2013,** 19, (4), 308-326.

130. Boateng, J. S.; Matthews, K. H.; Stevens, H. N. E.; Eccleston, G. M., Wound healing dressings and drug delivery systems: A review. *Journal of Pharmaceutical Sciences* **2008,** 97, (8), 2892-2923.

131. Madry, H.; Rey-Rico, A.; Venkatesan, J. K.; Johnstone, B.; Cucchiarini, M., Transforming Growth Factor Beta- Releasing Scaffolds for Cartilage Tissue Engineering. *Tissue Engineering Part B-Reviews* **2014,** 20, (2), 106-125.

132. Li, J. T.; Pei, M., Optimization of an In Vitro Three-Dimensional Microenvironment to Reprogram Synovium-Derived Stem Cells for Cartilage Tissue Engineering. *Tissue Engineering Part A* **2011,** 17, (5-6), 703-712.

133. Gu, X. S.; Ding, F.; Yang, Y. M.; Liu, J., Construction of tissue engineered nerve grafts and their application in peripheral nerve regeneration. *Prog. Neurobiol.* **2011,** 93, (2), 204-230.

134. Ohta, M.; Suzuki, Y.; Chou, H.; Ishikawa, N.; Suzuki, S.; Tanihara, M.; Mizushima, Y.; Dezawa, M.; Ide, C., Novel heparin/alginate gel combined with basic fibroblast growth factor promotes nerve regeneration in rat sciatic nerve. *J. Biomed. Mater. Res., Part A* **2004,** 71A, (4), 661-668.

135. Wang, S. G.; Cai, Q.; Hou, J. W.; Bei, J. Z.; Zhang, T.; Yang, J.; Wan, Y. Q., Acceleration effect of basic fibroblast growth factor on the regeneration of peripheral nerve through a 15-mm gap. *J. Biomed. Mater. Res., Part A* **2003,** 66A, (3), 522-531.

136. Chen, W.; Shi, C. Y.; Yi, S. H.; Chen, B.; Zhang, W. W.; Fang, Z. Q.; Wei, Z. L.; Jiang, S. X.; Sun, X. C.; Hou, X. L.; Xiao, Z. F.; Ye, G.; Dai, J. W., Bladder Regeneration by Collagen Scaffolds With Collagen Binding Human Basic Fibroblast Growth Factor. *J. Urol.* **2010,** 183, (6), 2432-2439.

137. Kurane, A.; Simionescu, D. T.; Vyavahare, N. R., In vivo cellular repopulation of tubular elastin scaffolds mediated by basic fibroblast growth factor. *Biomaterials* **2007,** 28, (18), 2830-2838.

138. Huang, X.; Yang, D. S.; Yan, W. Q.; Shi, Z. L.; Feng, J.; Gao, Y. B.; Weng, W. J.; Yan, S. G., Osteochondral repair using the combination of fibroblast growth factor and amorphous calcium phosphate/poly(L-lactic acid) hybrid materials. *Biomaterials* **2007,** 28, (20), 3091-3100.

139. Laham, R. J.; Rezaee, M.; Post, M.; Xu, X. Y.; Sellke, F. W., Intrapericardial administration of basic fibroblast growth factor: Myocardial and tissue distribution and comparison with intracoronary and intravenous administration. *Catheter. Cardiovasc. Interv.* **2003,** 58, (3), 375-381.

140. Fansa, H.; Schneider, W.; Wolf, G.; Keilhoff, G., Influence of insulin-like growth factor-I (IGF-I) on nerve autografts and tissue-engineered nerve grafts. *Muscle & Nerve* **2002,** 26, (1), 87-93.

141. Wood, M. D.; Hunter, D.; Mackinnon, S. E.; Sakiyama-Elbert, S. E., Heparin-Binding-Affinity-Based Delivery Systems Releasing Nerve Growth Factor Enhance Sciatic Nerve Regeneration. *Journal of Biomaterials Science-Polymer Edition* **2010,** 21, (6-7), 771-787.

142. Zeng, W.; Yuan, W.; Li, L.; Mi, J.; Xu, S.; Wen, C.; Zhou, Z.; Xiong, J.; Sun, J.; Ying, D.; Yang, M.; Li, X.; Zhu, C., The promotion of endothelial progenitor cells recruitment by nerve growth factors in tissue-engineered blood vessels. *Biomaterials* **2010,** 31, (7), 1636-1645.

143. Yang, Y.-H.; Barabino, G. A., Differential Morphology and Homogeneity of Tissue-Engineered Cartilage in Hydrodynamic Cultivation with Transient Exposure to Insulin-Like Growth Factor-1 and Transforming Growth Factor-beta 1. *Tissue Engineering Part A* **2013,** 19, (21-22), 2349-2360.

144. Kim, K.; Lam, J.; Lu, S.; Spicer, P. P.; Lueckgen, A.; Tabata, Y.; Wong, M. E.; Jansen, J. A.; Mikos, A. G.; Kasper, F. K., Osteochondral tissue regeneration using a bilayered composite hydrogel with modulating dual growth factor release kinetics in a rabbit model. *Journal of Controlled Release* **2013,** 168, (2), 166-178.

145. Puetzer, J. L.; Brown, B. N.; Ballyns, J. J.; Bonassar, L. J., The Effect of IGF-I on Anatomically Shaped Tissue-Engineered Menisci. *Tissue Engineering Part A* **2013,** 19, (11-12), 1443-1450.

146. Ertan, A. B.; Yilgor, P.; Bayyurt, B.; Calikoglu, A. C.; Kaspar, C.; Kok, F. N.; Kose, G. T.; Hasirci, V., Effect of double growth factor release on cartilage tissue engineering. *Journal of Tissue Engineering and Regenerative Medicine* **2013,** 7, (2), 149-160.

147. Seyednejad, H.; Ji, W.; Yang, F.; van Nostrum, C. F.; Vermonden, T.; van den Beucken, J.; Dhert, W. J. A.; Hennink, W. E.; Jansen, J. A., Coaxially Electrospun Scaffolds Based on Hydroxyl-Functionalized Poly(epsilon-caprolactone) and Loaded with VEGF for Tissue Engineering Applications. *Biomacromolecules* **2012,** 13, (11), 3650-3660.

148. van den Berg, W. B., The role of cytokines and growth factors in cartilage destruction in osteoarthritis and rheumatoid arthritis. *Zeitschrift Fur Rheumatologie* **1999,** 58, (3), 136-141.

149. Lucaciu, O. P.; Soritau, O.; Baciut, G.; Lucaciu, D.; Baciut, M.; Campian, R.; Bran, S., The Role of Bone Morphogenetic Proteins in Tissue Engineering Particulate Bone Grafts. *Particulate Science and Technology* **2014,** 32, (4), 377-383.

150. Hanada, K.; Dennis, J. E.; Caplan, A. I., Stimulatory effects of basic fibroblast growth factor and bone morphogenetic protein-2 on osteogenic differentiation of rat bone marrow-derived mesenchymal stem cells. *Journal of Bone and Mineral Research* **1997,** 12, (10), 1606-1614.

151. Chim, H.; Miller, E.; Gliniak, C.; Alsberg, E., Stromal-cell-derived factor (SDF) 1-alpha in combination with BMP-2 and TGF-beta 1 induces site-directed cell homing and osteogenic and chondrogenic differentiation for tissue engineering without the requirement for cell seeding. *Cell and Tissue Research* **2012,** 350, (1), 89-94.

152. Shintani, N.; Siebenrock, K. A.; Hunziker, E. B., TGF-beta 1 Enhances the BMP-2-Induced Chondrogenesis of Bovine Synovial Explants and Arrests Downstream Differentiation at an Early Stage of Hypertrophy. *Plos One* **2013,** 8, (1).

153. Chia, S. L.; Sawaji, Y.; Burleigh, A.; McLean, C.; Inglis, J.; Saklatvala, J.; Vincent, T., Fibroblast Growth Factor 2 Is an Intrinsic Chondroprotective Agent That Suppresses ADAMTS-5 and Delays Cartilage Degradation in Murine Osteoarthritis. *Arthritis and Rheumatism* **2009,** 60, (7), 2019-2027.

154. Deng, M.; Kumbar, S. G.; Nair, L. S.; Weikel, A. L.; Allcock, H. R.; Laurencin, C. T., Biomimetic Structures: Biological Implications of Dipeptide-Substituted Polyphosphazene-Polyester Blend Nanofiber Matrices for Load-Bearing Bone Regeneration. *Advanced Functional Materials* **2011,** 21, (14), 2641-2651.

155. Tessmar, J. K.; Gopferich, A. M., Matrices and scaffolds for protein delivery in tissue engineering. *Adv. Drug Delivery Rev.* **2007,** 59, (4-5), 274-291.

156. Kim, S. H. K. S. H.; Turnbull, J.; Guimond, S., Extracellular matrix and cell signalling: the dynamic cooperation of integrin, proteoglycan and growth factor receptor. *Journal of Endocrinology* **2011,** 209, (2), 139-151.

157. Macri, L.; Silverstein, D.; Clark, R. A. F., Growth factor binding to the pericellular matrix and its importance in tissue engineering. *Advanced Drug Delivery Reviews* **2007,** 59, (13), 1366-1381.

158. Hortensius, R. A.; Harley, B. A. C., The use of bioinspired alterations in the glycosaminoglycan content of collagen-GAG scaffolds to regulate cell activity. *Biomaterials* **2013,** 34, (31), 7645-7652.

159. Almodovar, J.; Guillot, R.; Monge, C.; Vollaire, J.; Selimovic, S.; Coll, J.-L.; Khademhosseini, A.; Picart, C., Spatial patterning of BMP-2 and BMP-7 on biopolymeric films and the guidance of muscle cell fate. *Biomaterials* **2014,** 35, (13), 3975-3985.

160. Koo, S.; Muhammad, R.; Peh, G. S. L.; Mehta, J. S.; Yim, E. K. F., Micro- and nanotopography with extracellular matrix coating modulate human corneal endothelial cell behavior. *Acta Biomaterialia* **2014,** 10, (5), 1975-1984.

161. Vasconcellos, F. C.; Swiston, A. J.; Beppu, M. M.; Cohen, R. E.; Rubner, M. F., Bioactive Polyelectrolyte Multilayers: Hyaluronic Acid Mediated B Lymphocyte Adhesion. *Biomacromolecules* **2010,** 11, (9), 2407-2414.

162. Silva, J. M.; Georgi, N.; Costa, R.; Sher, P.; Reis, R. L.; Van Blitterswijk, C. A.; Karperien, M.; Mano, J. F., Nanostructured 3D Constructs Based on Chitosan and Chondroitin Sulphate Multilayers for Cartilage Tissue Engineering. *Plos One* **2013,** 8, (2).

163. Chung, Y. I.; Tae, G.; Yuk, S. H., A facile method to prepare heparin-functionalized nanoparticles for controlled release of growth factors. *Biomaterials* **2006,** 27, (12), 2621-2626.

164. Rajam, A. M.; Jithendra, P.; Rose, C.; Mandal, A. B., In vitro evaluation of dual growth factor-incorporated chitosan nanoparticle impregnated collagen-chitosan scaffold for tissue engineering. *Journal of Bioactive and Compatible Polymers* **2012,** 27, (3), 265-277.

165. Du, M. C.; Zhu, Y. M.; Yuan, L. H.; Liang, H.; Mou, C. C.; Li, X. R.; Sun, J.; Zhuang, Y.; Zhang, W.; Shi, Q.; Chen, B.; Dai, J. W., Assembled 3D cell niches in chitosan hydrogel network to mimic extracellular matrix. *Colloids and Surfaces a-Physicochemical and Engineering Aspects* **2013,** 434, 78-87.

166. Halili, A. N.; Hasirci, N.; Hasirci, V., A multilayer tissue engineered meniscus substitute. *Journal of Materials Science-Materials in Medicine* **2014,** 25, (4), 1195-1209.

167. Chen, Z. G.; Wang, P. W.; Wei, B.; Mo, X. M.; Cui, F. Z., Electrospun collagen-chitosan nanofiber: A biomimetic extracellular matrix for endothelial cell and smooth muscle cell. *Acta Biomaterialia* **2010,** 6, (2), 372-382.

168. Levett, P. A.; Melchels, F. P. W.; Schrobback, K.; Hutmacher, D. W.; Malda, J.; Klein, T. J., A biomimetic extracellular matrix for cartilage tissue engineering centered on photocurable gelatin, hyaluronic acid and chondroitin sulfate. *Acta Biomaterialia* **2014,** 10, (1), 214-223.

169. Yun, Y.-P.; Yang, D. H.; Kim, S.-W.; Park, K.; Ohe, J.-Y.; Lee, B.-S.; Choi, B.-J.; Kim, S. E., Local delivery of recombinant human bone morphogenic protein-2 (rhBMP-2) from rhBMP-2/heparin complex fixed to a chitosan scaffold enhances osteoblast behavior. *Tissue Engineering and Regenerative Medicine* **2014,** 11, (2), 163-170.

170. Choi, Y. C.; Choi, J. S.; Kim, B. S.; Kim, J. D.; Yoon, H. I.; Cho, Y. W., Decellularized Extracellular Matrix Derived from Porcine Adipose Tissue as a Xenogeneic Biomaterial for Tissue Engineering. *Tissue Engineering Part C-Methods* **2012,** 18, (11), 866-876.

171. Shin, Y. S.; Lee, B. H.; Choi, J. W.; Min, B.-H.; Chang, J. W.; Yang, S. S.; Kim, C.-H., Tissue-engineered tracheal reconstruction using chondrocyte seeded on a porcine cartilage-derived substance scaffold. *International Journal of Pediatric Otorhinolaryngology* **2014,** 78, (1), 32-38.

172. Cheung, H. K.; Han, T. T. Y.; Marecak, D. M.; Watkins, J. F.; Amsden, B. G.; Flynn, L. E., Composite hydrogel scaffolds incorporating decellularized adipose tissue for soft tissue engineering with adipose-derived stem cells. *Biomaterials* **2014,** 35, (6), 1914-1923.

173. Paderi, J. E.; Panitch, A., Design of a synthetic collagen-binding peptidoglycan that modulates collagen fibrillogenesis. *Biomacromolecules* **2008,** 9, (9), 2562-2566.

174. Paderi, J. E.; Sistiabudi, R.; Ivanisevic, A.; Panitch, A., Collagen-Binding Peptidoglycans: A Biomimetic Approach to Modulate Collagen Fibrillogenesis for Tissue Engineering Applications. *Tissue Engineering Part A* **2009,** 15, (10), 2991-2999.

175. Kishore, V.; Paderi, J. E.; Akkus, A.; Smith, K. M.; Balachandran, D.; Beaudoin, S.; Panitch, A.; Akkus, O., Incorporation of a decorin biomimetic enhances the mechanical properties of electrochemically aligned collagen threads. *Acta Biomaterialia* **2011,** 7, (6), 2428-2436.

176. Sharma, S.; Panitch, A.; Neu, C. P., Incorporation of an aggrecan mimic prevents proteolytic degradation of anisotropic cartilage analogs. *Acta Biomaterialia* **2013,** 9, (1), 4618-4625.

177. Paderi, J. E.; Stuart, K.; Sturek, M.; Park, K.; Panitch, A., The inhibition of platelet adhesion and activation on collagen during balloon angioplasty by collagen-binding peptidoglycans. *Biomaterials* **2011,** 32, (10), 2516-2523.

178. Scott, R. A.; Paderi, J. E.; Sturek, M.; Panitch, A., Decorin Mimic Inhibits Vascular Smooth Muscle Proliferation and Migration. *Plos One* **2013,** 8, (11).

179. Sharma, S.; Lee, A.; Choi, K.; Kim, K.; Youn, I.; Trippel, S. B.; Panitch, A., Biomimetic Aggrecan Reduces Cartilage Extracellular Matrix From Degradation and Lowers Catabolic Activity in Ex Vivo and In Vivo Models. *Macromolecular Bioscience* **2013,** 13, (9), 1228-1237.

180. Stuart, K.; Paderi, J.; Snyder, P. W.; Freeman, L.; Panitch, A., Collagen-Binding Peptidoglycans Inhibit MMP Mediated Collagen Degradation and Reduce Dermal Scarring. *Plos One* **2011,** 6, (7).

181. Sarkar, S.; Lightfoot-Vidal, S. E.; Schauer, C. L.; Vresilovic, E.; Marcolongo, M., Terminal-end functionalization of chondroitin sulfate for the synthesis of biomimetic proteoglycans. *Carbohydrate Polymers* **2012,** 90, (1), 431-440.

182. Tran, V. M.; Nguyen, T. K. N.; Sorna, V.; Loganathan, D.; Kuberan, B., Synthesis and Assessment of Glycosaminoglycan Priming Activity of Cluster-xylosides for Potential Use as Proteoglycan Mimetics. *Acs Chemical Biology* **2013,** 8, (5), 949-957.

CHAPTER 3

Aggrecan-Mimetic, Glycosaminoglycan-Containing Nanoparticles for Growth Factor Stabilization and Delivery[1]

3.1 SUMMARY.

The direct delivery of growth factors to sites of tissue healing is complicated by their relative instability. In many tissues, the glycosaminoglycan (GAG) side chains of proteoglycans like aggrecan stabilize growth factors in the pericellular and extracellular space, creating a local reservoir that can be accessed during a wound healing response. GAGs also regulate growth factor-receptor interactions at the cell surface. Here we report the development of nanoparticles for growth factor delivery that mimic the size, GAG composition, and growth factor binding and stabilization of aggrecan. The aggrecan-mimetic nanoparticles are easy to assemble, and their structure and composition can be readily tuned to alter their physical and biological properties. We use basic fibroblast growth factor (FGF-2) as a model heparin-binding growth factor, demonstrating that aggrecan-mimetic nanoparticles can preserve its activity for more than three weeks. We evaluate FGF-2 activity by measuring both the proliferation and metabolic activity of bone marrow stromal cells to demonstrate that chondroitin sulfate-based aggrecan-mimics are as effective as aggrecan, and heparin-based aggrecan mimics are superior to aggrecan as delivery vehicles for FGF-2.

[1]Portions of this chapter appear in the following:
Place, L.W., Sekyi, M., and Kipper, M.J.; "Aggrecan-Mimetic, Glycosaminoglycan-Containing Nanoparticles for Growth Factor Stabilization and Delivery", *Biomacromolecules*, 15 (2014) 680-689. DOI:10.1021/bm401736c.

3.2 INTRODUCTION.

Growth factors hold much promise as therapeutics in regenerative medicine. They control cell proliferation, differentiation, and migration, and are involved in a number of metabolic pathways.[1-3] Growth factors have been used clinically in wound healing, bone disease, and in clinical trials for treating coronary artery disease.[4] They have also been proposed for tissue engineering of nerves, bladders, blood vessels, and osteochondral defects.[5-11] However, these proteins are unstable in plasma and require high doses to affect clinical outcomes.[12, 13] Realizing the potential of growth factors in regenerative medicine will require strategies for maintaining growth factor stability over time scales associated with tissue healing and for delivery of growth factors to the site of disease or injury.

Polymeric nanoparticles can be designed to protect growth factors from enzymatic degradation, and to release growth factors at a desired rate. Furthermore, their size allows them to cross the epithelium.[14] For example, Gu et al. formulated nanoparticles from glycidyl methacrylated dextran and gelatin for fibroblast growth factor (FGF) delivery to mouse mesenchymal stem cells.[15] They showed increased cellular activity for as long as ten days. In another study, Ho et al. synthesized a sulfated chitosan and then complexed it with unmodified chitosan to form polyelectrolyte complex nanoparticles (PCNs). These PCNs were used to deliver FGF to fibroblasts. They tested cell viability for five days, demonstrating that viability was improved using PCNs to deliver FGF, but that PCNs did not perform as well as the glycosaminoglycan heparin.[16] Huang et al. demonstrated preservation of the mitogenic activity of vascular endothelial growth factor (VEGF) for up to five days by encapsulation in PCNs of dextran sulfate with three polycations: chitosan, poly(L-lysine), and poly(ethyleneimine)).[17] Tan et al. immobilized chitosan-heparin nanoparticles onto a decellularized vein scaffold and used

them to localize vascular endothelial growth factor (VEGF) to improve vascularization of the scaffold. They showed controlled release over 30 days and improved cell infiltration, proliferation, ECM production, and vascularization.[18] Our group has also demonstrated controlled release of FGF complexed to chitosan-heparin PCNs from nanofiber scaffolds, which maintained FGF activity for over 30 days.[19] Rajam et al. was able to show a steady release of growth factor from a nanoparticle impregnated collagen-chitosan scaffold for 50 days.[20]

In normal tissues, growth factors are stabilized and presented to cells in a complex milieu of various other stimuli. Thus, in addition to stabilizing growth factors, a growth factor delivery vehicle might be designed to present growth factors in a biomimetic context that interacts favorably with these other signals. In the extracellular and pericellular space of many tissues, the glycosaminoglycan (GAG) side chains of proteoglycans, such as aggrecan, versican, and perlecan serve as a reservoir of stabilized growth factors, and regulate their signaling by also binding to their cell surface receptors.[21-28] GAGs might therefore make excellent materials for growth factor delivery. These GAGs are polyanionic polysaccharides, such as heparin and chondroitin sulfate. The so-called heparin-binding growth factors that bind to GAGs include members of the FGF family and the transforming growth factor-β (TGF-β) superfamily (including some bone morphogenetic proteins). Heparin has been shown to preserve the stability of or to enhance the delivery of a variety of growth factors including, FGFs, TGF-β, VEGF, nerve growth factor (NGF), and platelet-derived growth factor (PDGF).[29] This is the motivation for using sulfated glycosaminoglycans like heparin and their analogs as polymers for growth factor delivery.

In addition to their biochemical functions, proteoglycans also perform important biophysical functions that are dependent upon their nanoscale structure.[30] Aggrecan is the most

highly glycosylated of the proteoglycans, with up to 100 GAGs (chondroitin sulfate and keratin sulfate) attached to a core protein. In solution it adopts a dense, bottle-brush structure bearing a high concentration of negatively charged sulfate groups, with a hydrodynamic diameter of about 400 nm.[31-35] The high negative charge density and resulting high osmotic pressure of aggrecan give cartilage its compressive strength and lubricity.[34]

The aim of this work is to develop nanoparticles for growth factor delivery that mimic the composition, biochemical function, and size of aggrecan for growth factor stabilization and delivery. We use FGF-2 as a model growth factor because it is relatively unstable, and its binding to GAGs is known to influence both its stability and its presentation to growth factor receptors.[36] The aggrecan-mimetic nanoparticles are formed by the complexation of anionic and cationic polysaccharides to form polyelectrolyte complex nanoparticles (PCNs), which has been extensively studied by several groups.[37-42] The cationic polysaccharides chitosan (Chi) and *N*,*N*,*N*-trimethyl chitosan (TMC) are complexed with the anionic GAGs heparin (Hep) and chondroitin sulfate (CS) in solution with the polyanion in excess, so that the resulting PCNs have a colloidally stable, negatively charged structure that mimics the size and chemistry of aggrecan The structures of the polyelectrolytes used are shown in Figure 3.1 and a schematic of the PCNs and aggrecan are shown in Figure 3.2

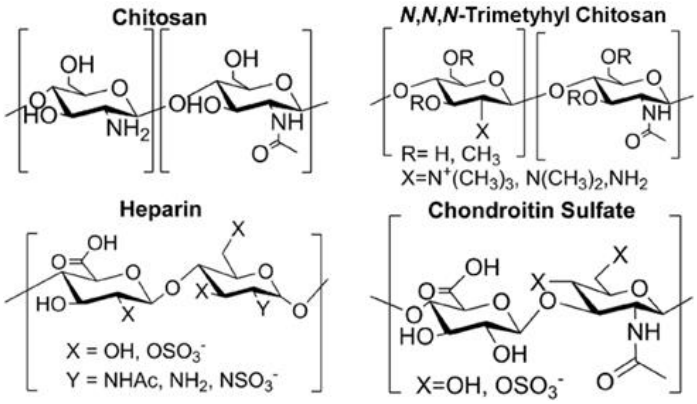

Figure 3.1. Chemical structures of the polysaccharides used in this work.

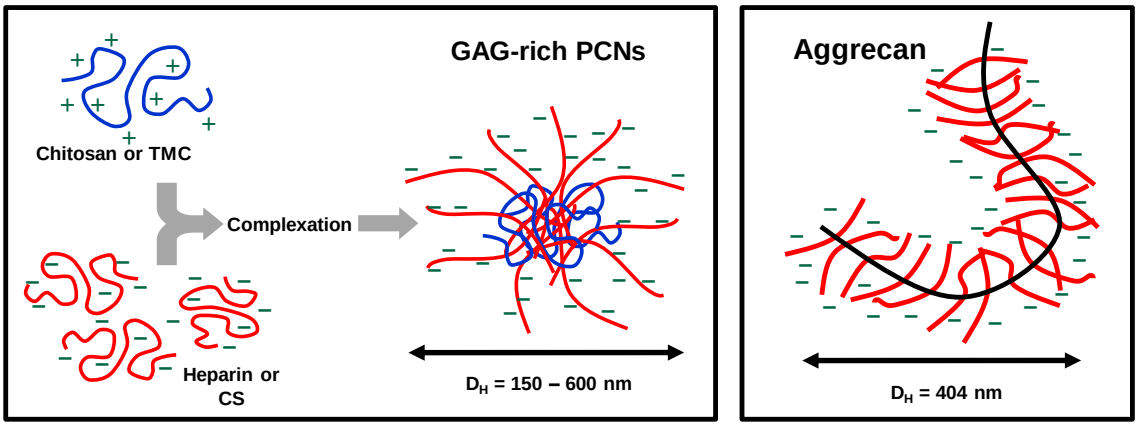

Figure 3.2. GAG-rich PCNs are formed by the complexation of polycationic chitosan or TMC (blue) with the polyanionic GAGs heparin or CS (red) in excess. This results in negatively charged particles presenting the GAGs that have similar size in solution and composition to the proteoglycan aggrecan. Aggrecan is a highly glycosylated protein (black) with up to 100 CS and keratin sulfate chains (red). The hydrodynamic diameter of aggrecan in solution is taken from Papagiannopoulos et al.[31]

Our group has previously studied growth factor binding, stabilization, and delivery using Hep-Chi PCNs, and Hep-Chi and Hep-TMC polyelectrolyte multilayers.[1, 19, 43] In the current work, PCNs from the four polyanion-polycation pairs – Hep-Chi, Hep-TMC, CS-Chi, and CS-TMC – are characterized, including the particle yield, size, zeta potential, and ability to bind FGF-2. The ability of the PCNs to maintain FGF-2 activity over 21 days is also demonstrated here, using assays that measure both the overall metabolic activity and the mitogenic activity of ovine marrow stromal cells (MSCs) to FGF-2. The ability to stabilize and deliver FGF-2 is compared to natural aggrecan and to FGF-2 delivered in solution with no polymer protection.

3.3 MATERIALS AND METHODS.

3.3.1 Materials. Chitosan was purchased from Novamatrix (Protosan UP B 90/20, 5 % acetylated determined by 1H NMR, Mw = 80 kDa; PDI = 1.52; Sandvika, Norway). Heparin sodium was purchased from Celsus Laboratories (from porcine intestinal mucosa, 12.5 % sulfur, Mw = 14.4 kDa; PDI = 1.14, Cincinnati, OH). Chondroitin sulfate sodium salt (CS) (from shark cartilage, 6 % sulfur, 6 sulfate/4 sulfate = 1.24, Mw = 84.3 kDa; PDI = 1.94), rhodamine B

isothiocyanate, and aggrecan from bovine articular cartilage were purchased from Sigma-Aldrich (St. Louis, MO). *N*,*N*,*N*-Trimethyl chitosan (TMC) was synthesized following a procedure described by De Britto and Assis, and characterized as we have done previously.[43, 44] Sodium acetate, sodium chloride, potassium chloride, sodium phosphate dibasic, potassium phosphate monobasic, and dimethyl sulfoxide (DMSO) were purchased from Fisher Scientific (Pittsburgh, PA). Glacial acetic acid and glutaraldehyde 8 % in water were purchased from Acros Organics (Geel, Belgium). Recombinant human FGF basic (FGF-2) 146 aa (carrier free) and Quantikine® ELISA Human FGF basic were purchased from R&D Systems (Minneapolis, MN). 4′6 Diamidino-2-phenylindole•2HCl (DAPI) was purchased from Thermo-Scientific (Rockford, IL). LIVE/DEAD® Viability/Cytotoxicity Kit for mammalian cells was purchased from Invitrogen (Eugene, OR). CellTiter 96® Non-Radioactive Cell Proliferation Assay (modified MTT assay) was purchased from Promega (Madison, WI). Fetal bovine serum (FBS), 0.25 % trypsin with EDTA, low-glucose Dulbecco's modified Eagle's medium (D-MEM), minimum essential medium alpha (α-MEM; supplemented with L-glutamine, ribonucleosides, and deoxyribonucleosides), and Dulbecco's phosphate buffered saline (DPBS) without Ca^{2+} and Mg^{2+} were purchased from HyClone (Logan, UT). Antibiotic-antimycotic (anti/anti), 1 M HEPES buffer solution, and Dulbecco's phosphate buffered saline with Ca^{2+} and Mg^{2+} were purchased from Gibco (Grand Island, NY). A Millipore Synthesis water purification unit (Millipore, Billerica, MA) was used to obtain ultrapure; 18.2 MΩ•cm water (DI water), used for making all aqueous solutions. Fluorimetric and UV-vis spectrophotometric techniques were performed using a fluorescence microplate reader (FLUOstar Omega, BMG Labtech, Durham, NC). Fluorescence microscopy was performed using an Olympus IX70 epifluorescence microscope (Center Valley, PA) with appropriate filters.

3.3.2 Formation and Characterization of Polyelectrolyte Complex Nanoparticles (PCNs). All PCNs were formed by the "one-shot" addition of a solution of the polycation to a solution of the polyanion, under vigorous stirring, with the polyanion in excess.[41, 42, 45, 46] Four different polycation-polyanion pairs were used to create PCNs with different compositions: heparin with chitosan (Hep-Chi), heparin with TMC (Hep-TMC), chondroitin sulfate with chitosan (CS-Chi), and chondroitin sulfate with TMC (CS-TMC). For Hep-Chi PCNs, heparin (0.95 mg mL−1) and chitosan (0.9 mg mL−1) were each dissolved in 0.1 M acetate buffer at pH 5 and then filtered using 0.22 μm polyvinylidene fluoride syringe filters (Fisher Scientific, PA). The chitosan solution was added in one shot to the stirring heparin solution in a 1:6 volume ratio (6 mL chitosan solution to 36 mL heparin solution), vigorously stirred for three hours, then left to settle overnight to remove any aggregates. The solution containing Hep-Chi PCNs and uncomplexed polymer was decanted from the settled aggregates and centrifuged (9000 rcf for 15 min). The supernatant was decanted to remove any uncomplexed polymer and the pelleted PCNs were resuspended in 100 μl of DI water. At this concentration PCNs do aggregate over time and are not used if they are older than 1 month. Before being diluted for analysis or use in an experiment, PCNs were briefly vortexed, which was sufficient to break up aggregates and resuspend them. A similar procedure was used for Hep-TMC, CS-Chi, and CS-TMC PCNs with the following modifications: For CS-Chi and CS-TMC PCNs, the chondroitin sulfate solution was 1.8 mg mL^{-1} because it contains approximately half as many sulfate groups as heparin. The Hep-TMC and CS-Chi PCNs were centrifuged at 2000 rcf for 30 min (instead of 9000 rcf for 15 min), because at higher speeds, the resulting pellet was not readily resuspended. The Hep-TMC, CS-Chi, and CS-TMC PCNs were resuspended in PBS, because they did not readily resuspend in DI water. Different centrifugation conditions might yield different particle size distributions. The

conditions used here for each type of PCN were chosen based on our ability to pellet the particles and also subsequently resuspend them.

Particle yield was determined on a polycation (chitosan or TMC) basis by fluorescence. Chitosan and TMC were tagged with rhodamine.[19] Chitosan or TMC (10 mg mL^{-1}) was dissolved in 10 mL of 0.1 M acetate buffer pH 5, then an equal volume of methanol was added. Rhodamine B isothiocyanate was dissolved in methanol (2 mg mL^{-1}) and 3.25 mL of this was added to the 20 mL chitosan or TMC solution. These were left to stir overnight and then dialyzed against DI water for 24 hours using 20 kDa MWCO dialysis cassettes (Slide-A-Lyzer, Thermo Scientific, PA). The resulting solutions were then lyophilized. The entire procedure and storage were done in the dark to protect against photobleaching. Each of the tagged polycations was mixed with untagged polycation in a 1:10 ratio. These were dissolved in 0.1 M acetate buffer pH 5, filtered, and then used to make PCNs as described above. The fluorescence intensity of the PCNs (λ_{ex} = 544 nm and λ_{em} = 590 nm) was compared to a standard curve created from the 1:10 mixture of tagged and untagged chitosan or TMC to calculate particle yield on a polycation basis. Fluorescently labelled polycations were only used for determining the PCN yields. All other experiments used only non-labelled polycations.

Hydrodynamic radius of the PCNs was measured by dynamic light scattering (DLS) using a 90Plus/BI-MAS (Brookhaven Instruments, Holtsville, NY). All PCN samples were diluted to 2-5 mg mL^{-1} in PBS to give samples of 1-2 mL. Measurements were taken at 25 °C at a fixed angle of 90°, 1 min per measurement. The values reported are the mean effective diameter and the mean polydispersity for each sample. Zeta potential was measured using the same instrument and the same samples used for DLS, via electrophoretic light scattering (ELS).

Each sample was measured five times at 25 °C and the values reported are the mean zeta potential for each sample ± the standard error of the mean.

3.3.3 FGF-2 PCN Loading. An ELISA (Quantikine® ELISA Human FGF basic, R&D Systems) was used to determine the loading efficiency of FGF-2 to the PCNs and to aggrecan. FGF-2 standards had concentrations from 11 pg mL^{-1} to 700 pg mL^{-1}. FGF-2 loading was performed in duplicate for all conditions. FGF-2 (100 ng mL^{-1}) in DPBS was mixed with each PCN type and with aggrecan (1 mg mL^{-1}) for 30 min. These were then centrifuged (9000 rcf for 15 min). The supernatants were removed and diluted 1:166 for the FGF-2 concentration to be within the range of the ELISA. The FGF-2 concentration in the supernatants was subtracted from the original amount in the solution used for loading to determine the amount of FGF-2 bound to the PCNs and to aggrecan.

3.3.4 Cell Harvest and Culture. The cell harvesting and expansion procedure is described in detail in our previous work.[1] Bone marrow aspirates from the iliac crest of three different female sheep were centrifuged. The supernatant containing the nucleated cells was mixed with growth media (low-glucose D-MEM with 10 % FBS, 1 % anti/anti, and 2.5 % HEPES) and seeded into culture flasks. After 24 h, the media was changed to remove all non-adherent cells. The marrow stromal cell (MSC) colonies were allowed to grow for at least seven days, then the cells were trypsinized, counted, and reseeded in culture flasks using maintenance media for culture expansion (α-MEM with 10 % FBS, 1 % anti/anti, and 2.5 % HEPES). MSCs were cryo-preserved prior to seeding into experimental conditions. Cells were not used beyond the fifth passage.

3.3.5 PCN Cytocompatibility. The compatibility of the PCNs towards MSCs was evaluated by dosing cell cultures from one donor animal with different PCN concentrations.

MSCs were seeded in a 48-well plate at 10,000 cells cm^{-2} and allowed to attach for three hours with 0.5 mL of untreated α-MEM containing 10 % FBS. Each of the treatments, Hep-Chi, Hep-TMC, CS Chi, and CS-TMC, were diluted with low-serum media (α-MEM containing 2.5 % FBS) to five different concentrations (0.5, 5, 10, 20, and 40 μg mL^{-1}). After the three-hour attachment, the media was aspirated and replaced with 0.5 mL of low-serum media containing PCNs. Two untreated wells in low-serum media were also cultured. In this low-serum condition, we have previously found that ovine MSCs survive, but do not proliferate well, unless exogenous FGF-2 is added to the cultures.[1] Cells were then incubated at 37 °C for 48 h. After 48 hours one untreated well was exposed to 70 % ethanol for 30 min as a control for the dead stain. The media was aspirated, each well was rinsed with DPBS with Ca^{2+} and Mg^{2+}, and Live/Dead stain was applied according to the vendor's instructions. The Live/Dead kit contained calcein AM (4 mM in DMSO) and ethidium homodimer-1 (2 mM in DMSO). These stock solutions were diluted to 2 μM calcein AM and 0.8 μM ethidium homodimer-1 in DPBS without Ca^{2+} and Mg^{2+}. Dye solution (200 μl) was added to each well and the plates were incubated in the dark at room temperature for 45 min before being imaged by fluorescence microscopy. For each well, three non-overlapping fields of view were imaged, totaling six images per well, at 4× magnification, approximately covering 25 % of the surface area in each well. The corresponding images taken with each filter were merged and qualitatively evaluated using Adobe Photoshop.

3.3.6 Preconditioning FGF-2, PCNs, and Aggrecan. To evaluate the ability of PCNs to stabilize FGF-2, FGF-2-loaded PCNs, FGF 2 bound to aggrecan, and un-complexed FGF-2 were first preconditioned by incubating in media containing 10 % FBS for 0, 3, 7, 14, or 21 days, to allow destabilization of the FGF-2. After preconditioning the activity of FGF-2 was assayed by

measuring the mitosis and metabolic activity of ovine MSCs. These assays are described in the next section.

FGF-2 was bound to each PCN type and to aggrecan using the same procedure as in the loading study above, without the final centrifugation step. Aliquots (125 to 250 µl in PBS) of FGF-2-loaded PCNs, FGF-2-loaded aggrecan, or FGF-2 alone were stored frozen. The aliquots reserved for 21 days of preconditioning were removed first and added to α MEM with 10 % FBS. These were placed in the incubator at 37 °C for 21 days. After seven days, the 14-day aliquots were removed from the freezer and the same procedure was done. These remained in the incubator for 14 days. This was repeated for the 7-day and 3-day aliquots on the appropriate days. On the day on which MSCs were seeded, the zero-day aliquots were thawed and prepared.

3.3.7 MSC Response to FGF-2, PCNSs, and Preconditioned FGF-2-Loaded PCNs and Aggrecan. To evaluate the ability of PCNs and aggrecan to stabilize growth factors, MSCs were treated with the preconditioned FGF-2 in low-serum media. MSC mitogenic activity was evaluated after 4 days of culture, by staining, imaging, and counting cell nuclei, and their metabolic activity was measured using the CellTiter 96® assay after 48 hrs of culture.

3.3.7.1 Mitogenic Activity Assay. The FGF-2 activity after 0, 3, 7, and 14 days of preconditioning in media containing 10 % serum at 37 °C was evaluated in an MSC proliferation assay. All treatments were conducted in duplicate wells on cells from each of the three donor animals seeded at 7000 cells cm^{-2}. These were allowed to attach for three hours in a 48-well plate with 0.5 mL of untreated, α-MEM containing 10 % FBS. After the three-hour attachment period, the seeding media was aspirated and replaced with 0.5 mL of low-serum media containing the treatment (preconditioned FGF-2-loaded PCNs, FGF-2 bound to aggrecan, PCNs without FGF-2, aggrecan without FGF-2, or FGF-2 in solution). PCN and aggrecan treatments

were diluted to 10 μg mL^{-1} (PCN or aggrecan), which corresponds to 1 ng mL^{-1} total FGF-2 (including both bound and unbound FGF-2). Unbound FGF-2 was also diluted to 1 ng mL^{-1}. These were cultured for four days with one media change after two days of culture, where the media change also contained the treatment. The treatment-containing media used for the media change was also stored in the jacketed incubator at 37 °C in α-MEM 2.5 % FBS (5 % CO_2) for the first two days of culture.

After the four-day culture period the cells were stained with calcein AM, fixed 2 % glutaraldehyde, and counter-stained with DAPI. The media was aspirated and each well was rinsed with DPBS with Ca^{2+} and Mg^{2+}. A 2 μM solution of calcein AM in DPBS with Ca^{2+} and Mg^{2+} was added to each well and incubated at 37 °C in the dark for 30 min. This dye was aspirated, wells were rinsed, and 2 % glutaraldehyde in DPBS with Ca^{2+} and Mg^{2+} was added to each well. This was incubated at 4 °C in the dark for 40 min. The glutaraldehyde solution was aspirated, each well was rinsed with DPBS with Ca^{2+} and Mg^{2+}, DAPI (1 μg mL^{-1}) in DPBS with Ca^{2+} and Mg^{2+} was added to each well, and this was incubated at room temperature for 15 min. The dye solution was aspirated and a final rinse was done with DPBS with Ca^{2+} and Mg^{2+}. The well plates were stored at 4 °C in the dark until imaging was performed. Three non-overlapping images were taken per well (25 % of the surface area). Images were processed using the ImageJ 1.41o software (National Institutes of Health, U.S.A.). The blue channel contained only the DAPI stained nuclei, and was counted using the particle analyzer algorithm in the ImageJ software, to obtain cell numbers per area. The FGF-2 activity is reported as the average cells per area for each treatment, normalized by the average cells per area in the untreated control samples.

3.3.7.1 Metabolic Activity Assay. To further understand how the FGF-2 is affecting the cultures during the mitosis assay, the FGF-2 activity after 0, 7, 14, and 21 days of preconditioning in media containing 10 % serum at 37 °C was evaluated using a modified MTT assay for cell metabolic activity. Ovine MSCs isolated from one donor animal were used for each treatment. All treatments were conducted in triplicate wells on cells seeded at 10,000 cells cm^{-2}. These were allowed to attach for three hours in a 48-well plate with 0.5 mL of untreated α-MEM containing 10 % FBS. After the three-hour attachment period, the seeding media was aspirated and replaced with 0.5 mL of low-serum media containing the treatment (preconditioned FGF-2-loaded PCNs, FGF-2 bound to aggrecan, PCNs without FGF-2, aggrecan without FGF-2, or FGF-2 in solution). Treatments were all diluted to the same concentrations used for the mitosis assay described above. Each treatment was evaluated in triplicate.

After a 48-hour culture period the CellTiter 96® (modified MTT) assay was performed according to the manufacturer's instructions. The FGF-2 activity is reported as the average of nine readings (triplicate readings from each of three replicates) for each condition, normalized by the negative control (no FGF-2).

3.3.8 Statistics. Data analysis was performed using Minitab (Minitab, Inc., State College, PA), version 16. For the FGF-2 stability/activity assay, comparisons between groups were performed via analysis of variance (ANOVA) models with Tukey's multiple comparison tests. Comparisons of each treatment group to the negative control were done using ANOVA with Dunnett's tests. Differences with $p < 0.05$ were considered statistically significant. Mitogenic activity data are expressed as the mean ± standard error of the mean ($n = 6$). Cell metabolic activity data were obtained from triplicate samples taken from each well; each treatment was also performed in triplicate ($n = 9$).

3.4 RESULTS AND DISCUSSION.

3.4.1 PCN Formation and Characterization. Four different compositions of PCNs were made by electrostatic complexation of a polyanion (either Hep or CS) and a polycation (either Chi or TMC) with the polyanion in excess. The PCN yield was determined on a polycation basis from fluorescence measurements of PCNs formed with rhodamine-labeled polycations. The FGF-2 loading was determined by difference using an ELISA for FGF-2, and the size and zeta potentials of PCNs before and after FGF-2 loading were determined by DLS and ELS, respectively. These results are shown in Table 3.1.

Table 3.1. PCN characterization. For Hep-Chi, CS-Chi, and CS-TMC PCNs the mean hydrodynamic diameter, PDI, and zeta potential are shown both before and after loading with FGF-2.

composition	yield (%)	FGF-2 loading (ng/mg)	mean D_H (nm)	PDI	ζ-potential (mV)
Hep-Chi	63 ± 7		260	0.152	−48 ± 0.3
Hep-Chi-FGF-2		51 ± 14	260	0.153	−3.87 ± 0.05
Hep-TMC	39 ± 3		170	0.005	−10 ± 2
Hep-TMC-FGF-2		56 ± 11	-[2]	-[2]	-[2]
CS-Chi	34 ± 5		260	0.05	−40 ± 3
CS-Chi-FGF-2		47 ± 3	230	0.038	−4.1 ± 0.1
CS-TMC	39 ± 6		540	0.161	−34 ± 0.8
CS-TMC-FGF-2		48 ± 12	380	0.161	−4.55 ± 0.05
Aggrecan	-	50 ± 5	400[3]	-	-

[2]Instability of Hep-TMC PCNs prevented the measurement of their size and □-potential after isolation by dialysis.

[3]From Papagiannopoulos et al.[31]

The Hep-Chi PCNs exhibited the highest yield (63 %) while the other three types were all in the 35-40 % range. The Hep-TMC PCNs were the most difficult to re-suspend and material was lost in the purification process. All PCNs had hydrodynamic diameters < 1 μm, and each type had a monomodal size distribution with polydispersity index less than 0.2.[37] The Hep-TMC particles were the smallest (mean D_H = 170 nm), the CS-TMC particles were the largest (mean D_H = 540 nm), and both Hep-Chi and CS-Chi had diameters of 260 nm. These results are similar to those observed previously by our group and other groups making similar particles.[37, 46-48] The hydrodynamic diameter of aggrecan reported by others is in the middle of the observed range of sizes for these PCNs.[31] (We did not independently measure the aggrecan by DLS or zeta potential because the large sample size and concentration required.) The Hep-Chi particles displayed the most negative zeta potential of −48 mV and the Hep-TMC particles had the least negative zeta potential of −10 mV. The size and zeta potential of PCNs after FGF-2 loading are also reported in Table 1. The magnitude of the zeta potential drops substantially after complexing PCNs with FGF-2 for all PCNs. For the Hep-TMC PCNs, they become colloidally unstable so that their size and zeta potential cannot be measured.

The size and zeta potential of PCNs can be affected by their composition and by the molecular weight and charge density of the constituent polyelectrolytes.[46, 49, 50] For both the heparin-containing and the CS-containing PCNs, the charge density of the polycation affects the zeta potential. Pairing the polyanion with chitosan results in a more negative zeta potential than the corresponding PCNs formed with TMC as the polycation. The two types of PCNs formed with TMC as the polycation also provide an interesting comparison of PCNs made with a small polyanion (heparin, MW = 14.4 kDa) and a large polyanion (CS, MW = 84.3 kDa), both containing strong anionic sulfate groups. The Hep-TMC particles formed here have the smallest

size and the least negative zeta potential of all of the PCNs. This would make them relatively unstable, and likely contributes to the observed difficulty in re-suspending them after binding FGF-2. The CS-TMC particles are the largest PCNs. The CS used here has a much higher molecular weight than the heparin. A previous study done in our lab showed that ion pairing between these two strong polyions at surfaces leads to hydrophilic complexes that swell with water.[51] This could be due to inefficient ion pairing, requiring that the PCNs retain a large number of small-molecular weight counterions. Dautzenberg and Jaeger also found that particle size increases when polyelectrolyte ion pairing is reduced, due to increased swelling with water.[50] This leads to retention of counter ions, high osmotic pressure, and swelling of the complexes.

Each of the PCNs and aggrecan all bound approximately 50 ng FGF-2 per mg of PCN or aggrecan. The polyanion GAG FGF-2 binding occurs primarily via electrostatic interactions between the sulfate groups in the GAG and pendent amine groups in the FGF-2.[52] In work by Asada et al. the authors observed that heparin may bind more FGF-2 than CS, likely because heparin is more highly sulfated.[53] In the present work, we used more polyanion when preparing the CS-containing PCNs than when preparing the heparin-containing PCNs to compensate for the reduced degree of sulfation of CS. Hence, the FGF-2 loading of the heparin- and CS-containing PCNs is approximately the same (Table 1).

3.4.2 PCN Cytocompatibility. The cytocompatibility of PCNs with respect to MSCs was evaluated to determine how the dose of PCNs affects MSC viability. Five doses of PCNs (0.5, 5.0, 10, 20, and 40 μg mL^{-1}) in low-serum media were compared to the negative control (no PCNs) and to a cytotoxic ethanol treatment (70 % ethanol), in a 48 h cytocompatibility assay. Representative images of each PCN treatment (Hep-Chi, Hep-TMC, CS-Chi, and CS-TMC) at

0.5 μg mL^{-1}, 10 μg mL^{-1}, 40 μg mL^{-1}, the negative control, and the ethanol-treated cells are shown in Figure 3.3. The Live/Dead stain indicates live cells in green and dead cells in red. At the 10 μg mL^{-1} dose, the total number of live cells and the degree of cell spreading appears to be reduced for all PCN formulations. At the 40 μg mL^{-1} dose, of all PCN formulations, there are far more dead cells than there are at the lower PCN doses. Since these cells are anchorage dependent, this inhibition of attachment and spreading may contribute to the apparent cytotoxicity observed at high PCN doses. The CS-TMC PCNs appear to have the least negative effect on cell spreading and viability, while Hep-Chi PCNs caused reduced cell spreading, even at the lowest dose, 0.5 μg mL^{-1}. While some effect of PCN delivery on MSC cultures is observed for all formulations at 10 μg mL^{-1}, we chose to use this dose for the subsequent FGF-2 activity assays, to achieve a 1 ng mL^{-1} total dose of FGF-2. The 1 ng mL^{-1} total dose of FGF-2 was identified as the optimally mitogenic dose for ovine MSCs in our previous work.[1]

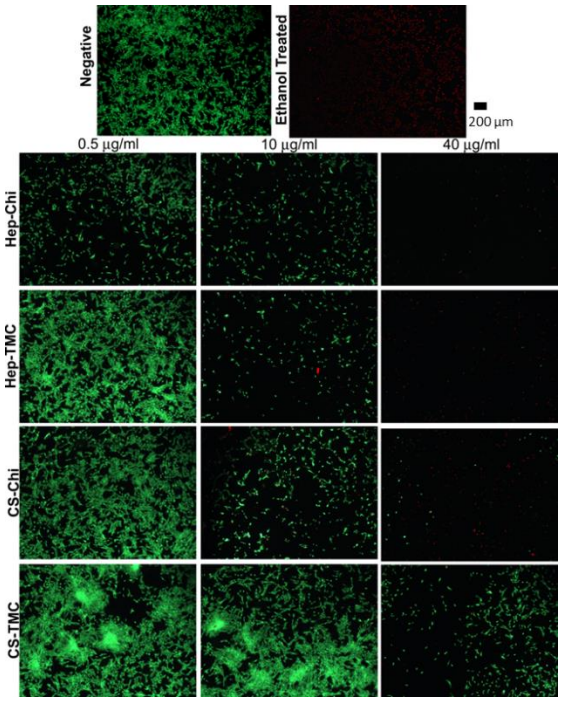

Figure 3.3. Cytocompatibility using Live/Dead stain. Each row represents a different PCN type dosed with increasing PCN concentrations (0.5 μg mL^{-1} to 40 μg mL^{-1}) from left to right. Some cytotoxicity of the PCNs is observed for doses greater than 10 μg mL^{-1}.

3.4.3 MSC Response to FGF-2, PCNs, and Preconditioned FGF-2-Loaded PCNs and Aggrecan.

3.4.3.1 Mitogenic Activity Assay. To evaluate the ability of PCNs to preserve the activity of FGF-2, cells were treated with PCNs, FGF-2-loaded PCNs, FGF-2 bound to aggrecan, or un-complexed FGF-2 that had been preconditioned at 37 °C in media containing 10 % FBS for 0, 3, 7, or 14 days. In separate experiments, cells were also treated with PCNs and aggrecan with no FGF-2.

We previously reported a biphasic dose response of ovine MSCs to FGF-2 in solution, with and optimally mitogenic dose in the range of 1 ng mL^{-1} to 10 ng mL^{-1} under the same conditions used here (four-day culture in low-serum media).[1] We also showed that the response to FGF-2 was enhanced when the FGF-2 was bound to heparin-containing surface coatings on glass rather than delivered in solution.[1] More recently, we demonstrated significant response to FGF-2 bound to Hep-Chi PCNs at an equivalent FGF-2 dose of approximately 0.2 ng mL^{-1} under the same conditions.[19] These experiments demonstrate that binding FGF-2 to heparin-containing PCNs or surfaces may reduce the dose required to achieve a functional response, compared to FGF-2 delivered in solution. Hence in the present work, we used an equivalent FGF-2 dose of 1 ng mL^{-1} and 10 μg mL^{-1} PCNs or aggrecan. The FGF-2 loading of each PCN type is displayed in Table 3.1. In all cases, approximately 50 % of the FGF-2 is bound to the PCNs or aggrecan. For the FGF-2 activity experiments, there is no separation step to remove unbound FGF-2. Thus, each condition uses an equal amount of total FGF-2.

Figure 3.4. shows the cell counts (cells per area after four days of culture) for the PCNs and aggrecan with no FGF-2. The negative control (no treatment) shows that MSCs do not proliferate in this low-serum condition over four days of cell culture without exogenous FGF-2. (Cells were initially seeded at 7000 cells per cm^2.) None of the PCN treatments resulted in a

positive response over the negative control. The aggrecan and CS-containing PCNs were not statistically different from the negative control. However, the heparin-containing PCNs had cell numbers statistically lower than the other conditions. This corresponds to the interference with cell attachment seen at 10 μg mL^{-1} in the cytocompatibility study. Representative microscopy images of DAPI-stained nuclei from which these cell numbers were obtained are shown in the Appendix.

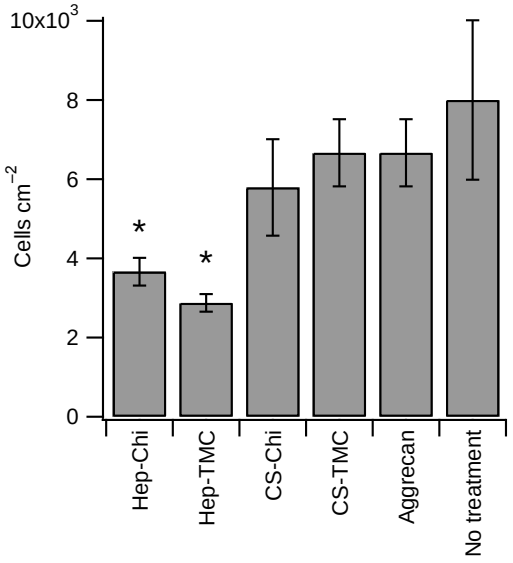

Figure 3.4. Cells per cm^2 obtained after four days of culture in low-serum media, treated with PCNs and aggrecan, compared to no treatment. * indicates statistical difference from the negative control ($p < 0.05$). Cells were seeded at 7000 cells per cm^2.

Previous studies have found that both heparin and CS may inhibit cell attachment.[54] Other sulfated polysaccharides have been shown to exhibit antiproliferative or cytotoxic effects on mammalian cells.[55, 56] Delivery of Hep-containing PCNs at 10 μg mL^{-1} may reduce the ability of cells to attach and spread, resulting in the reduced cell numbers seen here.

Figure 3.5. shows representative fluorescence micrographs (DAPI-stained nuclei) after four days of culture in low-serum media for untreated MSCs, MSCs treated with FGF-2 bound to PCNs (Hep-Chi and CS-Chi) or aggrecan, and FGF-2 delivered in solution, for different preconditioning times. The normalized cell numbers for each type of FGF-2-PCN treatment is

compared to the FGF-2-aggrecan and FGF-2 only treatments in Figure 3.6. In the low-serum condition, untreated cells do not proliferate; cells cultured with FGF-2 alone do proliferate, but not to as high of an extent as cells exposed to PCN-bound FGF-2. After 0 days preconditioning, the normalized cell numbers for the FGF-2 alone are statistically lower than the CS-Chi PCNs, and after 7 or 14 days of preconditioning they are statistically lower than the Hep-containing PCNs, but are not statistically different from the negative control after all preconditioning periods.

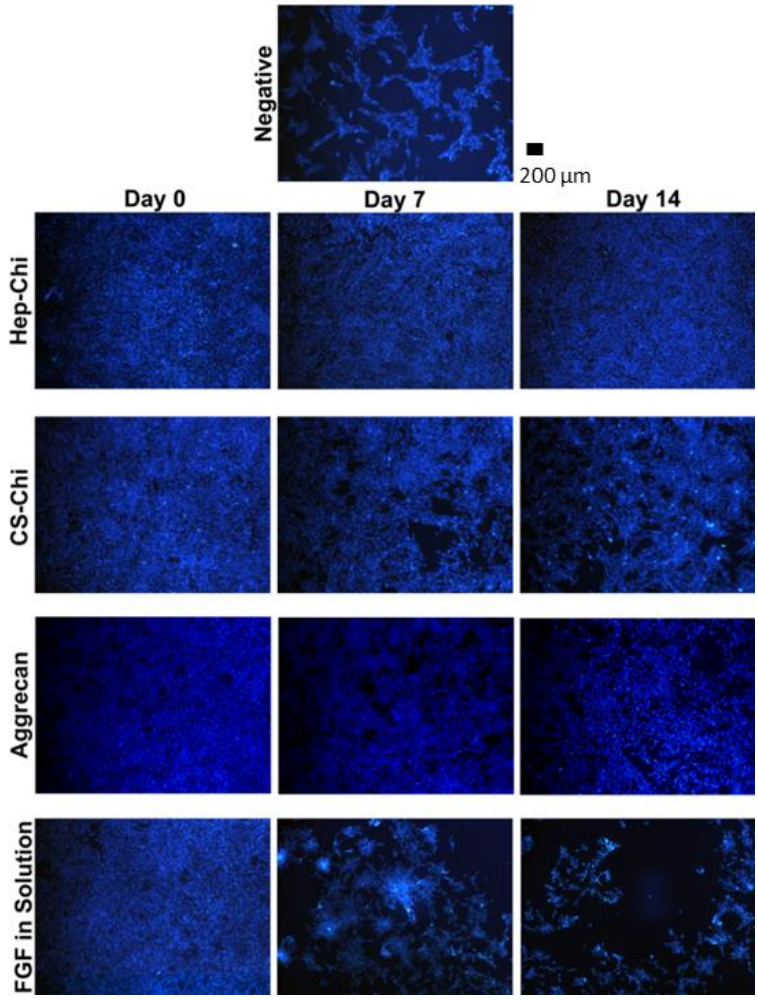

Figure 3.5. Representative fluorescence micrographs of DAPI-stained MSC nuclei after four days of culture with, no treatment, FGF-2-loaded PCNs or aggrecan, and FGF-2 in solution. Preconditioning time does not appear to have an effect on mitogenic activity, however treatment type does.

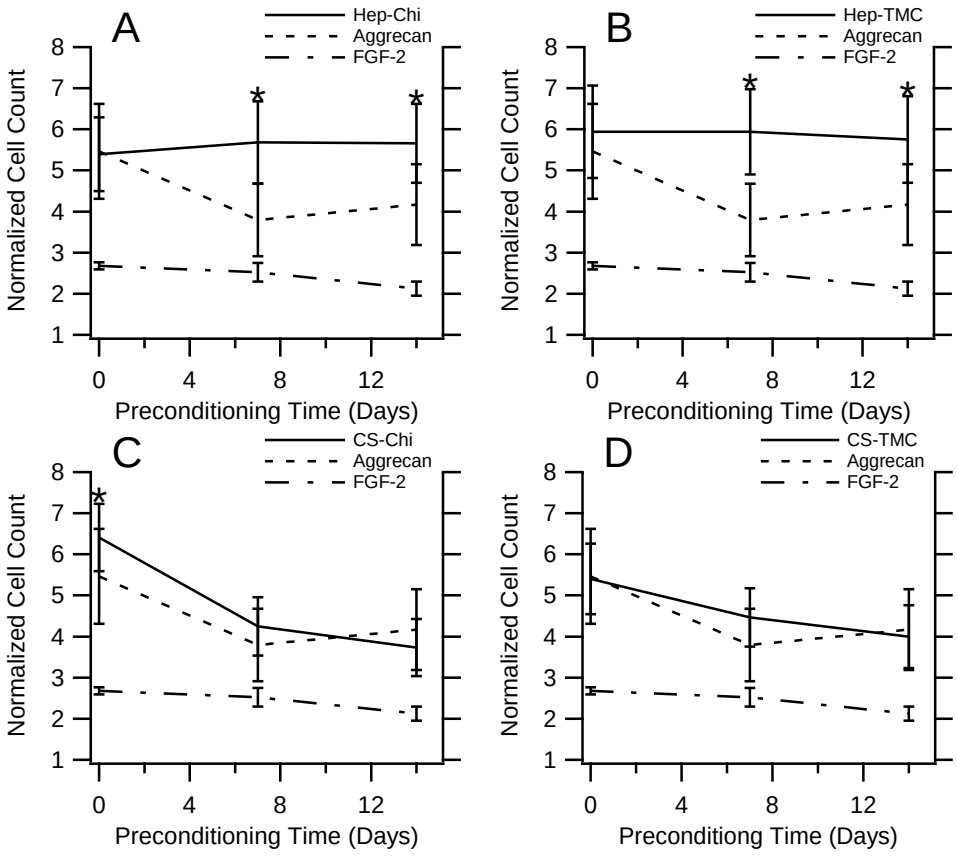

Figure 3.6. FGF-2 mitogenic activity in 4-day MSC culture, for FGF-2-loaded PCNs, FGF-2-loaded aggrecan, and FGF-2 in solution. The numbers represent cell count normalized to cell counts from the negative control. Panels A-D represent Hep-Chi, Hep-TMC, CS-Chi, and CS-TMC respectively. Each PCN type is compared to aggrecan and FGF-2 in solution; * indicates points that have statistically higher cell counts compared to FGF-2 in solution that was preconditioned for the same amount of time. Hep-containing PCNs remain consistent over preconditioning time while CS containing PCNs and aggrecan exhibit lower cell numbers for increased preconditioning time.

Despite the apparent inhibition of cell proliferation observed above for PCNs with no FGF-2 (Figure 3.4.), all of the treatments with FGF-2 result in increased cell numbers compared to cells cultured with no FGF-2 (normalized cell counts are all greater than 1). The mitogenic activity of FGF-2 bound to PCNs is also greater than the mitogenic activity of unbound FGF-2 for all PCNs at all time points. The Hep-Chi and Hep-TMC PCNs maintain a high level of FGF-2 mitogenic activity over the entire 14 day preconditioning, while the CS-Chi and CS-TMC PCNs and aggrecan exhibit some apparent loss of FGF-2 mitogenic activity with increased

preconditioning time (Figure 3.6.). Since the unbound FGF-2 in solution has a much lower mitogenic activity than FGF-2 bound to PCNs, we conclude that the FGF-2 bound to the PCNs is primarily responsible for the high level of activity in the PCN conditions. For the heparin-containing PCNs a substantial amount of FGF-2 must remain bound to the PCNs over the preconditioning time. The CS-containing PCNs and aggrecan may be slowly releasing some FGF-2 into solution, resulting in the observed drop in mitogenic activity with increasing preconditioning time.

3.4.3.2 Metabolic Activity Assay. To better understand how the cells respond to the preconditioned FGF-2 during the four-day mitosis experiments, a modified MTT assay was used to evaluate MSC metabolic activity. The modified MTT assay was performed on cells cultured for 48 hrs, treated with FGF-2, PCNs, FGF-2-loaded PCNs, or aggrecan preconditioned for 0, 7, 14, or 21 days. For treatments with no FGF-2, the MSC metabolic activity was the same across all four PCN types and the same as the negative control (not shown). Hence, although PCNs reduce attachment and spreading (Figures 3.3. and 3.4.) the MSC metabolic activity is not affected. Figure 3.7. shows the results of the metabolic activity assay for the FGF-2-containing treatments. The aggrecan and CS-containing PCNs showed no statistical difference across preconditioning time, indicating that FGF-2 activity in relation to metabolic activity for these treatments is stable. However, the Hep-containing PCNs exhibited increased metabolic activity after 21 days of preconditioning compared to 0 days, and FGF-2 alone showed reduced metabolic activity after 21 days of preconditioning compared to 7 days of preconditioning. When treatments were compared within individual time points, there were statistical differences between groups. At 7 days of preconditioning all treatments elicit the same MSC response, but as preconditioning time increases differences emerge indicating that there is some loss of activity

over time. After 14 days of preconditioning (Figure 3.7.C), CS-TMC and Hep-TMC elicit a higher metabolic response than aggrecan. After 21 days of preconditioning (Figure 3.7.D), three PCN types (Hep-TMC, Hep-Chi, and CS-TMC) are superior to FGF-2 alone and to FGF-2 bound to aggrecan. All PCN treatments stimulate more metabolic activity at all preconditioning times than the negative control, indicating that some FGF-2 activity remains over the 21 days.

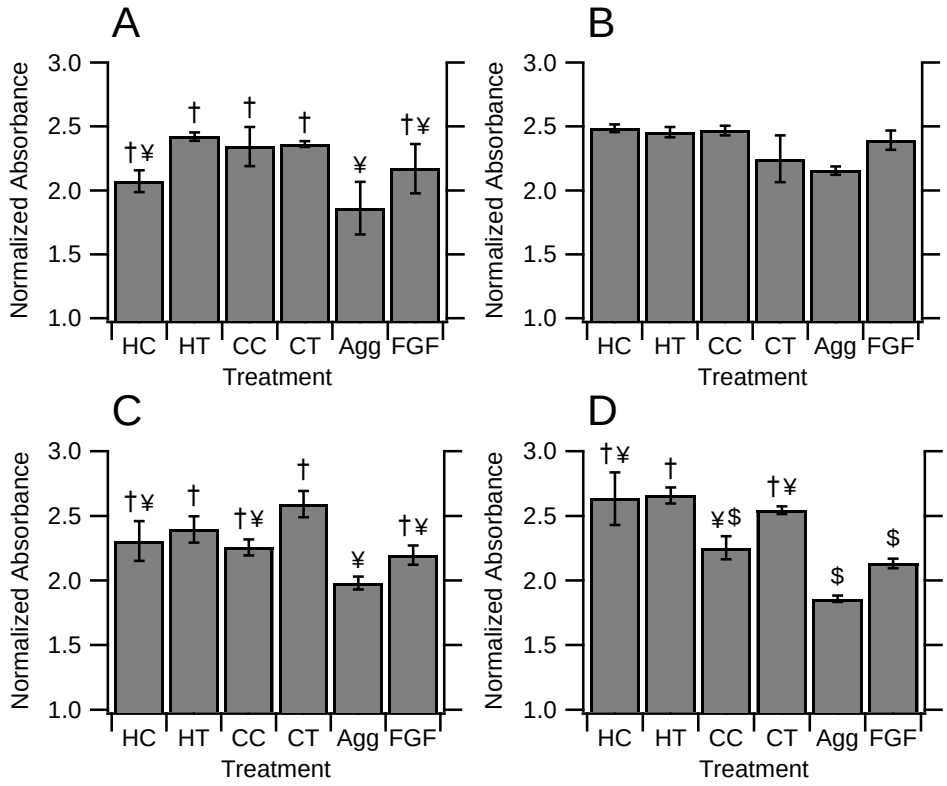

Figure 3.7. Metabolic activity after 2 days of culture with FGF-2-loaded PCNs, FGF-2-loaded aggrecan, and FGF-2 in solution (treatments were preconditioned in media for (A) 0, (B) 7, (C) 14, or (D) 21 days). Metabolic activity of MSCs exposed to treatment was normalized to the metabolic activity of untreated MSCs. In each panel, bars marked with the same symbol are not statistically different from one another within each figure. There was no statistical difference between any of the treatments after 7 days of preconditioning (B). After 14 days of preconditioning, Hep-TMC and CS-TMC elicit a higher response than aggrecan (C). After 21 days of preconditioning, Hep-TMC, Hep-Chi, and CS-TMC all elicit a higher response than aggrecan and FGF-2 in solution (D). All PCN treatments are statistically higher than the negative control regardless of preconditioning time.

Both CS and heparin are highly sulfated polysaccharides (Figure 3.2.) that can bind FGF-2 electrostatically, evidenced by the change in zeta potential upon FGF-2 binding (Table 3.1.).

However, the heparin-containing PCNs are more effective at stabilizing FGF-2 than the CS-containing PCNs and the CS-containing aggrecan. The high-specificity binding sequence of heparin and heparan sulfate for FGF-2 requires two *N*-sulfonates and a 2-*O*-sulfated iduronic acid.[21, 52] This high specificity binding of FGF-2 to heparin might also impart higher stability to FGF-2 bound to heparin-containing PCNs. The CS used in this work is primarily 4-*O*-sulfated and 6-*O*-sulfated, and therefore lacks the FGF-2-binding sulfation pattern found in heparin. Aggrecan contains mostly CS and some keratan sulfate, which is also 6-*O*-sulfated.[57, 58] The lack of specificity may make CS and aggrecan less effective at stabilizing FGF-2.

3.5 CONCLUSIONS.

The aggrecan-mimetic PCNs described here have a size and high density of GAGs similar to aggrecan. The manufacturing process is simple, reproducible, and requires no additional crosslinking to form the particles or additional chemical modification to bind the growth factor. At doses of 10 μg mL^{-1} and above they may inhibit cell attachment to tissue-culture polystyrene, and at higher doses, they may be cytotoxic toward MSCs. At a dose of 10 μg mL^{-1}, the Hep-containing PCNs result in reduced cell numbers compared to aggrecan and untreated controls in a four-day MSC culture assay. Nonetheless, these PCNs bind and stabilize FGF-2 enhancing both the mitogenic activity and the metabolic activity of MSCs in low-serum media.

In these experiments, we did not find a direct correlation between cell number and cell metabolic activity. While the MTT and similar assays can be highly correlated to cell number under some conditions, these cells are approaching confluence in the four-day cell culture, under the most mitogenic conditions. This likely results in contact inhibition, causing the results of the metabolic activity and mitogenesis assays to diverge.

This work shows that the mitogenic activity of FGF-2 is best maintained by binding to Hep-containing PCNs. Over the same preconditioning time period, delivery of FGF-2 using PCNs results in higher metabolic activity than delivery of FGF-2 using aggrecan. Furthermore, after 21 days of preconditioning, all of the PCN formulations are superior to aggrecan, and the Hep-containing PCNs are superior to FGF-2 in solution at stimulating metabolic activity of MSCs. FGF-2 in solution has no significant mitogenic activity after any of the preconditioning periods (normalized cell numbers were not statistically different from the untreated control). FGF-2 bound to aggrecan and CS-based PCNs lost some mitogenic activity during the 14-day preconditioning. But FGF-2 bound to heparin-containing PCNs exhibited no loss of activity during the 14-day preconditioning. The metabolic activity assay showed that after 14 days of preconditioning, two of the PCN types were superior to aggrecan at maintaining the FGF-2 activity, and after 21 days of preconditioning, the PCNs were superior to both aggrecan and FGF-2 alone.

We have previously demonstrated that similar PCNs can be bound to surfaces and used to deliver heparin-binding growth factors like FGF-2.[19, 45] Therefore, these aggrecan-mimetic PCNs might be used for growth factor delivery either in soluble form or bound to surfaces. This could improve the prospects for therapeutic delivery of heparin-binding growth factors and cytokines for tissue engineering and wound healing applications.

REFERENCES

1. Almodovar, J.; Bacon, S.; Gogolski, J.; Kisiday, J. D.; Kipper, M. J., Polysaccharide-Based Polyelectrolyte Multi layer Surface Coatings can Enhance Mesenchymal Stem Cell Response to Adsorbed Growth Factors. *Biomacromolecules* **2010,** 11, (10), 2629-2639.

2. Babensee, J. E.; McIntire, L. V.; Mikos, A. G., Growth factor delivery for tissue engineering. *Pharm. Res.* **2000,** 17, (5), 497-504.

3. Li, J. T.; Pei, M., Optimization of an In Vitro Three-Dimensional Microenvironment to Reprogram Synovium-Derived Stem Cells for Cartilage Tissue Engineering. *Tissue Eng., Part A.* **2011,** 17, (5-6), 703-712.

4. Chen, R. R.; Mooney, D. J., Polymeric growth factor delivery strategies for tissue engineering. *Pharm. Res.* **2003,** 20, (8), 1103-1112.

5. Gu, X. S.; Ding, F.; Yang, Y. M.; Liu, J., Construction of tissue engineered nerve grafts and their application in peripheral nerve regeneration. *Prog. Neurobiol.* **2011,** 93, (2), 204-230.

6. Ohta, M.; Suzuki, Y.; Chou, H.; Ishikawa, N.; Suzuki, S.; Tanihara, M.; Mizushima, Y.; Dezawa, M.; Ide, C., Novel heparin/alginate gel combined with basic fibroblast growth factor promotes nerve regeneration in rat sciatic nerve. *J. Biomed. Mater. Res., Part A* **2004,** 71A, (4), 661-668.

7. Wang, S. G.; Cai, Q.; Hou, J. W.; Bei, J. Z.; Zhang, T.; Yang, J.; Wan, Y. Q., Acceleration effect of basic fibroblast growth factor on the regeneration of peripheral nerve through a 15-mm gap. *J. Biomed. Mater. Res., Part A* **2003,** 66A, (3), 522-531.

8. Chen, W.; Shi, C. Y.; Yi, S. H.; Chen, B.; Zhang, W. W.; Fang, Z. Q.; Wei, Z. L.; Jiang, S. X.; Sun, X. C.; Hou, X. L.; Xiao, Z. F.; Ye, G.; Dai, J. W., Bladder Regeneration by Collagen

Scaffolds With Collagen Binding Human Basic Fibroblast Growth Factor. *J. Urol.* **2010,** 183, (6), 2432-2439.

9. Kurane, A.; Simionescu, D. T.; Vyavahare, N. R., In vivo cellular repopulation of tubular elastin scaffolds mediated by basic fibroblast growth factor. *Biomaterials* **2007,** 28, (18), 2830-2838.

10. Huang, X.; Yang, D. S.; Yan, W. Q.; Shi, Z. L.; Feng, J.; Gao, Y. B.; Weng, W. J.; Yan, S. G., Osteochondral repair using the combination of fibroblast growth factor and amorphous calcium phosphate/poly(L-lactic acid) hybrid materials. *Biomaterials* **2007,** 28, (20), 3091-3100.

11. Laham, R. J.; Rezaee, M.; Post, M.; Xu, X. Y.; Sellke, F. W., Intrapericardial administration of basic fibroblast growth factor: Myocardial and tissue distribution and comparison with intracoronary and intravenous administration. *Catheter. Cardiovasc. Interv.* **2003,** 58, (3), 375-381.

12. Richardson, T. P.; Peters, M. C.; Ennett, A. B.; Mooney, D. J., Polymeric system for dual growth factor delivery. *Nat. Biotechnol.* **2001,** 19, (11), 1029-1034.

13. Tessmar, J. K.; Gopferich, A. M., Matrices and scaffolds for protein delivery in tissue engineering. *Adv. Drug Delivery Rev.* **2007,** 59, (4-5), 274-291.

14. Grenha, A., Chitosan nanoparticles: a survey of preparation methods. *J. Drug Targeting* **2012,** 20, (4), 291-300.

15. Gu, C. H.; Zheng, R. H.; Yang, Z. F.; Wen, A. D.; Wu, H.; Zhang, H.; Yi, D. H., Novel glycidyl methacrylated dextran/gelatin nanoparticles loaded with basic fibroblast growth factor: formulation and characteristics. *Drug Dev. Ind. Pharm.* **2009,** 35, (12), 1419-1429.

16. Ho, Y. C.; Wu, S. J.; Mi, F. L.; Chiu, Y. L.; Yu, S. H.; Panda, N.; Sung, H. W., Thiol-Modified Chitosan Sulfate Nanoparticles for Protection and Release of Basic Fibroblast Growth Factor. *Bioconjugate Chem.* **2010,** 21, (1), 28-38.

17. Huang, M.; Vitharana, S. N.; Peek, L. J.; Coop, T.; Berkland, C., Polyelectrolyte complexes stabilize and controllably release vascular endothelial growth factor. *Biomacromolecules* **2007,** 8, (5), 1607-1614.

18. Tan, Q.; Tang, H.; Hu, J. G.; Hu, Y. R.; Zhou, X. M.; Tao, Y. M.; Wu, Z. S., Controlled release of chitosan/heparin nanoparticle-delivered VEGF enhances regeneration of decellularized tissue-engineered scaffolds. *Int. J. Nanomed.* **2011,** 6, 929-942.

19. Volpato, F. Z.; Almodovar, J.; Erickson, K.; Popat, K. C.; Migliaresi, C.; Kipper, M. J., Preservation of FGF-2 bioactivity using heparin-based nanoparticles, and their delivery from electrospun chitosan fibers. *Acta Biomater.* **2012,** 8, (4), 1551-1559.

20. Rajam, A. M.; Jithendra, P.; Rose, C.; Mandal, A. B., In vitro evaluation of dual growth factor-incorporated chitosan nanoparticle impregnated collagen-chitosan scaffold for tissue engineering. *J. Bioact. Compat. Polym.* **2012,** 27, (3), 265-277.

21. Harmer, N. J.; Ilag, L. L.; Mulloy, B.; Pellegrini, L.; Robinson, C. V.; Blundell, T. I., Towards a resolution of the stoichiometry of the fibroblast growth factor (FGF)-FGIF receptor - Heparin complex. *J. Mol. Biol.* **2004,** 339, (4), 821-834.

22. Frescaline, G.; Bouderlique, T.; Huynh, M. B.; Papy-Garcia, D.; Courty, J.; Albanese, P., Glycosaminoglycans mimetics potentiate the clonogenicity, proliferation, migration and differentiation properties of rat mesenchymal stem cells. *Stem Cell Res.* **2012,** 8, (2), 180-192.

23. Maccarana, M.; Casu, B.; Lindahl, U., Minimal Sequence in Heparin Heparan-Sulfate Required for Binding of Basic Fibroblast Growth-Factor. *J. Biol. Chem.* **1993,** 268, (32), 23898-23905.

24. Smith, S. M. L.; West, L. A.; Govindraj, P.; Zhang, X. Q.; Ornitz, D. M.; Hassell, J. R., Heparan and chondroitin sulfate on growth plate perlecan mediate binding and delivery of FGF-2 to FGF receptors. *Matrix Biol.* **2007,** 26, (3), 175-184.

25. Mccaffrey, T. A.; Falcone, D. J.; Du, B. H., Transforming Growth Factor-Beta-1 Is a Heparin-Binding Protein - Identification of Putative Heparin-Binding Regions and Isolation of Heparins with Varying Affinity for Tgf-Beta-1. *J. Cell. Physiol.* **1992,** 152, (2), 430-440.

26. Guimond, S.; Maccarana, M.; Olwin, B. B.; Lindahl, U.; Rapraeger, A. C., Activating and Inhibitory Heparin Sequences for FGF-2 (Basic FGF) - Distinct Requirements for FGF-1, FGF-2, and FGF-4. *J. Biol. Chem.* **1993,** 268, (32), 23906-23914.

27. Berry, D.; Kwan, C. P.; Shriver, Z.; Venkataraman, G.; Sasisekharan, R., Distinct heparan sulfate glycosaminoglycans are responsible for mediating fibroblast growth factor-2 biological activity through different fibroblast growth factor receptors. *FASEB J.* **2001,** 15, (6), 1422-1424.

28. Taylor, K. R.; Rudisill, J. A.; Gallo, R. L., Structural and sequence motifs in dermatan sulfate for promoting fibroblast growth factor-2 (FGF-2) and FGF-7 activity. *J. Biol. Chem.* **2005,** 280, (7), 5300-5306.

29. Princz, M. A.; Sheardown, H., Heparin-modified dendrimer cross-linked collagen matrices for the delivery of basic fibroblast growth factor (FGF-2). *J. Biomater. Sci., Polym. Ed.* **2008,** 19, (9), 1201-1218.

30. Boddohi, S.; Kipper, M. J., Engineering Nanoassemblies of Polysaccharides. *Adv. Mater.* **2010,** 22, (28), 2998-3016.

31. Papagiannopoulos, A.; Waigh, T. A.; Hardingham, T.; Heinrich, M., Solution structure and dynamics of cartilage aggrecan. *Biomacromolecules* **2006,** 7, (7), 2162-2172.

32. Knudson, C. B.; Knudson, W., Cartilage proteoglycans. *Semin. Cell Dev. Biol.* **2001,** 12, (2), 69-78.

33. Zoeller, J. J.; Whitelock, J. M.; Iozzo, R. V., Perlecan regulates developmental angiogenesis by modulating the VEGF-VEGFR2 axis. *Matrix Biol.* **2009,** 28, (5), 284-291.

34. Ng, L.; Grodzinsky, A. J.; Patwari, P.; Sandy, J.; Plaas, A.; Ortiz, C., Individual cartilage aggrecan macromolecules and their constituent glycosaminoglycans visualized via atomic force microscopy. *J. Struct. Biol.* **2003,** 143, (3), 242-257.

35. Horkay, F.; Basser, P. J.; Hecht, A. M.; Geissler, E., Gel-like behavior in aggrecan assemblies. *J. Chem. Phys.* **2008,** 128, (13).

36. Sakiyama-Elbert, S. E.; Hubbell, J. A., Development of fibrin derivatives for controlled release of heparin-binding growth factors. *J. Controlled Release* **2000,** 65, (3), 389-402.

37. Liu, Z. G.; Jiao, Y. P.; Liu, F. N.; Zhang, Z. Y., Heparin/chitosan nanoparticle carriers prepared by polyelectrolyte complexation. *J. Biomed. Mater. Res., Part A* **2007,** 83A, (3), 806-812.

38. Chen, M. C.; Wong, H. S.; Lin, K. J.; Chen, H. L.; Wey, S. P.; Sonaje, K.; Lin, Y. H.; Chu, C. Y.; Sung, H. W., The characteristics, biodistribution and bioavailability of a chitosan-based nanoparticulate system for the oral delivery of heparin. *Biomaterials* **2009,** 30, (34), 6629-6637.

39. Martins, A. F.; Pereira, A. G. B.; Fajardo, A. R.; Rubira, A. F.; Muniz, E. C., Characterization of polyelectrolytes complexes based on N,N,N-trimethyl chitosan/heparin prepared at different pH conditions. *Carbohydr. Polym.* **2011,** 86, (3), 1266-1272.

40. Fajardo, A. R.; Lopes, L. C.; Valente, A. J. M.; Rubira, A. F.; Muniz, E. C., Effect of stoichiometry and pH on the structure and properties of Chitosan/Chondroitin sulfate complexes. *Colloid Polym. Sci.* **2011,** 289, (15-16), 1739-1748.

41. Drogoz, A.; David, L.; Rochas, C.; Domard, A.; Delair, T., Polyelectrolyte complexes from polysaccharides: Formation and stoichiometry monitoring. *Langmuir* **2007,** 23, (22), 10950-10958.

42. Schatz, C.; Domard, A.; Viton, C.; Pichot, C.; Delair, T., Versatile and efficient formation of colloids of biopolymer-based polyelectrolyte complexes. *Biomacromolecules* **2004,** 5, (5), 1882-1892.

43. Almodovar, J.; Kipper, M. J., Coating Electrospun Chitosan Nanofibers with Polyelectrolyte Multilayers Using the Polysaccharides Heparin and N,N,N-Trimethyl Chitosan. *Macromol. Biosci.* **2011,** 11, (1), 72-76.

44. de Britto, D.; Assis, O. B. G., A novel method for obtaining a quaternary salt of chitosan. *Carbohydr. Polym.* **2007,** 69, (2), 305-310.

45. Boddohi, S.; Almodovar, J.; Zhang, H.; Johnson, P. A.; Kipper, M. J., Layer-by-layer assembly of polysaccharide-based nanostructured surfaces containing polyelectrolyte complex nanoparticles. *Colloids Surf., B* **2010,** 77, (1), 60-68.

46. Boddohi, S.; Moore, N.; Johnson, P. A.; Kipper, M. J., Polysaccharide-Based Polyelectrolyte Complex Nanoparticles from Chitosan, Heparin, and Hyaluronan. *Biomacromolecules* **2009,** 10, (6), 1402-1409.

47. Paliwal, R.; Paliwal, S. R.; Agrawal, G. P.; Vyas, S. P., Chitosan nanoconstructs for improved oral delivery of low molecular weight heparin: In vitro and in vivo evaluation. *Int. J. Pharm.* **2012,** 422, (1-2), 179-184.

48. Yeh, M. K.; Cheng, K. M.; Hu, C. S.; Huang, Y. C.; Young, J. J., Novel protein-loaded chondroitin sulfate-chitosan nanoparticles: Preparation and characterization. *Acta Biomater.* **2011,** 7, (10), 3804-3812.

49. Chauvierre, C.; Labarre, D.; Couvreur, P.; Vauthier, C., Novel polysaccharide-decorated poly(isobutyl cyanoacrylate) nanoparticles. *Pharm. Res.* **2003,** 20, (11), 1786-1793.

50. Dautzenberg, H.; Jaeger, W., Effect of charge density on the formation and salt stability of polyelectrolyte complexes. *Macromol. Chem. Phys.* **2002,** 203, (14), 2095-2102.

51. Almodovar, J.; Place, L. W.; Gogolski, J.; Erickson, K.; Kipper, M. J., Layer-by-Layer Assembly of Polysaccharide-Based Polyelectrolyte Multilayers: A Spectroscopic Study of Hydrophilicity, Composition, and Ion Pairing. *Biomacromolecules* **2011,** 12, (7), 2755-2765.

52. Mulloy, B.; Rider, C. C., Cytokines and proteoglycans: an introductory overview. *Biochem. Soc. Trans.* **2006,** 34, 409-413.

53. Asada, M.; Shinomiya, M.; Suzuki, M.; Honda, E.; Sugimoto, R.; Ikekita, M.; Imamura, T., Glycosaminoglycan affinity of the complete fibroblast growth factor family. *Biochim. Biophys. Acta, Gen. Subj.* **2009,** 1790, (1), 40-48.

54. Sanantonio, J. D.; Lander, A. D.; Wright, T. C.; Karnovsky, M. J., Heparin Inhibits the Attachment and Growth of BALB/C-3T3 Fibroblacsts on Collagen Substrata. *J. Cell. Physiol.* **1992,** 150, (1), 8-16.

55. Costa, L. S.; Fidelis, G. P.; Cordeiro, S. L.; Oliveira, R. M.; Sabry, D. A.; Camara, R. B. G.; Nobre, L.; Costa, M.; Almeida-Lima, J.; Farias, E. H. C.; Leite, E. L.; Rocha, H. A. O.,

Biological activities of sulfated polysaccharides from tropical seaweeds. *Biomed. Pharmacother.* **2010,** 64, (1), 21-28.

56. Stevan, F.; Oliveira, M.; Bucchi, D.; Noseda, M.; Iacomini, M.; Duarte, M., Cytotoxic effects against HeLa cells of polysaccharides from seaweeds. *J. Submicrosc. Cytol. Pathol* **2001,** 33, 477-484.

57. Chandran, P. L.; Horkay, F., Aggrecan, an unusual polyelectrolyte: Review of solution behavior and physiological implications. *Acta Biomater.* **2012,** 8, (1), 3-12.

58. Funderburgh, J. L., Keratan sulfate: structure, biosynthesis, and function. *Glycobiology* **2000,** 10, (10), 951-958.

CHAPTER 4

Synthesis and Characterization of Proteoglycan-mimetic Graft Copolymers[4]

4.1 SUMMARY.

Proteoglycans are found on the cell surface and in the extracellular matrix (ECM). They are made up of a core protein with glycosaminoglycan (GAG) side chains. Proteoglycans derive the majority of their function from their GAG side chains. Variations in composition and number of GAG side chains lead to a vast array of proteoglycan sizes and functionalities. Here we present a reaction scheme for the synthesis of a proteoglycan-mimetic graft copolymer with tunable side-chain composition. This is done using three different GAGs, hyaluronan, chondroitin sulfate, and heparin. Hyaluronan is modified along its backbone with thiols and then functionalized with a maleimide-hydrazide bifunctional coupling agent. Finally, either chondroitin sulfate or heparin is grafted on to the hyaluronan backbone through reductive amination. This is done with four different ratios of GAG side chain to produce graft copolymers over a range of sizes. The chemistry was confirmed through ATR-FTIR and proton NMR. Effective hydrodynamic diameter and zeta potential were determined using dynamic light scattering and electrophoretic mobility. Graft copolymers were tested for their ability to bind and deliver basic fibroblast growth factor (FGF-2) to mesenchymal stem cells (MSCs) and a pilot study was done to test their mechanical properties. Peak changes in the ATR-FTIR and the proton NMR spectra confirmed the success of the proposed reaction scheme. Dynamic light

[4]Portions of this chapter appear in the following:
Place, L.W., Kelly, S. M., and Kipper, M.J.; "Synthesis and Characterization of Proteoglycan-mimetic Graft Copolymers", in prep for submission to *Biomacromolecules,* 2014.
Kelly, S.M., "Synthesis of Proteoglycan Mimetic Graft Copolymers for Application in Regenerative Medicine in the Inflammatory Disease Osteoarthritis", Colorado State University Honors Thesis (Fort Collins, CO), May 2014.

scattering showed an increase in effective hydrodynamic diameter with grafting density resulting in a range from 90-500 nm. Zeta potential was negative for all conditions and generally becomes more negative with higher grafting density. In the FGF-2 study, the CS containing graft copolymers exhibited higher MSC activity than the Hep 1:1, but was similar to the Hep 1:30. The CS conditions and the Hep 1:30 performed equally as well as when FGF-2 was delivered in solution. When preliminary dynamic mechanical testing was performed, hydrogels containing the copolymers saw changes in maximum modulus with compression frequency. These results show much promise for the use of these graft copolymers to impart bio-functionality to a tissue engineering scaffold.

4.2 INTRODUCTION.

Proteoglycans are important in proper tissue function. They are found on the cell surface and in the extracellular matrix (ECM). [1, 2] Proteoglycans are made up of a core protein with glycosaminoglycan (GAG) side chains.[3, 4] Due to variations in composition and number of GAG side chains, proteoglycans come in a wide array of sizes and functionalities. GAGs are linear polysaccharides made up of repeating disaccharide units. There are five major types of GAGs, keratan, dermatan, heparan, chondroitin, and hyaluronan. This work focuses on heparin (Hep), chondroitin sulfate (CS), and hyaluronan (HA). Representative chemical structures of these are shown in Figure 4.1.

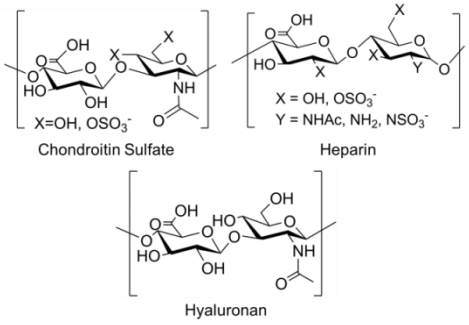

Figure 4.1. Chemical structures of GAGs used in this proposed synthesis

CS and Hep are both sulfated, whereas HA is not, all three are negatively charged at physiological pH, and can have molecular weights ranging from thousands to millions of Daltons. In proteoglycans the GAG chains are often in close proximity resulting in high anionic charge density, and thus, high osmotic pressure. [5-7] This leads to hydrophilicity, providing lubricity and compressive strength to tissues.

Additionally, GAGs play a variety of roles in cell signaling. They bind to cell surface integrins and localize cytokines in the ECM. This sequesters the cytokines in a reservoir and protects them from proteinase degradation.[8-10] They often form a GAG-cell-cytokine complex that enhances regulation of cell adhesion, migration, proliferation, and differentiation.

CS is found in many proteoglycans including aggrecan, biglycan, and syndecan. Aggrecan is the largest proteoglycan, containing up to 100 CS side chains.[5] Strong electrostatic repulsions between the CS chains results in the bottle-brush structure seen in Figure 4.2.

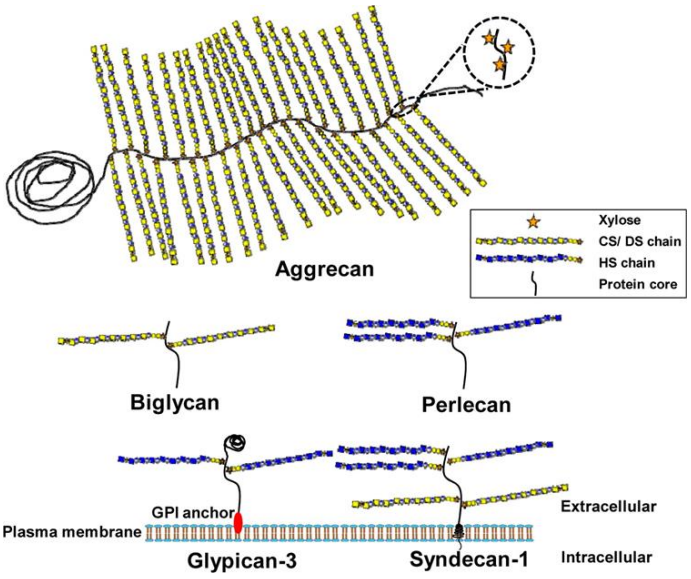

Figure 4.2. Schematic of common proteoglycans. (Reprinted from ACS Chemical Biology, 8/5, V.M. Tran, T.K.N. Nguyen, V. Sorna, D. Loganathan, B. Kuberan, Synthesis and Assessment of Glycosaminoglycan Priming Activity of Cluster-xylosides for Potential Use as Proteoglycan Mimetics, 949-957, Copyright 2013,with permission from American Chemical Society.)

The high charge density of aggrecan makes it very hydrophilic and causes it to swell in solution. Several studies have found that it exhibits a contour length of 300–500 nm.[5, 11] In this swollen state aggrecan imparts lubricity and compressive strength to tissues such as cartilage, the intervertebral disc, and the vitreous humor of the eye. [5, 12] In addition to biomechanical properties, CS also participates in biochemical signaling. CS binds growth factors and supports cell function when used in tissue engineering scaffolds.[6, 13-15] It also improves wound healing and has been used for the treatment of osteoarthritis and atherosclerosis[13, 16-20]

Hep is generally found in intracellular granules of mast cells. [5, 21] It has the highest negative charge density of any known biopolymer, and is structurally similar to the GAG heparan sulfate (HS). HS is found as side chains on proteoglycans such as syndecan, glypican, and perlecan. Because of its similarity to HS and commercial availability, Hep is often used in place of HS in experimental work.[8] These HS containing proteoglycans are the primary proteoglycans found in the glycocalyx. The glycocalyx is a coating found on the surface of most eukaryotic cells, and is of particular importance in the endothelium.[5] Syndecan and glypican are bound to the cell membrane and perlecan is excreted into the ECM where it assembles with collagen to form the structure of the basement membrane. A schematic of these various proteoglycans is displayed in Figure 4.2. These proteoglycans assemble with other macromolecules to form a hydrophilic network that shapes the function of the endothelial glycocalyx.[22-24] This structure is lubricious, aiding in the motion of red blood cells and inhibiting platelet and leukocyte adhesion.[5, 25, 26] This layer governs the interactions of all blood components with the endothelium including plasma proteins, enzymes, growth factors, and cytokines, which are crucial for homeostasis and preventing thrombosis.[5, 22, 25] Similar to CS, Hep also has the ability to bind and stabilize growth factors. There is a class of growth factors

that are referred to as "heparin-binding" because they are stabilized through interactions with Hep/HS. Additionally, Hep/HS exhibit ligands to integrins on the cell surface that aid in signaling. [1, 27]

HA is the only un-sulfated GAG and tends to have a much higher molecular weight than other GAGs. [6] HA is widely distributed throughout many tissues including skin, eye, connective, epithelial, endothelial, and neural tissues, where it provides lubricity and plays an active role in wound healing. [6, 13, 25, 28] It is used clinically to treat osteoarthritis. An injection directly into the joint is reported to restore lubricity and improve joint function.[13, 29, 30]

Cytokines such as growth factors provide signaling cues to cells for adhesion, migration, proliferation, and differentiation. They are involved in a variety of pathways: for wound healing, differentiation, and vascularization. [31-35] They have been used clinically to treat cardiovascular and bone diseases, and have been proposed for tissue engineering of nerves, bladders, blood vessels, and osteochondral defects.[35-42] However, the therapeutic potential of growth factors is mitigated by their relative instability. Members of the fibroblast growth factor (FGF) family have half-lives on the order of minutes.[31, 43, 44] As a result, large doses and multiple treatments are required for clinical effectiveness.[31, 45-47] Thus, stabilization is essential if the potential of these proteins is to be exploited. It has been well demonstrated in literature and by our group that both Hep and CS bind growth factor for delivery to cells.[35, 43, 45, 48]

Proteoglycans impart crucial functionality to tissues. Attempts have been made to mimic the structure and function of various proteoglycans for tissue engineering applications. The Panitch group has published several papers on the synthesis and functionality of proteoglycan-mimics using dermatan sulfate, CS, and a peptide chain, dubbed peptidoglycans.[49-52] They demonstrated that their dermatan sulfate-based peptidoglycans bind to collagen, delay

fibrillogenesis, and increase mechanical properties of a collagen gel and of aligned collagen threads.[49-51] In another study, this group showed that their CS-based peptidoglycans enhance the mechanical properties of a collagen scaffold, protect the scaffold from proteolytic degradation, and regulate chondrocyte gene expression.[52] In proteoglycans, GAGs are bound only at their terminal end, thus functionalizing GAGs with a unique end-group is one strategy for synthesizing a proteoglycan-mimic. Sarkar et al. successfully functionalized a terminal group on CS with vinyl monomers to these ends. [53] Tran et al. designed a library of xylosides which are able to activate multiple GAG chains to bind to a scaffold to mimic proteoglycans.[54] Our group has created polyelectrolyte complexed nanoparticles (PCNs) through electrostatic interactions of Hep and CS with chitosan. These have similar size and composition to the proteoglycan aggrecan. We have also demonstrated that Hep-containing PCNs were superior to aggrecan for growth factor stabilization.[45]

The work herein proposes a method to synthesize proteoglycan-mimetic graft copolymers with variable composition and side chain density. This is done using HA as the backbone and either CS or Hep grafted on as the side chains. These can be tailored by type and number of side chains to create a library of graft copolymers that mimic any number of proteoglycans seen endogenously. Additionally, these graft copolymers were tested for their ability to bind and deliver growth factor to cells and pilot tests were done to explore their mechanical properties. We demonstrate successful synthesis of these graft copolymers with a wide range of sizes through attenuated total reflectance Fourier transform infrared spectroscopy, proton nuclear magnetic resonance, dynamic light scattering, and zeta potential measurements. We also illustrate the functionality of these graft copolymers through basic fibroblast growth factor delivery to mesenchymal stem cells and dynamic mechanical testing.

4.3 MATERIALS AND METHODS.

4.3.1 Materials. Chitosan (Chi; Protosan UP B 90/20, 5 % acetylated determined by ^{1}H NMR, M_w = 80 kDa; PDI = 1.52) was purchased from Novamatrix (Sandvika, Norway). Chondroitin sulfate sodium salt (CS; from shark cartilage, 6% sulfur, 6sulfate/4sulfate = 1.24, M_w = 84.3 kDa; PDI = 1.94), *N,N*-dimethylformamide (DMF; 99.8%, M_w = 73.09 g mol^{-1}), *N* (3-dimethylaminopropyl)-*N*′-ethylcarbodiimide hydrochloride (EDC; 98%), *N*-hydroxysuccinimide (NHS; 98%), MES sodium salt (99%, M_w = 217.22 g mol^{-1}), sodium chloride (99%, M_w = 58.44 g mol^{-1}), sodium hydroxide (97%, M_w = 40.00 g mol^{-1}), cysteamine hydrochloride (98%, M_w = 113.61 g mol^{-1}), and sodium triacetoxyborohydride (STAB; 97%, M_w = 211.94 g mol^{-1}) were purchased from Sigma-Aldrich (St. Louis, MO). Heparin sodium was purchased from Celsus Laboratories (Hep; from porcine intestinal mucosa, 12.5 % sulfur, Mw = 14.4 kDa; PDI = 1.14, Cincinnati, OH). 5,5'-Dithio-bis-[2-nitrobenzoic acid] (Ellman's reagent; M_w = 396.35 g mol^{-1}), *N*-[ß-maleimidopropionic acid] hydrazide trifluoroacetic acid salt (BMPH; M_w = 297.19 g mol^{-1}), seamless cellulose dialysis tubing (12kDa MWCO), sodium hyaluronate (HA; 95%, M_w = 740 kDa), sodium acetate, sodium phosphate dibasic, sodium phosphate monobasic, agarose, tris(2-carboxyethyl)phosphine hydrochloride (TCEP-HCl; M_w = 286.65 g mol^{-1}), and Zeba Spin Desalting Columns (10 mL, 7K MWCO) were purchased from Thermo Fisher Scientific (Waltham, MA). Biotech cellulose ester membrane dialysis tubing (300kDa MWCO) was purchased from Spectrum Laboratories (Rancho Dominguez, CA). Glacial acetic acid was purchased from Acros Organics (Geel, Belgium). Recombinant human FGF basic (FGF-2) 146 aa (carrier free) was purchased from R&D Systems (Minneapolis, MN). Human fibronectin was purchased from BD Biosciences (Bedford, MA). 4′6 Diamidino-2-phenylindole•2HCl (DAPI) was purchased from Thermo-Scientific

(Rockford, IL). CellTiter-Blue® Cell Viability Assay was purchased from Promega (Madison, WI). Fetal bovine serum (FBS), 0.25 % trypsin with EDTA, low-glucose Dulbecco's modified Eagle's medium (D-MEM), minimum essential medium alpha (α-MEM; supplemented with L-glutamine, ribonucleosides, and deoxyribonucleosides), and Dulbecco's phosphate buffered saline (DPBS) without Ca^{2+} and Mg^{2+} were purchased from HyClone (Logan, UT). Antibiotic-antimycotic (anti/anti), 1 M HEPES buffer solution, and Dulbecco's phosphate buffered saline with Ca^{2+} and Mg^{2+} were purchased from Gibco (Grand Island, NY). A Millipore Synthesis water purification unit (Millipore, Billerica, MA) was used to obtain ultrapure; 18.2 MΩ•cm water (diH_2O), used for making all aqueous solutions.

4.3.2 Synthesis. There are three reactions in the synthesis of these graft copolymers: thiolation of HA (Figure 4.3.), BMPH modification of HA (Figure 4.4), and GAG coupling via reductive amination (Figure 4.5).

4.3.2.1 Thiolation of HA. The procedure used by Damodaran et al. to thiolate dextran was adapted for thiolating HA.[55] 250 mg of HA was dissolved into 50 mL of MES activation buffer (0.1 M MES, 0.5 M NaCl, pH 6.0) in a 45 °C oil bath and allowed to dissolve overnight. The solution was cooled to room temperature the following morning. EDC-HCl was added to the activation buffer in a 10× molar excess (0.645 g, 191.7 g mol^{-1}) and allowed to react for two hours in order to activate the carboxylate functional group on HA. Following the two hour activation step, the pH was raised to 7.2 using sodium hydroxide. Cysteamine hydrochloride (0.88 g, 23× molar excess compared to HA starting material) was added to the reaction solution and the reaction was allowed to continue for five hours. After this time, the mixture was taken off of the stir plate and placed in dialysis tubing (12 kDa MWCO), where they were dialyzed over the period of 5 days from 0.5 M NaCl to 0.25 M NaCl, 0.1 M NaCl, 0.05 M NaCl, and

finally to diH_2O in order to rid the sample solution of excess cysteamine hydrochloride and EDC. Following the dialysis step, the samples were lyophilized in order to recover a solid, pure thiolated HA (HA-SH) intermediate (324 mg). This intermediate was analyzed for thiol content using the Ellman's reagent test according to manufacturer's instructions.

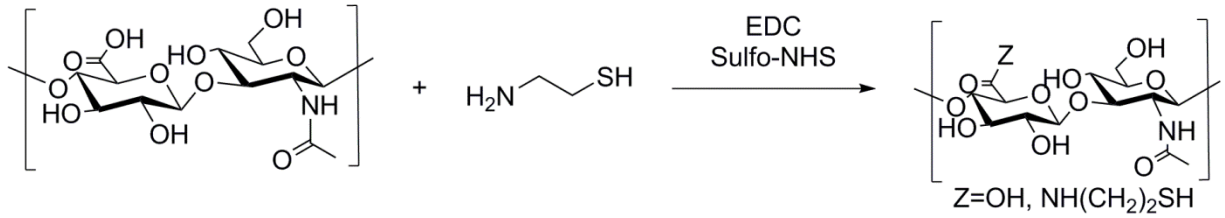

Figure 4.3. Schematic of HA thiolation with cysteamine through EDC, sulfo-NHS coupling to form HA-SH.

4.3.2.2 Coupling BMPH to HA-SH. Before coupling BMPH to HA-SH, HA-SH was reacted with TCEP to reduce any disulfide bonds. This was accomplished by dissolving 100 mg of HA-SH in 20 mL of phosphate buffered saline (PBS) (0.1 M sodium phosphate, 0.15 M NaCl, pH 8). TCEP (114 mg) was dissolved in the solution and the reduction was carried out for one hour. After one hour, the reaction solution was passed through desalting columns to exchange the reaction solution with PBS (0.1M sodium phosphate, 0.15M NaCl, pH 7.2).

Next, 73 mg of BMPH was added to the solution and the coupling reaction proceeded for two hours at room temperature. The solution was then dialyzed as in the thiolation reaction to remove any unreacted BMPH and lyophilized, yielding pure solid HA-BMPH (110 mg).

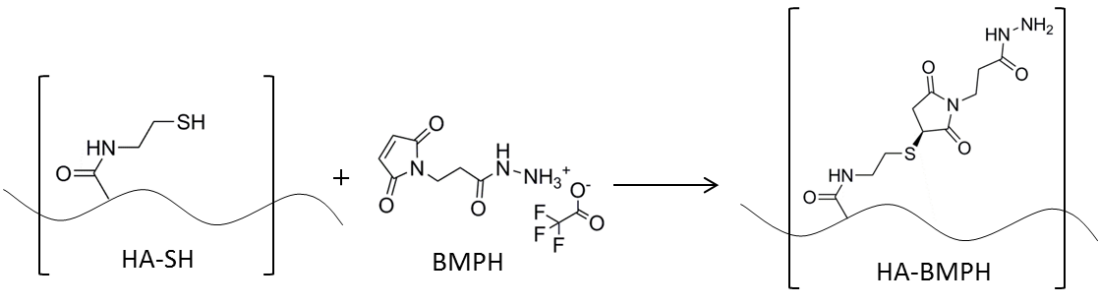

Figure 4.4. Schematic of HA-SH activation with BMPH through maleimide-thiol coupling to form HA-BMPH.

4.3.2.3 Coupling CS/Hep to HA-BMPH via Reductive Amination. Eight different compositions of graft copolymers were synthesized; four different ratios of either CS or Hep to HA-BMPH (1:1, 1:3, 1:10, and 1:30). The ratios were determined on a thiol content basis determined by Ellman's reagent described in the previous section. The 1:1 ratio is one CS or Hep chain for every one thiol group on an HA-SH chain, 1:3 is one CS or Hep chain for every three thiols, 1:10 is one CS or Hep chain for every ten thiols, and 1:30 is one CS or Hep chain for every 30 thiols. This protocol was adapted from Sisu et al. and Dalpathado et al.[56, 57] HA-BMPH (15 mg) was placed into a round-bottom flask, the flask was sealed, and 10 mL of anhydrous DMF were added. The flask was then purged with nitrogen. After purging, 350 μL of acetic acid was added and the reaction vessel was step-wise heated from 25 °C to 85 °C in 10 °C increments over a period of two hours. During this time, 1 g of sodium triacetoxyborohydride (STAB, 100x molar excess) was dissolved in 10 mL of anhydrous DMF in a separate round-bottom flask and purged with nitrogen. After the two hour heating, 356 μL of STAB was added to the reaction vessel, and every two hours for a total of ten hours (1.78 mL of STAB). The reaction was allowed to run overnight. After reaction, samples were heated to 60 °C under vacuum to remove DMF, dissolved in diH_2O and dialyzed as described above. The samples were then lyophilized and the recovered product was a white powder.

4.3.4 Chemical Characterization. Neat polymers, synthesis intermediates, and products at the different ratios were analyzed using attenuated total reflectance Fourier transform infrared spectroscopy (ATR-FTIR) and proton nuclear magnetic resonance (^{1}H NMR).

4.3.4.1 ATR-FTIR. A Nicolet 6700 spectrometer (Thermo Electron Corporation, Madison, WI) was used to perform ATR-FTIR on intermediate samples and graft copolymer

products to confirm coupling chemistry. A Smart iTR ATR sampling accessory was used with a ZnSe crystal to collect spectra from 4000 - 650 cm^{-1}.

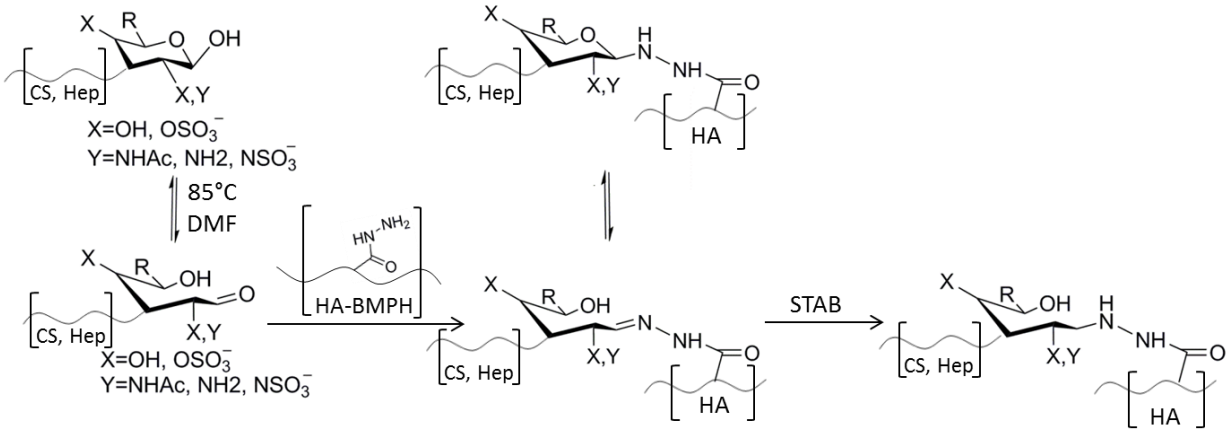

Figure 4.5. Schematic of GAG coupling with HA-BMPH to form graft copolymers through reductive amination.

4.3.4.2 NMR. The samples were dissolved in D_2O at concentrations of 1-5 mg mL^{-1} depending on sample solubility. A 400 MHz spectrometer (Agilent Varian 400MR) equipped with automated tuning and a 7600 sample changer was used for ^1H NMR spectra acquisition. The following parameters were used, of 64 scans, 5 seconds relaxation time, and 25 °C.

4.3.3 DLS and Zeta Potential. Hydrodynamic diameter of the graft copolymers and the neat polymers was measured by dynamic light scattering (DLS) using a 90Plus/BI-MAS (Brookhaven Instruments, Holtsville, NY). All samples were dissolved in PBS to concentrations of 5 mg mL^{-1}. Measurements were taken at 25 °C at a fixed angle of 90°, 1 min per measurement. The values reported are the mean effective diameter for each sample. For zeta potential, samples were dialyzed against diH_2O (300 kDa MWCO) for 24 hours to remove any unreacted polymer, lyophilized and dissolved in PBS at 5 mg mL^{-1}. The zeta potential was then measured using the same instrument as in DLS, via electrophoretic light scattering (ELS). Each sample was measured five times, 30 scans each, at 25 °C and the values reported are the mean zeta potential for each sample ± the standard error of the mean.

4.3.5 Cell Harvest and Culture. The cell harvesting and expansion procedure is described in detail in our previous work.[31] Bone marrow aspirates from the iliac crest of female sheep were centrifuged. The supernatant containing the nucleated cells was mixed with growth media (low-glucose D-MEM with 10 % FBS, 1 % anti/anti, and 2.5 % HEPES) and seeded into culture flasks. After 24 h, the media was changed to remove all non-adherent cells. The marrow stromal cell (MSC) colonies were allowed to grow for at least seven days, then the cells were trypsinized, counted, and reseeded in culture flasks using maintenance media for culture expansion (α-MEM with 10 % FBS, 1 % anti/anti, and 2.5 % HEPES). MSCs were cryo-preserved prior to seeding into experimental conditions. Cells were not used beyond the fifth passage.

4.3.6 Preparing Surfaces for FGF Delivery. To test FGF-2 delivery from graft copolymers, a tissue culture polystyrene (TCPS) 96-well plate was coated with Chi-Hep or Chi-CS polyelectrolyte multilayers (PEMs) with Chi, Hep, CS, or different compositions of graft copolymers as the terminal layer, and FGF-2 was delivered via adsorption, solution as the positive control, or not at all for the negative control. Experimental conditions are displayed in Table 4.1 The deposition of PEMs is a facile method to coat a surface whereby two solutions containing oppositely charged polyelectrolytes are alternated until a desired thickness is attained. The procedure used here was adapted from Boddohi et al.[58] Chi, Hep, CS, and graft copolymer solutions were prepared in acetate buffer (0.2 M, pH 5). Chi and Hep were dissolved at a concentration of 0.01 M (on a saccharide unit basis). CS was prepared at a concentration of 0.02 M because it has half as many sulfate groups as Hep. Graft copolymers were dissolved at 5 mg mL^{-1}. A rinse solution was prepared by adjusting the pH of diH_2O to 4 with acetic acid. Chi, Hep, CS, and rinse solutions were filtered with a 0.22 μm polyvinylidene fluoride (PVDF)

syringe filters (Fisher Scientific). All graft copolymers were dialyzed (300 kDa MWCO) against diH_2O for 24 hours and lyophilized before use. PEM construction was done by alternating adsorption and rinse steps as follows.; 100 μL of solution was added to each well and adsorbed under gentle agitation for five minutes. Five layers of either Chi-Hep or Chi-CS were adsorbed. The sixth layer contained Hep, CS, or graft copolymer, and Chi-terminated samples were constructed with seven layers. All surfaces were produced in triplicate. Surfaces were then sterilized with 70 % ethanol for 15 minutes, and rinsed with sterile PBS prior to protein adsorption and cell seeding. For adsorbing FGF-2, 100 μL (100 ng mL^{-1} in diH_2O) was placed in each well of the 96-well plate and allowed to adsorb for two hours under gentle agitation. The FGF-2 solution was then aspirated, and the wells were rinsed with sterile PBS. All surfaces were coated with fibronectin (10 μg mL^{-1} in diH_2O); 100 μL was placed in each well of the 96-well plate for one hour under static conditions. The fibronectin solution was then aspirated and the surfaces were rinsed with sterile PBS.

Table 4.1. Conditions for MSC response to FGF-2 delivered from surfaces.

PEM Type	Mode of FGF Delivery		
$[Chi\text{-}CS]_3$-Chi	None	Soluble	Adsorbed
$[Chi\text{-}CS]_3$	None	Soluble	Adsorbed
$[Chi\text{-}CS]_2$-ChiCS1-1	None	Soluble	Adsorbed
$[Chi\text{-}CS]_2$-Chi-CS 1-30	None	Soluble	Adsorbed
$[Chi\text{-}Hep]_3$-Chi	None	Soluble	Adsorbed
$[Chi\text{-}Hep]_3$	None	Soluble	Adsorbed
$[Chi\text{-}Hep]_2$-Chi-Hep 1-1	None	Soluble	Adsorbed
$[Chi\text{-}Hep]_2$-Chi-Hep 1-30	None	Soluble	Adsorbed

4.3.7 MSC Response to FGF-2, Graft Copolymers, and FGF-2 bound to Graft Copolymers. MSCs were seeded at a density of 7000 cells cm^{-2} in α-MEM (10 % FBS) and allowed to attach for three hours. At this time the media was aspirated and replaced with low-serum media (2.5 % FBS) because under these conditions ovine MSCs do not proliferate

unless stimulated by FGF-2.[45] FGF-2 delivered in solution at 1 ng mL^{-1} has been identified as the optimal mitogenic dose for ovine MSCs and thus was used as the positive control.[31] Cultures were maintained for four days, with a medium change on day two with FGF-2 (1 ng mL^{-1}) included in the media change for positive control samples, no additional FGF-2 was provided for samples with FGF-2 adsorbed on the surface. To evaluate FGF-2 delivery CellTiter-Blue Cell Viability Assay was performed on day two and day four. Additionally, on day four, cultures were evaluated via microscopy. Cells were fixed with glutaraldehyde (2 % in DPBS with Ca^{2+} and Mg^{2+}) for 45 minutes at 4 °C, and then stained with DAPI (1 μg mL^{-1} in DPBS with Ca^{2+} and Mg^{2+}) for 15 minutes at room temperature. The wells were rinsed with DPBS with Ca^{2+} and Mg^{2+} between each step, and protected from light. After fixing and staining, surfaces were stored dry, protected from light, at 4 °C until microscopy was performed. Images were obtained using a 4× objective on an Olympus IX70 epi-fluorescence microscope (Center Valley, PA) equipped with a QImaging Micropublisher camera with an appropriate filter for DAPI.

4.3.8 Dynamic Mechanical Analysis (DMA). A pilot study to test mechanical properties of the graft copolymers was performed. Hydrogels containing 2.5 % w/v polymer in diH_2O were formed using agarose or a mixture of 90 % agarose 10 % GAG or graft copolymer. Different compositions of hydrogels tested are displayed in Table 4.3. Agarose powder was mixed with diH_2O and heated to 90 °C for three hours for dissolution, at this time the temperature was allowed to cool to 60 °C. GAG or graft copolymer was added and solutions were stirred for one hour at 60 °C. Solutions were then poured into an untreated 48-well plate and left to set overnight. DMA was performed on a servo-hydraulic mechanical test system (Bionic Model 370.02 MTS Corp, Eden Prairie, MN) with 10 lb S beam load cell (LSB303 Futek, Irvine, CA). Samples were first preloaded with 0.05 N, and then subjected to cyclic loading between 0 and 10

% compressive strain at 0.05 Hz, 0.5 Hz, and 5 Hz for 5 cycles. Stress, strain, phase, and amplitude were calculated using a custom Matlab (Mathworks, Natick, MA) code. Stress versus strain was then graphed and fit with a two-parameter function to find the modulus at 0 % strain and at 10 % strain for each sample using a custom code written in IgorPro (version 5.0.5.7, Wave Metrics, Portland, OR). The two-parameter function, shown in Equation 4.1, was adapted from Park et al.[59]

$$-\sigma = A\left(1 - e^{-B(1-\lambda)}\right) \qquad \textbf{Equation 4.1}$$

Where $-\sigma$ is stress, $(1-\lambda)$ is strain, and A and B are fit parameters.

Table 4.2. List of Hydrogel Types for DMA Testing.

Gel Type		Composition
Control Hydrogels	Agarose	2.5 % Agarose
	HA	2.25 % Agarose, 0.25 % HA
	CS	2.25 % Agarose, 0.25 % CS
	Hep	2.25 % Agarose, 0.25 % Hep
Copolymer Hydrogels	CS 1:1	2.25 % Agarose, 0.25 % CS 1:1
	CS 1:30	2.25 % Agarose, 0.25 % CS1:30
	Hep 1:1	2.25 % Agarose, 0.25 % Hep 1:1
	Hep 1:30	2.25 % Agarose, 0.25 % Hep 1:30

4.3.9 Statistics. Data analysis was performed using Minitab (Minitab, Inc., State College, PA), version 16. For CellTiter-Blue assay testing, comparisons between groups were performed via analysis of variance (ANOVA) models with Tukey's multiple comparison tests. Differences with $p < 0.05$ were considered statistically significant. CellTiter-Blue Data are expressed as the mean ± standard error of the mean ($n = 3$).

4.4 RESULTS AND DISCUSSION.

4.4.1 Chemical Characterization. Ellman's reagent was used to calculate thiol content on the HA-SH intermediate. It was found that approximately 50 % of the carboxylate groups,

present on each disaccharide of HA, were modified with thiol. This result was the basis used to determine stoichiometric ratios of GAG side chain to available grafting sites on HA. The 1:1 ratio is one CS or Hep chain for every one thiol group on an HA-SH backbone, 1:3 is one CS or Hep chain for every three thiols, 1:10 is one CS or Hep chain for every ten thiols, and 1:30 is one CS or Hep chain for every 30 thiols. This notation will be used throughout the results.

ATR-FTIR was conducted to qualitatively assess changes in the magnitude of characteristic peaks associated with the reaction scheme. A peak corresponding to the carbon-nitrogen bond formed when the sulfated GAGs are grafted onto the HA backbone was identified at approximately 1540 cm^{-1} and the peak for sulfate appears at approximately 1260 cm^{-1}. The spectra of the graft copolymers are displayed in Figure 4.6.

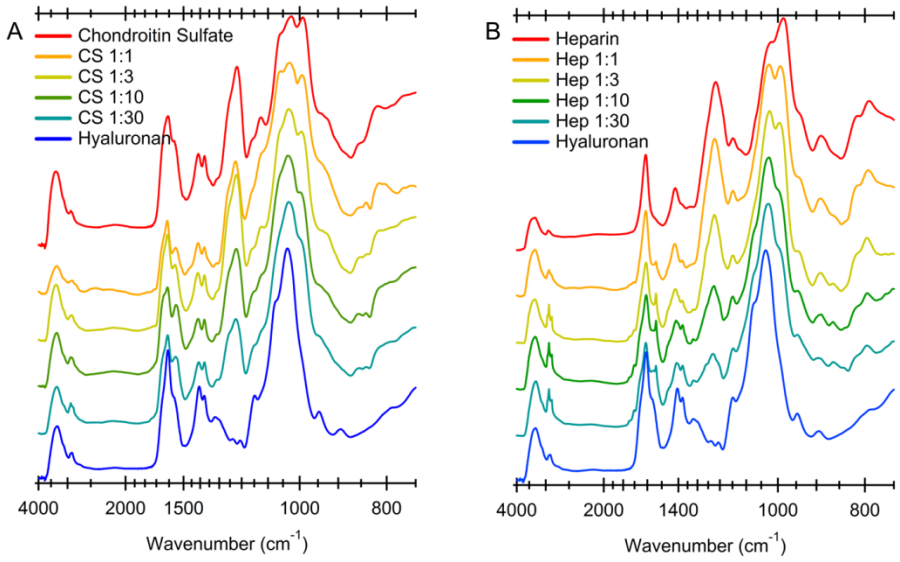

Figure 4.6. ATR-FTIR spectra of neat GAGs and graft copolymers made with A.) CS and B.) Hep. Carbon-nitrogen peak associated with grafting is located at 1540 cm^{-1} and sulfate peak is located at 1260 cm^{-1}. Changes in both peaks can be seen with change in grafting density.

The carbon-nitrogen bond formed during grafting presents as a sharp peak in the Hep spectra and as a shoulder in the CS spectra. The peak decreases with increasing grafting density because it is diluted by the addition of more GAG, additionally it has been seen that the presence of water reduces peak intensities of molecules involved in hydrogen bonding.[60] When more

hydrophilic GAG is present the relative humidity may also increase adding to the reduction in this peak. This peak is not seen in the HA-BMPH, spectra shown in the Appendix, indicating that coupling was successful. Sulfate groups are on CS and Hep, but not HA, thus changes in this peak are associated with the amount of CS or Hep present. For both the CS and Hep copolymers, a peak associated with the bond formed during grafting appear and the magnitude of the sulfate peak increases. This indicates that the CS and Hep are reacting with the hydrazide functional groups of the HA-BMPH backbone. There is also a large peak at 1000 cm^{-1} that is associated with saccharide ring breathing. There are shifts in shoulders on this peak between 1150 and 1050 cm^{-1}, and between 1000 and 950 cm^{-1} that occur with grafting density. Other spectra including samples before and after dialysis are shown in the Appendix. Additionally, ^{1}H NMR was done to further verify the chemistry. The spectra confirmed the thiolation and addition of BMPH onto HA. Upon modification with CS or Hep, the spectra exhibit changes which support the success of reductive amination. These spectra are shown in the Appendix.

4.4.2 DLS and Zeta Potential. DLS was conducted to determine the effective hydrodynamic diameter of each copolymer sample and the neat polymers. The diameters of both the CS and Hep bound copolymers increase with increasing grafting density. The CS copolymers range from approximately 90 nm to 450 nm in diameter. The Hep copolymers range from approximately 80 nm to 550 nm in diameter. The effective hydrodynamic diameters of the neat polymers are less than ten in all cases. A histogram of the results can be seen Figure 4.7. The DLS results indicate that synthesis of the graft copolymers has not only been achieved, but that controlling the degree of binding is possible as the size of the copolymers increases with increasing stoichiometric ratio. At the 1:1 stoichiometric ratio, both the CS and Hep copolymers have an effective hydrodynamic diameter of approximately 500 nm, which is comparable to that

of aggrecan.[11, 45] Proteoglycans come in a variety of compositions and sizes, with core proteins ranging from 20-400 kDa and from 1 to over 100 GAG side chains.[22, 61, 62] This results in a wide range of hydrodynamic diameters. The graft copolymers synthesized here exhibit an array of sizes from 90-500 nm.

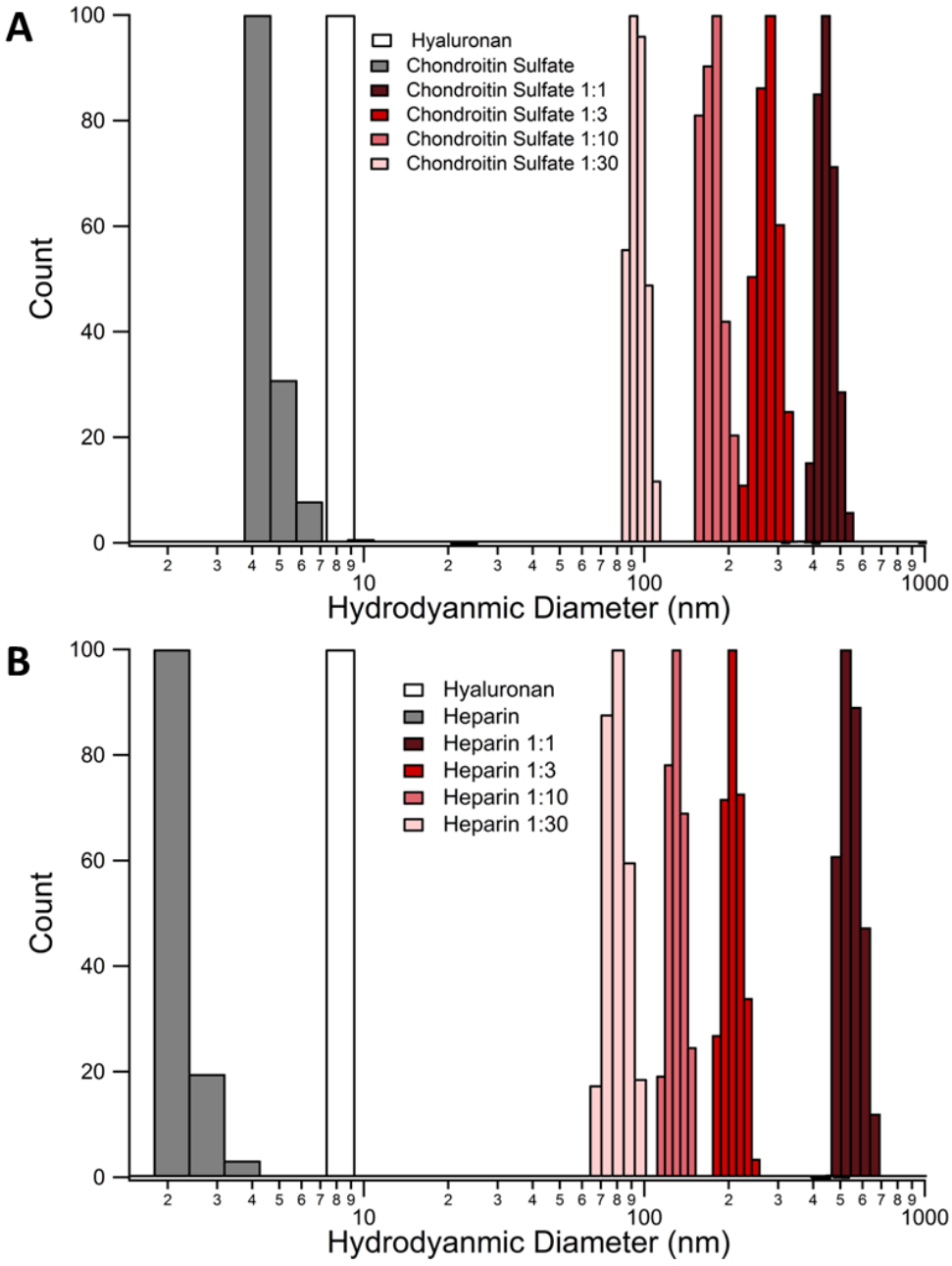

Figure 4.7. Histograms of the effective hydrodynamic diameter of neat polymers and graft copolymers made with A.) CS or B.) Hep.

Table 4.3. Zeta Potential Results.

Composition	ζ-Potential (mV)
HA	-23 ± 0.9
CS	-22 ± 1.3
CS 1:1	-34 ± 0.8
CS 1:3	-27 ± 0.9
CS 1:10	-29 ± 2.4
CS 1:30	-12 ± 1.8
Hep	-26 ± 2
Hep 1:1	-29 ± 0.9
Hep 1:3	-26 ± 2
Hep 1:10	-23 ± 2
Hep 1:30	-23 ± 1.6

Zeta potential measurements were also taken of the neat GAGs and the graft copolymers. The change in zeta potential with grafting density is shown in Table 4.4. The polymers HA, CS and Hep all have negative zeta potentials. For the graft copolymers, the charge density tends to decrease with increasing CS or Hep grafting density. In both cases the neat CS or Hep has a zeta potential corresponding to an intermediate copolymer graft density. After performing ATR-FTIR, ^{1}HNMR, DLS, and ZLS it is evident that both the CS and Hep side chains have bound to the HA backbone via BMPH to form these graft copolymers with an array of grafting densities.

4.4.3 MSC Response to FGF-2 delivered in solution or adsorbed to surfaces. Graft copolymers were tested for their ability to deliver FGF-2 to MSCs. Surfaces were coated with either Chi-CS or Chi-Hep PEMs, with the terminal layer being Chi, CS, Hep, CS 1:1, CS 1:30, Hep 1:1, or Hep 1:30. FGF-2 was then adsorbed to surfaces of each type in triplicate. MSCs were seeded onto these surfaces, onto surfaces without FGF-2 adsorbed but with FGF-2 delivered in solution, and onto surfaces with no FGF-2, and then cultured for four days. Samples were evaluated for cell activity via CellTiter-Blue Cell Viability Assay and stained with DAPI for imaging. The CellTiter-Blue results are displayed in Figure 4.8.

The surfaces containing CS are consistently higher than those containing Hep. In the CS case, the CS-terminated, CS 1:1-terminated, and CS 1:30-terminated surfaces do not perform any differently from each other, and on day 4 all perform better than the Chi-terminated samples. Additionally, all of these surfaces exhibit higher cell activity than their counterparts with no FGF-2. This indicates that both graft copolymer densities are able to deliver FGF-2 to MSCs as well as CS coated on the surface and as well as delivery in solution. The surfaces containing Hep generally exhibit lower cell activity than the CS surfaces. However, in the Hep1:30-terminated case activity levels are similar to those seen on CS surfaces. Additionally, FGF-2 adsorbed to the Hep 1:30 demonstrates similar levels as FGF-2 delivered in solution. Hep has been reported to interfere with cell attachment.[45] Low cell attachment could result in the lower levels of cell activity observed here. The Hep 1:30-terminated surface may contain less Hep than the other conditions resulting in higher initial cell adhesion. These results suggest that both grafting densities on the CS copolymer and the 1:30 Hep copolymer are able to bind FGF-2 and enhance cell activity. After culture, cells were fixed and stained with DAPI for imaging to further support the CellTiter-Blue data. The results from microscopy are in agreement with the cell activity assay. Images of the CS 1:30-terminated and the Hep 1:30-terminated samples with no FGF-2, FGF-2 delivered in solution, and FGF-2 adsorbed to the surface are displayed in Figure 4.9. Very few cells are seen in the samples with no FGF-2, and samples with FGF-2 delivered in solution look similar to those with FGF-2 adsorbed. This increase in cell number in the presence of FGF-2 indicates that the FGF-2 is active both when adsorbed to graft copolymers and when delivered in solution. These results are similar to those shown previously by our group with the use of GAG-rich PCNs. We have bound FGF-2 to GAG-rich PCNs and delivered them in solution and from electrospun nanofibers to MSCs. The MSCs exhibited upregulated cellular activity when

exposed to FGF-2 delivered from our PCNs and in some cases when delivered in solution.[43, 45] Delivery of growth factors in solution *in vivo* is impractical. Growth factors have a short half-life in the body on the order of minutes.[45, 63] In our previous work we demonstrated that while FGF-2 delivered in solution lost activity over time, our GAG-rich PCNs were able to sustain activity over 30 days.[43, 45] The graft copolymers described in this work exhibit the ability to bind FGF-2 and have the potential for incorporation into an implant for delivery of growth factor to sites of healing.

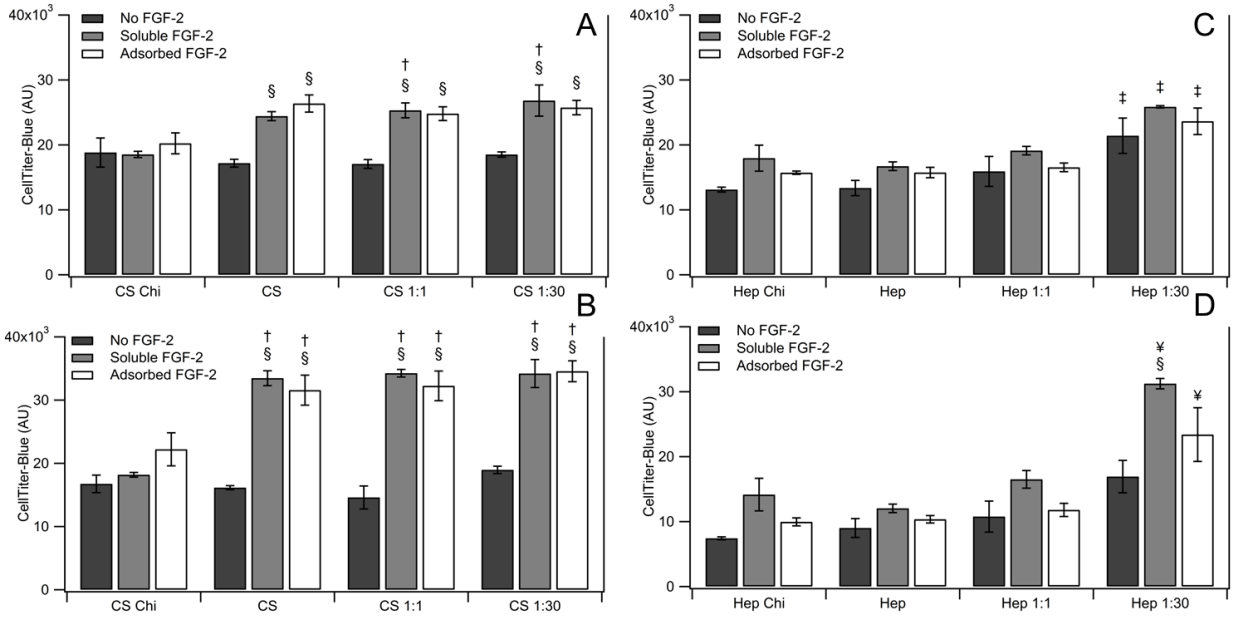

Figure 4.8. CellTiter-Blue data for A.) CS on Day 2, B.) CS on Day 4, C.) Hep on Day 2, and D.) Hep on Day 4. A Tukey's multiple comparisons test was performed to distinguish between groups. A "§" indicates that that treatment was higher than the same condition with no FGF-2, a "†" indicates that that treatment is higher than its Chi-terminated counterpart, a "‡" indicates that that treatment is higher than its Chi-terminated counterpart and its neat GAG terminated counterpart, "¥" indicates that the treatment is higher than its Chi-terminated, GAG-terminated, and Copolymer 1:1-terminated counterparts.

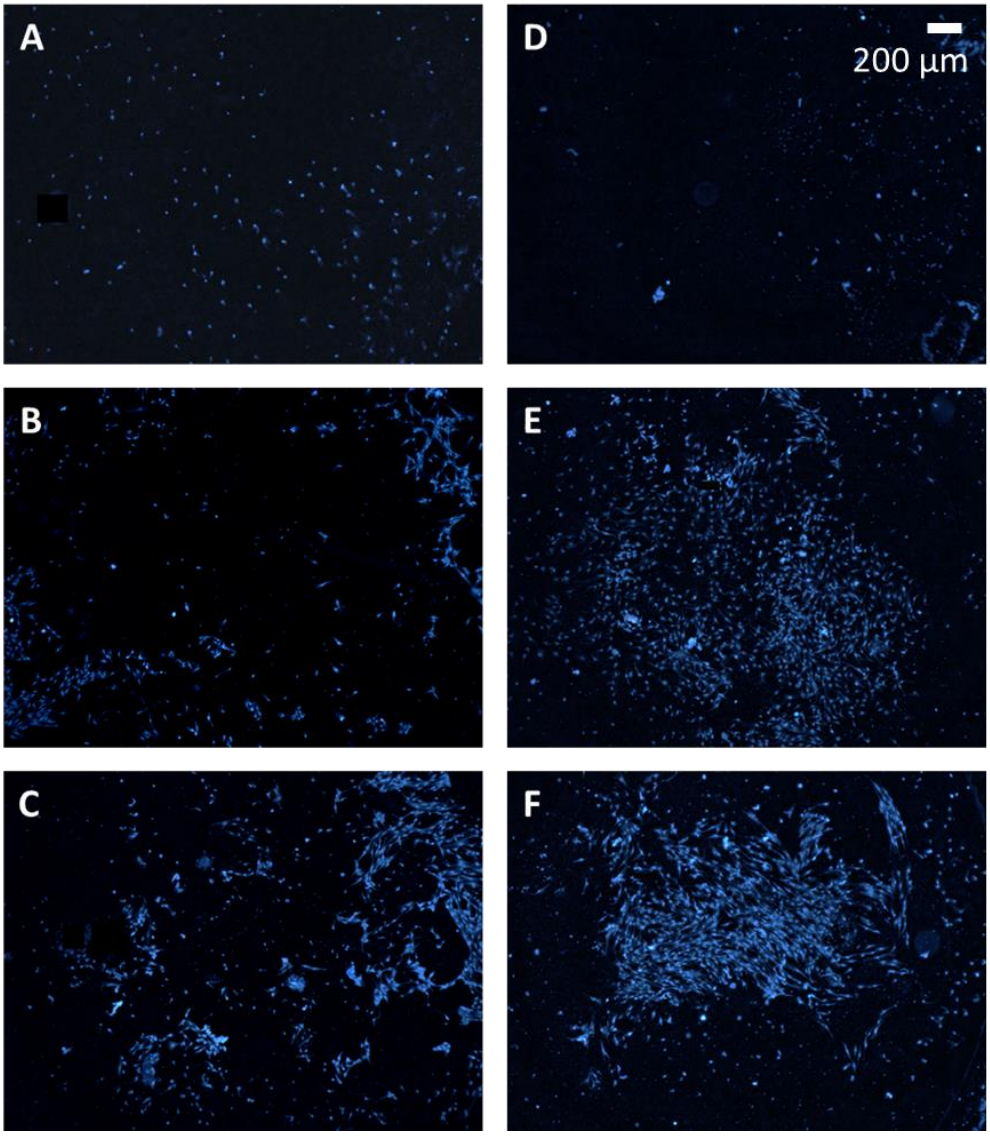

Figure 4.9. Microscopy of cells cultured on 1:30 ratio graft copolymer surfaces A.) CS 1:30 no FGF-2, B.) CS 1:30 FGF-2 delivered in solution, C.) CS 1:30 FGF-2 adsorbed, D.) Hep 1:30 no FGF-2, E.) Hep 1:30 FGF-2 delivered in solution, F.) Hep 1:30 FGF-2 adsorbed.

4.4.4 DMA of Graft Copolymer Impregnated Hydrogels. In a pilot study, graft copolymers were added to hydrogels to test their effect on mechanical properties. The results are displayed in Table 4.5. The minimum modulus (E_{min}), observed at 0 % strain, and the maximum modulus (E_{max}), seen at 10% strain, are shown for each sample. Representative stress versus strain and stress versus cycle number curves are shown in Figure 4.10. There is wide variability in compressive modulus between samples and within a sample; this is particularly evident at 5

Hz. There does not appear to be much difference in compressive modulus between the gels containing GAGs and those containing graft copolymers, but both types of hydrogels do generally exhibit higher compressive moduli than the agarose hydrogels. Additionally, hydrogels containing graft copolymers see an increase in compressive modulus with cycle frequency, whereas the agarose gels do not. This is characteristic of cartilage due to its viscoelastic properties.[59] The proteoglycans in cartilage play a significant role in producing these mechanical properties. The proteoglycan-mimetic graft copolymers created here may be able to duplicate these characteristics. A full study is planned to explore this phenomena. Unconfined compression testing with cyclic loading in a PBS bath will be performed. More samples will be prepared in a reproducible manner. More frequencies will be tested with a focus on physiologically relevant loading from 0.01-2 Hz. The results will again be fit with the model used in the pilot study to calculate E_{min} and E_{max}.

Table 4.4. Minimum and Maximum Modulus (E_{min} and E_{max}) for each hydrogel sample.

Hydrogel Type	0.05 Hz		0.5 Hz		5 Hz	
	E_{min} (kPa)	E_{max} (kPa)	E_{min} (kPa)	E_{max} (kPa)	E_{min} (kPa)	E_{max} (kPa)
Agarose	29 ± 0.8	69 ± 2.4	34 ± 2.3	52 ± 4.1	19 ± 6.1	81 ± 14
HA	23 ± 0.4	75 ± 1.7	30 ± 1.1	98 ± 4.8	44 ± 9.4	89 ± 4.0
HA	36 ± 0.5	99 ± 2.1	37 ± 1.7	100 ± 6	60 ± 6.5	75 ± 10
CS	47 ± 2.9	62 ± 4.2	51 ± 2.2	110 ± 6	70 ± 4.4	84 ± 4.2
CS	47 ± 3.0	75 ± 5.8	50 ± 2.1	120 ± 7	75 ± 3.6	110 ± 21
Hep	52 ± 0.8	94 ± 1.9	54 ± 2.0	130 ± 6	80 ± 3.4	110 ± 18
Hep	49 ± 1.0	91 ± 2.3	53 ± 1.8	130 ± 6	74 ± 5.0	110 ± 7
CS 1:1	35 ± 0.8	70 ± 2.1	40 ± 1.7	130 ± 8	50 ± 14	91 ± 6.3
CS 1:1	27 ± 0.8	45 ± 1.5	33 ± 1.7	73 ± 4.8	53 ± 3.7	69 ± 20
CS 1:30	29 ± 1.1	65 ± 3.2	38 ± 1.2	99 ± 4.3	34 ± 17	44 ± 3.6
CS 1:30	29 ± 0.6	54 ± 1.5	33 ± 2.2	91 ± 8.2	25 ± 21	74 ± 4.8
Hep 1:1	48 ± 1.0	93 ± 2.4	48 ± 1.3	130 ± 4.6	64 ± 22	140 ± 63
Hep 1:1	33 ± 0.6	89 ± 2.1	44 ± 1.6	110 ± 5.3	73 ± 5.2	100 ± 6
Hep 1:1	32 ± 1.0	63 ± 2.6	34 ± 2.0	77 ± 5.8	52 ± 6.2	76 ± 5.8
Hep 1:30	34 ± 0.8	75 ± 2.4	40 ± 3	110 ± 12	66 ± 19	76 ± 4.6

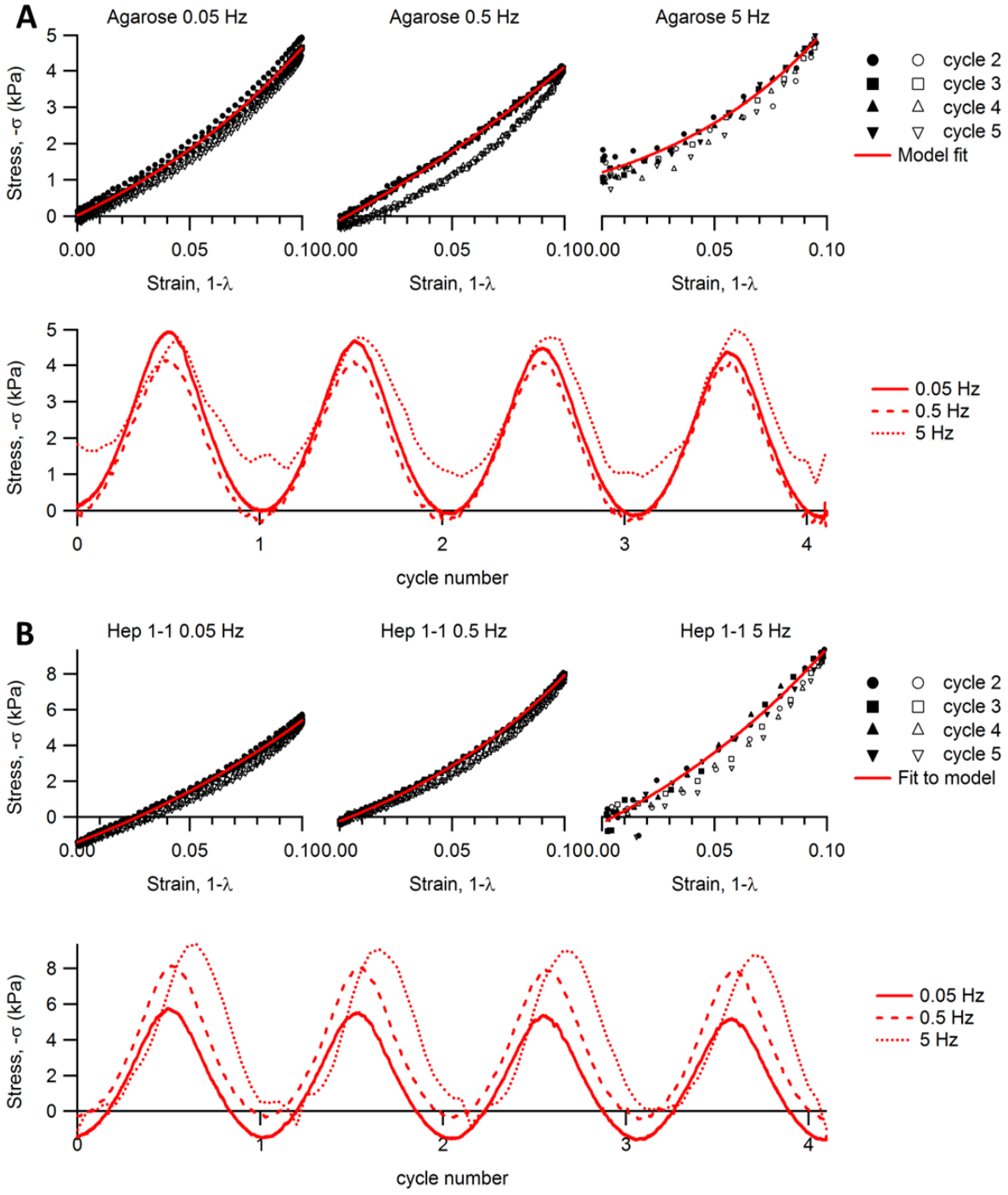

Figure 4.10. Representative stress vs strain and stress vs cycle curves for A.) Agarose and B.) Heparin 1:1.. The modulus increases more from 0 % strain to 10 % strain at higher frequencies in the Heparin 1:1 gel whereas no difference is observed with frequency in the agarose only gels.

.

4.5 CONCLUSIONS.

The synthesis of proteoglycan-mimetic graft copolymers using HA as the backbone and either CS or Hep as the side chains with controllable grafting density was successful. Confirmation of the proposed chemistry was done via ATR-FTIR and ^{1}H NMR. Characteristic peaks associated with the coupling agent and the sulfate groups on the GAG side chains were identified and analyzed for changes due to reaction. Alterations in peak magnitude and morphology confirmed the success of the coupling chemistry. The different compositions exhibit effective hydrodynamic diameters ranging from 90-500 nm as measured by DLS, and all demonstrated negative zeta potentials indicating a negative surface charge. A cell study was done to test the ability of the graft copolymers to deliver FGF-2 to MSCs. The CS containing graft copolymers exhibited higher cell activity than the Hep 1:1, but was similar to the Hep 1:30. The CS conditions and the Hep 1:30 performed as well as when FGF-2 was delivered in solution. Finally, a pilot study to explore the mechanical properties of the graft copolymers was performed. Hydrogels containing the copolymers exhibited changes in compressive modulus with compression frequency similar to the phenomena seen in cartilage. These results show much promise for the use of these graft copolymers to impart bio-functionality to a tissue engineering scaffold.

REFERENCES

1. Senni, K.; Pereira, J.; Gueniche, F.; Delbarre-Ladrat, C.; Sinquin, C.; Ratiskol, J.; Godeau, G.; Fischer, A.-M.; Helley, D.; Colliec-Jouault, S., Marine Polysaccharides: A Source of Bioactive Molecules for Cell Therapy and Tissue Engineering. *Marine Drugs* **2011,** 9, (9), 1664-1681.

2. Sasisekharan, R.; Raman, R.; Prabhakar, V., Glycomics approach to structure-function relationships of glycosaminoglycans. In *Annual Review of Biomedical Engineering*, 2006; Vol. 8, pp 181-231.

3. Schaefer, L.; Schaefer, R. M., Proteoglycans: from structural compounds to signaling molecules. *Cell and Tissue Research* **2010,** 339, (1), 237-246.

4. Suh, J. K. F.; Matthew, H. W. T., Application of chitosan-based polysaccharide biomaterials in cartilage tissue engineering: a review. *Biomaterials* **2000,** 21, (24), 2589-2598.

5. Boddohi, S.; Kipper, M. J., Engineering Nanoassemblies of Polysaccharides. *Advanced Materials* **2010,** 22, (28), 2998-3016.

6. Salbach, J.; Rachner, T. D.; Rauner, M.; Hempel, U.; Anderegg, U.; Franz, S.; Simon, J.-C.; Hofbauer, L. C., Regenerative potential of glycosaminoglycans for skin and bone. *Journal of Molecular Medicine-Jmm* **2012,** 90, (6), 625-635.

7. Yanagishita, M., Function of Proteoglycans in the Extracellular-Matrix. *Acta Pathologica Japonica* **1993,** 43, (6), 283-293.

8. Mulloy, B.; Rider, C. C., Cytokines and proteoglycans: an introductory overview. *Biochemical Society Transactions* **2006,** 34, 409-413.

9. Zeyland, J.; Lipinski, D.; Juzwa, W.; Plawski, A.; Slomski, R., Structure and application of select glycosaminoglycans. *Medycyna Weterynaryjna* **2006,** 62, (2), 139-144.

10. Stevens, M. M.; George, J. H., Exploring and engineering the cell surface interface. *Science* **2005,** 310, (5751), 1135-1138.

11. Papagiannopoulos, A.; Waigh, T. A.; Hardingham, T.; Heinrich, M., Solution structure and dynamics of cartilage aggrecan. *Biomacromolecules* **2006,** 7, (7), 2162-2172.

12. Roughley, P. J.; Lee, E. R., Cartilage Proteoglycans - Structure and Potential Functions. *Microscopy Research and Technique* **1994,** 28, (5), 385-397.

13. Li, Y.; Rodrigues, J.; Tomas, H., Injectable and biodegradable hydrogels: gelation, biodegradation and biomedical applications. *Chemical Society Reviews* **2012,** 41, (6), 2193-2221.

14. Miller, R. E.; Grodzinsky, A. J.; Cummings, K.; Plaas, A. H. K.; Cole, A. A.; Lee, R. T.; Patwari, P., Intraarticular Injection of Heparin-Binding Insulin-like Growth Factor 1 Sustains Delivery of Insulin-like Growth Factor 1 to Cartilage Through Binding to Chondroitin Sulfate. *Arthritis and Rheumatism* **2010,** 62, (12), 3686-3694.

15. Thelin, M. A.; Bartolini, B.; Axelsson, J.; Gustafsson, R.; Tykesson, E.; Pera, E.; Oldberg, A.; Maccarana, M.; Malmstrom, A., Biological functions of iduronic acid in chondroitin/dermatan sulfate. *Febs Journal* **2013,** 280, (10), 2431-2446.

16. Volpi, N., Therapeutic applications of glycosaminoglycans. *Current Medicinal Chemistry* **2006,** 13, (15), 1799-1810.

17. Balakrishnan, B.; Banerjee, R., Biopolymer-Based Hydrogels for Cartilage Tissue Engineering. *Chemical Reviews* **2011,** 111, (8), 4453-4474.

18. Asada, M.; Shinomiya, M.; Suzuki, M.; Honda, E.; Sugimoto, R.; Ikekita, M.; Imamura, T., Glycosaminoglycan affinity of the complete fibroblast growth factor family. *Biochimica Et Biophysica Acta-General Subjects* **2009,** 1790, (1), 40-48.

19. Zou, X. H.; Foong, W. C.; Cao, T.; Bay, B. H.; Ouyang, H. W.; Yip, G. W., Chondroitin sulfate in palatal wound healing. *Journal of Dental Research* **2004,** 83, (11), 880-885.

20. Kosir, M. A.; Quinn, C. C. V.; Wang, W. L.; Tromp, G., Matrix glycosaminoglycans in the growth phase of fibroblasts: More of the story in wound healing. *Journal of Surgical Research* **2000,** 92, (1), 45-52.

21. Gandhi, N. S.; Mancera, R. L., The Structure of Glycosaminoglycans and their Interactions with Proteins. *Chemical Biology & Drug Design* **2008,** 72, (6), 455-482.

22. Reitsma, S.; Slaaf, D. W.; Vink, H.; van Zandvoort, M. A. M. J.; Egbrink, M. G. A. o., The endothelial glycocalyx: composition, functions, and visualization. *Pflugers Archiv-European Journal of Physiology* **2007,** 454, (3), 345-359.

23. Florian, J. A.; Kosky, J. R.; Ainslie, K.; Pang, Z. Y.; Dull, R. O.; Tarbell, J. M., Heparan sulfate proteoglycan is a mechanosensor on endothelial cells. *Circulation Research* **2003,** 93, (10), E136-E142.

24. Becker, B. F.; Chappell, D.; Bruegger, D.; Annecke, T.; Jacob, M., Therapeutic strategies targeting the endothelial glycocalyx: acute deficits, but great potential. *Cardiovascular Research* **2010,** 87, (2), 300-310.

25. Weinbaum, S.; Tarbell, J. M.; Damiano, E. R., The structure and function of the endothelial glycocalyx layer. *Annual Review of Biomedical Engineering* **2007,** 9, 121-167.

26. Becker, T. A.; Kipke, D. R.; Brandon, T., Calcium alginate gel: A biocompatible and mechanically stable polymer for endovascular embolization. *Journal of Biomedical Materials Research* **2001,** 54, (1), 76-86.

27. Baldwin, A. D.; Kiick, K. L., Polysaccharide-Modified Synthetic Polymeric Biomaterials. *Biopolymers* **2010,** 94, (1), 128-140.

28. Bastow, E. R.; Byers, S.; Golub, S. B.; Clarkin, C. E.; Pitsillides, A. A.; Fosang, A. J., Hyaluronan synthesis and degradation in cartilage and bone. *Cellular and Molecular Life Sciences* **2008,** 65, (3), 395-413.

29. Muzzarelli, R. A. A.; Greco, F.; Busilacchi, A.; Sollazzo, V.; Gigante, A., Chitosan, hyaluronan and chondroitin sulfate in tissue engineering for cartilage regeneration: A review. *Carbohydrate Polymers* **2012,** 89, (3), 723-739.

30. Itano, N.; Kimata, K., Hyaluronan synthase: New directions for hyaluronan research. *Trends in Glycoscience and Glycotechnology* **1998,** 10, (51), 23-38.

31. Almodovar, J.; Bacon, S.; Gogolski, J.; Kisiday, J. D.; Kipper, M. J., Polysaccharide-Based Polyelectrolyte Multi layer Surface Coatings can Enhance Mesenchymal Stem Cell Response to Adsorbed Growth Factors. *Biomacromolecules* **2010,** 11, (10), 2629-2639.

32. Babensee, J. E.; McIntire, L. V.; Mikos, A. G., Growth factor delivery for tissue engineering. *Pharm. Res.* **2000,** 17, (5), 497-504.

33. Li, J. T.; Pei, M., Optimization of an In Vitro Three-Dimensional Microenvironment to Reprogram Synovium-Derived Stem Cells for Cartilage Tissue Engineering. *Tissue Eng., Part A.* **2011,** 17, (5-6), 703-712.

34. Somers, P.; Cornelissen, R.; Thierens, H.; Van Nooten, G., An optimized growth factor cocktail for ovine mesenchymal stem cells. *Growth Factors* **2012,** 30, (1), 37-48.

35. Chen, R. R.; Mooney, D. J., Polymeric growth factor delivery strategies for tissue engineering. *Pharmaceutical Research* **2003,** 20, (8), 1103-1112.

36. Gu, X. S.; Ding, F.; Yang, Y. M.; Liu, J., Construction of tissue engineered nerve grafts and their application in peripheral nerve regeneration. *Prog. Neurobiol.* **2011,** 93, (2), 204-230.

37. Ohta, M.; Suzuki, Y.; Chou, H.; Ishikawa, N.; Suzuki, S.; Tanihara, M.; Mizushima, Y.; Dezawa, M.; Ide, C., Novel heparin/alginate gel combined with basic fibroblast growth factor promotes nerve regeneration in rat sciatic nerve. *J. Biomed. Mater. Res., Part A* **2004,** 71A, (4), 661-668.

38. Wang, S. G.; Cai, Q.; Hou, J. W.; Bei, J. Z.; Zhang, T.; Yang, J.; Wan, Y. Q., Acceleration effect of basic fibroblast growth factor on the regeneration of peripheral nerve through a 15-mm gap. *J. Biomed. Mater. Res., Part A* **2003,** 66A, (3), 522-531.

39. Chen, W.; Shi, C. Y.; Yi, S. H.; Chen, B.; Zhang, W. W.; Fang, Z. Q.; Wei, Z. L.; Jiang, S. X.; Sun, X. C.; Hou, X. L.; Xiao, Z. F.; Ye, G.; Dai, J. W., Bladder Regeneration by Collagen Scaffolds With Collagen Binding Human Basic Fibroblast Growth Factor. *J. Urol.* **2010,** 183, (6), 2432-2439.

40. Kurane, A.; Simionescu, D. T.; Vyavahare, N. R., In vivo cellular repopulation of tubular elastin scaffolds mediated by basic fibroblast growth factor. *Biomaterials* **2007,** 28, (18), 2830-2838.

41. Huang, X.; Yang, D. S.; Yan, W. Q.; Shi, Z. L.; Feng, J.; Gao, Y. B.; Weng, W. J.; Yan, S. G., Osteochondral repair using the combination of fibroblast growth factor and amorphous calcium phosphate/poly(L-lactic acid) hybrid materials. *Biomaterials* **2007,** 28, (20), 3091-3100.

42. Laham, R. J.; Rezaee, M.; Post, M.; Xu, X. Y.; Sellke, F. W., Intrapericardial administration of basic fibroblast growth factor: Myocardial and tissue distribution and

comparison with intracoronary and intravenous administration. *Catheter. Cardiovasc. Interv.* **2003,** 58, (3), 375-381.

43. Volpato, F. Z.; Almodovar, J.; Erickson, K.; Popat, K. C.; Migliaresi, C.; Kipper, M. J., Preservation of FGF-2 bioactivity using heparin-based nanoparticles, and their delivery from electrospun chitosan fibers. *Acta Biomaterialia* **2012,** 8, (4), 1551-1559.

44. Sakiyama-Elbert, S. E.; Hubbell, J. A., Development of fibrin derivatives for controlled release of heparin-binding growth factors. *Journal of Controlled Release* **2000,** 65, (3), 389-402.

45. Place, L. W.; Sekyi, M.; Kipper, M. J., Aggrecan-Mimetic, Glycosaminoglycan-Containing Nanoparticles for Growth Factor Stabilization and Delivery. *Biomacromolecules* **2014,** 15, (2), 680-689.

46. Richardson, T. P.; Peters, M. C.; Ennett, A. B.; Mooney, D. J., Polymeric system for dual growth factor delivery. *Nat. Biotechnol.* **2001,** 19, (11), 1029-1034.

47. Tessmar, J. K.; Gopferich, A. M., Matrices and scaffolds for protein delivery in tissue engineering. *Adv. Drug Delivery Rev.* **2007,** 59, (4-5), 274-291.

48. Santo, V. E.; Gomes, M. E.; Mano, J. F.; Reis, R. L., Chitosan-chondroitin sulphate nanoparticles for controlled delivery of platelet lysates in bone regenerative medicine. *Journal of Tissue Engineering and Regenerative Medicine* **2012,** 6, s47-s59.

49. Paderi, J. E.; Panitch, A., Design of a synthetic collagen-binding peptidoglycan that modulates collagen fibrillogenesis. *Biomacromolecules* **2008,** 9, (9), 2562-2566.

50. Paderi, J. E.; Sistiabudi, R.; Ivanisevic, A.; Panitch, A., Collagen-Binding Peptidoglycans: A Biomimetic Approach to Modulate Collagen Fibrillogenesis for Tissue Engineering Applications. *Tissue Engineering Part A* **2009,** 15, (10), 2991-2999.

51. Kishore, V.; Paderi, J. E.; Akkus, A.; Smith, K. M.; Balachandran, D.; Beaudoin, S.; Panitch, A.; Akkus, O., Incorporation of a decorin biomimetic enhances the mechanical properties of electrochemically aligned collagen threads. *Acta Biomaterialia* **2011,** 7, (6), 2428-2436.

52. Sharma, S.; Panitch, A.; Neu, C. P., Incorporation of an aggrecan mimic prevents proteolytic degradation of anisotropic cartilage analogs. *Acta Biomaterialia* **2013,** 9, (1), 4618-4625.

53. Sarkar, S.; Lightfoot-Vidal, S. E.; Schauer, C. L.; Vresilovic, E.; Marcolongo, M., Terminal-end functionalization of chondroitin sulfate for the synthesis of biomimetic proteoglycans. *Carbohydrate Polymers* **2012,** 90, (1), 431-440.

54. Tran, V. M.; Nguyen, T. K. N.; Sorna, V.; Loganathan, D.; Kuberan, B., Synthesis and Assessment of Glycosaminoglycan Priming Activity of Cluster-xylosides for Potential Use as Proteoglycan Mimetics. *Acs Chemical Biology* **2013,** 8, (5), 949-957.

55. Damodaran, V. B.; Place, L. W.; Kipper, M. J.; Reynolds, M. M., Enzymatically degradable nitric oxide releasing S-nitrosated dextran thiomers for biomedical applications. *Journal of Materials Chemistry* **2012,** 22, (43), 23038-23048.

56. Sisu, I.; Udrescu, V.; Flangea, C.; Tudor, S.; Dinca, N.; Rusnac, L.; Zamfir, A. D.; Sisu, E., Synthesis and structural characterization of amino-functionalized polysaccharides. *Central European Journal of Chemistry* **2009,** 7, (1), 66-73.

57. Dalpathado, D. S.; Jiang, H.; Kater, M. A.; Desaire, H., Reductive amination of carbohydrates using NaBH(OAc)(3). *Analytical and Bioanalytical Chemistry* **2005,** 381, (6), 1130-1137.

58. Boddohi, S.; Almodovar, J.; Zhang, H.; Johnson, P. A.; Kipper, M. J., Layer-by-layer assembly of polysaccharide-based nanostructured surfaces containing polyelectrolyte complex nanoparticles. *Colloids and Surfaces B-Biointerfaces* **2010,** 77, (1), 60-68.

59. Park, S.; Hung, C. T.; Ateshian, G. A., Mechanical response of bovine articular cartilage under dynamic unconfined compression loading at physiological stress levels. *Osteoarthritis and Cartilage* **2004,** 12, (1), 65-73.

60. Servaty, R.; Schiller, J.; Binder, H.; Arnold, K., Hydration of polymeric components of cartilage - an infrared spectroscopic study on hyaluronic acid and chondroitin sulfate. *International Journal of Biological Macromolecules* **2001,** 28, (2), 121-127.

61. Margolis, R. U.; Margolis, R. K., Aggrecan-Versican-Neurocan Family of Proteoglycans. *Extracellular Matrix Components* **1994,** 245, 105-126.

62. Gasimli, L.; Linhardt, R. J.; Dordick, J. S., Proteoglycans in stem cells. *Biotechnology and Applied Biochemistry* **2012,** 59, (2), 65-76.

63. d'Angelo, I.; Garcia-Fuentes, M.; Parajo, Y.; Welle, A.; Vantus, T.; Horvath, A.; Bokonyi, G.; Keri, G.; Alonso, M. J., Nanoparticles Based on PLGA:Poloxamer Blends for the Delivery of Proangiogenic Growth Factors. *Molecular Pharmaceutics* **2010,** 7, (5), 1724-1733.

CHAPTER 5

Two-Phase Emulsion and Coaxial Electrospinning to Incorporate Growth Factors into Electrospun Nanofibers[5]

5.1 SUMMARY.

Cells are surrounded by an information-rich extracellular matrix (ECM) made of a complex network of macromolecules. This network provides both cell signaling and structural support. One strategy for tissue engineering scaffolds is to mimic both of these. Growth factors are prevalent in the ECM and provide cues for cell adhesion, migration, proliferation, and differentiation. However, the use of growth factors is complicated by their relative instability. In the ECM, glycosaminoglycan (GAG) side chains of proteoglycans bind and stabilize growth factors, creating a local reservoir. Electrospinning is a method for creating a scaffold of nanofibers on the same size scale as features found in the ECM. Here we report the development of two electrospinning techniques, using an emulsion and a coaxial needle, for incorporating growth factor into electrospun nanofibers. We use basic fibroblast growth factor (FGF-2) as a model growth factor, and bind it to GAG-rich polyelectrolyte complex nanoparticles (PCNs) for stabilization throughout electrospinning. The two techniques are characterized for morphology, nanoparticle and FGF-2 incorporation, cytocompatibility, and FGF-2 delivery. We demonstrate that both techniques result in nanofibers within the size range of collagen fiber bundles found in

[5]Portions of this chapter appear in the following:
Place, L.W., Seyki, M., Taussig, J.E.,and Kipper, M.J.; "Two-Phase Emulsion and Coaxial Electrospinning to Incorporate Growth Factors into Electrospun Nanofibers", in prep for submission to *Macromolecular Bioscience,* 2014.
Taussig, J.E.; "Formulation and Analysis of Emulsion-Electrospun Nanofibers with Embedded Nanoparticle-Bound Fibroblast Growth Factor-2 (FGF-2)", Colorado State University Honors Thesis (Fort Collins, CO), May 2014.
Seyki, M.; "Electrospinning Nanoparticle/Nanofiber Mats for Growth Factor Stabilization and Delivery", Colorado State University Honors Thesis (Fort Collins, CO), May 2014.

the ECM and dispersion of PCNs throughout the fiber mat, and exhibit cytocompatibility. We evaluate FGF-2 incorporation via an ELISA and determine that the coaxial technique is superior to the emulsion for growth factor incorporation. Finally, FGF-2 delivery to MSCs from coaxially electrospun nanofibers is assessed using a cell activity assay. The results suggest that binding FGF-2 to GAG-rich nanoparticles protects it from degradation during coaxial electrospinning making this technique a viable option for producing a bioactive tissue engineering scaffold.

5.2 INTRODUCTION.

Tissues are made up of cells surrounded by the extracellular matrix (ECM). The ECM consists of an intricate network of macromolecules made up of polysaccharides and cytokines surrounded by a framework of structural proteins which are typically secreted and assembled by the cells in their locality.[1, 2] This creates a microenvironment rich in information for regulating cell adhesion, migration, proliferation, and differentiation.[1, 3, 4] ECM is organized in a hierarchical structure that directs tissue function. For example, fibrous proteins such as collagen and elastin align in complex arrangements producing the unique mechanical properties seen in tendons and blood vessels.[5, 6] Nanoscale features are a significant focus in the design of scaffolds for tissue engineering, as cells involved in tissue repair respond to nanoscale topographical features and nanomechanical properties through migration, differentiation, and cytokine profiles.[7-15] Differences in ratios and geometrical arrangements of the macromolecular components of the ECM at the nanometer and micrometer levels are responsible for the wide variety seen in structure, topography, and physical properties of tissues.[1, 6, 16] Mimicking these nanostructures can enhance the functionality of a scaffold.

In addition to structural support, the ECM governs cell adhesion, cell-to-cell communication and differentiation through the presentation of signaling molecules, such as

adhesion ligands and growth factors.[17] Growth factors stimulate cells to proliferate, differentiation, migrate, and regulate wound healing processes.[18-22] They have clinical applications in the treatment of cardiovascular and bone diseases, and wound healing applications, and have been proposed for tissue engineering of nerves, bladders, blood vessels, and osteochondral defects.[22-29] However, the therapeutic nature of growth factors has limitations. They are highly unstable in plasma and as a result, require large doses to be clinically effective.[18, 30-32] Members of the fibroblast growth factor (FGF) family have half-lives that can be measured in minutes.[18, 33, 34] Thus, in order to harness the potential of these proteins, stabilization is imperative.

In the ECM of many tissues, glycosaminoglycan (GAG) side chains of proteoglycans, such as aggrecan, versican, and perlecan serve as a repository of stabilized growth factors, and direct signaling by interacting with integrins on the cell surface.[35-42] GAGs are anionic linear polysaccharides that are involved in a wide variety of roles in tissue function. The GAG heparin protects and enhances the delivery of many growth factors including members of the FGF family, the transforming growth factor-β (TGF-β) superfamily (including some bone morphogenetic proteins), vascular endothelial growth factor (VEGF), nerve growth factor (NGF), and platelet-derived growth factor (PDGF).[34, 43]

Polyelectrolyte complexed nanoparticles (PCNs) are formed by the electrostatic interaction of anionic and cationic polysaccharides which has been comprehensively investigated by several groups.[44-49] Mori et al. created PCNs through the complexation of heparin, and the polycation protamine and demonstrated their ability to stabilize fibroblast growth factor 2 (FGF-2) for seven days, against thermal degradation.[50] Tan et al. impregnated a decellularized vein scaffold with chitosan-heparin nanoparticles to localize VEGF for improved vascularization

of the scaffold. They showed controlled release over 30 days and enhanced cell infiltration, proliferation, ECM production, and angiogenesis.[51] Our group has previously studied growth factor binding, stabilization, and delivery using GAG-rich PCNs made from various combinations of the GAGs heparin and chondroitin sulfate and the polycations chitosan and trimethyl chitosan, and from heparin-chitosan and heparin-trimethyl chitosan polyelectrolyte multilayers.[18, 30, 33, 52] We demonstrated improved stabilization and delivery when FGF-2 was bound to PCNs over naked delivery.[30] Additionally, we showed that heparin-chitosan PCNs were superior to chondroitin sulfate-based PCNs at stabilizing and delivering FGF-2. Thus the study herein uses the heparin-chitosan formulation. A schematic of the formation of these GAG-rich PCNs is shown in Figure 5.1.

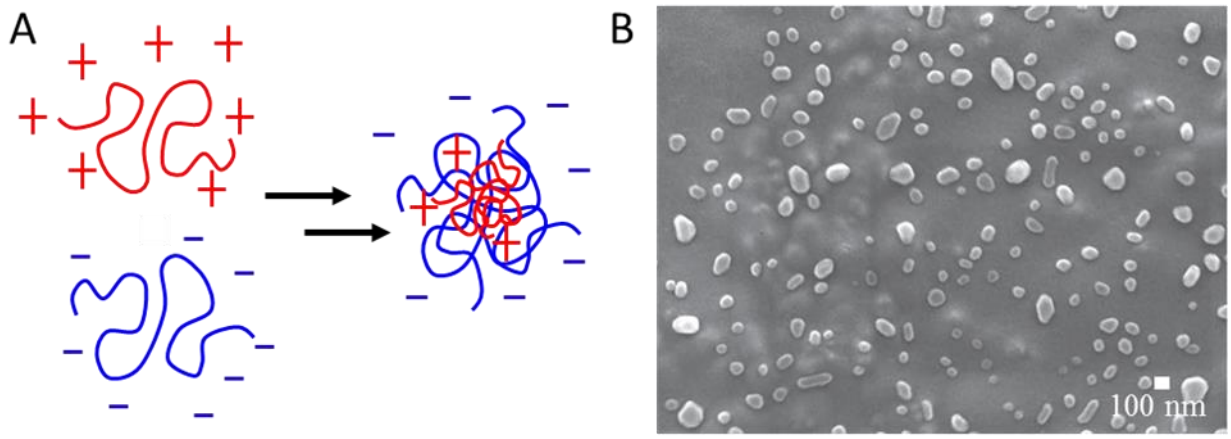

Figure 5.1. A.) Schematic of GAG-rich PCNs created by our group. B.) SEM image of GAG-rich PCNs

Electrospinning is a versatile technique that produces biomimetic nanofibers with high porosity, and surface area.[53-55] They are created by dissolving a polymer in a semi-viscous, volatile solution and passing it through a needle in the presence of an electric field. The electric field pulls the polymer to a grounded collector plate. Most of the solvent evaporates by the time the polymer fiber lands. Adding drugs or protein to the initial polymer solution is a strategy to

impregnate the fiber mat with therapeutic molecules. However, electrospinning typically uses harsh organic solvents that would destroy any therapeutic potential of the molecule. Thus, creative methods are being developed to protect molecules from degradation.

Emulsion electrospinning is a specialized method which allows for the combination of immiscible solvents. This technique makes the mixing of an organic electrospinning solvent with an aqueous phase possible. Many bioactive molecules need to remain under physiological conditions to maintain their activity. An emulsion can provide enough separation between the two phases to protect the therapeutic species. Briggs et al. were successful in the use of emulsion electrospinning to create polycaprolactone and poly(ethylene oxide) blends, for the release of PDGF and demonstrated that the scaffolds enhanced osteogenic differentiation of human mesenchymal stem cells.[56] Xu et al. demonstrated the controlled release of doxorubicin hydrochloride, a water soluble anticancer drug, from nanofibers electrospun from an emulsion. The doxorubicin hydrochloride incorporated in the nanofibers exhibited antitumor activity against mouse glioma cells.[57] In a study performed by Zhao et al., FGF-2 was loaded into a scaffold electrospun from an emulsion containing the synthetic polymer, poly(lactide-co-glycolide). The scaffold exhibited bioactivity of FGF-2 for 3 weeks.[58] These studies show promise for the use of an emulsion technique to create an electrospun scaffold impregnated with active growth factor.

A second technique for electrospinning immiscible phases is coaxial electrospinning. This system uses a compound needle with two separate feeds that keeps the solutions separate until they reach the tip of the needle. This minimizes the time the two phases are in contact with each other, protecting a sensitive molecule from the organic phase.[59] Thuy et al. created porous coaxial nanofibers containing polylactic acid and salicylic acid in polyethylene glycol as a carrier

polymer. They found that they could alter the release profile by changing the porosity of the coaxial nanofibers.[60] Recently, Man et al. fabricated coaxially electrospun nanofibers containing TGF-β and coated with bone marrow derived stem cells-specific affinity peptide E7 for cartilage tissue engineering. The incorporation of peptide E7 and TGF- β resulted in increased cell adhesion and chondrocyte differentiation.[61] Ji et al. studied blend and coaxially electrospun polycaprolactone-based nanofibers for protein integration. Both techniques resulted in protein incorporation, however coaxial electrospinning resulted in more sustained release and higher protein activity.[62]

Though the several groups have been successful in their growth factor release studies, Liu et al. and Ji et al. found that protein was susceptible to degradation during the electrospinning process, reducing its biological activity.[62, 63] As mentioned earlier, growth factors are unstable in solution, but binding them to GAGs may provide the necessary protection. The intent of this work is to develop and compare two techniques, an emulsion and coaxial electrospinning, for incorporating growth factor into electrospun nanofibers. Furthermore, this work strives to demonstrate growth factor stabilization throughout electrospinning through the use of GAG-rich PCNs. This is accomplished through electrospinning the natural polysaccharide chitosan, which has a chemical structure similar to that of GAGs, FGF-2, GAG-rich PCNs, water, and polyvinyl alcohol (PVA) as a carrier polymer to create nanofibers loaded with growth factor. Schematics of the two different techniques are displayed in Figure 5.1. Both techniques allow for the separation of the growth factor-loaded aqueous phase from the organic phase.

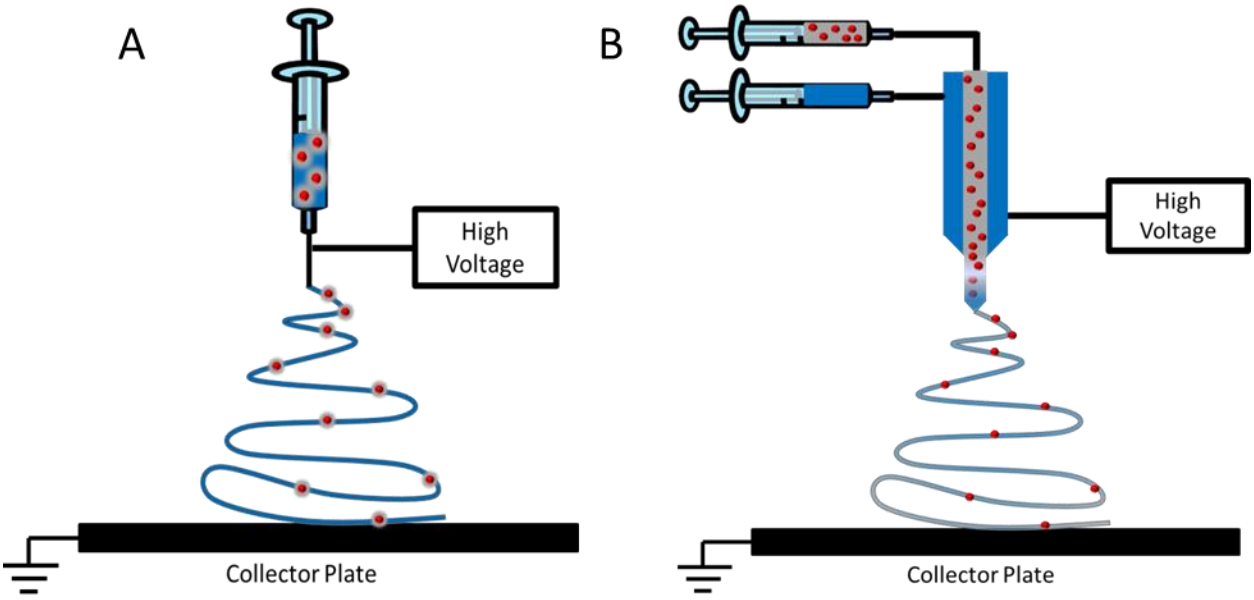

Figure 5.2. Schematic of A.) Emulsion and B.) Coaxial Electrospinning. The blue solution represents the chitosan phase, the red dots represent the GAG-rich PCNs containing growth factor, and the gray represents the aqueous phase.

5.3 MATERIALS AND METHODS.

5.3.1 Materials. A coaxial needle was purchased from Ramé-Hart (Succasunna, NJ). Chitosan (80 kDa, 5% acetylated confirmed through 1H NMR, Protosan UP B 90/20, PDI=1.52) was purchased from Novamatrix (Sandvika, Norway). Heparin sodium (from porcine intestinal mucosa, 14.4 kDa, 12.5% sulfur, PDI=1.14) was purchased from Celsus Laboratories (Cincinnati, OH). Polyvinyl alcohol (87-89% hydrolyzed, 166 kDa), rhodamine B isothiocyanate (RITC), fluorescein isothiocyanate isomer I (FITC), ammonium hydroxide, and albumin from bovine serum (BSA) were purchased from Sigma-Aldrich (St. Louis, MO). Dichloromethane (DCM), trifluoroacetic acid (TFA), tween-20, and glacial acetic acid were purchased from Acros Organics (Geel, Belgium). Sodium hydroxide, methanol, sodium acetate, sodium chloride, potassium chloride, sodium phosphate dibasic anhydrous, potassium phosphate monobasic, and 0.22 μm polyvinylidene fluoride filter syringe tips, were purchased from Thermo-Fisher Scientific (Waltham, MA). Slide-A-Lyzer dialysis cassettes MWCO of 3,500 Daltons were

purchased from Thermo-Scientific (Rockford, IL). Recombinant human FGF basic (FGF-2) 146 aa (carrier free), and human FGF basic ELISA DuoSet were purchased from R&D Systems (Minneapolis, MN). Human fibronectin was purchased from BD Biosciences (Bedford, MA). LIVE/DEAD® Viability/Cytotoxicity Kit for mammalian cells was purchased from Invitrogen (Eugene, OR). CellTiter-Blue® Cell Viability Assay was purchased from Promega (Madison, WI). Fetal bovine serum (FBS), 0.25 % trypsin with EDTA, low-glucose Dulbecco's modified Eagle's medium (D-MEM), minimum essential medium alpha (α-MEM; supplemented with L-glutamine, ribonucleosides, and deoxyribonucleosides), and Dulbecco's phosphate buffered saline (DPBS) without Ca^{2+} and Mg^{2+} were purchased from HyClone (Logan, UT). Antibiotic-antimycotic (anti/anti), 1 M HEPES buffer solution, and Dulbecco's phosphate buffered saline with Ca^{2+} and Mg^{2+} were purchased from Gibco (Grand Island, NY). A Millipore Synthesis water purification unit (Millipore, Billerica, MA) was used to obtain 18.2 MΩ•cm water (DI water), used for making aqueous solutions.

5.3.2 PCN Formation. The procedure for creating PCNs is described in detail in our previous work.[30] Briefly, heparin (0.95 mg mL^{-1}) and chitosan (0.9 mg mL^{-1}) were each dissolved in 0.1 M acetate buffer at pH 5 and then filtered. The chitosan solution was added in one shot to the stirring heparin solution in a 1:6 volume ratio and vigorously stirred for three hours, then left to settle overnight to remove any aggregates. The solution containing PCNs and uncomplexed polymer was decanted from the settled aggregates and centrifuged (9000 rcf for 15 min). The supernatant was decanted to remove any uncomplexed polymer and the pelleted PCNs were resuspended in 100 μl of DI water, this yields PCNs at 8 mg mL^{-1}. At these concentrations PCNs do aggregate over time and are not used if they are older than 1 month.

Before being diluted for analysis or used in an experiment, PCNs were briefly vortexed, which was sufficient to break up aggregates and resuspend them.

5.3.3 FGF-2 Loading onto PCNs. FGF-2 was reconstituted in PBS with 0.1 % BSA at a concentration of 100 μg mL^{-1}. For loading, FGF-2 (100 ng mL^{-1}) and PCNs (1 mg mL^{-1}) were combined and mixed vigorously for 30 min. This procedure has been shown to result in about 50 % binding of FGF-2 to PCNs.[30]

5.3.4 Electrospinning Emulsion. The organic phase used in the emulsion consists of 7 wt % chitosan in a 70:30 volume ratio of TFA to DCM. Chitosan was dissolved in TFA for three hours with minimal stirring, at which point DCM was added and stirred overnight. The aqueous phase containing, PCNs, FGF-2 or FGF-2 bound to PCNs, with 0.4 % tween-20 were mixed at a 1:10 volume ratio (aqueous to organic) for 15 minutes.

First, a base layer containing only the 7 % chitosan in 70:30 TFA:DCM was electrospun at 1 mL h^{-1}, 18 kV, and a collector distance of 7 in for two hours. Next, the emulsion was electrospun at 1 mL h^{-1}, 15 kV, and a collector distance of 6 in for three hours. The electrospun nanofibers were collected onto aluminum foil covering a 0.5 in thick copper plate.

5.3.5 Coaxial Electrospinning. Chitosan (3 wt %) was dissolved in a 70:30 volume ratio of glacial acetic acid to water for 1 week. PVA (8 wt %) was dissolved in water for 24 h at 40 °C. Water, FGF-2 (100 ng mL^{-1}), PCNs (1 mg mL^{-1}), or FGF-2 bound to PCNs (100 ng mL^{-1}, 1 mg mL^{-1} respectively) were added to the 8 % PVA solution in a 3:5 volume ratio to make a 5 % PVA solution. This solution was stirred for one hour prior to electrospinning.

A custom coaxial needle was purchased from Ramé-Hart with a 22 gauge inner needle and a 16 gauge outer needle pictured in Figure 5.2. Two arrangements were electrospun using the two solutions described above, chitosan fed to the outer needle and PVA fed to the inner

needle and the reverse arrangement. These arrangements were electrospun at 18 kV, and a collector distance of 7 in for five hours with the solution fed to the outer needle at 2 mL h^{-1} and the solution fed to the inner needle at 1 mL h^{-1}. The electrospun nanofibers were collected onto aluminum foil covering a 0.5 in thick copper plate.

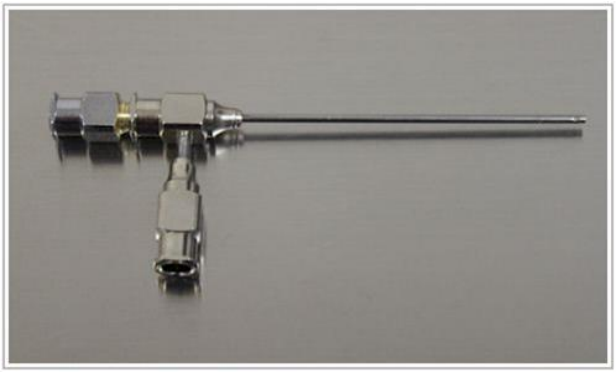

Figure 5.3. Coaxial needle purchased from Ramé-Hart.

5.3.6 Fluorescent Tagging of Chitosan. Fluorescent microscopy was performed to confirm the presence of PCNs within the fibers. For these experiments, chitosan to be used in electrospinning or in PCNs was tagged with either RITC or FITC. When using tagged chitosan in electrospinning or PCN formulation, a 1:10 ratio of tagged to untagged chitosan was used; all other procedures were identical. When electrospinning the tagged emulsion, tagged chitosan was only used in the emulsion layer. Chitosan in the base layer was untagged. The tagged chitosan was not used in any other experiments.

The procedure for making FITC- and RITC-tagged chitosan was previously described by Volpato et al.[33] The method used to produce FITC- and RITC-tagged chitosan was identical aside from the dye concentrations. First, 100 mg of chitosan was dissolved in 10 mL of 0.10 M acetic acid. 10 mL of methanol was added to the solution followed by, 3.25 mL of 1.77 mg mL^{-1} FITC in methanol. When making RITC-tagged chitosan, 3.25 mL of 2 mg mL^{-1} RITC dye

solution was used. The solution was mixed overnight, followed by dialysis to remove any unreacted dye, and finally lyophilized and stored at 4 °C.

5.3.7 Preparation of Electrospun Nanofibers for Cell Culture. Electrospun sheets were peeled off of the aluminum foil collector. The sheet was folded twice to make four laminated layers and samples were cut out using an 8 mm biopsy punch to create scaffolds. Before being used in cell culture experiments, scaffolds were neutralized, sterilized, and coated with fibronectin.

5.3.7.1 Neutralization. Nanofiber scaffolds were placed in a 48-well plate with 0.5 mL of 5 M ammonium hydroxide. These were placed on a shaker plate for 30 min. The solutions were aspirated, and rinsed three times (10 min, 5 min, and 1 min) with PBS. Before neutralization, electrospun chitosan is water soluble. After neutralization using this procedure, electrospun chitosan is durable to aqueous processing, as we have shown previously.[33, 52]

5.3.7.2 Sterilization. Neutralized nanofiber scaffolds were then sterilized; the last rinse was aspirated and 0.5 mL of 70 % ethanol in water was added to each well. The scaffolds were in solution for 15 minutes. The ethanol solution was removed, and then three rinses (10 min, 5 min, and 1 min) were performed with sterile PBS.

5.3.7.3 Fibronectin Coating. Sterilized nanofiber scaffolds were coated with fibronectin to improve cell attachment; the last PBS rinse was aspirated and 0.5 ml of fibronectin (10 $\mu g\ mL^{-1}$) was added to each well. These were placed on a shaker plate for one hour. The solution was then aspirated and one PBS rinse was performed. Emulsion nanofiber scaffolds were used for cell culture on the same day.

5.3.8 Characterization of Electrospun Nanofibers. Nanofiber mats were analyzed using scanning electron microscopy (SEM) and total internal reflectance (TIRF) microscopy to

confirm nanofiber formation and even dispersion of PCNs. Emulsion nanofiber scaffolds containing only water, water + PCNs, water + FGF-2 and water + PCNs/FGF-2 in the aqueous phase and coaxial nanofiber samples containing PVA, PVA + PCNs, PVA + FGF-2, and PVA+ PCNs/FGF-2, and emulsion and coaxial samples that were treated for cell culture were coated with 10 nm of gold and imaged at 5-15 kV on a Jeol JSM-5600F SEM. TIRF microscopy was done on FITC tagged nanofibers containing RITC-tagged PCNs, using a custom built microscope with lasers at 473 and 532 nm.

5.3.9 Cell Harvest and Culture. The cell harvesting and expansion procedure is described in detail in our previous work.[18] Bone marrow aspirates from the iliac crest of female sheep were centrifuged. The supernatant containing the nucleated cells was mixed with growth media (low-glucose D-MEM with 10 % FBS, 1 % anti/anti, and 2.5 % HEPES) and seeded into culture flasks. After 24 h, the media was changed to remove all non-adherent cells. The marrow stromal cell (MSC) colonies were allowed to grow for at least seven days, then the cells were trypsinized, counted, and reseeded in culture flasks using maintenance media for culture expansion (α-MEM with 10 % FBS, 1 % anti/anti, and 2.5 % HEPES). MSCs were cryo-preserved prior to seeding into experimental conditions. Cells were not used beyond the fifth passage.

5.3.10 MSC Cytocomplatibility with Electrospun Nanofibers. MSCs were seeded onto emulsion, coaxial with chitosan in excess, and coaxial with PVA in excess nanofiber scaffolds (in triplicate), at a density of 100,000 cells per scaffold into an untreated 48-well plate with 0.2 mL of α-MEM with 10 % FBS and allowed to attach for three hours. After three hours, the media was aspirated and 0.5 mL of fresh media was added to each well. Cells were cultured on the nanofiber scaffolds for four days in α-MEM media containing 10 % FBS, 1 % anti/anti, and

2.5 % HEPES buffer. Media was changed on the second day of culture. On the fourth day of culture, media was removed and nanofiber samples were stained with LIVE/DEAD® Viability/Cytotoxicity Kit for mammalian cells according to manufacturer's instructions and imaged using a Zeiss fluorescence microscope with appropriate filters.

5.3.11 FGF-2 Quantification within Electrospun Nanofiber Scaffolds via ELISA. A human FGF Basic DuoSet ELISA kit was used to according to manufacturer's instructions to quantify FGF-2 within the nanofiber samples. The FGF-2 was released from the nanofibers by exposing the nanofibers to the ELISA diluent buffer without any neutralization step. Without the neutralization (described in section 5.3.7.1) the nanofibers are water soluble. Neat emulsion nanofiber scaffolds containing only water in the aqueous phase, emulsion nanofiber scaffolds containing FGF-2, coaxial nanofiber scaffolds containing only PVA, and coaxial nanofiber scaffolds containing PVA + FGF-2 (in both arrangements) were dissolved in diluent buffer in the ELISA plate coated with capture antibody for two hours. The rest of the manufacturer's protocol was then followed and the plate was read at 450 nm. Each condition was performed in triplicate.

5.3.12 MSC Dose Response to FGF-2 on Coaxial Fibers. MSCs were seeded onto coaxial nanofiber samples containing only PVA at a density of 20,000 cells per nanofiber scaffold into an untreated 48-well plate with 50 µL of α-MEM with 10 % FBS and allowed to attach for three hours. After three hours, the samples were moved to a fresh untreated 48-well plate and 0.5 mL of low serum α-MEM (2.5 % FBS) was added. Media was supplemented with 0, 0.5, 1, 5, 10, or 50 ng mL^{-1} FGF-2. Cells were cultured on the nanofiber scaffolds for 4 days in α-MEM media with 2.5 % FBS, 1 % anti/anti, and 2.5 % HEPES buffer. Low-serum media was used because it has been previously shown that under these conditions ovine MSCs can survive, but do not proliferate unless provided with FGF-2. [30] Media containing the different

levels of FGF-2 was prepared and stored in the incubator during the culture period. Media was changed on the second day of culture using the prepared media containing FGF-2.

On the second day of culture CellTiter-Blue Cell Viability Assay was performed according to manufacturer's instructions. Briefly, 100 µL of dye was added to each well and incubated for 16 h. At this time, samples were taken from each well and read at 544 nm excitation and 590 nm emission. Samples were then rinsed twice with media to remove any residual dye and fresh media containing the appropriate amount of FGF-2 was added to each well. On the fourth day of culture, the CellTiter-Blue assay was repeated.

5.3.13 MSC Response to FGF-2 delivered via Coaxial Fibers. The same protocol as in the dose response study was used, with the following modifications. MSCs were seeded onto, coaxial electrospun samples with the PVA phase containing only PVA, PVA + PCNs, PVA + FGF-2, PVA + PCNs/FGF-2. After attachment, samples were moved to a 96-well plate and 100 µL of α-MEM containing 2.5 % FBS, 1 % anti/anti, and 2.5 % HEPES buffer without any exogenous FGF-2 was added to each well. The CellTiter-Blue assay was performed in the same way except, 20 µL was added to each well. The media changes and microscopy were done the same as above.

5.3.14 Statistics. Data analysis was performed using Minitab (Minitab, Inc., State College, PA), version 16. For the dose response study and the FGF-2 delivery study, comparisons between groups were performed via analysis of variance (ANOVA) models with Tukey's multiple comparison tests. Differences with $p < 0.05$ were considered statistically significant. Cell activity data as detected by CellTiter-Blue are expressed as the mean ± standard error of the mean ($n = 3$).

5.4 RESULTS AND DISCUSSION.

5.4.1 Characterization of Electrospun Nanofibers. Electrospun nanofibers were analyzed via SEM and TIRF microscopy for fiber morphology and even distribution of PCNs. SEM was performed on emulsion and coaxial samples containing no additives, PCNs, FGF-2, and PCNs/FGF-2. However no differences were observed in fiber morphology, thus representative images of emulsion and coaxial nanofibers without additives are displayed in Figure 5.4.

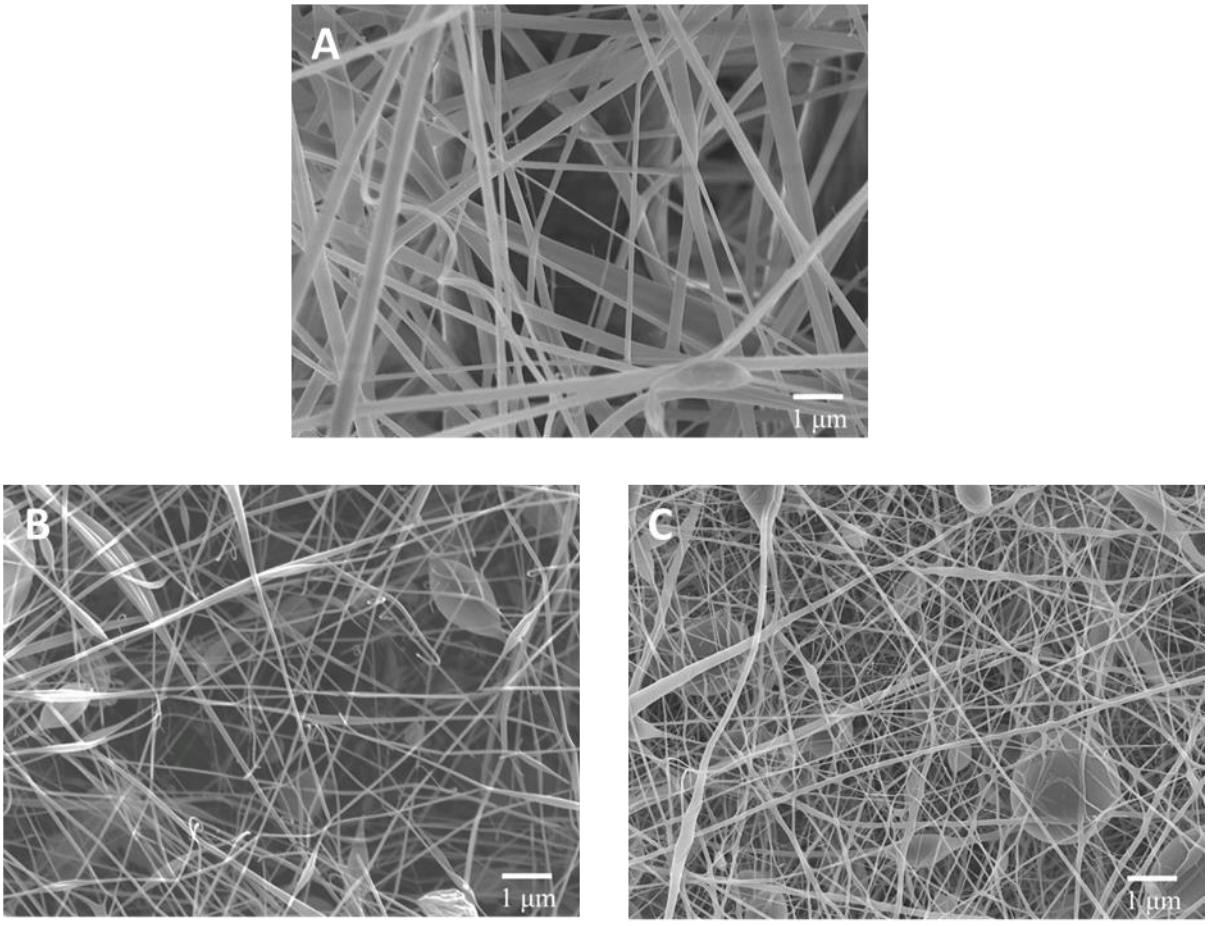

Figure 5.4. A.) Emulsion nanofibers, B.) Coaxial nanofibers with chitosan in excess, C.) Coaxial nanofibers with PVA in excess.

The emulsion layer is spun on top of a plain chitosan layer, there appears to be two different phases of fibers with the plain chitosan fibers being much larger than those from the

emulsion. Nanofibers from all electrospinning arrangements are submicron and contain beading. This indicates that there is some electrospraying occurring in conjunction with electrospinning.

SEM images were taken of samples treated for cell culture to investigate any morphological changes. These are shown in Figure 5.5.

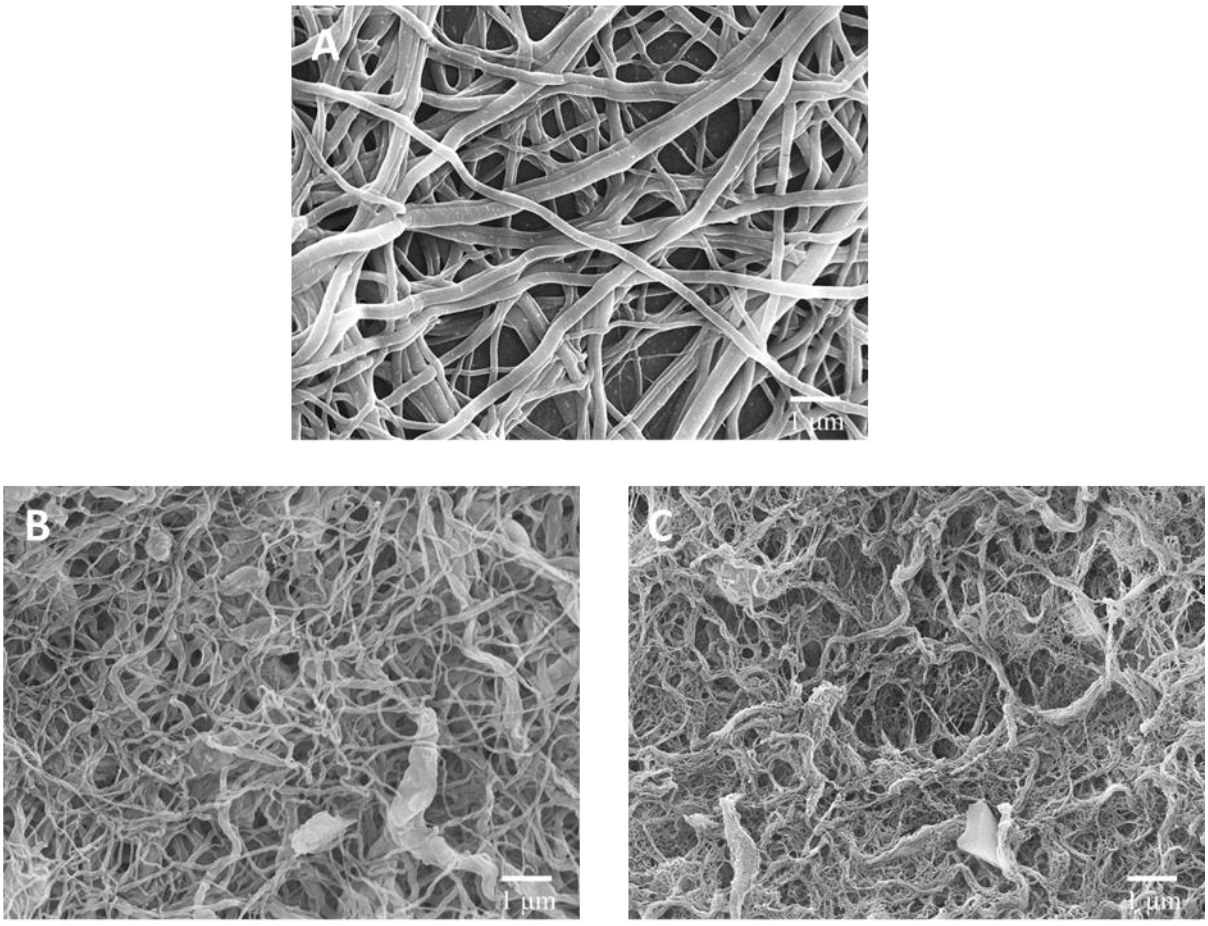

Figure 5.5. Representative images of nanofiber scaffolds after treatment for cell culture. All three experience morphological changes. A.) Emulsion nanofibers, B.) Coaxial nanofibers with chitosan in excess, C.) Coaxial nanofibers with PVA in excess

The nanofibers electrospun from the emulsion show swelling and mild crimping after cell culture treatment. The coaxial nanofibers exhibit more striking morphological changes. The fibers containing chitosan in excess display some swelling and exhibit crimping. The fibers containing PVA in excess also show crimping, but in addition they appear to have pores within

the fibers. PVA is water soluble; generally high temperature and extended amounts of time are required for complete dissolution, but electrospinning results in high surface area which would allow PVA to dissolve more easily. Thus, nanofibers containing higher amounts of PVA may be losing more material and would display a porous structure. The nanofibers containing more chitosan (which is only soluble at acidic pH) do not dissolve, but are able to absorb more water causing swelling. These changes are also apparent macroscopically; the scaffolds containing PVA in excess shrink during the treatment process whereas the scaffolds containing chitosan in excess swell. Although morphology is altered, a fibrous structure with high porosity and biomimetic nanofeatures is still present in all cases.

TIRF microscopy was used to confirm the presence and distribution of PCNs throughout the nanofiber mats. Chitosan used in the TIRF experiments was tagged with FITC causing fibers to appear green; PCNs were tagged with RITC and appear red, shown in figure 5.6. below.

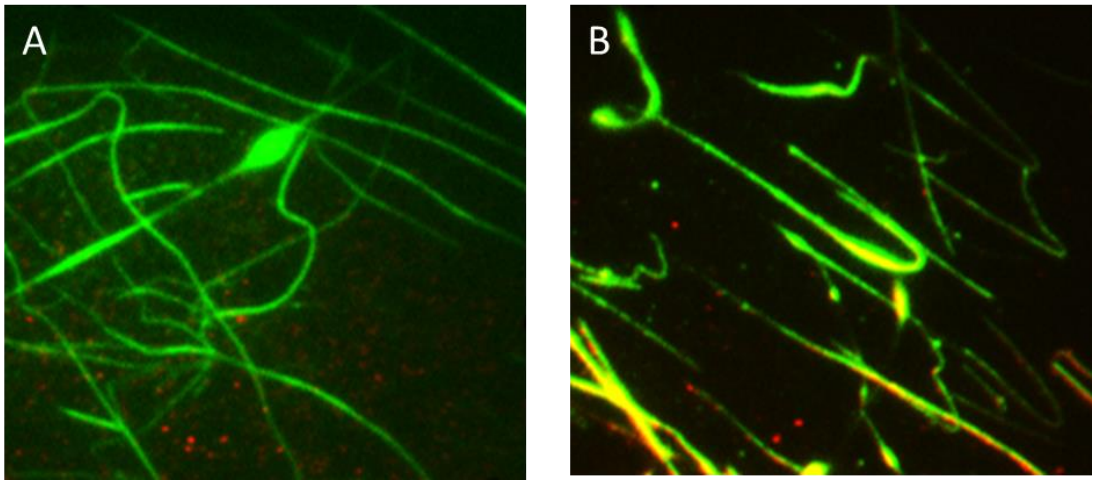

Figure 5.6. TIRF microscopy of A.) Emulsion nanofibers tagged with FITC impregnated with RITC tagged PCNs and B.) Coaxial nanofibers tagged with FITC impregnated with RITC tagged PCNs.

Green fibers can be clearly seen in both conditions. Red can be seen both within the fibers and scattered around the fibers. There is also beading apparent and green dots present around the fibers. These agree with the observations made in the SEM images. In addition to

electrospinning there is electrospraying occurring. It has been previously seen in emulsion electrospinning that the rheological properties of the two phases may change under the stresses experienced in the Taylor cone. [64] Additionally over long electrospinning times there is a risk of phase separation both of which may lead to electrospraying. Despite electrospraying, nanoscale fibers similar in diameter to collagen fiber bundles (50-500 nm) found in the ECM are prevalent.[65] Microscopy confirms the formation of ECM mimetic fibers and distribution of PCNs throughout the fiber mat.

5.4.2 MSC Cytocompatiblity with Electrospun Nanofibers. MSCs were cultured on nanofiber scaffolds and stained using a LIVE/DEAD kit to test for cytocompatibility. MSCs were cultured on nanofiber scaffolds for four days and then stained for imaging. Results are shown in Figure 5.7., live cells are stained green and dead cells appear red.

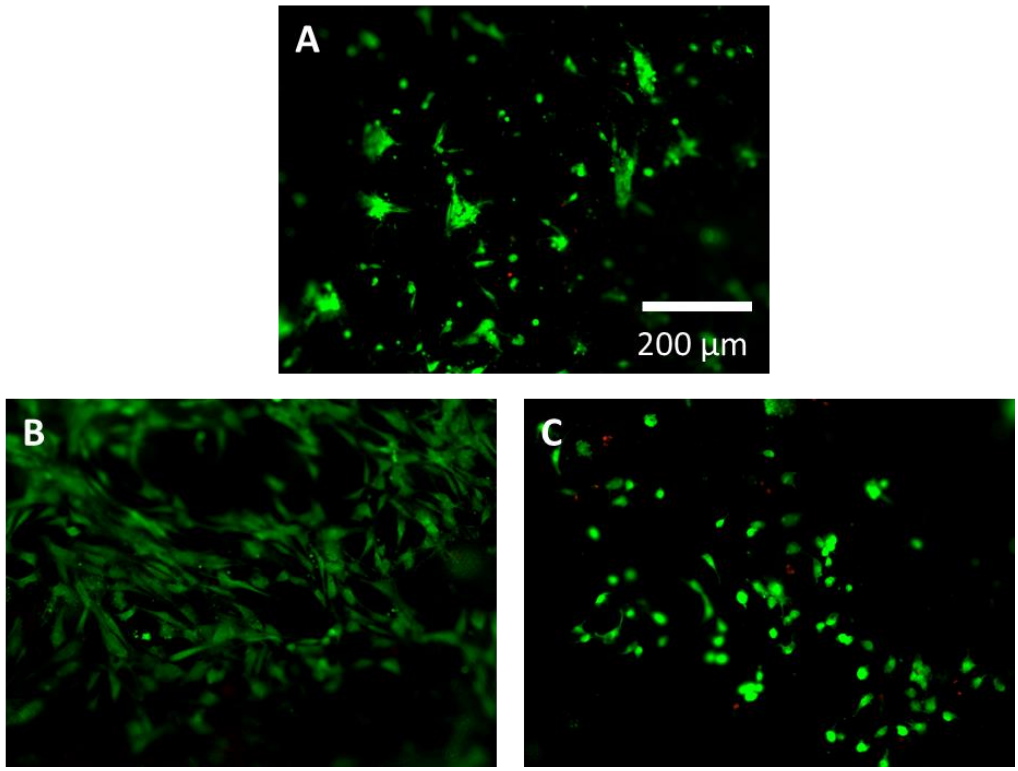

Figure 5.7. Fluorescent microscopy of MSCs growing on A.) An emulsion nanofiber scaffold, B.) A coaxial nanofiber scaffold with chitosan in excess, and C.) A coaxial nanofibers scaffold with PVA in excess.

There are differences in cell morphology on the three different scaffold types. The MSCs growing on the emulsion scaffold have abstract shapes, not round, not spindle. Some cells appear to be spreading and interacting with the fiber network, but overall a morphological pattern is not displayed. The MSCs growing on the coaxial scaffold with chitosan in excess exhibit a typical MSC spindle shape and show good spreading and interaction with the surface. The cells growing on the coaxial scaffold with PVA in excess have a round morphology similar to that of chondrocytes grown in a hydrogel. In all three cases very few red cells are observed and cells are interacting with the material, suggesting cytocompatibility. Although fewer cells are observed on the emulsion and the coaxial fibers with PVA in excess, the incorporation of growth factor could alter cellular response, thus all scaffold types may be useful as tissue engineering scaffolds and drug delivery systems.

5.4.3 FGF-2 Quantification within Electrospun Nanofiber Scaffolds via ELISA. Human FGF basic ELISA was used to quantify FGF-2 within emulsion and coaxial nanofiber samples. Neat samples were incubated with capture antibody in a 96-well plate for two hours. Because the samples had not been neutralized, the emulsion scaffold and the coaxial scaffold with PVA in excess both dissolved. The coaxial scaffold with chitosan in excess remained macroscopically intact, but after analysis with SEM it was found that all nanostructure is lost (image available in the Appendix), thus FGF-2 inside the scaffold has been released and would bind to the capture antibody. Results are displayed in Table 5.1.

Table 5.1. FGF-2 Quantification via ELISA

	FGF-2 detected ng/scaffold ± SE	Maximum FGF-2 possible	% Yield
Emulsion	-	0.27	0
Coaxial Chi in Excess	0.34 ± 0.044	1.7	20
Coaxial PVA in Exces	0.20 ± 0.038	3.4	5.9

The emulsion scaffolds containing FGF-2 gave the same or lower readings as the blank emulsion nanofiber scaffolds without any FGF-2. This indicates that emulsion nanofibers contain no detectable FGF-2. When proteins come into contact with harsh solvents they can denature. It is possible that the emulsion did not offer enough protection from the TFA/DCM solvent system, denaturing the FGF-2. Denatured FGF-2 would not have the same reactivity with the ELISA, leading to lower readings. In the coaxial case, the ELISA shows that there is between 0.2 and 0.4 ng of FGF-2 per scaffold, if used in a 96-well plate with 100 μL of media, there are 2-4 ng mL^{-1} delivered to MSCs. According to a previous study done by our group this should be within the range for optimal mitogenic dose (0.1-10 ng mL^{-1}).[18] While there appears to be a sufficient amount of FGF-2 loaded into the nanofibers, the yield is between 6 and 20 %. The low yields in both cases could be due to several factors. As discussed earlier, any denatured FGF-2 will have reduced affinity for the capture antibody, and electrospinning can be inefficient, with much of the material not being captured on the collector plate. Incorporating PCNs into the nanofibers may offer protection for the FGF-2 resulting in higher loading efficiency. However, when FGF-2 is bound to PCNs steric hindrance inhibits binding to the capture antibody, thus ELISA was not performed on these scaffold types.

ELISA is very sensitive, detecting FGF-2 at concentrations as low as pg mL^{-1}. While PCNs should increase loading efficiency, since no FGF-2 was detectable via ELISA in the emulsion nanofibers it is not believed that that technique will incorporate a therapeutic dose. Thus, only the coaxial nanofibers were pursued for FGF-2 delivery to MSCs. Although, the ability of the emulsion nanofibers to deliver FGF-2 is limited, they may still be useful for delivering small molecules that are not as sensitive to their surrounding environment such as antibiotics or antitumor drugs.

5.4.4 MSC Dose Response to FGF-2 on Coaxial Fibers. MSCs were exposed to exogenous FGF-2 in doses ranging from 0 to 50 ng mL^{-1}, and then tested for cell proliferation using CellTiter-Blue assay. Results are displayed in Figure 5.8.

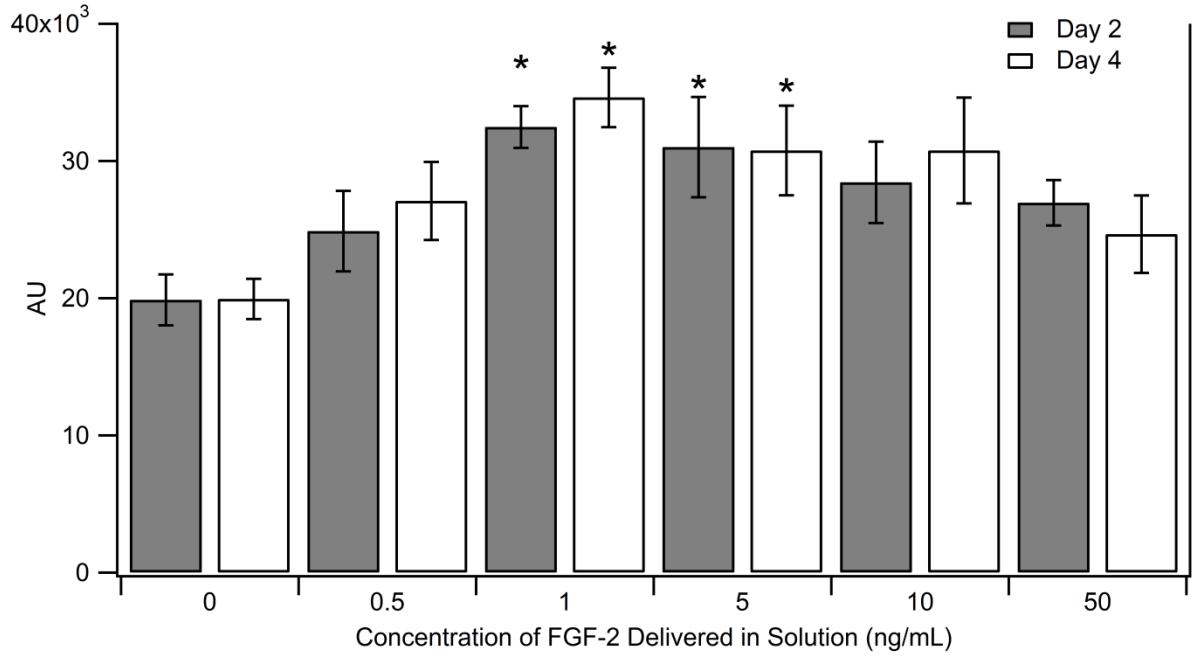

Figure 5.8. CellTiter-Blue results from response of MSCs to different doses of FGF-2 delivered in solution. 1 ng/mL and 5 ng/mL elicited the most metabolic activity from cells on both day 2 and day 4 of culture. "*" indicates statistical difference from the negative control.

There is more cell activity at doses between 1-10 ng mL^{-1} than at zero and above 10 ng mL^{-1}, which agrees with a previous dose-response study performed by our group on tissue culture polystyrene.[18] However, only doses at 1 and 5 ng mL^{-1} are statistically significant from no FGF-2. The ELISA results show that the coaxial nanofibers are capable of delivering an FGF-2 dose of 2-4 ng mL^{-1} to MSCs in a 96-well plate format which falls within this optimal range.

5.4.5 MSC Response to FGF-2 delivered via Coaxial Fibers. MSCs were seeded onto coaxial nanofibers containing only PVA, PCNs, FGF-2, or PCNs/FGF-2 and cultured for four

days in α-MEM (2.5 % FBS). CellTiter-Blue cell proliferation assay was used to determine cell activity on the different nanofiber formulations. Results are show in figure 5.9.

On day 2, FGF-2 delivered in solution to both coaxial arrangements appear to be higher than the other conditions, and are statistically different from fibers with PVA in excess containing FGF-2, PVA in excess containing FGF-2 bound to PCNs, and both coaxial arrangements containing PCNs. On day 4, FGF-2 delivered in solution continues to elicit the highest response, and statistical differences remain similar, however other conditions saw a rise in cell activity from day to 2 to day 4 as exhibited by the ratio of cell activity on day 4 to that of day 2. The nanofibers containing PCNs and FGF-2 bound to PCNs exhibit a higher response than their counterpart on day 2 (ratios are greater than 1) indicating proliferation, while FGF-2 delivered in solution does not change. However, there are no statistical differences in cell proliferation. It should be noted that while the fibers containing only PCNs exhibit proliferation, they have relatively low cell activity compared to FGF-2 delivered in solution on both days. On day 4 FGF-2 delivered in solution exhibits the highest amount of cell activity followed by FGF-2 bound to PCNs, when chitosan is in excess. All other conditions, including those containing FGF-2 without PCN protection, behave similarly to nanofibers without FGF-2. This suggests that FGF-2 is degraded by the electrospinning process and PCNs may offer protection when coaxially electrospun with chitosan in excess, making this technique a viable option for incorporating growth factor into an electrospun scaffold for tissue engineering.

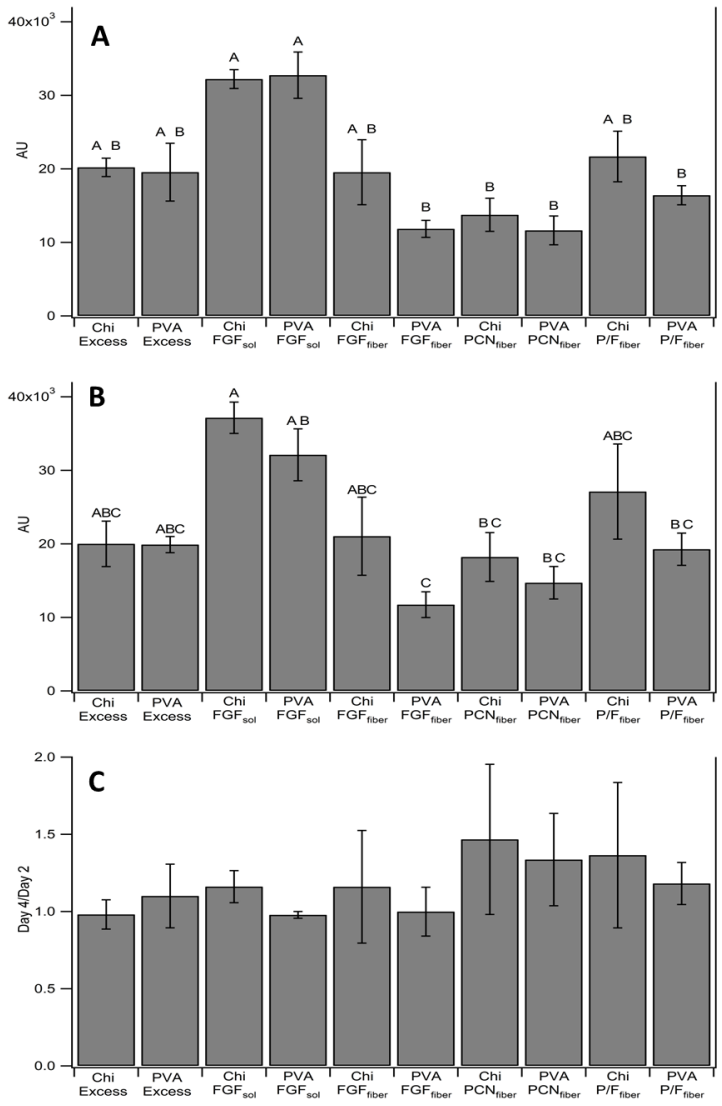

Figure 5.9. CellTiter-Blue results from MSC response to FGF-2 delivered from different formulations of coaxial nanofibers, chitosan in excess and PVA in excess with no additives (Chi Excess, PVA Excess), chitosan in excess and PVA in excess with FGF-2 delivered in solution at 1 ng mL^{-1} (Chi FGF_{sol} and PVA FGF_{sol}), chitosan in excess and PVA in excess with FGF-2 incorporated into the nanofibers (Chi FGF_{fiber} and PVA FGF_{fiber}), chitosan in excess and PVA in excess with PCNs incorporated into the nanofibers (Chi PCN_{fiber} and PVA PCN_{fiber}), and chitosan in excess and PVA in excess with FGF-2 bound to PCNs incorporated into the nanofibers (Chi P/F_{fiber} and PVA P/F_{fiber}) A.) Day 2 cell response, B.) Day 4 cell response, C.) Day 4 cell response divided by day 2 cell response, indicating proliferation if the result is greater than 1. Bars labeled with the same letter indicate same statistical group, there were no statistical differences in day 4 divided by day 2.

In our previous work we saw that when unprotected FGF-2 was preconditioned at 37 °C activity was lost over time. However, when FGF-2 was bound to our GAG-rich PCNs stability

was maintained for more than 21 days.[30] Additionally we have demonstrated sustained release of adsorbed FGF-2/PCN complexes from electrospun nanofibers over a period of 30 days.[33] In this work we have established a method for incorporating these complexes into electrospun nanofibers and shown that the FGF-2 remains active throughout processing. The activity levels are not statistically different from FGF-2 delivered in solution that did not undergo any processing. This suggests that this technique could be used to localize active growth factor into an implant for presentation to cells at a site of injury, mitigating the need for multiple bolus injections of growth factor.

5.5 CONCLUSIONS.

Electrospinning using an emulsion and a coaxial technique both successfully created nanofibers within the size range of collagen fiber bundles found in the ECM and resulted in dispersion of PCNs throughout the fiber mat. All three scaffold types exhibited cytocompatibility, with coaxial fibers with chitosan in excess showing the greatest amount of cell adhesion and spreading, emulsion fibers showing heterogeneous interactions, and coaxial fibers with PVA in excess demonstrating round cell morphology similar to that of chondrocytes. Emulsion fibers were not able to incorporate a stable clinical dose of FGF-2, but may be applicable for the delivery of small molecules that are resistant to organic solvents. Coaxial fibers were loaded with therapeutic levels of FGF-2. While there were no statistical differences, when FGF-2 was bound to GAG-rich PCNs and delivered via coaxial nanofibers with chitosan in excess, cell activity appeared to be higher than fibers containing FGF-2 with no PCNs, suggesting that the PCNs protect FGF-2 throughout the electrospinning process. Thus, coaxial electrospinning is a viable option for producing a bioactive scaffold for tissue engineering.

REFERENCES

1. Stevens, M. M.; George, J. H., Exploring and engineering the cell surface interface. *Science* **2005,** 310, (5751), 1135-1138.

2. Chen, R.; Hunt, J. A., Biomimetic materials processing for tissue-engineering processes. *Journal of Materials Chemistry* **2007,** 17, (38), 3974-3979.

3. Yang, S. F.; Leong, K. F.; Du, Z. H.; Chua, C. K., The design of scaffolds for use in tissue engineering. Part 1. Traditional factors. *Tissue Engineering* **2001,** 7, (6), 679-689.

4. Hubbell, J. A., Biomaterials in Tissue Engineering. *Bio-Technology* **1995,** 13, (6), 565-576.

5. Balakrishnan, B.; Banerjee, R., Biopolymer-Based Hydrogels for Cartilage Tissue Engineering. *Chemical Reviews* **2011,** 111, (8), 4453-4474.

6. Gasiorowski, J. Z.; Murphy, C. J.; Nealey, P. F., Biophysical Cues and Cell Behavior: The Big Impact of Little Things. *Annual Review of Biomedical Engineering, Vol 15* **2013,** 15, 155-176.

7. Mendonça, G.; Mendonça, D. B. S.; Simões, L. G. P.; Araújo, A. L.; Leite, E. R.; Duarte, W. R.; Aragão, F. J. L.; Cooper, L. F., The effects of implant surface nanoscale features on osteoblast-specific gene expression. *Biomaterials* **2009,** 30, (25), 4053-4062.

8. Yim, E. K. F.; Pang, S. W.; Leong, K. W., Synthetic nanostructures inducing differentiation of human mesenchymal stem cells into neuronal lineage. *Exp. Cell Res.* **2007,** 313, (9), 1820-1829.

9. Gittens, R. A.; McLachlan, T.; Olivares-Navarrete, R.; Cai, Y.; Berner, S.; Tannenbaum, R.; Schwartz, Z.; Sandhage, K. H.; Boyan, B. D., The effects of combined micron-/submicron-

scale surface roughness and nanoscale features on cell proliferation and differentiation. *Biomaterials* **2011,** 32, (13), 3395-3403.

10. Andersson, A.-S.; Bäckhed, F.; von Euler, A.; Richter-Dahlfors, A.; Sutherland, D.; Kasemo, B., Nanoscale features influence epithelial cell morphology and cytokine production. *Biomaterials* **2003,** 24, (20), 3427-3436.

11. Popat, K. C.; Eltgroth, M.; LaTempa, T. J.; Grimes, C. A.; Desai, T. A., Titania Nanotubes: A Novel Platform for Drug-Eluting Coatings for Medical Implants? *Small* **2007,** 3, (11), 1878-1881.

12. Cui, F.-Z.; Ge, J., New observations of the hierarchical structure of human enamel, from nanoscale to microscale. *J. Tissue Eng. Regener. Med.* **2007,** 1, (3), 185-191.

13. Wang, X.; Kim, H. J.; Wong, C.; Vepari, C.; Matsumoto, A.; Kaplan, D. L., Fibrous proteins and tissue engineering. *Mater. Today (Oxford, U. K.)* **2006,** 9, (12), 44-53.

14. Boddohi, S.; Kipper, M. J., Engineering Nanoassemblies of Polysaccharides. *Adv. Mater.* **2010,** 22, 2298-3016.

15. Ruckh, T. T.; Kumar, K.; Kipper, M. J.; Popat, K. C., Osteogenic differentiation of bone marrow stromal cells on poly([epsilon]-caprolactone) nanofiber scaffolds. *Acta Biomater.* **2010,** 6, 2949-2959.

16. Thiele, J.; Ma, Y.; Bruekers, S. M. C.; Ma, S.; Huck, W. T. S., 25th Anniversary Article: Designer Hydrogels for Cell Cultures: A Materials Selection Guide. *Advanced Materials* **2014,** 26, (1), 125-148.

17. Alberts, B.; Johnson, A.; Lewis, J.; Raff, M.; Roberts, K.; Walter, P., The Extracellular Matrix of Animals. In *Molecular Biology of the Cell*, 4 ed.; Garland Science: New York, 2002.

18. Almodovar, J.; Bacon, S.; Gogolski, J.; Kisiday, J. D.; Kipper, M. J., Polysaccharide-Based Polyelectrolyte Multi layer Surface Coatings can Enhance Mesenchymal Stem Cell Response to Adsorbed Growth Factors. *Biomacromolecules* **2010,** 11, (10), 2629-2639.

19. Babensee, J. E.; McIntire, L. V.; Mikos, A. G., Growth factor delivery for tissue engineering. *Pharm. Res.* **2000,** 17, (5), 497-504.

20. Li, J. T.; Pei, M., Optimization of an In Vitro Three-Dimensional Microenvironment to Reprogram Synovium-Derived Stem Cells for Cartilage Tissue Engineering. *Tissue Eng., Part A.* **2011,** 17, (5-6), 703-712.

21. Somers, P.; Cornelissen, R.; Thierens, H.; Van Nooten, G., An optimized growth factor cocktail for ovine mesenchymal stem cells. *Growth Factors* **2012,** 30, (1), 37-48.

22. Chen, R. R.; Mooney, D. J., Polymeric growth factor delivery strategies for tissue engineering. *Pharmaceutical Research* **2003,** 20, (8), 1103-1112.

23. Gu, X. S.; Ding, F.; Yang, Y. M.; Liu, J., Construction of tissue engineered nerve grafts and their application in peripheral nerve regeneration. *Prog. Neurobiol.* **2011,** 93, (2), 204-230.

24. Ohta, M.; Suzuki, Y.; Chou, H.; Ishikawa, N.; Suzuki, S.; Tanihara, M.; Mizushima, Y.; Dezawa, M.; Ide, C., Novel heparin/alginate gel combined with basic fibroblast growth factor promotes nerve regeneration in rat sciatic nerve. *J. Biomed. Mater. Res., Part A* **2004,** 71A, (4), 661-668.

25. Wang, S. G.; Cai, Q.; Hou, J. W.; Bei, J. Z.; Zhang, T.; Yang, J.; Wan, Y. Q., Acceleration effect of basic fibroblast growth factor on the regeneration of peripheral nerve through a 15-mm gap. *J. Biomed. Mater. Res., Part A* **2003,** 66A, (3), 522-531.

26. Chen, W.; Shi, C. Y.; Yi, S. H.; Chen, B.; Zhang, W. W.; Fang, Z. Q.; Wei, Z. L.; Jiang, S. X.; Sun, X. C.; Hou, X. L.; Xiao, Z. F.; Ye, G.; Dai, J. W., Bladder Regeneration by Collagen

Scaffolds With Collagen Binding Human Basic Fibroblast Growth Factor. *J. Urol.* **2010,** 183, (6), 2432-2439.

27. Kurane, A.; Simionescu, D. T.; Vyavahare, N. R., In vivo cellular repopulation of tubular elastin scaffolds mediated by basic fibroblast growth factor. *Biomaterials* **2007,** 28, (18), 2830-2838.

28. Huang, X.; Yang, D. S.; Yan, W. Q.; Shi, Z. L.; Feng, J.; Gao, Y. B.; Weng, W. J.; Yan, S. G., Osteochondral repair using the combination of fibroblast growth factor and amorphous calcium phosphate/poly(L-lactic acid) hybrid materials. *Biomaterials* **2007,** 28, (20), 3091-3100.

29. Laham, R. J.; Rezaee, M.; Post, M.; Xu, X. Y.; Sellke, F. W., Intrapericardial administration of basic fibroblast growth factor: Myocardial and tissue distribution and comparison with intracoronary and intravenous administration. *Catheter. Cardiovasc. Interv.* **2003,** 58, (3), 375-381.

30. Place, L. W.; Sekyi, M.; Kipper, M. J., Aggrecan-Mimetic, Glycosaminoglycan-Containing Nanoparticles for Growth Factor Stabilization and Delivery. *Biomacromolecules* **2014,** 15, (2), 680-689.

31. Richardson, T. P.; Peters, M. C.; Ennett, A. B.; Mooney, D. J., Polymeric system for dual growth factor delivery. *Nat. Biotechnol.* **2001,** 19, (11), 1029-1034.

32. Tessmar, J. K.; Gopferich, A. M., Matrices and scaffolds for protein delivery in tissue engineering. *Adv. Drug Delivery Rev.* **2007,** 59, (4-5), 274-291.

33. Volpato, F. Z.; Almodovar, J.; Erickson, K.; Popat, K. C.; Migliaresi, C.; Kipper, M. J., Preservation of FGF-2 bioactivity using heparin-based nanoparticles, and their delivery from electrospun chitosan fibers. *Acta Biomaterialia* **2012,** 8, (4), 1551-1559.

34. Sakiyama-Elbert, S. E.; Hubbell, J. A., Development of fibrin derivatives for controlled release of heparin-binding growth factors. *Journal of Controlled Release* **2000,** 65, (3), 389-402.

35. Harmer, N. J.; Ilag, L. L.; Mulloy, B.; Pellegrini, L.; Robinson, C. V.; Blundell, T. I., Towards a resolution of the stoichiometry of the fibroblast growth factor (FGF)-FGIF receptor - Heparin complex. *J. Mol. Biol.* **2004,** 339, (4), 821-834.

36. Frescaline, G.; Bouderlique, T.; Huynh, M. B.; Papy-Garcia, D.; Courty, J.; Albanese, P., Glycosaminoglycans mimetics potentiate the clonogenicity, proliferation, migration and differentiation properties of rat mesenchymal stem cells. *Stem Cell Res.* **2012,** 8, (2), 180-192.

37. Maccarana, M.; Casu, B.; Lindahl, U., Minimal Sequence in Heparin Heparan-Sulfate Required for Binding of Basic Fibroblast Growth-Factor. *J. Biol. Chem.* **1993,** 268, (32), 23898-23905.

38. Smith, S. M. L.; West, L. A.; Govindraj, P.; Zhang, X. Q.; Ornitz, D. M.; Hassell, J. R., Heparan and chondroitin sulfate on growth plate perlecan mediate binding and delivery of FGF-2 to FGF receptors. *Matrix Biol.* **2007,** 26, (3), 175-184.

39. Mccaffrey, T. A.; Falcone, D. J.; Du, B. H., Transforming Growth Factor-Beta-1 Is a Heparin-Binding Protein - Identification of Putative Heparin-Binding Regions and Isolation of Heparins with Varying Affinity for Tgf-Beta-1. *J. Cell. Physiol.* **1992,** 152, (2), 430-440.

40. Guimond, S.; Maccarana, M.; Olwin, B. B.; Lindahl, U.; Rapraeger, A. C., Activating and Inhibitory Heparin Sequences for FGF-2 (Basic FGF) - Distinct Requirements for FGF-1, FGF-2, and FGF-4. *J. Biol. Chem.* **1993,** 268, (32), 23906-23914.

41. Berry, D.; Kwan, C. P.; Shriver, Z.; Venkataraman, G.; Sasisekharan, R., Distinct heparan sulfate glycosaminoglycans are responsible for mediating fibroblast growth factor-2

biological activity through different fibroblast growth factor receptors. *FASEB J.* **2001,** 15, (6), 1422-1424.

42. Taylor, K. R.; Rudisill, J. A.; Gallo, R. L., Structural and sequence motifs in dermatan sulfate for promoting fibroblast growth factor-2 (FGF-2) and FGF-7 activity. *J. Biol. Chem.* **2005,** 280, (7), 5300-5306.

43. Princz, M. A.; Sheardown, H., Heparin-modified dendrimer cross-linked collagen matrices for the delivery of basic fibroblast growth factor (FGF-2). *J. Biomater. Sci., Polym. Ed.* **2008,** 19, (9), 1201-1218.

44. Liu, Z. G.; Jiao, Y. P.; Liu, F. N.; Zhang, Z. Y., Heparin/chitosan nanoparticle carriers prepared by polyelectrolyte complexation. *J. Biomed. Mater. Res., Part A* **2007,** 83A, (3), 806-812.

45. Chen, M. C.; Wong, H. S.; Lin, K. J.; Chen, H. L.; Wey, S. P.; Sonaje, K.; Lin, Y. H.; Chu, C. Y.; Sung, H. W., The characteristics, biodistribution and bioavailability of a chitosan-based nanoparticulate system for the oral delivery of heparin. *Biomaterials* **2009,** 30, (34), 6629-6637.

46. Martins, A. F.; Pereira, A. G. B.; Fajardo, A. R.; Rubira, A. F.; Muniz, E. C., Characterization of polyelectrolytes complexes based on N,N,N-trimethyl chitosan/heparin prepared at different pH conditions. *Carbohydr. Polym.* **2011,** 86, (3), 1266-1272.

47. Fajardo, A. R.; Lopes, L. C.; Valente, A. J. M.; Rubira, A. F.; Muniz, E. C., Effect of stoichiometry and pH on the structure and properties of Chitosan/Chondroitin sulfate complexes. *Colloid Polym. Sci.* **2011,** 289, (15-16), 1739-1748.

48. Drogoz, A.; David, L.; Rochas, C.; Domard, A.; Delair, T., Polyelectrolyte complexes from polysaccharides: Formation and stoichiometry monitoring. *Langmuir* **2007,** 23, (22), 10950-10958.

49. Schatz, C.; Domard, A.; Viton, C.; Pichot, C.; Delair, T., Versatile and efficient formation of colloids of biopolymer-based polyelectrolyte complexes. *Biomacromolecules* **2004,** 5, (5), 1882-1892.

50. Mori, Y.; Nakamura, S.; Kishimoto, S.; Kawakami, M.; Suzuki, S.; Matsui, T.; Ishihara, M., Preparation and characterization of low-molecular-weight heparin/protamine nanoparticles (LMW-H/P NPs) as FGF-2 carrier. *International Journal of Nanomedicine* **2010,** 5, 147-155.

51. Tan, Q.; Tang, H.; Hu, J. G.; Hu, Y. R.; Zhou, X. M.; Tao, Y. M.; Wu, Z. S., Controlled release of chitosan/heparin nanoparticle-delivered VEGF enhances regeneration of decellularized tissue-engineered scaffolds. *Int. J. Nanomed.* **2011,** 6, 929-942.

52. Almodovar, J.; Kipper, M. J., Coating Electrospun Chitosan Nanofibers with Polyelectrolyte Multilayers Using the Polysaccharides Heparin and N,N,N-Trimethyl Chitosan. *Macromol. Biosci.* **2011,** 11, (1), 72-76.

53. Bellan, L. M.; Craighead, H. G., Nanomanufacturing Using Electrospinning. *Journal of Manufacturing Science and Engineering-Transactions of the Asme* **2009,** 131, (3), 4.

54. Bhardwaj, N.; Kundu, S. C., Electrospinning: A fascinating fiber fabrication technique. *Biotechnology Advances* **2010,** 28, (3), 325-347.

55. Crespy, D.; Friedemann, K.; Popa, A. M., Colloid-Electrospinning: Fabrication of Multicompartment Nanofibers by the Electrospinning of Organic or/and Inorganic Dispersions and Emulsions. *Macromolecular Rapid Communications* **2012,** 33, (23), 1978-1995.

56. Briggs, T.; Arinzeh, T. L., Examining the formulation of emulsion electrospinning for improving the release of bioactive proteins from electrospun fibers. *Journal of Biomedical Materials Research Part A* **2014,** 102, (3), 674-684.

57. Xu, X. L.; Yang, L. X.; Xu, X. Y.; Wang, X.; Chen, X. S.; Liang, Q. Z.; Zeng, J.; Jing, X. B., Ultrafine medicated fibers electrospun from W/O emulsions. *Journal of Controlled Release* **2005,** 108, (1), 33-42.

58. Zhao, S.; Zhao, J.; Dong, S.; Huangfu, X.; Li, B.; Yang, H.; Zhao, J.; Cui, W., Biological augmentation of rotator cuff repair using bFGF-loaded electrospun poly(lactide-co-glycolide) fibrous membranes. *International Journal of Nanomedicine* **2014,** 9, 2373-2385.

59. Bock, N.; Dargaville, T. R.; Woodruff, M. A., Electrospraying of polymers with therapeutic molecules: State of the art. *Progress in Polymer Science* **2012,** 37, (11), 1510-1551.

60. Thuy, T. T. N.; Ghosh, C.; Hwang, S. G.; Chanunpanich, N.; Park, J. S., Porous core/sheath composite nanofibers fabricated by coaxial electrospinning as a potential mat for drug release system. *International Journal of Pharmaceutics* **2012,** 439, (1-2), 296-306.

61. Man, Z.; Yin, L.; Shao, Z.; Zhang, X.; Hu, X.; Zhu, J.; Dai, L.; Huang, H.; Yuan, L.; Zhou, C.; Chen, H.; Ao, Y., The effects of co-delivery of BMSC-affinity peptide and rhTGF-beta 1 from coaxial electrospun scaffolds on chondrogenic differentiation. *Biomaterials* **2014,** 35, (19), 5250-5260.

62. Ji, W.; Yang, F.; van den Beucken, J.; Bian, Z. A.; Fan, M. W.; Chen, Z.; Jansen, J. A., Fibrous scaffolds loaded with protein prepared by blend or coaxial electrospinning. *Acta Biomaterialia* **2010,** 6, (11), 4199-4207.

63. Liu, S.; Qin, M. J.; Hu, C. M.; Wu, F.; Cui, W. G.; Jin, T.; Fan, C. Y., Tendon healing and anti-adhesion properties of electrospun fibrous membranes containing bFGF loaded nanoparticles. *Biomaterials* **2013,** 34, (19), 4690-4701.

64. Crespy, D.; Friedemann, K.; Popa, A.-M., Colloid-Electrospinning: Fabrication of Multicompartment Nanofibers by the Electrospinning of Organic or/and Inorganic Dispersions and Emulsions. *Macromolecular Rapid Communications* **2012,** 33, (23), 1978-1995.

65. Ma, P. X., Biomimetic materials for tissue engineering. *Advanced Drug Delivery Reviews* **2008,** 60, (2), 184-198.

CHAPTER 6

Nanostructured Biomaterials from Electrospun Demineralized Bone Matrix: A Survey of Processing and Crosslinking Strategies[6]

6.1 SUMMARY.

In the design of scaffolds for tissue engineering biochemical function and nanoscale features are of particular interest. Natural polymers provide a wealth of biochemical function, but do not have the processability of synthetic polymers, limiting their ability to mimic the hierarchy of structures in the natural extracellular matrix. Thus, they are often combined with synthetic carrier polymers to enable processing. Demineralized bone matrix (DBM), a natural polymer, is allograft bone with inorganic material removed. DBM contains the protein components of bone, which includes adhesion ligands and osteoinductive signals, such as important growth factors. Herein we describe a novel method for tuning the nanostructure of DBM through electrospinning without the use of a carrier polymer. This work surveys solvents and solvent blends for electrospinning DBM. Blends of hexafluoroisopropanol and trifluoroacetic acid are studied in detail. The effects of DBM concentration and dissolution time on solution viscosity are also reported and correlated to observed differences in electrospun fiber morphology. We also present a survey of techniques to stabilize the resultant fibers with respect to aqueous environments. Glutaraldehyde vapor treatment is successful at maintaining both macroscopic and microscopic structure of the electrospun DBM fibers. Finally, we report results from tensile testing of

[6]Portions of this chapter appear in the following:
Leszczak, V., Place, L.W., Franz, N., Popat, K.C., and Kipper, M.J.; "Nanostructured Biomaterials from Electrospun Demineralized Bone Matrix: A Survey of Processing and Crosslinking Strategies", *ACS Applied Materials and Interfaces*, In Press. DOI:10.1021/am501700e. Copyright ACS 2014. Used with permission.

stabilized DBM nanofiber mats, and preliminary evaluation of their cytocompatibility. The DBM nanofiber mats exhibit good cytocompatibility toward human dermal fibroblasts (HDF) in a 4-day culture; neither the electrospun solvents nor the crosslinking results in any measurable residual cytotoxicity toward HDF.

6.2 INTRODUCTION.

The hierarchy of structures at different length scales is a distinguishing characteristic of all human tissues. These structural features give rise to biological properties that govern tissue function and influence the myriad of processes involved in immune response and tissue repair. In the design of scaffolds for tissue engineering, features at the nanoscale are of particular interest, as cells involved in tissue repair respond to nanoscale topographical features and nanomechanical properties of materials by migrating, differentiating or de-differentiating, and altering their cytokine profiles, and other phenotype indicators.[1-9]

Both synthetic and natural polymers have been researched extensively to create nanoscale scaffolds for engineering various tissues. Synthetic polymers may have tunable degradation kinetics, processability and mechanical properties.[10] However, current scaffolds fabricated from synthetic polymers have surfaces that cells do not recognize unless proteins and peptides are introduced.[11] This lack of recognition may inhibit cell attachment, proliferation and differentiation.[2] Furthermore, synthetic polymers face a challenge when implanted into the body. Despite the fact that they are termed biocompatible and biodegradable, foreign body reactions inhibit the amount of tissue integration, which can ultimately lead to implant failure.[12-15] Natural polymers may be the solution to creating a scaffold that can drive cell proliferation and differentiation, while limiting foreign body reactions.[16, 17] Natural polymers such as collagen, glycosaminoglycans, chitosan and alginates are advantageous due to their low toxicity and low

chronic inflammatory response.[18] Unlike synthetic polymers, natural polymers have a complexity that consists of functional peptides, growth factors and bioactive factors which are already present in the body. Therefore, biologically derived materials can possibly provide both a scaffold and a signal for tissue engineering applications, without the addition of growth factors or cytokines.[19] However, many natural polymers do not have the processability of synthetic polymers, limiting their ability to mimic the hierarchy of structures in the natural ECM. Thus, they are often combined with synthetic carrier polymers to facilitate processing into tissue scaffolds.

Demineralized bone matrix (DBM), a natural polymer blend, is allograft bone with inorganic material removed. DBM contains the protein components of bone, including adhesion ligands and osteoinductive signals. It is the natural protein network in which osteocytes perform the anabolic and catabolic processes that maintain healthy bone. Therefore, it can be remodeled and it promotes mineralization. Hence, over the past 30 years, the use of DBM in orthopedic surgery has flourished. However, as prepared, DBM is a dry powder that is typically combined with carrier polymers or other materials to form a composite, paste, or putty that can be more readily used in an orthopedic surgery.[20] Commercial products containing DBM are now available in a variety of different shapes, sizes and forms including morsels, cubes, dowels, strips, etc. However, none of the aforementioned products have tunable nano-features inherent in the osteoconductive nanostructure of bone. Thus, natural polymers such as DBM would be greatly improved for tissue engineering applications if they could be processed into biomimetic nanostructures.

To realize the potential of donated human tissues to develop new tissue constructs, this work establishes techniques to design the nanostructure of DBM. Thus far, DBM products have

not been successfully manufactured without the use of a carrier. Further, no DBM products on the market have engineered nano-structured features. Engineering nanostructured materials from human tissues is potentially a simple, low-cost, reproducible strategy for imparting stable biological signals to tissue engineering scaffolds. This strategy may rival or surpass more expensive strategies like growth factor and gene delivery. Herein we describe a novel method for tuning the nanostructure of DBM through electrospinning, a versatile technique for the fabrication of nano-featured surfaces.[21]

To form electrospun nanofibers, a polymer solution is drawn into a fiber by a strong electric field (~kV cm^{-1}) between a nozzle and a grounded collector, while a syringe pump supplies polymer solution to the nozzle. The solvent rapidly evaporates as the polymer solution travels from the nozzle to the collector, resulting in the formation of a nanofiber, collected in a randomly oriented, non-woven mat. The polymer solution in a volatile solvent must have appropriate surface tension, viscosity, conductivity, and polymer concentration for the process to be successful. Nanofiber scaffolds can be prepared from a wide number of synthetic and natural polymers, providing a three-dimensional cell culture environment, nanoscale topographical and mechanical cues, and a porous network for nutrient and metabolite exchange. Nanofibers from natural polymers have been proposed as tissue engineering scaffolds, including collagen, chitosan, silk, synthetic elastin peptides, and DNA.[22, 23] Blends of natural and synthetic polymers (e.g. collagen/polyester and collagen/elastin/polyester) have also been used to make nanofiber scaffolds.[24] Very recently, human adipose tissue ECM has been proposed as a nanofiber scaffold material.[25] To our knowledge, this report from 2012 is the only report in the peer-reviewed literature in which a pure tissue ECM (rather than an ECM component) has been formed into nanofiber tissue scaffolds.

In this work, we survey techniques for production and stabilization of electrospun DBM nanofibers. This novel technique results in a biopolymer construct that is stable in aqueous conditions and contains nanoscale features that recapitulate features of tissue ECM, without the use of a synthetic carrier polymer. Finally, we demonstrate that crosslinked DBM nanofibers are cytocompatible using human dermal fibroblasts.

6.3 METHODS.

6.3.1 Materials. Morselized demineralized bone matrix (DBM) was generously supplied by Allosource (Centennial, CO). Chloroform, dimethylformamide (DMF), glycerol, methanol, and tetrahydrofuran (THF) were purchased from Mallinckrodt Chemicals (St. Louis, MO). Dichloromethane (DCM), ethanol, hexafluoro-2-propanol (HFIP), and trifluoroacetic acid (TFA), were purchased from Acros Organics (Geel, Belgium). Dimethylsulfoxide (DMSO) was purchased from EMD Chemicals (Darmstadt, Germany). Acetic acid was purchased from Fisher Scientific (Pittsburgh, PA). Ammonium hydroxide, glutaraldehyde (30 %), riboflavin, and tetrachloroethylene (TCE) were purchased from Sigma-Aldrich (St. Louis, MO). Isopropanol (IPA) was purchased from Macron Chemicals (Phillipsburg, NJ). 1-Ethyl-3-[3-dimethylaminopropyl]carbodiimide hydrochloride (EDC), HEPES buffer, and tissue culture polystyrene coverslips were purchased from Thermo (Waltham, MA). Phosphate buffered saline (PBS) and Trypsin 0.25% were purchased from HyClone (Logan, UT). Antibiotic-antimycotic (anti/anti) was purchased from Gibco (Grand Island, NY). Dulbecco's Modification of Eagle's Medium (DMEM, supplemented with 4.5 g L^{-1} glucose, L-glutamine, and sodium pyruvate) was purchased from Corning Cellgro® (Manassas, VA). Fetal Bovine Serum (FBS) was purchased from Atlanta Biologicals (Flowery Branch, GA). Human Dermal Fibroblasts (HDF) were purchased from Zen-Bio (Research Triangle Park, NC). LIVE/DEAD® Viability/Cytotoxicity

Kit for mammalian cells was purchased from Invitrogen (Eugene, OR). CellTiter-Blue® cell viability assay was purchased from Promega (Madison, WI). All chemicals were used as received unless indicated otherwise.

6.3.2 Determining Appropriate Solvents for DBM. Solutions were made by adding 0.5 g of DBM to 10 mL of the solvents listed in Table 1 at room temperature (RT) and 65 °C. Solutions of DBM with pure solvents were observed after 18-24 hrs according to Table 1. Solvent blends were made by combining DMF, DCM, HFIP and glycerol with TFA in 50:50, 70:30 and 90:10 ratios (Table 2). Solutions were made by adding 0.5 g DBM to these 10 mL solvent blends. Solutions of DBM with solvent blends were observed after 22 hrs at 40 °C.

6.3.3 Effect of DBM Concentration on Viscosity. To study the effect of DBM concentration on viscosity, solutions of 0.5 g, 0.8 g, 1.1 g, 1.4 g, 1.7 g and 2.0 g of DBM in a 10 mL solvent blend of 70:30 HFIP:TFA were made. Each solution was allowed to dissolve for 22 hrs at 40 °C. At 22 hrs, solutions were removed from heat and allowed to reach room temperature before taking viscosity measurements. Viscosity measurements were taken with a TL5 or TL6 spindle on a Fungilab viscometer attached to a water bath to maintain constant temperature at 25 °C. After taking viscosity measurements, solutions were immediately electrospun at 1 mL hr^{-1}, 15 kV and a collector distance of 6 in. Fibers were then coated with a 10-nm layer of gold and imaged at 7 kV on a Jeol JSM-5600F scanning electron microscope (SEM) to examine fiber structure. The images were analyzed using Image J, to measure fiber diameters. Between 320 and 450 fiber diameter measurements were obtained from multiple micrographs representing each condition.

6.3.4 Solution Stability. A solution of 1.1 g of DBM in a 10 mL solvent blend of 70:30 HFIP:TFA was made at 40 °C for 22 hrs. This solution was photographed digitally and then

incubated at RT for an additional 48 hrs. A second photograph was taken at this time and solution color was compared.

This same solution (five different vials for five different time points) was prepared and tested for change in viscosity over time. After 22 hrs of dissolution, the vials were allowed to cool to RT and the viscosity of the zero time point vial was tested using a TL5 spindle on a Fungilab viscometer attached to a water bath to maintain constant temperature at 25 °C. The other four vials were incubated at RT for 6, 12, 24, or 48 hrs. At each respective time point the sample viscosity was measured.

After taking viscosity measurements, each of the solutions was immediately electrospun at 1 mL hr^{-1}, 15 kV and a collector distance of 6 in. After spinning, each sample was coated with a 10-nm layer of gold and imaged at 7 kV using an SEM to examine fiber structure. The images were analyzed using Image J, to measure fiber diameters. Between 320 and 450 fiber diameter measurements were obtained from multiple micrographs representing each condition.

6.3.5 Stabilizing DBM Fibers. A solution of 1.1 g of DBM in a 10 mL solvent blend of 70:30 HFIP:TFA was made at 40 °C for 22 hrs and electrospun at 1 mL hr^{-1}, 15 kV and a collector distance of 6 in. After spinning, a sample of neat fibers was vacuum dried for 18 hrs. A number of solvents were investigated for extraction of residual fluorinated solvents from the fibers; these are listed in Table 3. Spot tests were done on neat fibers using these solvents to check for solvent compatibility with fibers. TCE was chosen as a likely solvent for the residual TFA and HFIP. Fibers were soaked in TCE for 18 hrs and dried for analysis. Neat fibers, vacuum dried fibers, TCE-treated fibers, and DBM powder were subjected to X-ray photoelectron spectroscopy (XPS) on a Physical Electronics 5800 spectrometer. Spectra were analyzed using Multipak.

Several crosslinking methods were attempted. Fibers underwent dehydrothermal (DHT) treatment and ultraviolet (UV) light treatment alone and in combination. For DHT treatment, they were placed in a vacuum oven at 150 °C for 18 hrs. Ultraviolet (UV) treatment was performed at 256 nm for 1 hr on each side of the fiber mat. Fibers were then exposed to water to check for stability.

Three covalent chemical crosslinking agents, genipin, 1-ethyl-3-[3-dimethylaminopropyl] carbodiimide hydrochloride (EDC), and riboflavin were studied. Suitable solvents from Table 3 were chosen for the crosslinking experiments. Suitable solvents in this case are non-solvents for DBM but are able to solubilize the crosslinker. Genipin, at 30 mM, was dissolved in isopropanol (IPA) and fibers were soaked in this solution for 18, 42, or 72 hours.[26] A 200 mM solution of EDC in IPA was made and fibers were soaked for 18, 42, or 72 hours. EDC-treated fiber mats were rinsed with sodium phosphate buffer (pH 7.4) for 2 hrs, followed by rinsing with phosphate buffered saline (PBS) for an additional 2 hrs. This method was adapted from Barnes.[27] This experiment was repeated using dichloromethane (DCM), chloroform, and TCE as solvents for 18 hrs. Samples of the fiber mats soaked in only the solvent, the solvent + EDC, and the solvent + EDC followed by PBS were then and coated with a 10 nm layer of gold and imaged at 7 kV using SEM.

In situ crosslinking via addition of EDC or riboflavin directly to the spinning solutions was also studied. EDC (38.5 mg mL^{-1}) or riboflavin (2 mg mL^{-1}) was mixed into the electrospinning solution immediately before spinning. The same electrospinning procedure previously described was used here. After electrospinning, the riboflavin sample was exposed to broad spectrum UV light for 1 hr. After spinning, fibers were exposed to water to test for stability. Fibers containing riboflavin before and after UV treatment were imaged using SEM.

Finally, crosslinking using glutaraldehyde vapor was investigated. After spinning, fibers supported with aluminum foil were placed into a desiccator with 10 mL of glutaraldehyde (50%). The dessicator was subjected to vacuum for 3 days. After 3 days, fibers were removed and exposed to DI water to remove unreacted glutaraldehyde and to test for stability.[28] Glutaraldehyde-crosslinked fibers before and after exposure to DI water were imaged using SEM.

6.3.6 Mechanical Testing. Uniaxial tensile testing of a dog-bone-shaped sample of glutaraldehyde crosslinked DBM nanofiber mat was performed using a servo-hydraulic mechanical test system (Bionic Model 370.02 MTS Corp, Eden Prairie, MN) equipped with a n 8.9 N load cell (Futek LSB200, Irvine, California). The fiber mat was hydrated with PBS and positioned into customized thin film grips. The fiber mat was speckle coated with India ink and surface images were captured during tensile testing (0.1 % per second with a 0.01 N preload) with a CCD camera (Flea3, Point Grey Research, Richmond, BC, Canada) until mechanical failure occurred.

To calculate strain, images were analyzed using a Matlab (Mathworks, Natick, MA)-based Digital Image Correlation code (E.M.C. Jones, University of Illinois) to track the displacement of the speckle pattern in the central region of each dog-bone-shaped sample. Stress was calculated by dividing the force values by the cross-sectional area of the central region of sample, which had a thickness of 65 μm. Tensile modulus was obtained from the slope of the linear region of the stress-strain curve.

6.3.7 Cytocompatibility Evaluation. DBM samples were soaked in PBS on a shaker plate for seven days with PBS changes every 24 h, to ensure the complete removal of glutaraldehyde after crosslinking. An 8-mm biopsy punch was used to cut samples of DBM and

TCPS for cell culture. These were then treated with ultraviolet light for 1 hour for sterilization. HDF were expanded and seeded in DMEM containing 10% FBS, 2.5% HEPES, and 1% anti/anti. HDF were seeded at 100,000 cells/sample (in 200 uL DMEM) in an untreated 48-well plate. Cells were allowed to attach for 3 h, then 300 uL DMEM was added to each well. Samples were moved to a new untreated 48-well plate with fresh DMEM the next day and samples were assayed for cell viability after 24 h of culture. Cell metabolic activity was assayed after 1 day and 4 days of culture, using the CellTiter-Blue® assay. Both the viability and metabolic activity of cells on nanofibers were compared to the cells on TCPS.

The Live/Dead® assay was used according to manufacturer's instructions. Briefly, three samples of TCPS and three samples of DBM seeded with HDF and one sample of blank DBM were stained with calcein (2 µM) and ethidium homodimer-1 (4 µM) in PBS for 35 min. Samples were imaged using a Zeiss fluorescence microscope with filter sets 62 HE BP 585/35 (red) and BP 474/28 (green). The CellTiter-Blue® cell viability assay was used according to manufacturer's instructions. Briefly, 100 µL of CellTiter-Blue dye was added to 500 µl of DMEM in an untreated 48-well plate containing, three samples of TCPS and three samples of DBM seeded with HDF and three samples of blank TCPS and three samples of blank DBM and incubated for 8 h at 37°C. Three 150 µL samples were taken from each sample and placed in a black 96-well plate and read in a fluorescence microplate reader (FLUOstar Omega, BMG Labtech, Durham, NC) at 544 nm excitation and 590 nm emission.

6.4 RESULTS AND DISCUSSION.

6.4.1 Determining appropriate solvents for DBM. Prior to electrospinning, an appropriate solvent or solvent blend capable of dissolving the DBM had to be determined. Initially, pure solvents were used to investigate the solubility of DBM. TFA is the only solvent

from Table 1 that can dissolve DBM completely at 5 g dL^{-1} (Table 1) at room temperature and at 65 °C, turning the solution a transparent dark brown color. The dark brown color of the solution may indicate that TFA oxidizes the DBM. TFA is a common electrospinning solvent for synthetic and natural polymers and polymer blends due to its volatility, miscibility with other solvents, and its acidity.[29-33] However, electrospinning the homogenous solution of DBM in TFA at 1 mL hr^{-1} was not successful over a range of voltages (0-6 kV) and tip-to-collector distances (5-7in). While attempting to electrospin charge build up and arcing occurred with no fiber formation, limiting the voltage to 6 kV. Therefore, the solution of DBM in TFA does not provide a solution with an ideal viscosity or electrical properties for electrospinning. Thus, blends of solvents with TFA were pursued to increase viscosity and decrease charging, while minimizing oxidation.

Table 6.1. Dissolution for DBM in pure solvents (5 % DBM), at room temperature and at 65 °C.

Non-polar solvents	Vapor pressure at 20 °C (Torr)	Dielectric constant	Soluble at RT	Soluble at 65 °C
Chloroform	158.4	4.8	No	No
Dichloromethane (DCM)	350	9.1	No	No
Polar aprotic solvents				
Tetrahydrofuran (THF)	142	7.6	No	No
Dimethylformamide (DMF)	2.7	36.7	No	No
Dimethylsulfoxide (DMSO)	<1	46.7	No	No
Polar protic solvents				
Acetic Acid	10.1	6.2	No	Partially
Trifluoroacetic acid (TFA)	97.5	8.6	***Yes***	***Yes***
Hexafluoroisopropanol (HFIP)	120	16.8	No	Partially
Glycerol	<1	42.5	No	No
Water	17.54	80.1	No	No

Next, solvent blends containing TFA were investigated (Table 6.2.). In order to potentially preserve the biological function of proteins in DBM, the dissolution temperature for the solvent blend experiments was reduced to 40 °C.[34] DMF:TFA blends do not dissolve DBM;

DCM:TFA and glycerol:TFA partially dissolve DBM at 50:50, 70:30 and 90:10 solvent ratios, and HFIP:TFA dissolve DBM at 50:50, 70:30 and 90:10 ratios after 22 hrs. In addition to not being capable of dissolving the DBM completely, the high volatility of DCM (boiling point = 39.6 ºC) hindered its use in preparing the electrospinning solution, and glycerol was too viscous and not volatile enough for use in the electrospinning process. Hence, HFIP was chosen as an appropriate solvent to blend with TFA. By visually inspecting the solutions, it was noted that the 90:10 HFIP:TFA solution was turbid, while the 50:50 HFIP:TFA blend was still dark brown in color (Figure 6.1.). Thus the blend of 70:30 HFIP:TFA was selected, as this composition minimizes the amount of TFA used, while still achieving complete dissolution of the DBM.

Table 6.2. Dissolution of DBM in solvent blends (5 % DBM at 40 ºC for 22 h).

	50:50	70:30	90:10
DMF:TFA	No	No	No
DCM:TFA	***Yes***	***Yes***	***Yes***
HFIP:TFA	***Yes***	***Yes***	***Yes***
Glycerol:TFA	***Yes***	***Yes***	***Yes***

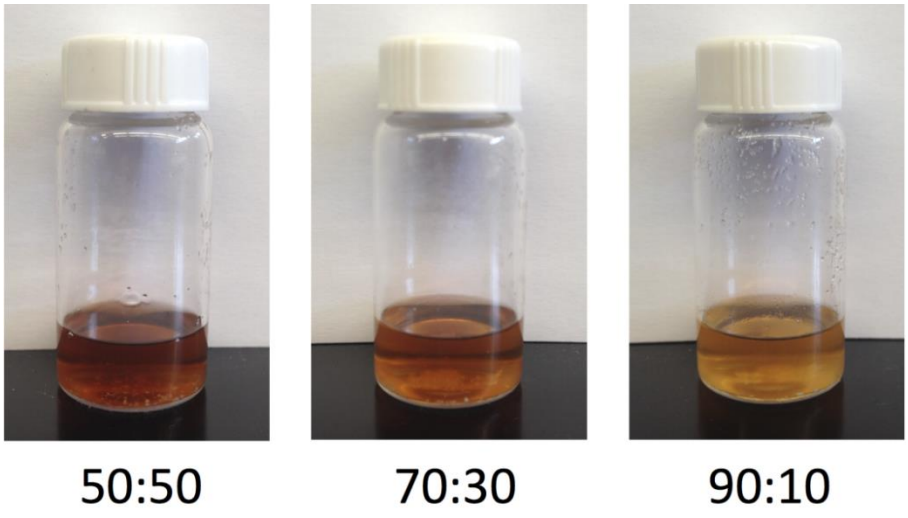

Figure 6.1. HFIP:TFA blends with 5 % DBM observed after 22 h at 40 °C. The 90:10 HFIP:TFA solution is turbid, while the 50:50 HFIP:TFA blend is still dark brown in color. Thus the 70:30 HFIP:TFA blend was further pursued.

6.4.2 Effect of concentration on viscosity. The size and uniformity of electrospun fibers is highly dependent on the viscosity of the solution. To reveal how viscosity affects the morphology of DBM fibers, various concentrations of DBM (5, 8, 11, 14, 17, and 20 g dL^{-1}) in 70:30 HFIP:TFA were electrospun. Viscosity of the solutions increased exponentially with solution concentration (Figure 6.2.).

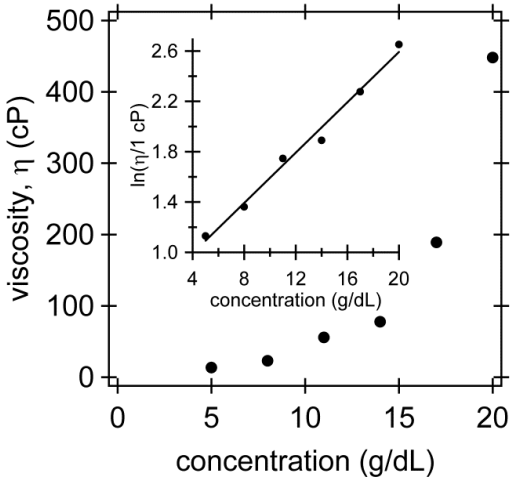

Figure 6.2. Viscosity of DBM in 70:30 HFIP:TFA increases exponentially with increasing concentration.

Each solution was electrospun and fiber structure was examined with SEM. Representative images and histograms of fiber diameters obtained from multiple images at each condition are shown in Figure 6.3. Electrospraying occurred when attempting to electrospin the 5 g dL^{-1} DBM solution (13.5 cP), evident by the presence of particulates in Figure 6.3. A. It is common at low concentrations, when surface tension of the solution is high, for there to be insufficient viscosity and electrical conductivity of the solution, producing beads.[35] As the concentration of DBM and the viscosity of the solution increase, fibers become more uniform and beads disappear. At high polymer concentrations chain entanglements are more readily created, which stabilize the electrospinning jet by inhibiting jet breakup. However, when polymer concentration gets too high, the electrospinning process is also inhibited. This can be seen at 17 g dL^{-1} (189 cP) and 20

g dL^{-1} DBM (448 cP) concentration. At these highest solution concentrations (17 g dL^{-1} and 20 g dL^{-1}) the distribution of fiber diameters becomes non-uniform with some very small fibers (< 100 nm) and some very large fibers (> 1 μm) (Figure 6.3. E and F). This indicates that the appropriate viscosity for electrospinning DBM in a 70:30 HFIP:TFA blend ranges from 23-78 cP. For further experiments the 11 g dL^{-1} DBM concentration (56 cP) was selected.

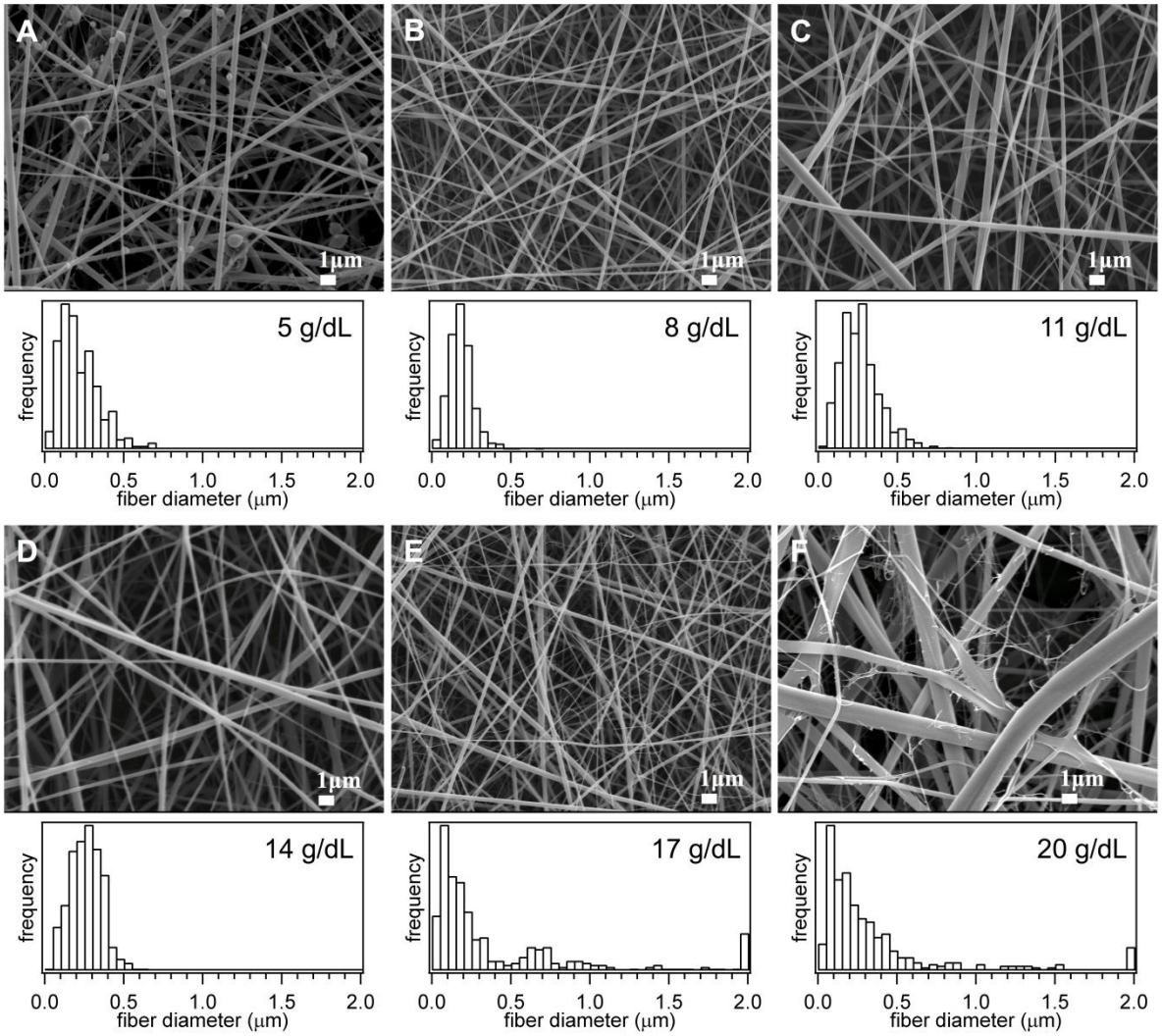

Figure 6.3. Representative SEM images and fiber diameter distributions reveal that the range of fiber diameter changes with increasing concentrations of DBM. (A) At low DBM concentration (5 g dL^{-1}) the fibers are thinner and beads are present. (B-D) As the concentration increases (8 g dL^{-1} to 14 g dL^{-1}) the fibers become uniform. (E-F) Once the concentration increases to 17 g dL^{-1} however, the fibers are no longer uniform and webbing is observed. In the histograms in E and F the bars at 2 μm also include all fiber diameters larger than 2 μm.

6.4.3 Solution Stability. To further investigate polymer instability, viscosity measurements were taken at 0, 6, 12, 24, and 48 hrs after dissolution of DBM (11 g dL^{-1} in 70:30 HFIP:TFA). Each of these solutions was then electrospun immediately after viscosity measurements were taken, and fibers were imaged using SEM (Figure 6.4.).

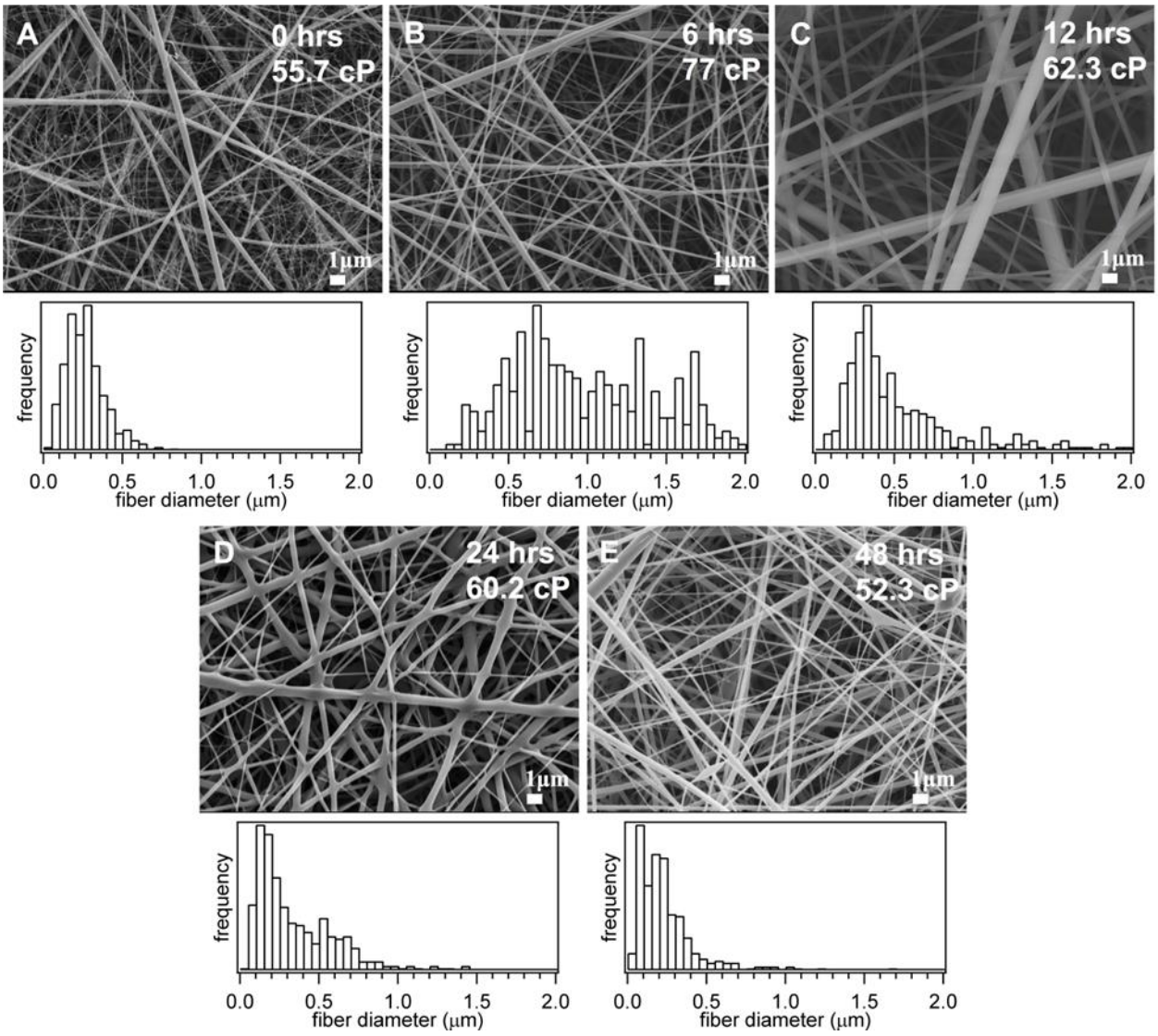

Figure 6.4. Representative SEM images and fiber diameter distributions of DBM fibers electrospun from solutions immediately after DBM dissolution (A), 6 (B), 12 (C), 24 (D), and 48 hrs (E) after dissolution. The higher viscosity solutions (B and C) result in least uniform fiber diameter distribution. As the solution ages and the viscosity goes down, the resulting fiber diameter and distribution width also decrease (D and E).

Over the first 6 hours the viscosity of the solution increases, and then the viscosity decreases over the next 42 hrs (Figure 6.4.). As previously stated, the polymer solution may be undergoing oxidation, indicating that the polymer is breaking down. Initially, degradation results in a higher concentration of polymer chains, increasing the solution viscosity. This results in the larger diameter fibers and broader fiber diameter distribution observed in Figure 6.4. B. As degradation continues from 6 to 48 hours after dissolution, the polymer chains get shorter, and the viscosity then decreases over time, suggesting that fewer entanglements are formed. This results in progressively smaller diameter fibers and narrower fiber diameter distributions as the solution ages (Figures 6.4. C-E). The solution color (not shown), viscosity, and fiber diameter changes over 48 hrs indicate that the polymer is breaking down over time. This suggests that the solution is unstable and should be used immediately upon preparation.

6.4.4 Stabilizing and Crosslinking DBM Fibers. After electrospinning from HFIP:TFA solvent blends, the DBM fibers are water soluble. In order for these to be used as a biomaterial, they must be stable in aqueous environments. X-ray photoelectron spectra (XPS) of electrospun fibers and the neat DBM powder are shown in Figure 6.5.

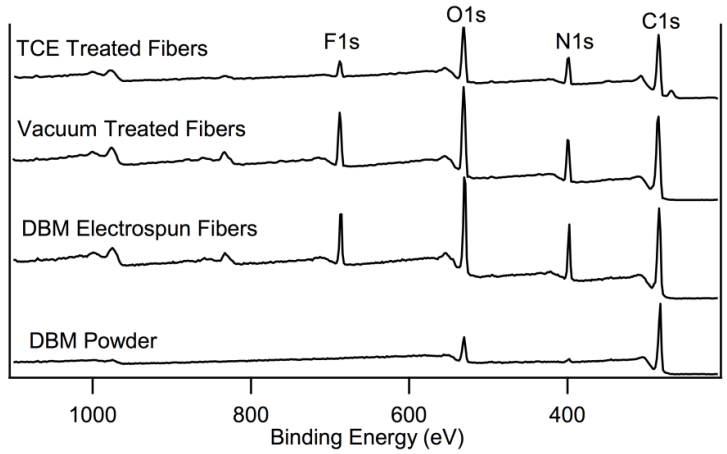

Figure 6.5. Representative XPS survey scans of DBM powder and electrospun DBM. After electrospinning a fluorine peak is evident, not present in the DBM powder. TCE treatment extracts 67 % of the residual fluorinated solvents (TFA and HFIP).

After electrospinning there is fluorine present that is not present in the DBM powder. This indicates that there is residual solvent remaining in the fibers. Vacuum drying for 18 hrs was done to remove volatile solvent and XPS was repeated. There was no change in the fluorine peak between neat fibers and vacuum dried fibers. It is possible that the solvent blend used denatured or partially degraded the protein components of the DBM, resulting in a large number of primary amines capable of forming salts with TFA.[29, 34, 36-39] These salts would make the DBM fibers soluble and cannot be removed by application of vacuum.[29]

To attempt to remove the residual fluorinated solvents, the fibers were exposed to the extractants shown in Table 6.3. to determine which of these do not solubilize the fibers. These solvents are, TCE, chloroform, DCM, and IPA. Of these extractants TCE was chosen as the most likely to extract the residual solvent. The fibers were exposed to TCE for 18 hrs and dried. XPS was done on neat fibers and TCE-treated fibers. The fluorine content was reduced by 67 % (XPS data shown in Figure 6.5.), however the fibers were still water soluble. Thus crosslinking was explored to stabilize the fibers.

Table 6.3. Stability of fibers in extractants.

Extractant	Stable
Tetrachloroethylene (TCE)	***Yes***
Chloroform	***Yes***
Dichloromethane (DCM)	***Yes***
Hexafluoroisopropanol (HFIP)	No
Dimethylformamide (DMF)	No
Dimethylsulfoxide (DMSO)	No
Isopropanol (IPA)	***Yes***
Ethanol	No
Methanol	No
Aqueous ammonium hydroxide (5 M)	No

The crosslinking methods explored are summarized in Table 6.4. DHT and UV treatment were investigated, along with four crosslinking agents, genipin, EDC, riboflavin, and glutaraldehyde. In Table 6.4., fiber mats that retained mechanical integrity after treatment were determined to be *macroscopically stable*; fiber mats that also retained the fiber nanostructure observed in SEM were determined to be *microscopically stable.* DHT alone did not stabilize the fibers, UV treatment and the combination of UV and DHT treatments made the fibers partially insoluble. Treatment with DHT crosslinks by forming a bond between amine and carboxylate groups through thermal dehydration.[40] Crosslinking via UV treatment is initiated by the formation of free radicals on aromatic rings (e.g. in tyrosine and phenylalanine residues).[41] These free radicals then react with each other to form crosslinks. The degree of UV crosslinking is limited by the amount of these structures available. Both DHT and UV treatment may also be limited to the surface of the fibers.[40] When the fibers are exposed to DI water, the water penetrates the fibers causing the mat to dissolve.

Table 6.4. Stability of fibers after different crosslinking protocols.

Crosslinking Conditions	Macroscopically Stable	Microscopically Stable
DHT Treatment	***Yes***	No
UV Treatment	Partially	No
DHT and UV Treatment	Partially	No
Genipin in IPA	No	No
EDC in Chloroform	***Yes***	No
EDC in DCM	***Yes***	No
EDC in IPA	***Yes***	No
EDC *in situ*	No	No
Riboflavin + UV	Partially	No
Glutaraldehyde vapor	***Yes***	***Yes***

Chemical treatments were then pursued to more fully crosslink. Genipin is a naturally occurring crosslinking agent derived from the plant *Gardenia jasminoides.*[42] In a study by Sung et al., it was found that genipin is 10,000 times less cytotoxic than glutaraldehyde, making genipin an attractive crosslinking agent for biomaterials. Genipin reacts with free amines found in amino acids and then can dimerize giving rise to both intermolecular and intramolecular bonds.[43] When genipin reacts with amino acids a dark blue pigment is produced. The presence of this pigment is an indication of crosslinking. In this study we dissolved genipin in IPA and soaked fiber mats in the solution for 18-72 hrs. Dark blue was visible in isolated spots on the fiber mat only after 72 hrs of treatment, fiber mats treated for shorter periods of time remained white. All genipin-treated fiber mats remained water soluble after treatment.

EDC forms crosslinks between amines and carboxylates. Here, EDC was dissolved in IPA and fiber mats were soaked for 18-72 hrs. After this treatment fiber mats did not appear water soluble to the naked eye. The EDC-treated mats were then subjected to a 2-hr rinse in phosphate buffer (pH 7.4) followed by a second rinse in phosphate buffered saline (PBS) for an additional 2 hrs. These were dried and imaged using SEM (Figure 6.6.). After the PBS rinse the fibers are swollen and appear fused. EDC treatment in less polar solvents, DCM, chloroform, and TCE was pursued to minimize fiber swelling. After treatment in DCM and chloroform the mat did not appear to be water soluble, but EDC was insoluble in TCE and unable to crosslink. Fiber mats were soaked in only the solvent, the solvent + EDC, or solvent + EDC followed by PBS and then imaged using SEM. Representative micrographs are shown in Figure 6.6. Chloroform + EDC treatment maintains the most fiber structure before the PBS rinse, but all nanostructure is lost after rinsing. The DCM + EDC treatment swells the fibers somewhat, but after rinsing all nanostructure is absent. IPA alone swells the fibers slightly. When EDC is added, a large amount

of porosity and some nanostructure is lost. Unlike the less polar solvents, a small amount of the structure is maintained after rinsing with PBS, however all porosity is eliminated.

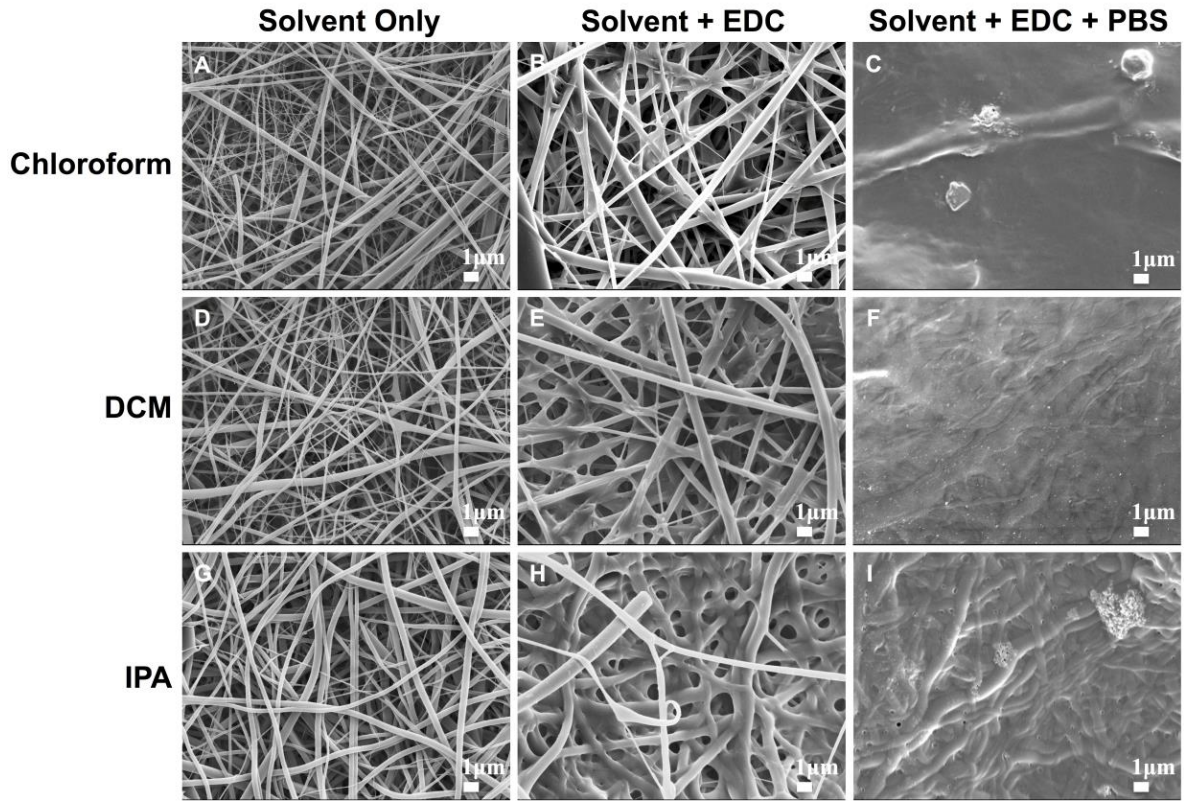

Figure 6.6. Representative SEM images of the fibers after soaking in the solvent alone (A, D, and G), the solvent + EDC (B, E, and H), and the solvent + EDC followed by a PBS rinse (C, F, and I). Even though crosslinking in chloroform, DCM, and IPA prevents the mats from completely dissolving, in PBS the nanostructure is lost.

A crosslinking agent must be incorporated throughout the fibers in order to successfully stabilize the nanostructure. In nonpolar solvents the EDC is unable to penetrate inside the fibers to crosslink, and stabilizing bonds are only formed on the outside. When fibers are placed in a polar solvent such as water, the water penetrates the fibers causing them to swell, and crosslinks present on the fiber surfaces are insufficient to preserve the nanostructure. IPA is the most polar of these solvents, thus, fibers swell to a greater extent and some EDC is able penetrate inside and form crosslinks within allowing some structure to be maintained.

To achieve more uniform distribution of EDC throughout the fibers, in situ crosslinking was attempted to stabilize the fibers from within. EDC was mixed into the electrospinning solution immediately before spinning. The same electrospinning procedure previously used was performed. Fibers were exposed to DI water and dissolved immediately. EDC binds amines to carboxylates and TFA contains carboxylates. Therefore, it is possible that the EDC reacted with the TFA instead of with the DBM and no crosslinking occurred within the polymer. A crosslinker that does not react with the solvent is needed. Riboflavin was chosen as a candidate because it crosslinks by forming free radicals when exposed to UV light, thus it can be incorporated throughout the fibers and activated when desired.[44] Riboflavin was added to the electrospinning solution, fibers were spun as described earlier, and UV treatment was then performed. The riboflavin incorporation turns the electrospun fibers neon yellow, but after UV exposure the fibers return to a light cream color. SEM images of the riboflavin-containing fibers after electrospinning and after subsequent UV treatment are displayed in Figure 6.7. The UV-treated fibers exhibit a curled appearance under SEM suggesting that crosslinks have been formed within the fibers. However, after UV treatment, these fibers were exposed to DI water and partially dissolved. The two chemical crosslinking agents that react primarily with amines, genipin and riboflavin, do not stabilize fibers, however EDC treatment (binds amines to carboxylates) resulted in a fiber mat that macroscopically remained intact after contact with water, but lacked fibrous nanostructure.

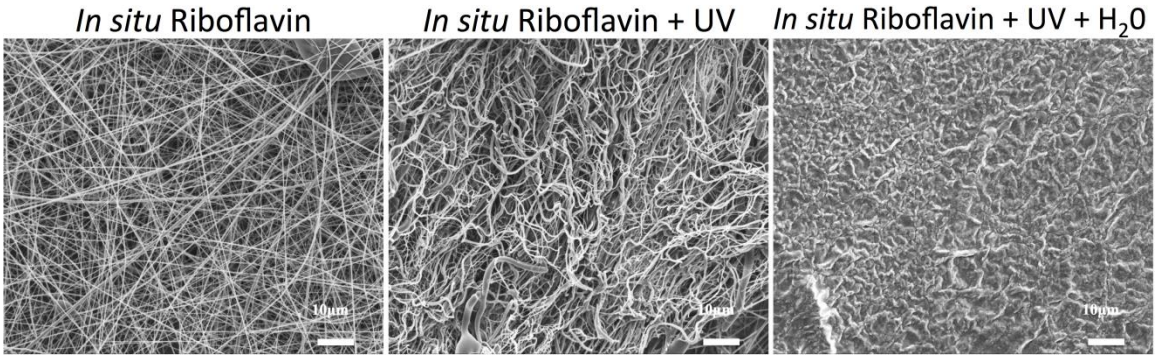

Figure 6.7. Representative SEM images of the riboflavin-incorporated fibers after electrospinning and after subsequent activation via UV treatment post-spinning. The riboflavin treatment was not able to preserve the nanostructure after exposure to water.

Unlike the other techniques reviewed above, crosslinking using glutaraldehyde vapor successfully preserves some fiber nanostructure and porosity. Glutaraldehyde creates intra and intermolecular crosslinks by forming an imine with the nonprotonated □-amino group of lysine.[45] After electrospinning, fibers were placed in a dessicator subjected to vacuum with glutaraldehyde for 3 days. Fibers exposed to this treatment were imaged before and after exposure to DI water. While there is significant change to the fiber and pore morphology upon crosslinking, the porous nanostructured network is preserved (Figure 6.8.). Furthermore, the same structure is seen after exposure to DI water, indicating that glutaraldehyde successfully crosslinked the DBM fibers.

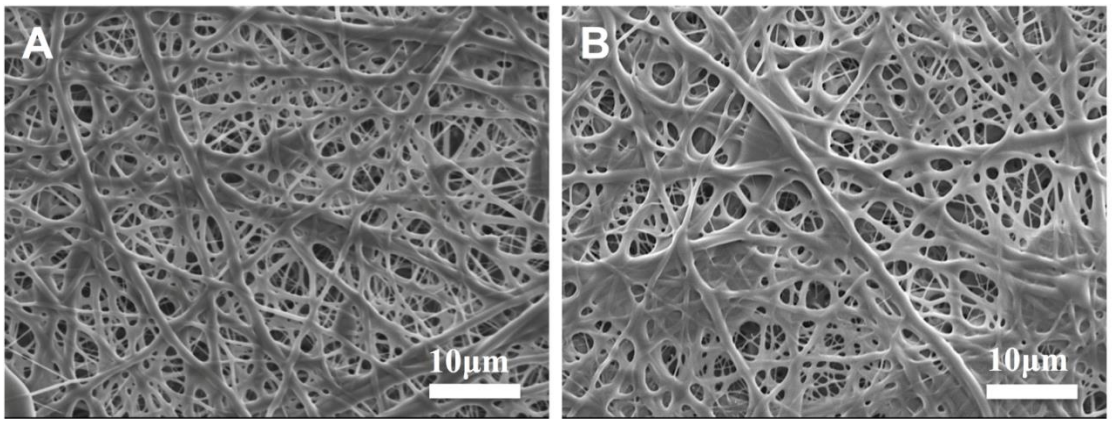

Figure 6.8. Representative SEM images of glutaraldehyde vapor-treated fibers before (A) and after (B) exposure to water. Glutaraldehyde vapor successfully stabilized the fibers, allowing them to maintain their nanostructure and porosity.

6.4.5 Mechanical Testing. Figure 6.9. shows the stress strain behavior of glutaraldehyde-crosslinked DBM nanofibers after rehydration. The sample exhibits a toe region from about 0 % to about 3 % strain, followed by a linear elastic region. The ultimate strain of this sample is 8.85 % and the Young's modulus obtained from the linear region of the stress-strain curve (between 4 % and 8.85 % strain) is 3.37 MPa.

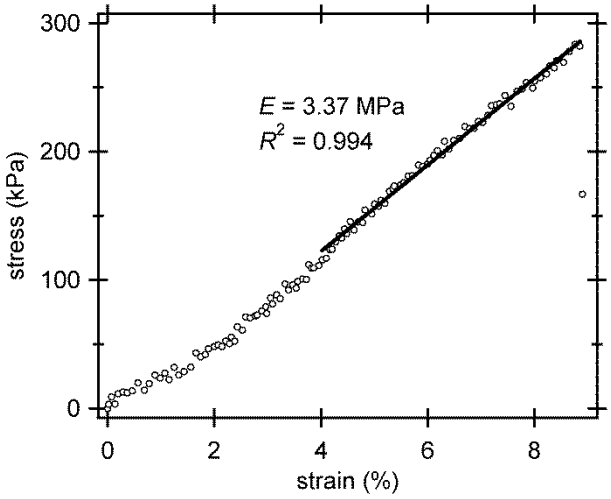

Figure 6.9. Stress-strain behavior of glutaraldehyde-crosslinked DBM nanofibers under uniaxial tensile testing.

6.4.6 Cytocompatibility Testing. Human dermal fibroblasts (HDF) were cultured on glutaraldehyde-crosslinked DBM nanofibers and on tissue culture polystyrene for 24 hrs and for 4 days. HDF viability was assayed using Live/Dead staining after 24 hrs, and metabolic activity was assayed by CellTiter-Blue assay after both 24 hrs and 4 days. Figure 6.10. shows a representative merged image of both the green ("live") and red ("dead") channels from fluorescence microscopy of HDF cultured on DBM nanofibers for 24 hours. Dead cells were so sparse, that they could not be meaningfully quantified from multiple fields of view and multiple DBM nanofiber samples, which is similar to the HDF cultured on TCPS (not shown). HDF on nanofibers shown in Figure 6.10. are well spread and interacting with the fibers. The metabolic

activity of HDF cultured on DBM nanofibers was about 40 % lower than that of HDF cultured on TCPS after 24 hours (not shown); based on the viability assay, we attribute this apparent reduction in metabolic activity to inefficient cell seeding on the nanofibers rather than to cytotoxicity. After 4 days, there was no change in the metabolic activity on either the HDF cultured on TCPS or HDF cultured DBM nanofibers, indicating good survival of cells on DBM nanofibers. These results confirm that after crosslinking with glutaraldehyde, the DBM nanofibers are stable in aqueous cell culture media, and support mammalian cell growth; neither the solvents used for electrospinning, nor the glutaraldehyde crosslinking result in measureable cytotoxicity toward HDF. Furthermore, the HDF on DBM nanofibers are well spread, indicating that DBM nanofibers require no exogenous adhesion ligand modification (e.g. addition of fibronectin, collagen, or RGD peptides) as are commonly required to promote cell adhesion to many synthetic polymer scaffolds.

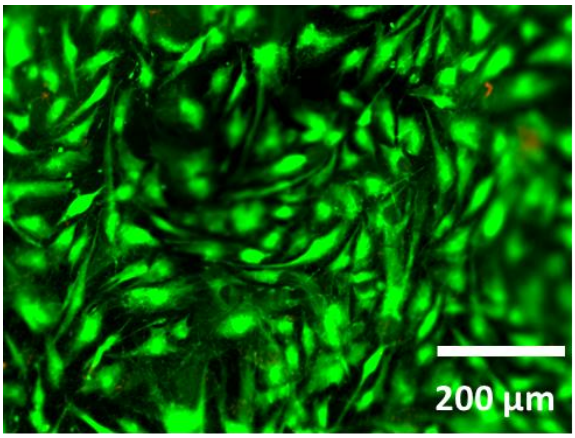

Figure 6.10. Merged red and green channel fluorescence micrographs of HDF on DBM nanofibers after 24 hours of culture. Dead (red) cells could not be quantified, indicating that the DBM nanofibers exhibit good cytocompatibility toward HDF.

6.5 CONCLUSIONS.

DBM is completely soluble in TFA, but the solution does not exhibit properties conducive to electrospinning. After exploring a number of solvent blends, 70:30 HFIP:TFA was

chosen as having ideal properties for electrospinning. DBM concentration in the spinning solution affects fiber morphology due to changes in viscosity and polymer entanglements. Electrospraying is observed at low concentrations, uniform fibers are observed at intermediate concentrations, and fiber diameter becomes widely variable at high concentrations. DBM is being degraded by the solvent mixture over time. This degradation affects solution viscosity, fiber morphology, and stability of fibers in aqueous environments. Initially, viscosity and fiber diameter increase due to a higher number of polymer chains in solution, but as degradation continues and polymer chains become shorter, viscosity and fiber diameter decrease. In order to have consistent fiber mats solutions may not be stored for later use. After the electrospinning process, the fiber mats are water soluble. Crosslinking is imperative for the success of using DBM as electrospun tissue engineering scaffolds. Thus far, the only crosslinking method that is capable of maintaining fiber structure and porosity is a glutaraldehyde vapor treatment. After glutaraldehyde crosslinking, rehydrated DBM nanofibers have good handling characteristics, and are stable in aqueous environments. Importantly, initial cytocompatibility testing gives no indication of cytotoxicity that might be caused by electrospinning solvents or residual glutaraldehyde, and the DBM nanofibers support cell attachment with no addition of exogenous adhesion ligands.

REFERENCES

1. Mendonça, G.; Mendonça, D. B. S.; Simões, L. G. P.; Araújo, A. L.; Leite, E. R.; Duarte, W. R.; Aragão, F. J. L.; Cooper, L. F., The effects of implant surface nanoscale features on osteoblast-specific gene expression. *Biomaterials* **2009,** 30, (25), 4053-4062.

2. Yim, E. K. F.; Pang, S. W.; Leong, K. W., Synthetic nanostructures inducing differentiation of human mesenchymal stem cells into neuronal lineage. *Exp. Cell Res.* **2007,** 313, (9), 1820-1829.

3. Gittens, R. A.; McLachlan, T.; Olivares-Navarrete, R.; Cai, Y.; Berner, S.; Tannenbaum, R.; Schwartz, Z.; Sandhage, K. H.; Boyan, B. D., The effects of combined micron-/submicron-scale surface roughness and nanoscale features on cell proliferation and differentiation. *Biomaterials* **2011,** 32, (13), 3395-3403.

4. Andersson, A.-S.; Bäckhed, F.; von Euler, A.; Richter-Dahlfors, A.; Sutherland, D.; Kasemo, B., Nanoscale features influence epithelial cell morphology and cytokine production. *Biomaterials* **2003,** 24, (20), 3427-3436.

5. Popat, K. C.; Eltgroth, M.; LaTempa, T. J.; Grimes, C. A.; Desai, T. A., Titania Nanotubes: A Novel Platform for Drug-Eluting Coatings for Medical Implants? *Small* **2007,** 3, (11), 1878-1881.

6. Cui, F.-Z.; Ge, J., New observations of the hierarchical structure of human enamel, from nanoscale to microscale. *J. Tissue Eng. Regener. Med.* **2007,** 1, (3), 185-191.

7. Wang, X.; Kim, H. J.; Wong, C.; Vepari, C.; Matsumoto, A.; Kaplan, D. L., Fibrous proteins and tissue engineering. *Mater. Today (Oxford, U. K.)* **2006,** 9, (12), 44-53.

8. Boddohi, S.; Kipper, M. J., Engineering Nanoassemblies of Polysaccharides. *Adv. Mater.* **2010,** 22, 2298-3016.

9. Ruckh, T. T.; Kumar, K.; Kipper, M. J.; Popat, K. C., Osteogenic differentiation of bone marrow stromal cells on poly([epsilon]-caprolactone) nanofiber scaffolds. *Acta Biomater.* **2010,** 6, 2949-2959.

10. Gunatillake, P. A.; Adhikari, R., Biodegradable synthetic polymers for tissue engineering. *Eur. Cells Mater.* **2003,** 5, 1-16.

11. Henderson, L. A.; Kipper, M. J.; Chiang, M. Y. M., Beyond Trial & Error: Tools to Advance the Engineering of Biomaterials. In *Polymers for Biomedical Applications*, Mahapatro, A.; Kulshrestha, A. S., Eds. ACS: Washington, D.C., 2008; Vol. 977, pp 118-152.

12. Marotta, J. S.; Widenhouse, C. W.; Habal, M. B.; Goldberg, E. P., Silicone gel breast implant failure and frequency of additional surgeries: Analysis of 35 studies reporting examination of more than 8000 explants. *J. Biomed. Mater. Res.* **1999,** 48, (3), 354-364.

13. Tullberg, T., Failure of a Carbon Fiber Implant: A Case Report. *Spine* **1998,** 23, (16), 1804-1806.

14. van der Giessen, W. J.; Lincoff, A. M.; Schwartz, R. S.; van Beusekom, H. M. M.; Serruys, P. W.; Holmes, D. R.; Ellis, S. G.; Topol, E. J., Marked Inflammatory Sequelae to Implantation of Biodegradable and Nonbiodegradable Polymers in Porcine Coronary Arteries. *Circulation* **1996,** 94, (7), 1690-1697.

15. Leszczak, V.; Smith, B. S.; Popat, K. C., Hemocompatibility of polymeric nanostructured surfaces. *J. Biomater. Sci.-Polym. Ed.* **2013,** 24, (13), 1529-1548.

16. Furst, E. M.; Pagac, E. S.; Tilton, R. D., Coadsorption of polylysine and the cationic surfactant cetyltrimethylammonium bromide on silica. *Ind. Eng. Chem. Res.* **1996,** 35, (5), 1566-1574.

17. Becker, T. A.; Kipke, D. R.; Brandon, T., Calcium alginate gel: A biocompatible and mechanically stable polymer for endovascular embolization. *J. Biomed. Mater. Res.* **2001,** 54, (1), 76-86.

18. Vats, A.; Tolley, N. S.; Polak, J. M.; Gough, J. E., Scaffolds and biomaterials for tissue engineering: a review of clinical applications. *Clin. Otolaryngol. Allied Sci.* **2003,** 28, (3), 165-172.

19. Renth, A. N.; Detamore, M. S., Leveraging "raw materials" as building blocks and bioactive signals in regenerative medicine. *Tissue Eng., Part B* **2012,** 18, (5), 341-62.

20. Gruskin, E.; Doll, B. A.; Futrell, F. W.; Schmitz, J. P.; Hollinger, J. O., Demineralized bone matrix in bone repair: History and use. *Adv. Drug Delivery Rev.* **2012,** 64, (12), 1063-1077.

21. Murugan, R.; Ramakrishna, S., Nano-featured scaffolds for tissue engineering: A review of spinning methodologies. *Tissue Eng.* **2006,** 12, (3), 435-447.

22. Holzwarth, J. M.; Ma, P. X., Biomimetic nanofibrous scaffolds for bone tissue engineering. *Biomaterials* **2011,** 32, (36), 9622-9629.

23. Pham, Q. P.; Sharma, U.; Mikos, A. G., Electrospinning of polymeric nanofibers for tissue engineering applications: A review. *Tissue Eng.* **2006,** 12, (5), 1197-1211.

24. Heydarkhan-Hagvall, S.; Schenke-Layland, K.; Dhanasopon, A. P.; Rofail, F.; Smith, H.; Wu, B. M.; Shemin, R.; Beygui, R. E.; MacLellan, W. R., Three-dimensional electrospun ECM-based hybrid scaffolds for cardiovascular tissue engineering. *Biomaterials* **2008,** 29, (19), 2907-2914.

25. Francis, M. P.; Sachs, P. C.; Madurantakam, P. A.; Sell, S. A.; Elmore, L. W.; Bowlin, G. L.; Holt, S. E., Electrospinning adipose tissue-derived extracellular matrix for adipose stem cell culture. *J. Biomed. Mater. Res., Part A* **2012,** 100A, (7), 1716-1724.

26. Yao, C. H.; Liu, B. S.; Chang, C. J.; Hsu, S. H.; Chen, Y. S., Preparation of networks of gelatin and genipin as degradable biomaterials. *Mater. Chem. Phys.* **2004,** 83, (2-3), 204-208.

27. Barnes, C. P.; Pemble, C. W.; Brand, D. D.; Simpson, D. G.; Bowlin, G. L., Cross-linking electrospun type II collagen tissue engineering scaffolds with carbodiimide in ethanol. *Tissue Eng* **2007,** 13, (7), 1593-605.

28. Zhang, Y. Z.; Venugopal, J.; Huang, Z. M.; Lim, C. T.; Ramakrishna, S., Crosslinking of the electrospun gelatin nanofibers. *Polymer* **2006,** 47, (8), 2911-2917.

29. Almodóvar, J.; Kipper, M. J., Coating electrospun chitosan nanofibers with polyelectrolyte multilayers using the polysaccharides heparin and N,N,N-trimethyl chitosan. *Macromol. Biosci.* **2011,** 11, (1), 72-76.

30. Devarayan, K.; Hanaoka, H.; Hachisu, M.; Araki, J.; Ohguchi, M.; Behera, B. K.; Ohkawa, K., Direct Electrospinning of Cellulose-Chitosan Composite Nanofiber. *Macromol. Mater. Eng.* **2013,** 298, (10), 1059-1064.

31. Ohkawa, K.; Cha, D. I.; Kim, H.; Nishida, A.; Yamamoto, H., Electrospinning of chitosan. *Macromol. Rapid Commun.* **2004,** 25, (18), 1600-1605.

32. Ohsawa, O.; Lee, K. H.; Kim, B. S.; Lee, S.; Kim, I. S., Preparation and characterization of polyketone (PK) fibrous membrane via electrospinning. *Polymer* **2010,** 51, (9), 2007-2012.

33. Chen, F.; Li, X. Q.; Mo, X. M.; He, C. L.; Wang, H. S.; Ikada, Y., Electrospun chitosan-P(LLA-CL) nanofibers for biomimetic extracellular matrix. *J. Biomater. Sci., Polym. Ed.* **2008,** 19, (5), 677-691.

34. Côté, M.-F.; Laroche, G.; Gagnon, E.; Chevallier, P.; Doillon, C. J., Denatured collagen as support for a FGF-2 delivery system: physicochemical characterizations and in vitro release kinetics and bioactivity. *Biomaterials* **2004,** 25, (17), 3761-3772.

35. Zheng, J.; He, A.; Li, J.; Xu, J.; Han, C. C., Studies on the controlled morphology and wettability of polystyrene surfaces by electrospinning or electrospraying. *Polymer* **2006,** 47, (20), 7095-7102.

36. Sangsanoh, P.; Supaphol, P., Stability improvement of electrospun chitosan nanofibrous membranes in neutral or weak basic aqueous solutions. *Biomacromolecules* **2006,** 7, (10), 2710-2714.

37. Jiang, Q. R.; Reddy, N.; Zhang, S. M.; Roscioli, N.; Yang, Y. Q., Water-stable electrospun collagen fibers from a non-toxic solvent and crosslinking system. *J. Biomed. Mater. Res., Part A* **2013,** 101A, (5), 1237-1247.

38. Arnoult, O. A Novel Benign Solution for Collagen Processing. Case Western Reserve University, 2010.

39. Chen, Z. G.; Wang, P. W.; Wei, B.; Mo, X. M.; Cui, F. Z., Electrospun collagen–chitosan nanofiber: A biomimetic extracellular matrix for endothelial cell and smooth muscle cell. *Acta Biomater.* **2010,** 6, (2), 372-382.

40. Ratanavaraporn, J.; Rangkupan, R.; Jeeratawatchai, H.; Kanokpanont, S.; Damrongsakkul, S., Influences of physical and chemical crosslinking techniques on electrospun type A and B gelatin fiber mats. *Int. J. Biol. Macromol.* **2010,** 47, (4), 431-438.

41. Weadock, K. S.; Miller, E. J.; Bellincampi, L. D.; Zawadsky, J. P.; Dunn, M. G., Physical Cross-Linking of Collagen-Fibers - Comparison of Ultrviolet-Irradiation and Dehydrothermal Treatment. *J. Biomed. Mater. Res.* **1995,** 29, (11), 1373-1379.

42. Muzzarelli, R. A. A., Genipin-crosslinked chitosan hydrogels as biomedical and pharmaceutical aids. *Carbohydr. Polym.* **2009,** 77, (1), 1-9.

43. Sung, H. W.; Chen, C. N.; Huang, R. N.; Hsu, J. C.; Chang, W. H., In vitro surface characterization of a biological patch fixed with a naturally occurring crosslinking agent. *Biomaterials* **2000,** 21, (13), 1353-1362.

44. Fawzy, A.; Nitisusanta, L.; Iqbal, K.; Daood, U.; Beng, L. T.; Neo, J., Characterization of Riboflavin-modified Dentin Collagen Matrix. *J. Dent. Res.* **2012,** 91, (11), 1049-1054.

45. Gough, J. E.; Scotchford, C. A.; Downes, S., Cytotoxicity of glutaraldehyde crosslinked collagen/poly(vinyl alcohol) films is by the mechanism of apoptosis. *J. Biomed. Mater. Res.* **2002,** 61, (1), 121-130.

CHAPTER 7

Conclusions and Future Work

7.1 CONCLUSIONS.

This dissertation investigated the inherent properties of natural polymers to create biomimetic nanomaterials for growth factor stabilization and delivery. This was done through a literature review followed by the investigation of four specific aims. Six biopolymers were used to create three different geometries of nanoassemblies. These include chitosan (CHI), *N*,*N*,*N*-trimethylchitosan (TMC), heparin (HEP), chondroitin sulfate (CS), hyaluronan (HA), and demineralized bone matrix (DBM). These biopolymers were used in combination with the basic fibroblast growth factor (FGF-2) to create and evaluate biomimetic nanoassemblies for use in tissue engineering.

7.1.1 Research Aims. The specific aims proposed were accomplished by:

Specific Aim 1: Polyelectrolyte complex nanoparticles (PCNs) were made from four different combinations of polysaccharides, FGF-2 was bound to them and they were compared to each other and to aggrecan to investigate stabilization of growth factors. This was addressed in chapter three.

Specific Aim 2: Proteoglycan-mimetic graft copolymers containing either heparin or chondroitin sulfate at four different grafting densities were synthesized and characterized. This was addressed in chapter four.

Specific Aim 3: Both emulsion and coaxial electrospinning techniques were developed to incorporate growth factor into electrospun nanofibers and were characterized for FGF-2 stability after processing. This was addressed in chapter five.

Specific Aim 4: Processing conditions to form a nanostructured tissue engineering scaffold made from demineralized bone matrix without a carrier polymer were determined. This was addressed in chapter six.

7.1.2 Literature Review. The literature supports the hypothesis that biopolymers have inherent biophysical and biochemical properties that can be exploited for growth factor stabilization and delivery. The ECM is made up of an intricate network of polysaccharides and proteins. Proteoglycans found in the ECM and on the cell surface are crucial to tissue function. They are made up of a core protein and GAG side chains. The composition and geometry of the GAGs dictate the function of the proteoglycan. GAGs impart a high anionic charge density to proteoglycans resulting in high osmotic pressure and hydrophilicity which is compounded to lubricity and compressive strength in tissues. Proteins form structural components of the ECM. They align into hierarchical structures that give rise to mechanical properties of tissue. Additionally, they interact with other macromolecules in the ECM participating in cell signaling. Growth factors are signaling molecules on the cell surface and in the ECM of tissues. They are implicated in metabolic pathways that regulate homeostasis and wound healing. Growth factors have great therapeutic potential, but are unstable in solution. In the ECM, GAGs bind to growth factors protecting them from proteolytic degradation and participating in cell surface receptor-growth factor interactions. Biopolymers for growth factor delivery have been designed in a wide array of shapes and sizes. Formats such as coatings, nanoparticles, three dimensional constructs, ECM-derived materials, and synthetic approaches have been studied. There has been much research on biopolymers and their functional roles in structure and cell signaling, but not to the same extent as synthetic polymers. Harnessing the intricate relationship between growth factors and the ECM is a powerful tool for the design of bioactive tissue engineering scaffolds.

7.1.3 Aggrecan-mimetic, Glycosaminoglycan-containing Nanoparticles for Growth Factor Stabilization and Delivery. The PCNs produced have a size and high density of GAGs similar to aggrecan. At doses of 10 μg mL^{-1} and above they may inhibit cell attachment to tissue-culture polystyrene, and at higher doses, they may be cytotoxic toward MSCs. Nonetheless, these PCNs bind and stabilize FGF-2 enhancing both the mitogenic activity and the metabolic activity of MSCs in low-serum media.

This work shows that the mitogenic activity of FGF-2 is best maintained by binding to Hep-containing PCNs. Over the same preconditioning time period, delivery of FGF-2 using PCNs results in higher metabolic activity than delivery of FGF-2 using aggrecan. Furthermore, after 21 days of preconditioning, all of the PCN formulations are superior to aggrecan, and the Hep-containing PCNs are superior to FGF-2 in solution at stimulating metabolic activity of MSCs. FGF-2 in solution has no significant mitogenic activity after any of the preconditioning periods (normalized cell numbers were not statistically different from the untreated control). FGF-2 bound to aggrecan and CS-based PCNs lost some mitogenic activity during the 14-day preconditioning, but FGF-2 bound to heparin-containing PCNs exhibited no loss of activity during the 14-day preconditioning. The metabolic activity assay showed that after 14 days of preconditioning, two of the PCN types were superior to aggrecan at maintaining the FGF-2 activity, and after 21 days of preconditioning the PCNs were superior to both aggrecan and FGF-2 alone. These aggrecan-mimetic PCNs may be used for growth factor delivery either in soluble form or bound to surfaces. This could improve the prospects for therapeutic delivery of heparin-binding growth factors and cytokines for tissue engineering and wound healing applications.

7.1.3 Synthesis and Characterization of Proteoglycan-mimetic Graft Copolymers. The synthesis of proteoglycan-mimetic graft copolymers using HA as the backbone and either CS or Hep as the side chains with controllable grafting density was successful. Confirmation of the proposed chemistry was done via ATR-FTIR and ^{1}H NMR. Characteristic peaks associated with the coupling agent and the sulfate groups on the GAG side chains were identified and analyzed for changes due to reaction. Alterations in peak magnitude and morphology confirmed the success of the coupling chemistry. The different compositions exhibit effective hydrodynamic diameters ranging from 90-500 nm as measured by DLS, and all demonstrated negative zeta potentials, indicating a negative surface charge. A cell study was done to test the ability of the graft copolymers to deliver FGF-2 to MSCs. The CS-containing graft copolymers exhibited higher cell activity than the Hep 1:1, but was similar to the Hep 1:30. The CS conditions and the Hep 1:30 performed equally as well as when FGF-2 was delivered in solution. Finally, preliminary mechanical testing was performed to test for physical properties of the graft copolymers. Hydrogels containing the copolymers exhibited changes in compressive modulus with cycle frequency. These results show much promise for these graft copolymers to impart bio-functionality to tissue engineering scaffolds.

7.1.5 Two-Phase Emulsion and Coaxial Electrospinning to Incorporate Growth Factors into Electrospun Nanofibers. Electrospinning using an emulsion and a coaxial technique both successfully created nanofibers within the size range of collagen fiber bundles found in the ECM and resulted in dispersion of PCNs throughout the fiber mat. All three scaffold types exhibited cytocompatibility, with coaxial fibers with chitosan in excess showing the greatest amount of cell adhesion and spreading, emulsion fibers showing heterogeneous interactions, and coaxial fibers with PVA in excess demonstrating round cell morphology similar

to that of chondrocytes. Emulsion fibers were not able to incorporate a stable bioactive dose of FGF-2, but may be applicable for the delivery of small molecules that are incompatible with organic solvents. Coaxial fibers were loaded with biologically active levels of FGF-2. While there were no statistical differences, when FGF-2 was bound to GAG-rich PCNs and delivered via coaxial nanofibers with chitosan in excess, cell activity appeared to be higher than fibers containing FGF-2 with no PCNs, suggesting that the PCNs protect FGF-2 throughout the electrospinning process. Thus, coaxial electrospinning is a viable option for producing a bioactive scaffold for tissue engineering.

7.1.6. Nanostructured Biomaterials from Electrospun Demineralized Bone Matrix: A Survey of Processing and Crosslinking Strategies. DBM is completely soluble in TFA, but the solution does not exhibit properties conducive to electrospinning. After exploring a number of solvent blends, 70:30 HFIP:TFA was chosen as having ideal properties for electrospinning. DBM concentration in the spinning solution affects fiber morphology due to changes in viscosity and polymer entanglements. Electrospraying is observed at low concentrations, uniform fibers are observed at intermediate concentrations, and fiber diameter becomes widely variable at high concentrations. DBM is being degraded by the solvent mixture over time. This degradation affects solution viscosity, fiber morphology, and stability of fibers in aqueous environments. Initially, viscosity and fiber diameter increase due to a higher number of polymer chains in solution, but as degradation continues and polymer chains become shorter, viscosity and fiber diameter decrease. In order to have consistent fiber mats solutions may not be stored for later use. After the electrospinning process, the fiber mats are water soluble. Crosslinking is imperative for the success of using DBM as electrospun tissue engineering scaffolds. Thus far, the only crosslinking method that is capable of maintaining fiber structure and porosity is a

glutaraldehyde vapor treatment. After glutaraldehyde crosslinking, rehydrated DBM nanofibers have good handling characteristics, and are stable in aqueous environments. Importantly, initial cytocompatibility testing gives no indication of cytotoxicity that might be caused by electrospinning solvents or residual glutaraldehyde, and the DBM nanofibers support cell attachment with no addition of exogenous adhesion ligands.

7.2 FUTURE WORK.

While considerable work has been done in this dissertation, future studies are needed to address experimental limitations, answer lingering questions, and expand this work to other applications. The experiments addressing the aggrecan-mimetic PCNs described in chapter three had some limitations including calculation of PCN yield and FGF-2 binding, characterization of aggrecan, and verification of cell activity. Yield was calculated using fluorescence on a polycation basis. This is an indirect method and did not account for the polyanions. The low mass of the particles and salt from the buffer prevent mass from being an option, however thermogravimetric analysis may be a better method to determine yield. Binding efficiency of FGF-2 to PCNs was determined by difference using an ELISA on the supernatant. When FGF-2 is bound to PCNs it does not interact with the capture antibody in the ELISA in the same manner as free FGF-2. Thus an ELISA could not be used directly. Measuring fluorescently tagged FGF-2 has been attempted, but is not as sensitive as an ELISA. This limitation also affected the ability to measure the amount of FGF-2 obtained in the emulsion and coaxial nanofibers described in chapter five. A method of directly measuring FGF-2 when it is bound to PCNs would provide more certainty in the evaluation of binding efficiency. The techniques used for measuring both mitogenic and metabolic activity are limited by the necessity of fixing the cells. Thus each sample could only be analyzed at one time point during culture. Multiple samples for evaluation

at different time points or an assay such as CellTiter-Blue which does not require fixation would have provided information on cell activity throughout the culture period.

In the future these PCNs could be expanded to deliver other growth factors and to deliver multiple growth factors. Growth factors that stimulate differentiation in a long-term culture would be an interesting experiment. Additionally, *in vivo* experiments would provide information on immune response elicited by the PCNs.

Emulsion and coaxial electrospinning, described in chapter five, are an extension of the work in chapter three. The same limitations of determining PCN yield and FGF-2 binding efficiency present uncertainties. These experiments were also hindered by difficulties in imaging a three dimensional construct and low initial cell attachment. To confirm the presence of PCNs in the nanofibers, PCNs and nanofibers were tagged with different fluorophores and then imaged using TIRF microscopy. The excitation and emission spectra of the two fluorophores chosen were similar, causing both to fluoresce when excited at 473 nm, the use of other fluorophores such as Texas Red would mitigate this problem. Additionally, the three dimensional nature of the nanofibers caused fluorescence from different planes to appear in imaging, this lead to issues in fiber characterization and cell imaging. CellTiter-Blue was thus used as a measure of cell activity and an indication of cell number. However it is difficult to separate metabolic activity and cell number which both give higher results in the CellTiter-Blue assay. Low cell numbers also made imaging difficult and required long incubation times with the CellTiter-Blue dye. Use of a higher seeding density, and a combination of confocal microscopy with metabolic assays would mitigate these limitations. Although complications were present throughout the experiments performed in chapter five, incorporation of PCNs into various scaffold types is an interesting

prospect. They can protect growth factor throughout processing conditions, or be used to pattern different growth factors throughout a scaffold.

The proteoglycan-mimetic graft copolymers described in chapter four have only just been developed. While NMR has been performed it needs to be more thoroughly analyzed to confirm the chemistry. Additionally, neutron scattering or atomic force microscopy would provide information on the structure of these graft copolymers. Longer growth factor stability studies are necessary to verify their ability to not only deliver, but protect growth factor from degradation. More in depth mechanical testing would provide information on solution dynamics, functionality in a hydrogel scaffold,and possible applications for these assemblies. More grafting densities should be explored, as well as different GAG side chains, such as dermatan and karatan, and combinations of GAG side chains should be used. It would be interesting to optimize growth factor-copolymer complex properties by varying brush composition with different growth factors. Similar to PCNs, differentiation and *in vivo* studies would provide a wealth of information.

The electrospun DBM reported in chapter six is also a young project. The study was limited by the availability of DBM as well as the ability to analyze it for content. Only DBM from one donor was used and only XPS was performed on the material. A thorough understanding of the components of DBM and differences between donors would help in determining an appropriate solvent system. Additionally, more mechanical testing and longer term cell studies for differentiation would help to define an application for this novel material. Tuning the structure into aligned fibers, layered constructs, and rolling into a three dimensional tube may define or open this material to a multitude of applications. Although the electrospun fibers are cytocompatible, the solvent system currently used for electrospinning is toxic.

Developing a benign and “green” solvent system would improve the biological potential of this material.

This dissertation contains a vast amount of information gained from the outlined specific aims. However, there remains much to be explored. The biomaterials developed here have promising therapeutic potential and could be tailored to any number of tissue engineering applications.

APPENDIX

A.1 SUPPORTING MATERIAL FOR CHAPTER 3.

A.1.1 MSC Response to FGF-2, PCNs, and Preconditioned FGF-2-Loaded PCNs and Aggrecan. MSCs were cultured with the different PCNs and aggrecan with and without FGF-2 for four days.

A.1.1.1 Mitogenic Activity Assay. After the culture period cells were fixed and stained with DAPI and counted using ImageJ. Figure A.1.1 shows representative microscopy images of cells cultured with no treatment, and with PCNs and aggrecan at 10 µg mL^{-1} without FGF-2.

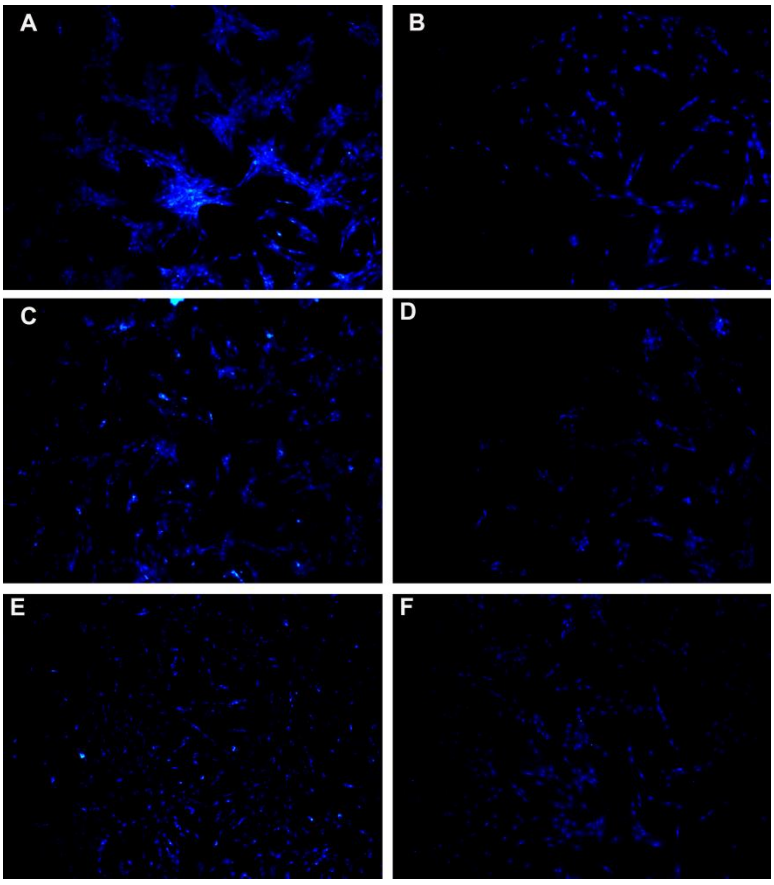

Figure A.1.1. Representative fluorescence micrographs of DAPI-stained MSC nuclei after four days of culture with (A) no treatment, and (B-F) 10 µg mL^{-1} aggrecan, Hep-Chi, Hep-TMC, CS-Chi, and CS-TMC without FGF-2, respectively. There is no apparent cell proliferation with any of these treatments.

A.2 SUPPORTING MATERIAL FOR CHAPTER 4.

A.2.1 Chemical Characterization. Graft copolymers were characterized using ATR-FTIR and proton NMR to confirm the chemical reaction.

A.2.1.1 ATR-FTIR. Chemistry was confirmed using ATR-FTIR on all graft copolymers synthesized. The spectra of HA, HA-SH, and HA-BMPH are shown in Figure A.2.1.

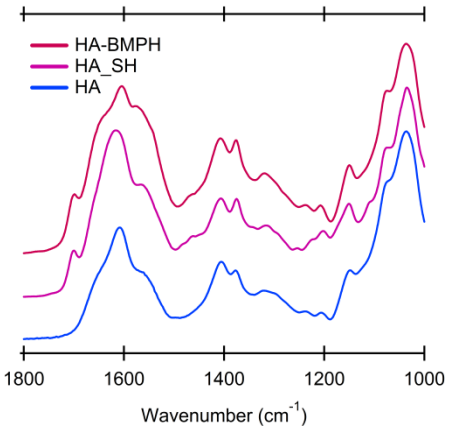

Figure A.2.1. ATR-FTIR spectra of HA, HA-SH, and HA-BMPH intermediates.

The sharp peak at 1540 cm^{-1} due to the carbon-nitrogen bond that forms during grafting is not present.

Dialysis against diH_2O in 300 kDa MWCO dialysis tubing was done to remove any uncomplexed GAG. FTIR was repeated after the dialysis. Results are shown in Figures A.2.2.

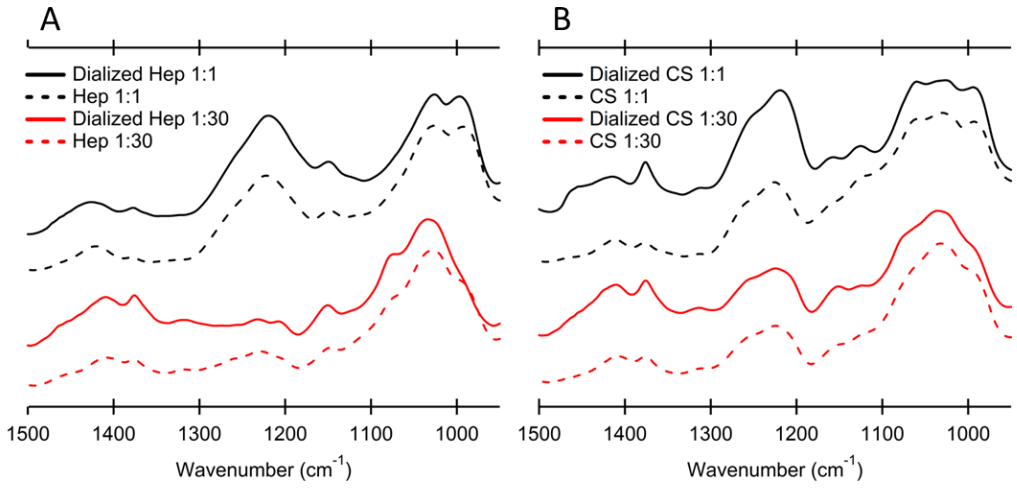

Figure A.2.2. ATR-FTIR spectra of A.) Hep 1:1 and 1:30 and B.) CS 1:1 and 1:30 graft copolymers before and after dialysis.

A.2.1.2 Proton NMR. Chemistry was confirmed through Proton NMR of intermediates and graft copolymers. Changes in peaks associated with the BMPH coupling agent are seen at ~2.3 and ~2.0 ppm. NMR spectra for neat CS and HA, and CS graft copolymers are presented in Figure A.2.3. Some peak assignments and integrals are shown, "*" indicates small molecule contamination. Peaks associated with the BMPH coupling agent are apparent in the CS 1:30 spectra.

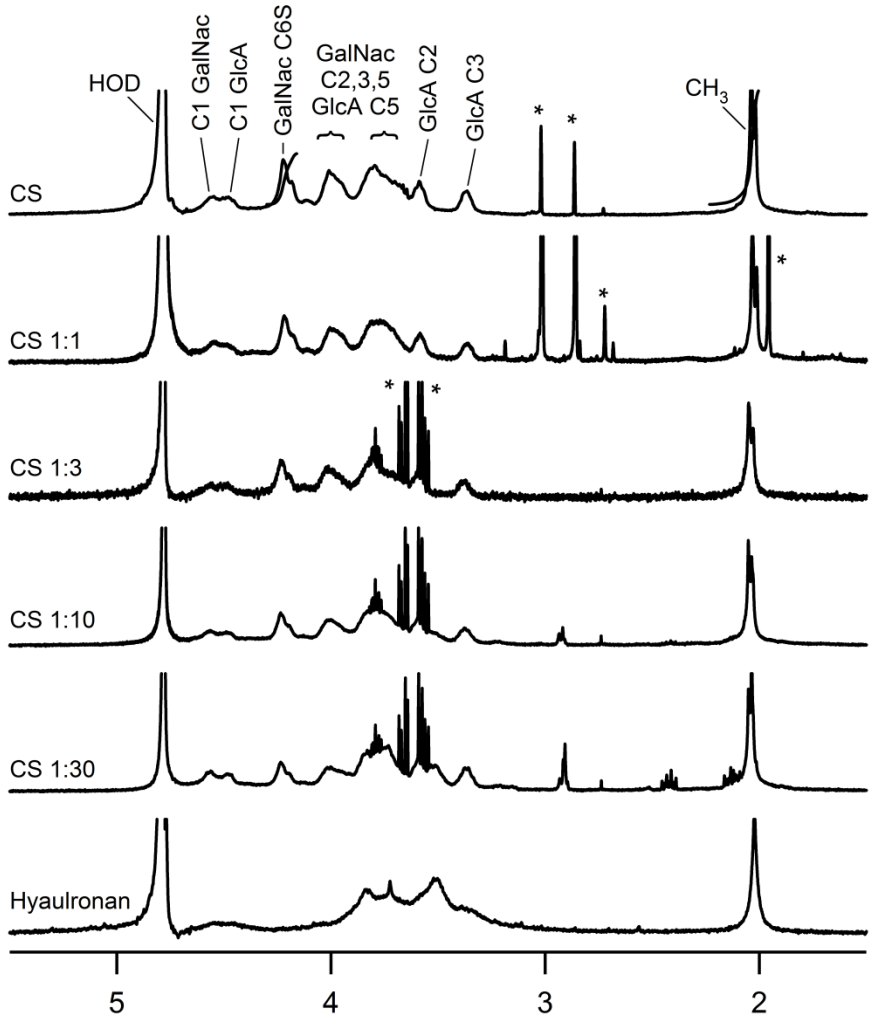

Figure A.2.3. NMR Spectra of neat CS, neat HA, and CS graft copolymers with some peak assignments and integrals. "*" indicates small molecule contamination. Peaks associated with the BMPH coupling agent are apparent in the CS 1:30 spectra.

Spectra for the Hep graft copolymers are displayed in Figure A.2.3. Peaks from the BMPH coupling agent are apparent in the 1:30, 1:10, and 1:3 samples.

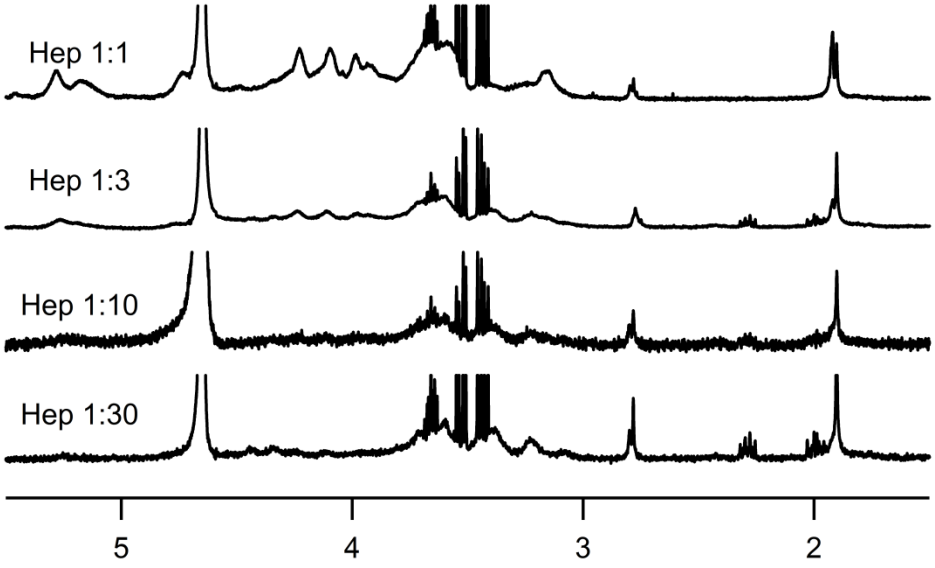

Figure A.2.4. NMR spectra of Hep graft copolymers.

The spectra for HA, HA-SH, and HA-BMPH intermediates are shown in Figure A.2.5.

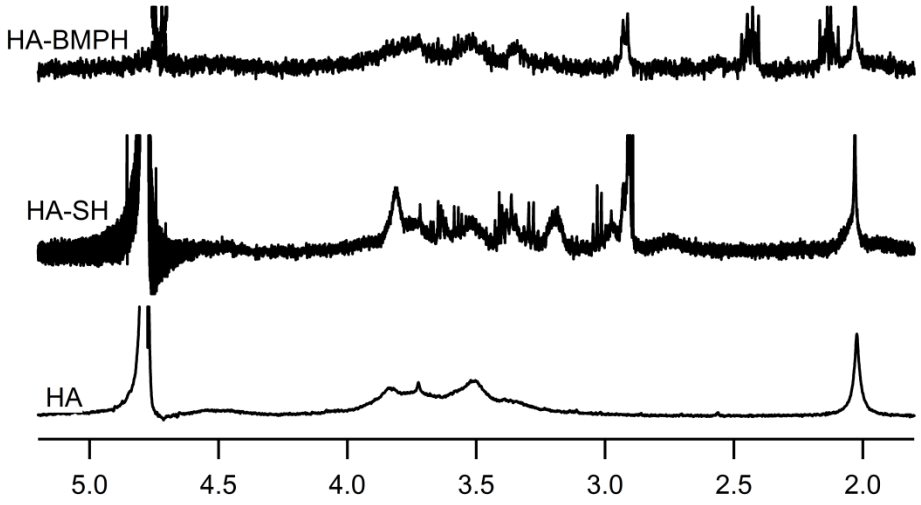

Figure A.2.5. NMR Spectra of HA intermediates.

A.3 SUPPORTING MATERIAL FOR CHAPTER 5.

A.3.1 FGF-2 Quantification within Electrospun Nanofiber Scaffolds via ELISA.

Without any neutralization step, scaffolds were placed in ELISA diluent buffer for two hours. The Emulsion and the PVA in excess coaxial scaffolds dissolved, however the chitosan in excess coaxial scaffold did not dissolve. It was imaged using SEM to investigate its nanostructure, shown in Figure A.3.1. All nanostructure is gone. It is assumed that all FGF-2 was released from the scaffold.

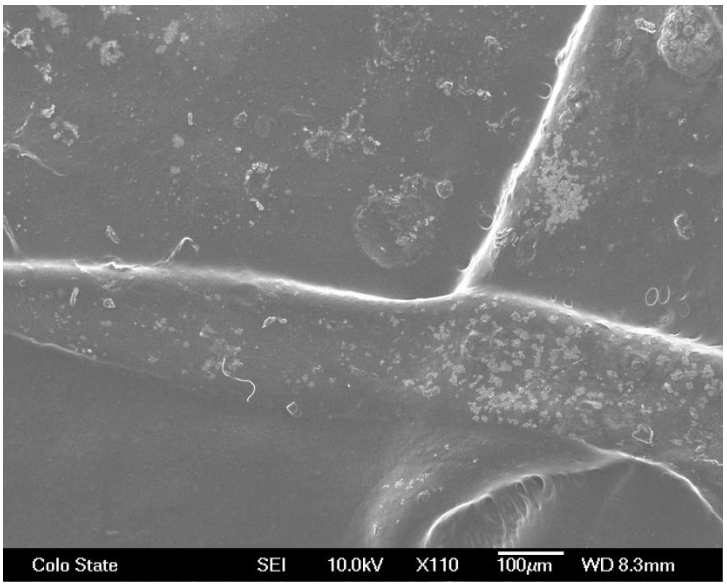

Figure A.3.1. SEM of Chi in excess coaxial scaffold after soaking in ELISA buffer for two hours.

CURRICULUM VITAE

LAURA WALKER PLACE
1500 Yount St.
Fort Collins, CO 80524
(918)740-2320
Laura.w.Place@gmail.com

EDUCATION:

Doctor of Philosophy Degree in Biomedical Engineering
Colorado State University, expected May 2014
Thesis Title: *Biopolymer Nanomaterials for Growth Factor Stabilization and Delivery*
Thesis Advisor: Dr. Matt J. Kipper

Bachelor of Science Degree in Chemical Engineering
University of Oklahoma, received December 2008

RESEARCH EXPERIENCE:

Colorado State University Graduate Research Assistant January 2010-Present
January 2010-Present. Fort Collins, CO
Advisor: Dr. Matt J. Kipper
Prepared novel polyelectrolyte complex nanoparticles with superior growth factor stabilization and delivery. Directly compared the biological activity to the proteoglycan aggrecan and determined nanoparticle compositions that improve biological performance to optimize growth factor delivery to stem cells.

Proteoglycan mimetic graft copolymers with tunable structure were created using synthetic chemistry. The grafting density and composition can be altered to mimic different proteoglycans. The chemistry was confirmed and the graft copolymers were characterized for size, zeta-potential, solution dynamics, and growth factor delivery.

In a collaboration with AlloSource, human demineralized bone matrix (DBM) was processed and electrospun into nanofibers with controllable morphology. These nanofibers contain bioactive components that occur naturally in DBM. A patent is pending on the processing methods.

Chitosan and polyvinyl alcohol (PVA) were coaxially electrospun to form nanofibers with a core/shell structure. These can be used for controlled delivery of growth factors to stem cells.

Polyelectrolyte multilayers were formed using different combinations of polysaccharides. These were characterized and relationships between ion-pairing, thickness, and

hydrophilicity were discerned. These properties can be employed to engineer these coatings for specific applications.

In addition to research projects I have trained and managed undergraduate students that work in the lab. I have taught them techniques and theory and helped them to design and implement research projects.

Louisiana Tech University Research Experience for Undergraduates
June 2008-August 2008. Ruston, LA
Advisor: Dr. Sidney P. Sit
The effects of direct current on fibroblasts seeded in a freeze dried chitosan scaffold were studied. Procedures for seeding cells uniformly throughout the scaffold and observing cell migration due to direct current were established.

Iowa State University Research Experience for Undergraduates
June 2007-August 2007. Ames, IA
Advisor: Dr. Robert C. Brown
Pyrolytic chars produced at different temperatures and mixed with bio-oil were evaluated for their effects on soil fertility. The pyrolysis byproduct was found to increase bacterial activity when mixed with soil.

University of Oklahoma Undergraduate Research Assistant
September 2004-May 2007. Norman, OK
Advisor: Dr. Vassilios I. Sikavitsas
Mesenchymal stem cells (MSCs) were seeded onto arginine-glycine-aspartic acid (RGD) modified Poly-l-lactic acid foam scaffolds in a flow perfusion bioreactor and evaluated for osteogenic differentiation. It was found that there was a synergistic effect of RGD and flow perfusion on osteogenic differentiation of MSCs.

Saint Francis Hospital Center for Genetic Testing Lab Technician
May 2006-August 2006, December 2006-January 2007. Tulsa, OK
Advisor: Dr. Frederick V. Schaefer
New probes were designed to test for the MAPT and TGFBR2 genes. The accuracy of the probes was then validated for use in genetic testing.

Laboratory Skills and Expertise
Electrospinning, layer-by-layer assembly of polyelectrolyte multilayers, formation of polyelectrolyte complex nanoparticles, mammalian cell culture, dynamic light scattering, enzyme-linked immunosorbent assay, polymerase chain reaction, gel electrophoresis, fluorescent staining and microscopy, MTT assay, cell titer blue, gel permeation chromatography, contact angle, viscometry, scanning electron microscopy, ellipsometry, thermogravimetric analysis, nuclear magnetic resonance, x-ray photoelectron spectroscopy, Fourier transform infrared spectroscopy, polarization modulation infrared reflection adsorption spectroscopy, Fourier transform surface plasmon resonance.

COLLABORATIONS:

Dr. Tammy Donahue and Hannah Pauly
Dynamic mechanical testing of hydrogels impregnated with proteoglycan-mimetic graft copolymers.

Dr. Salman Khetani and Christine Lee
Using GAG-based polyelectrolyte multilayers to deliver TGF-β to hepatocytes in a coculture model.

Dr. Ketul C. Popat, Victoria Leszczak, and AlloSource
Demineralized bone matrix was processed and electrospun into nanofibers, An invention disclosure has been filed on the processing methods.

Dr. Melissa Reynolds and Dr. Vinod Damodaran
The degradation of a biodegradable dextran derivative by dextranase was monitored through GPC.

PUBLICATIONS:

Place, L.W.; Seyki, M.; Taussig, J.E.; Kipper, M.J.; Two-Phase Emulsion and Coaxial Electrospinning to Incorporate Growth Factors into Electrospun Nanofibers. 2014, in preparation for submission to *Macromolecular Bioscience.*

Place, L.W.; Kelly, S.; Kipper, M.J.; Synthesis and Characterization of Proteoglycan-Mimetic Graft Copolymers. 2014, in preparation for submission to *Biomacromolecules.*

Leszczak, V.; Place, L.W.; Franz, N.; Popat, K.C.; Kipper, M.J.; Nanostructured Biomaterials from Electrospun Demineralized Bone Matrix: A Survey of Processing and Cross-Linking Strategies. *Applied Materials and Interfaces* 2014, In Press. DOI:10.1021/am501700e.

Place, L.W.; Seyki, M.; Kipper, M.J.; Aggrecan-Mimetic, Glycosaminoglycan-Containing Nanoparticles for Growth Factor Stabilization and Delivery. *Biomacromolecules* 2013, *15*(2), 680-689.

Damodaran, V. B.; Place, L. W.; Kipper, M. J.; Reynolds, M. M., Enzymatically degradable nitric oxide releasing S-nitrosated dextran thiomers for biomedical applications. *Journal of Materials Chemistry* 2012, *22* (43), 23038-23048.

Almodovar, J.; Place, L. W.; Gogolski, J.; Erickson, K.; Kipper, M. J., Layer-by-Layer Assembly of Polysaccharide-Based Polyelectrolyte Multilayers: A Spectroscopic Study of Hydrophilicity, Composition, and Ion Pairing. *Biomacromolecules* 2011, *12* (7), 2755-2765.

Alvarez-Barreto, J. F.; Landy, B.; VanGordon, S.; Place, L.; DeAngelis, P. L.; Sikavitsas, V. I., Enhanced osteoblastic differentiation of mesenchymal stem cells seeded in RGD-functionalized PLLA scaffolds and cultured in a flow perfusion bioreactor. *Journal of Tissue Engineering and Regenerative Medicine* 2011, *5* (6), 464-475.

CONFERENCES & PRESENTATIONS:

October 2013. *Biopolymer Nanomaterials for Growth Factor Stabilization and Delivery.* School of Biomedical Engineering Seminar Series, Fort Collins, CO.

September 2013. *Electrospinning Extracellular Matrix Proteins.* Biomedical Engineering Society annual meeting. Seattle, WA

November 2012. *Synthesis and characterization of an aggrecan-mimetic graft copolymer for biomedical applications.* American Insitute of Chemical Engineers annual meeting, Pittsburgh, PA.

October 2012. *Polyelectrolyte complex nanoparticles for the stabilization and delivery of FGF-2.* Biomedical Engineering Society annual meeting, Atlanta, GA.

November 2011. *Polysaccharide nanoassemblies for biomedical applications.* School of Biomedical Engineering Seminar Series, Fort Collins, CO.

October 2011. *Polysaccharide nanoassemblies for growth factor stabilization and delivery.* American Institute of Chemical Engineers annual meeting, Minneapolis, MN.

September 2011. *Aggrecan-mimetic polysaccharide nanoassemblies.* American Chemical Society annual meeting, Denver, CO.

PROFESSIONAL SOCIETIES:

Biomedical Engineering Society
2009-Present
American Institute of Chemical Engineers
2006-Present

UNIVERSITY SERVICE:

STEM Summer Instructor

- Northrop Grumman high school summer camp for biomedical engineering
  July 2014

Graduate Teaching Assistant

- BIOM 300, Problem-Based Learning Biomedical Engineering Lab
  January 2014- May 2014

Mentor to Undergraduate Students

- Training, supervising, and advising undergraduate research assistants during lab work for honors theses, work study, and volunteering

2010-Present

Biomedical Engineering Society-local chapter

- Graduate Student Advisor
  2011-Present
- Elementary School and Middle School Outreach
  2011
- Treasurer
  2010-2011
- Chapter Revitalization
  2010

School of Biomedical Engineering Seminar Series Committee

- Committee Member
  August 2012- May 2013

REFERENCES:

Dr. Matt J. Kipper
Associate Professor Chemical and Biological Engineering
Associate Professor Biomedical Engineering
Department of Chemical and Biological Engineering
Colorado State University
1370 Campus Delivery
Fort Collins, CO 80523
(970)491-0870
matthew.kipper@colostate.edu

Dr. Ketul C. Popat
Associate Professor Mechanical Engineering
Associate Professor Biomedical Engineering
Department of Mechanical Engineering
Colorado State University
1374 Campus Delivery
Fort Collins CO, 80523
(970)491-1468
ketul.popat@colostate.edu

Dr. Melissa M. Reynolds
Assistant Professor Chemistry
Assistant Professor Biomedical Engineering
Department of Chemistry
Colorado State University
Campus Delivery 1872
Fort Collins, CO 80523
(970)491-3775
melissa.reynolds@colostate.edu